UNIVERSITEIT VAN PRETORIA
UNIVERSITY OF PRETORIA
YUNIBESITHI YA PRETORIA
Denkleiers • Leading Minds • Dikgopolo tša Dihlalefi

A three-dimensional model for the Leeuwpoort tin mine and its application to exploration predictions

By:

Zandri Harris

Submitted in partial fulfilment of the requirements for the degree M.Sc. Geology in the Faculty of Natural and Agricultural Sciences

University of Pretoria

Pretoria

October 2017

UNIVERSITEIT VAN PRETORIA
UNIVERSITY OF PRETORIA
YUNIBESITHI YA PRETORIA

Title of Treatise: A three-dimensional model for the Leeuwpoort tin mine and its application to exploration prediction

Author: Zandri Harris

Supervisor: Professor R.K.W. Merkle

Department: Department of Geology, Faculty of Natural and Agricultural Sciences, University of Pretoria

Degree: M.Sc. Geology

ABSTRACT

Due to tighter financial margins, the need for better knowledge of grade data is required. Geological models allow the user to have a better understanding of the geological environment in which mining is taking place. Three dimensional (3D) geological, ore deposit, and mining models are therefore becoming increasingly important in the mining industry. 3D models are being used more frequently for mineral potential targeting, as well as resource assessment, because good quality geological models allow the user to determine grade domains within mineralized environments. The aim of this thesis is to create a geological model for Leeuwpoort Tin Mine (C-Mine) and test the applicability of this 3D model for exploration purposes. The 3D geological and interpolant models created of Leeuwpoort Mine was used to determine the probability of intersecting a lode of economic interest, if 500 drillholes were randomly drilled in a specific boundary. Resampling was conducted using the Bootstrap method, in order to determine how the probability will change as different borehole sample sizes are used.

When conducting a quantitative resource assessment of mineral deposits, grade-tonnage models form a fundamental part in the estimation and prediction process. Grade and tonnage models are used during quantitative resource assessment to predict the values of the known deposits for a specific type, and can also be used to determine the potential value of undiscovered deposits in a specific area. If sufficient geological data is available, the tonnage of mineralized bodies can be calculated and a grade-tonnage model can be created from the 3D geological model. 3D models can be used as a summary and visualization tool for geological environments. The 3D visualization of deposit give a much better representation of the orebody than 2D cross-sections from a few drillholes. The effectiveness of 3D model, as a possible tool for mining, is limited by the quality and quantity of the data. Poor quality data will result in poor quality models, whereas limited data will result in a higher level of uncertainty of the estimates based from these 3D models. However, even limited data can be used to visualize geological environments.

In the case of Leeuwpoort Mine, limited structural and lithological information was available to create the 3D models. However, the provided peg index noted the positions of the mine pegs, and consequently indicate where the lodes were mined. In this instance, with limited mine peg data, the lode “volumes” could be reconstructed. The peg index was used to delineate the mining area in order to model the lodes, as well as interpret geological features. Once the lode “volumes” were created in the 3D model, the specific orezone with the geometric relationship between individual lodes of Leeuwpoort Mine could be defined. In addition, the probability of

intersecting a certain number of lodes was derived from these modelled surfaces, resulting in the estimation for the predicted probability of success. The 3D geological and interpolant models created of Leeuwpoort Mine were used to determine the probability of intersecting a lode of economic interest, if exploration drilling were to be done. Resampling was conducted using the Bootstrap method, in order to determine how reliable this prediction is as a function of number of boreholes. The results obtained from the Bootstrap analysis indicates that the average probability of intersecting a lode of economic significance, for each of the different sample sizes stays the same. A higher level of confidence in the probability of intersecting a lode can be assumed for areas that have large quantities of drilling.

If a geological environment similar to that of Leeuwpoort Mine is considered for an exploration project, the chances of intersecting an economical orebody or lode during exploration is very low. When considering Greenfields exploration (virgin exploration), the chances of intersecting a mineralized body is extremely low, and a lot of money has to be invested to obtain meaningful results. However, if Brownfields exploration (exploration on a known area) takes place, the chances of intersecting a mineralized body is higher, because prior knowledge of the area exists and can be used to make informed decisions on where to drill. Less money needs to be invested for the drilling than for Greenfields exploration. In the case of Leeuwpoort Mine, unfortunately even Brownfields exploration will bear a very limited chance of identifying a mineralized body, which means that in such a scenario, the information about potential success rate of a drilling program is even more important for drilling and financial planning.

ACKNOWLEDGEMENTS

This thesis is dedicated to my parents, Terence Harris and Dilia Harris. Their continuous support, encouragement and unconditional love allowed the author the opportunity to excel.

It is my pleasure to acknowledge the roles of several individuals who were instrumental for completion of my M.Sc. thesis:

The thesis supervisor, *Prof Roland K. W. Merkle*, and mentor and consultant, *Mr. P.W.J Delport*, are thanked for providing guidance and assistance throughout this thesis. Their constant feedback and guidance on the thesis allowed the author to grow academically. Mr P.W.J. Delport is thanked for providing access to the fundamental historical data.

Mr B. Cohen and *Mrs. M.M. Cohen* are thanked for their hospitality during the numerous site visits. Mr Ben Cohan is thanked for allowing the author access to the mine premesis.

The *Leapfrog Geo South Africa Support Team* are thanked for allowing the author unenterupted access to the Leapfrog Geo software. They are especially thanked for their assistance, guidance and training throughout this thesis.

Mr. F.A.S. Reyneke is thanked for his contribution and assistance throughout the thesis. His guidance and experience in data processing and bootstrapping analysis was most beneficial. His feedback and assistance on the thesis was most helpful.

Ms K. Byrch and *Mr Q. Hall* are thanked for their assistance with the data capturing and data processing of the historical data.

Mr K. Petzer is thanked for this assistance and guidance throughout the thesis.

The *Council of Geoscience* is thanked for granting the author a bursary to complete a Master's Degree.

DECLARATION OF ORIGINALITY

The **Department of Geology (University of Pretoria)** places great emphasis upon integrity and ethical conduct in the preparation of all written work submitted for academic evaluation. While academic staff teach you about referencing techniques and how to avoid plagiarism, you too have a responsibility in this regard. If you are at any stage uncertain as to what is required, you should speak to your lecturer before any written work is submitted.

You are guilty of plagiarism if you copy something from another author's work (eg a book, an article or a website) without acknowledging the source and pass it off as your own. In effect you are stealing something that belongs to someone else. This is not only the case when you copy work word-for-word (verbatim), but also when you submit someone else's work in a slightly altered form (paraphrase) or use a line of argument without acknowledging it. You are not allowed to use work previously produced by another Students) for a ruling. Plagiarism is regarded as a serious contravention of the University's rules student. You are also not allowed to let anybody copy your work with the intention of passing if off as his/her work.

Students who commit plagiarism will not be given any credit for plagiarised work. The matter may also be referred to the Disciplinary Committee (and can lead to expulsion from the University. The declaration which follows must accompany all written work submitted while you are a student of the **Department of Geology (University of Pretoria)**. No written work will be accepted unless the declaration has been completed and attached.

I, the undersigned, declare that:

1. I understand what plagiarism is and am aware of the University's policy in this regard.
2. I declare that the thesis/dissertation, thesis (e.g. essay, report, thesis, assignment, dissertation, thesis, etc.) is my own original work. Where other people's work has been used (either from a printed source, Internet or any other source), this has been properly acknowledged and referenced in accordance with departmental requirements.
3. I have not used work previously produced by another student or any other person to hand in as my own.
4. I have not allowed, and will not allow, anyone to copy my work with the intention of passing it off as his or her own work.

Full names of student: Zandri Harris

Student number: 13045050

Topic of work: A three-dimensional model for the Leeuwpoort tin mine and its application to exploration predictions

Signature: _____

TABLE OF CONTENTS

LIST OF FIGURES

LIST OF TABLES

1. INTRODUCTION

Due to tighter financial margins, the need for better knowledge of grade data is required. Geological models allow the user to have a better understanding of the geological environment in which mining is taking place. Three dimensional (3D) geological, ore deposit, and mining models are therefore becoming increasingly important in the mining industry. 3D modelling software is preferred to manual hand-written or hand-drawn models of geological environments, because the use of modelling software reduces the time consumed when developing the models (Cowan et al., 2002; Reid, 2017; Zu et al., 2012; Yan-lin et al., 2011). The technological advancements in 3D models has allowed users to effectively store, manage, process and display large quantities of obtained geological information (Wu et al., 2005). 3D models are being used more frequently for mineral potential targeting, as well as resource assessment, because good quality geological models allow the user to determine grade domains within mineralized environments (Wang et al., 2011).

When conducting a quantitative resource assessment of mineral deposits, grade-tonnage models form a fundamental part in the estimation and prediction process. Grade and tonnage models are used during quantitative resource assessment to predict the values of the known deposits for a specific type, and can also be used to determine the potential value of undiscovered deposits in a specific area. If sufficient geological data is available, the tonnage of mineralized bodies can be calculated and a grade-tonnage model can be created form the 3D geological model. The aim of this thesis is to create a geological model for Leeuwpoort Tin Mine and test the applicability of this 3D model for exploration purposes. Geostatistical analysis will be done on the exploration results and will be used to determine if the 3D models can be used as a geological exploration tool.

1.1. Importance and significance of tin

Tin (Sn) is a silver transition metal that is soft, malleable and chemically stable. This metal is non-toxic and has a low melting point, 231.9 ˚C. Tin is used for industrial purposes to coat other metals to prevent corrosion and as a lead free solder (Du Toit and Pringle, 1998). The latter has increased the market value of tin significantly, as lead based solder has been classified as environmentally damaging. Tin is used to produce paint, glass decorations and pewters, whereas organo-tin is used in the manufacturing of industrial plastics, PVC's and pesticides.

Tin is known to be a constituent in 79 valid mineral species, but the two most economic minerals are stannite and cassiterite. Stannite (Cu_2FeSnS_4) is a copper-iron-tin bearing sulphide that has a high metallic lustre and is silver or black in colour. Stannite is mainly found in hydrothermal vein deposits occurring with chalcopyrite, pyrite, tetrahedrite, sphalerite, arsenopyrite, cassiterite, and wolframite. Stannite contains approximately 28% tin, which is significantly lower than Cassiterite (SnO_2). Cassiterite (Figure 1) is brown to black in colour but some colour varieties of red, yellow and colourless are also possible. Cassiterite contain approximately 78.6% tin and is the only significant tin ore (Du Toit and Pringle, 1998; Ivanov et al., 1980; Ivanov et al., 1982).

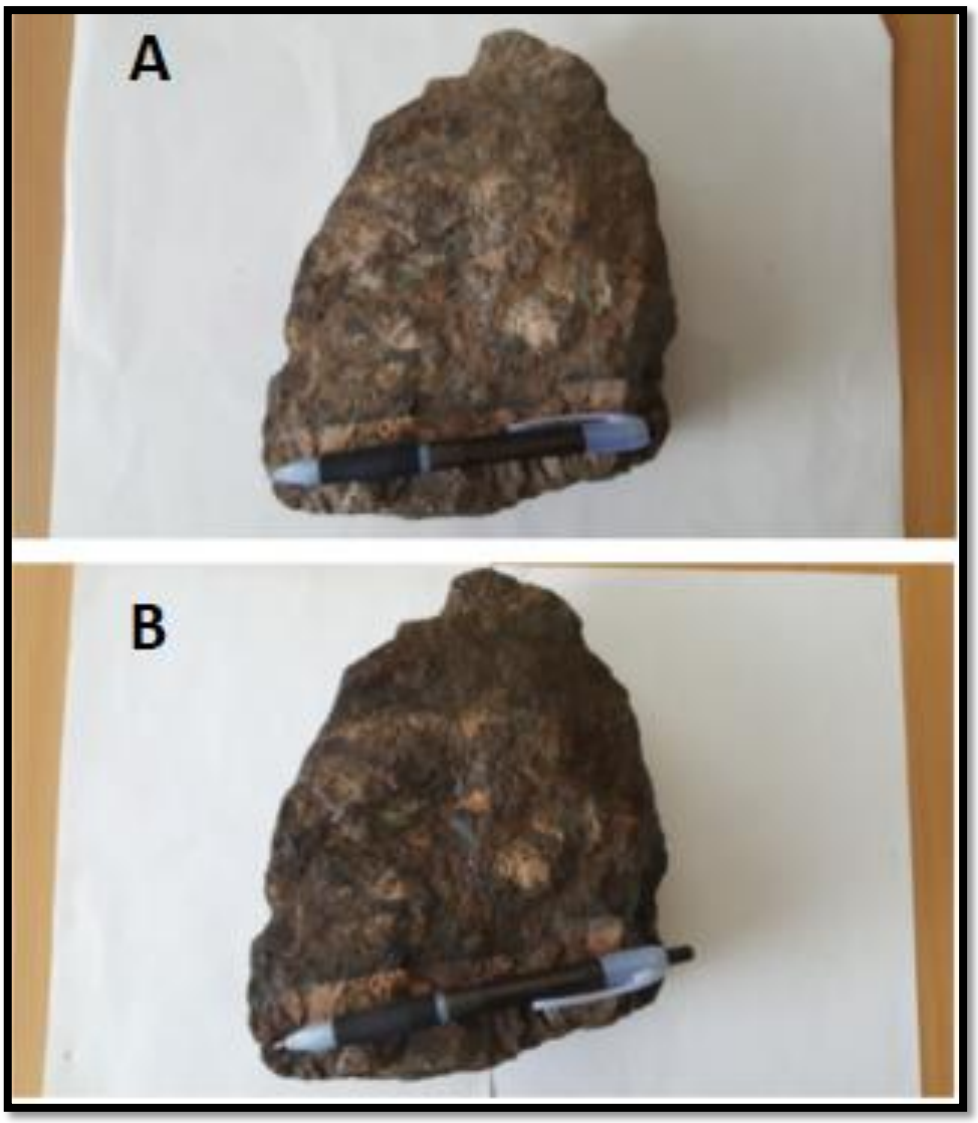

Figure 1: Hand specimen of cassiterite minerals (dark minerals) within an arkose, from Leeuwpoort Mine. A) Dry hand specimen sample of cassiterite minerals (dark minerals) within an arkose, pen for scale. B) Wet hand specimen sample of cassiterite minerals (dark minerals) within an arkose, pen for scale.

1.2. Occurrences of tin in South Africa

Tin mineralization can be found throughout South Africa (Figure 2).The economically significant tin deposits can be found in the Cape Granite Suite near Cape Town and in the Bushveld Complex (Lenthall, 1974; Falcon, 1989). Tin deposits in the Northern and Mpumalanga provinces (Figure 2 points 1-6) are associated with the acidic phase of the Bushveld Complex, where a total of 88 tin occurrences have been identified. The tin deposits in the Bushveld Complex can be classified as either endogranitic deposits or as exogranitic deposits (Du Toit and Pringle, 1998). Tin mineralization in the Archean Granite (Figure 2 points 7-8) are the only two cassiterite occurrences in this region, however, both of these mineralization are subeconomical (Rozendaal et al., 1986; Du Toit and Pringle, 1998). Tin deposits are primarily cassiterite rich in the Cape Granite Suite (Figure 2 point 15) and are associated with syn- and post-tectonic granitoids. These granitoids intruded into the volcano-sedimentary Malmesbury Group and underwent low-grade regional metamorphism (Du Toit and Pringle, 1998).

1.3. Tin mining in South Africa

The world's main supply of cassiterite is sourced from stanniferous (tin rich) alluvial deposits that are derived from mineralized zones in the surrounding areas (Du Toit and Pringle, 1998; Rozendaal et al., 1986). The main source of tin in South Africa is located in the Bushveld Complex, and a total of six tin fields are distinguished between: Potgietersrus, Olifants, Elands, Rooiberg, Nylstroom and Moloto (Figure 3 and Table 1). Three mines produced the largest quantities of tin: Rooiberg, Zaaiplaats, and Union Tin. Figure 3 depicts the total tin production as a pie chart for each tin field. Rooiberg tin field was the largest producer of tin in the Bushveld complex.

Table 1 indicates the total tonnes of metallic tin produced for each of the tin fields (Du Toit and Pringle, 1998). Of these tin fields, Rooiberg, Potgietersrus, and Nylstroom produced 90% of the total metallic tin of South Africa. An old timber prop was discovered at Rooiberg, dated at 1515 AD, the South African Iron Age, which suggests that tin was mined in the Rooiberg area 500 years ago (Falcon, 1989; Grant, 1999; Friede, 1976; Buchanan, 2006). However, archaeological evidence indicates that tin mining was done long before then (Grant, 1999).

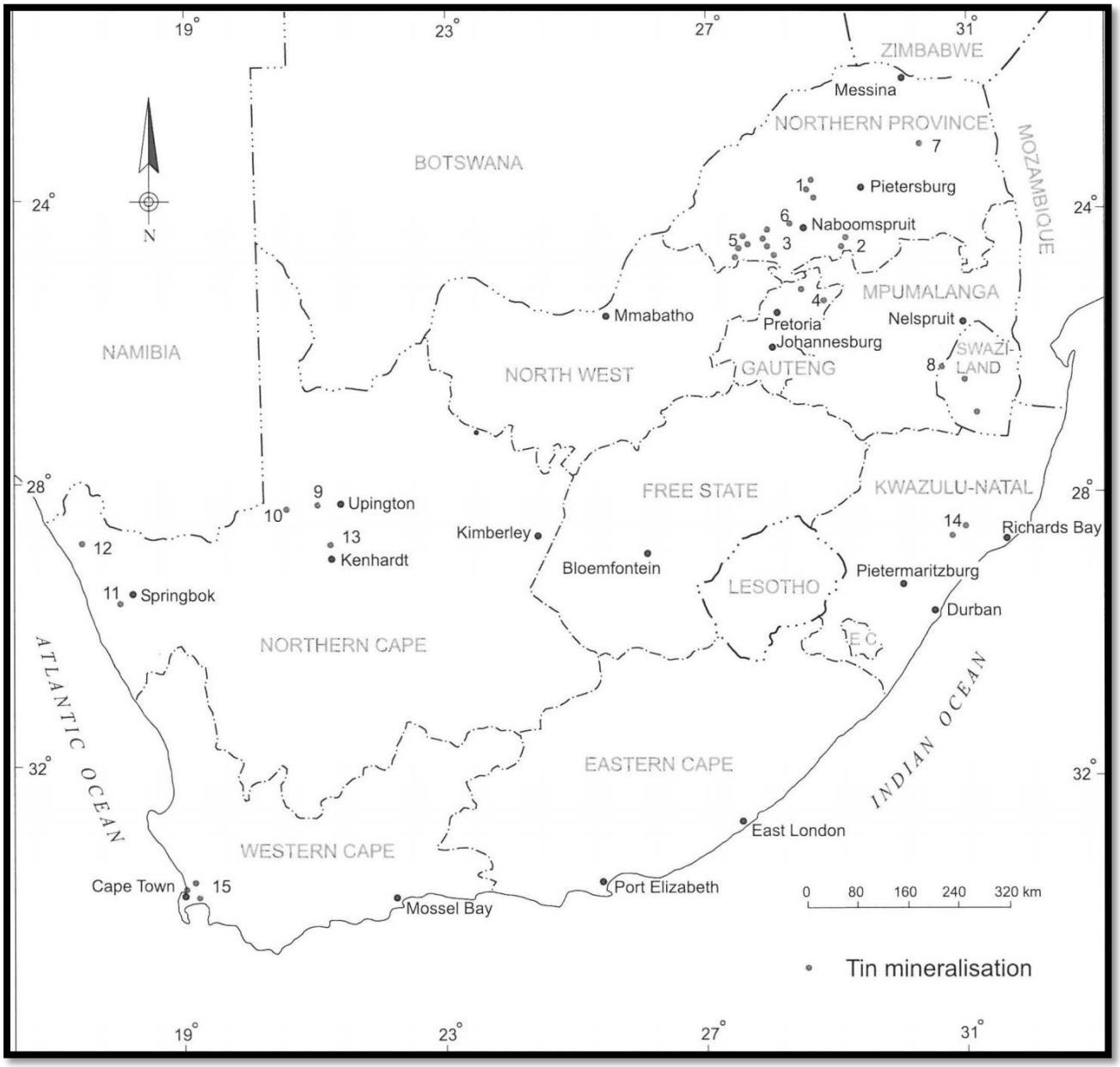

Figure 2: Tin deposits of South Africa. The major tin deposits are indicated with a dot. Northern and Mpumalanga Province: 1) Potgietersrus, 2) Olifants, 3) Elands, 4) Rooiberg, 5) Nylstroom and 6) Moloto. Archean Granite region: 7) Klein Letaba and 8) Oshoek. Northern Cape Province: 9) Van Rooy's Vley, 10) Renosterkop, 11) Tweedam, 12) Stinkfontein, 13) N'Rougas and 14) Umfuli. Cape Granite: Cape Granite Suite. Sourced from Du Toit and Pringle (1998).

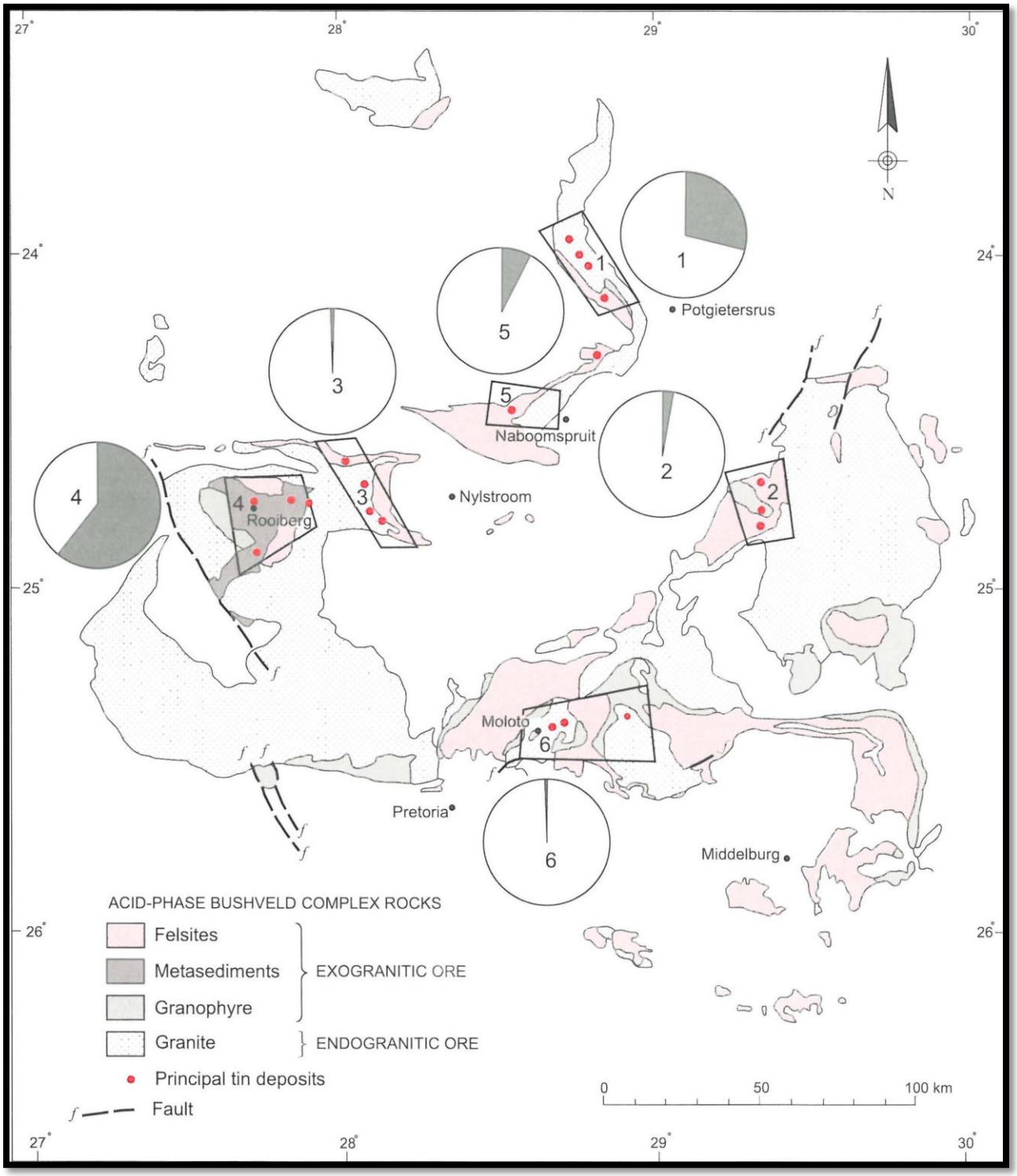

Figure 3: Location of the tin fields in the Bushveld Complex. 1) Potgietersrus, 2) Olifants, 3) Elands, 4) Rooiberg, 5) Nylstroom and 6) Moloto. The total percentage of metallic tin production is expressed as a pie diagram. These pie diagrams can be related to Table 1. Sourced from Du Toit and Pringle (1998).

The two largest producers, Rooiberg Tin Limited (formerly Rooiberg Minerals) and Zaaiplaats Tin, started mining operations in 1908. Leeuwpoort Tin was operational by 1911 and was taken over by Rooiberg Tin Limited in 1932 (Falcon, 1989; Du Toit and Pringle, 1998). The collapse of the Tin Council resulted in a decrease of the tin price after 1980, and subsequently led to the closure of the mines after 87 years of underground production, which yielded 100000 tons of tin metal. Rooiberg Tin Limited was the last active tin producer in the Bushveld Complex and closed down in November 1993 (Falcon, 1989; Du Toit and Pringle, 1998; Godsell, 2011).

1.4. Mining in the Rooiberg tin field

In 1979, Rooiberg Tin Limited held 17 000 ha of mineral rights and 5330 ha of freehold rights in the Rooiberg tin field (Falcon, 1989). Five production mines were established on the property: Rooiberg (A-Mine), Nieuwpoort (B-Mine), Leeuwpoort (C-Mine), Blaauwbank (D-Mine), and Vellefontein (Stumpfl, 1977).

Table 1: Total tonnage of metallic tin produced for the tin fields of the Bushveld Complex. These tin fields can be referred back to Figure 2 and Figure 3. Sourced from Du Toit and Pringle (1998).

	TIN FIELD	%	METAL-LIC TIN (t)	HOST ROCK
1	POTGIETERSRUS **Mines:** Zaaiplaats Roodepoort (Groenfontein) Solomon's Temple Welgevonden	29,3	~40 000	Granite
2	OLIFANTS **Mines:** Mutue Fides Stavoren Roodewal Vlakfontein	2,2	3 026	Granite
3	ELANDS **Mines:** Elandsfontein - 4 sites	0,1	118	Felsite
4	ROOIBERG **Mines:** Vellefontein Rooiberg (A-Mine) Nieuwpoort (B-Mine) Leeuwpoort (C-Mine) Blaauwbank (D-Mine)	61,1	84 000	Metasedi-ments
5	NYLSTROOM **Mines:** Union Mine	7,3	10 000	Felsite
6	MOLOTO **Mines:** Enkeldoorn (Zustershoek) Vlaklaagte Allemansdrift	0,01	104	Granite
TOTAL METALLIC TIN		**100**	**137 248**	

.

2. GEOLOGY

This section will outline the regional and local geology of the Rooiberg tin field, with specific reference to Leeuwpoort Tin Mine (C Mine).

2.1. Geology of the Rooiberg tin field in the Bushveld Complex

As mentioned previously, the Bushveld Complex hosts the main economic tin fields of South Africa, which are located in the western portion of the Bushveld Igneous Complex (Figure 3) (Leube and Stumpfl, 1963; Du Toit and Pringle, 1998). The Rooiberg tin field is located on arkosites and shales of the upper portion of the Precambrian Transvaal Supergroup, which is a folded remnant or roof pendent of the Bushveld granites in this region (Figure 4) (Falcon, 1989; Du Toit and Pringle, 1998; Stumpfl and Leube, 1963; Rozendaal et al., 1986). A well-developed shale band, also known as the Main Shale, formed a cap rock which efficiently trapped the ascending mineralizing solutions (Phillips, 1982; Rozendaal et al., 1986). The prevention of fluid mobilization resulted in the precipitation of cassiterite along with fluorspar and copper-iron sulphides (Lenthall, 1974). However, Phillips (1982) noted that steep fractures did allow mineralization through and into the Blaauwbank Shale Member of the Leeuwpoort Formation. The Rooiberg tin field, and more specifically Leeuwpoort Mine, which is the main focus of this report, is located on the Rooiberg Fragment.

2.2. Geology of the Rooiberg tin field in the Rooiberg Fragment

The Rooiberg Fragment, is located on the western lobe of the Bushveld Complex (Falcon, 1989; Rozendaal et al., 1995a). The Rooiberg Fragment has a triangular shape and covers an aerial extent of 800 km^2 (Hartzer, 1995; Rozendaal et al., 1986). The Rooiberg Fragment is composed of volcano-sedimentary rocks of the Transvaal sequence that has an approximate early Palaeoproterozoic age (Buchanan, 2006). These rocks are surrounded by granitoid intrusive rocks of the Bushveld Complex: Lebowa Granite Suite (LGS) as well as the Rashoop Granophyre Suite (Figure 4) (Rozendaal et al., 1995a).

The Rooiberg Fragment consists of the sedimentary rocks of the Pretoria Group that forms part of the Transvaal Supergroup. The Pretoria Group is conformably overlain by the volcanic rocks of the Dullstroom Formation that is part of the Rooiberg Group (Schreiber et al., 1991) (Eriksson et al., 1995) (Eriksson et al., 2006) (Buchanan, 2006). An intracratonic rifting event resulted in the deposition of volcanic rocks in the Dullstroom Formation (Eriksson et al., 1995). The subsequent detachment of the volcanic rocks from the Dullstroom Formation occurred approximately 2.050 Ga during the mafic to ultramafic intrusion of magma into the Bushveld

Complex (Eriksson et al., 1995) (Buchanan, 2006). Hartzer (1995) suggested that the Smelterskop and Rinkhalskop Formations were the basal units of the Rooiberg Group. Eriksson et al. (1993) suggested that the Leeuwpoort Formation and Mackekaan Formations should be included as basal units as well.

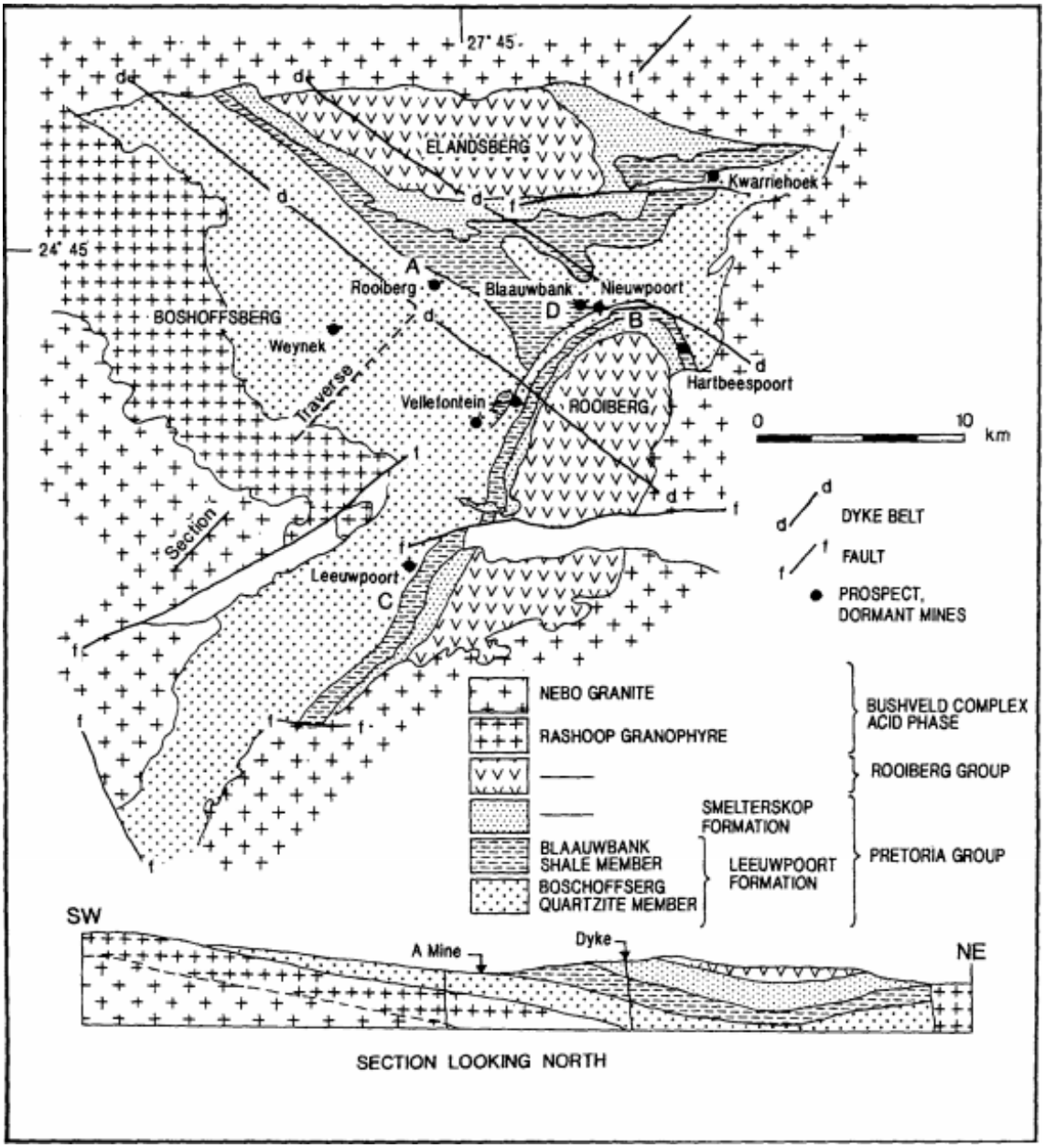

Figure 4: Regional geology and tectonic features of the Rooiberg Fragment as well as the location of the important tin producers. Sourced from Rozendaal et al. (1995).

The Leeuwpoort Formation can be subdivided into two Members: the lower Boschoffsberg Quartzite Member and the upper Blaauwbank Shale Member (Figure 5) (Rozendaal et al., 1995a; Rozendaal et al., 1986; Kent and Matthews, 1980). The nomenclature division of the Leeuwpoort Formation was used throughout the mining period of Leeuwpoort Mine as a

mining term. The nomenclature of the Boschoffsberg Quartzite Member and Blaauwbank Shale Member was used throughout this thesis to avoid any confusion when referring to the historical data. The nomenclature of the Leeuwpoort Formation has since been changed to the lower Boschoffsberg Member and upper Blaauwbank Member.

The Boschoffsberg Quartzite Member is composed of feldspathic sandstone and quartzite with minor poorly sorted basal conglomerates that has identifiable trough and planar cross-bedding. Two units can be identified within the Blaauwbank Shale Member: 1) a lower shaly arkose that marks the gradational transition between the arkosites and shales, and 2) and an overlying shale unit. (Rozendaal et al., 1995a; Eriksson et al., 1993; Rozendaal et al., 1986). The Smelterskop Formation conformably overlies the Leeuwpoort Formation, and is characterised by an alternating sequence of magnesium rich andesites, cross-bedding dominated arenites and thin, laminated intercalated shales (Figure 5) (Eriksson et al., 1993; Rozendaal et al., 1995a). The extrusive felsic volcanic rocks of the Rooiberg Group is located at the top of the stratigraphy and conformably to paraconformably overlie the sequence.

All tin deposits in this region are located in the quartzites at the transitional boundary of the Boschoffsberg Quartzite Member (Hartzer, 1995; Eriksson et al., 1993; Rozendaal et al., 1995a). The concept of regionally developed continuous stanniferous zones was developed based on the stratabound distribution of individual ore deposits (Rozendaal et al., 1995a). The mines located within the Rooiberg tin fields are dominated by different styles of mineralization which includes the following:

- Tourmaline pockets or orbicules
- Disseminated cassiterite
- Steep and flat dipping sulphide fractures
- Hydrothermal carbonate breccias

The mineralization was classified according to two types by Rozendaal et al. (1986): conformable and unconformable mineralization. Conformable mineralization includes pockets, bedding-plane mineralization, bedded lodes, and bedded stringers. Unconformable mineralization includes steeply dipping lodes that have a strike parallel to the major fracture direction.

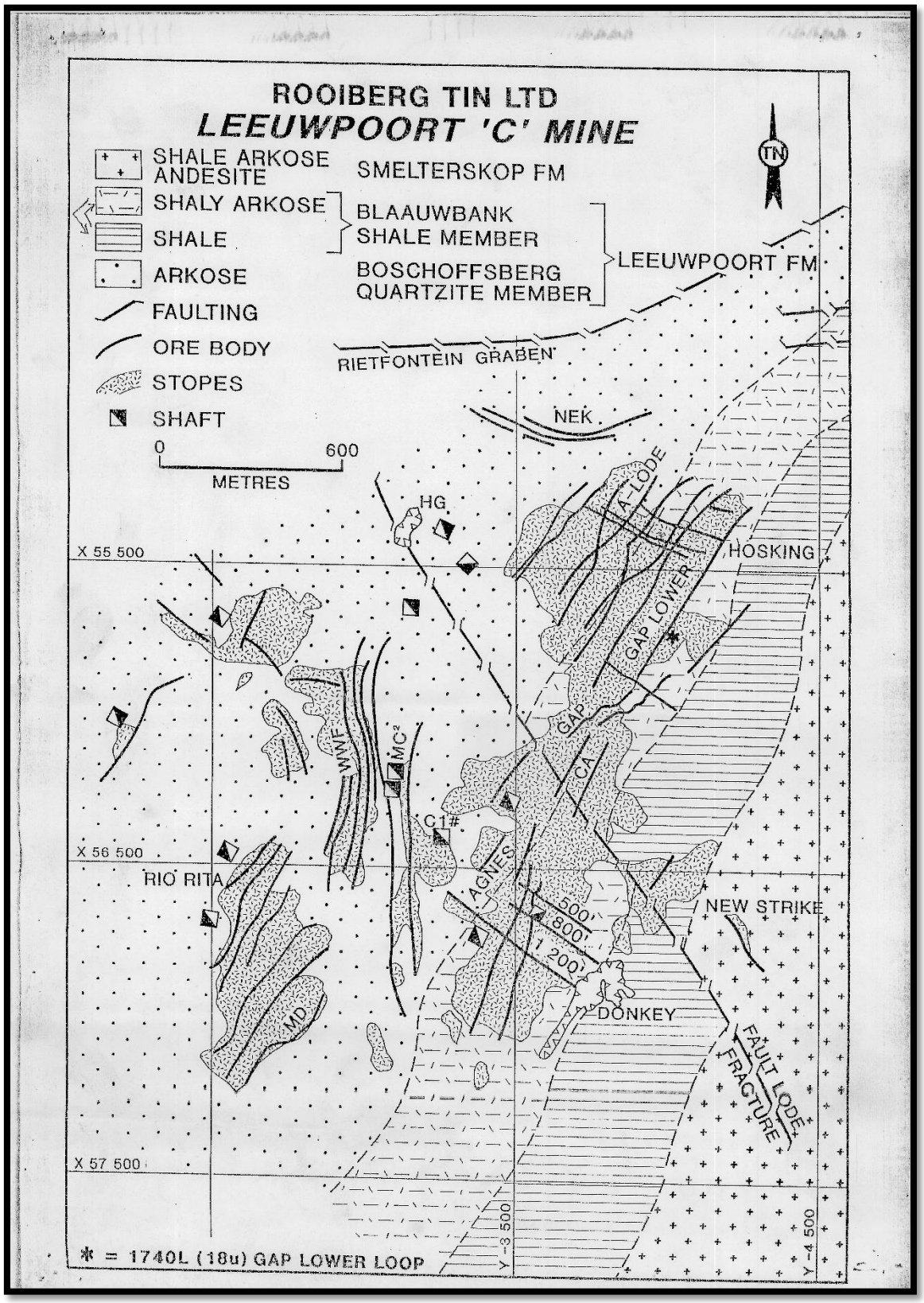

Figure 5: Local geology of Leeuwpoort (C-Mine). The major mineralized stopes were projected onto surface. Sourced form an unpublished map of Rooiberg Tin Ltd.

Cassiterite can be formed through two main geological processes. The first process is associated with granitic intrusions. Cassiterite occurs as an accessory constituent in late-stage granitic intrusion and is mainly focused in veins and fissures (Labuschagne, 2004; Falcon, 1989). The second process is mainly associated with alluvial and placer deposits. Cassiterite is mainly associated with highly acidic granitic rocks and does not occur in situ anywhere in the world except when granites are in close proximity (Falcon, 1989).

The tin deposits in South Africa can generally be classified in two main deposit types:

1. Syngenetic deposit types are characterised by pipes and disseminations in young granitic rocks.
2. Epigenetic deposit types are characterised by veins, fault breccias and replacement systems. Zaaiplaats, Groenfontein, Mutue Fides, Stavaren, Union Tin, Solomons Temple, Rooiberg, and Leeuwpoort Mines all form part of the epigenetic deposit type. Table 2 list the mines in the Bushveld Complex along with their associated geology in which the epigenetic replacement takes place (Falcon, 1989).

Table 2: Mines within the Bushveld Complex with replacement bodies of tin within associated geology.

Mines within the Bushveld Complex	Associated geology in which replacement bodies occurs
Zaaiplaats and Groenfontein	Main granites
Mutue Fides and Stavaren	Granophyres
Union Tin and Solomons Temple	Felsites
Rooiberg and Leeuwpoort	Roof sediments

2.3. Structural influences on tin mineralization at Rooiberg tin field

The influence of structural evolution on ore mineralization has long been debated by scholars. The tin mineralization of the Rooiberg Fragment can be related to the tectonic structures associated with the emplacement of the Bushveld Complex (Figure 6). The structural evolution of the Bushveld Complex can be separated into pre-Bushveld interference folding and syn-Bushveld fracturing (Rozendaal et al., 1995a; Leube and Stumpfl, 1963; Labuschagne, 2004). The pre-Bushveld fragment is characterised by interference folding that deformed the fragment and originated from multilateral compression. The folding and deformation caused moderate doming and basining which led to the fold limbs having a dip angle of approximately 18° (Leube and Stumpfl, 1963; Hartzer, 1995; Rozendaal et al., 1995a).

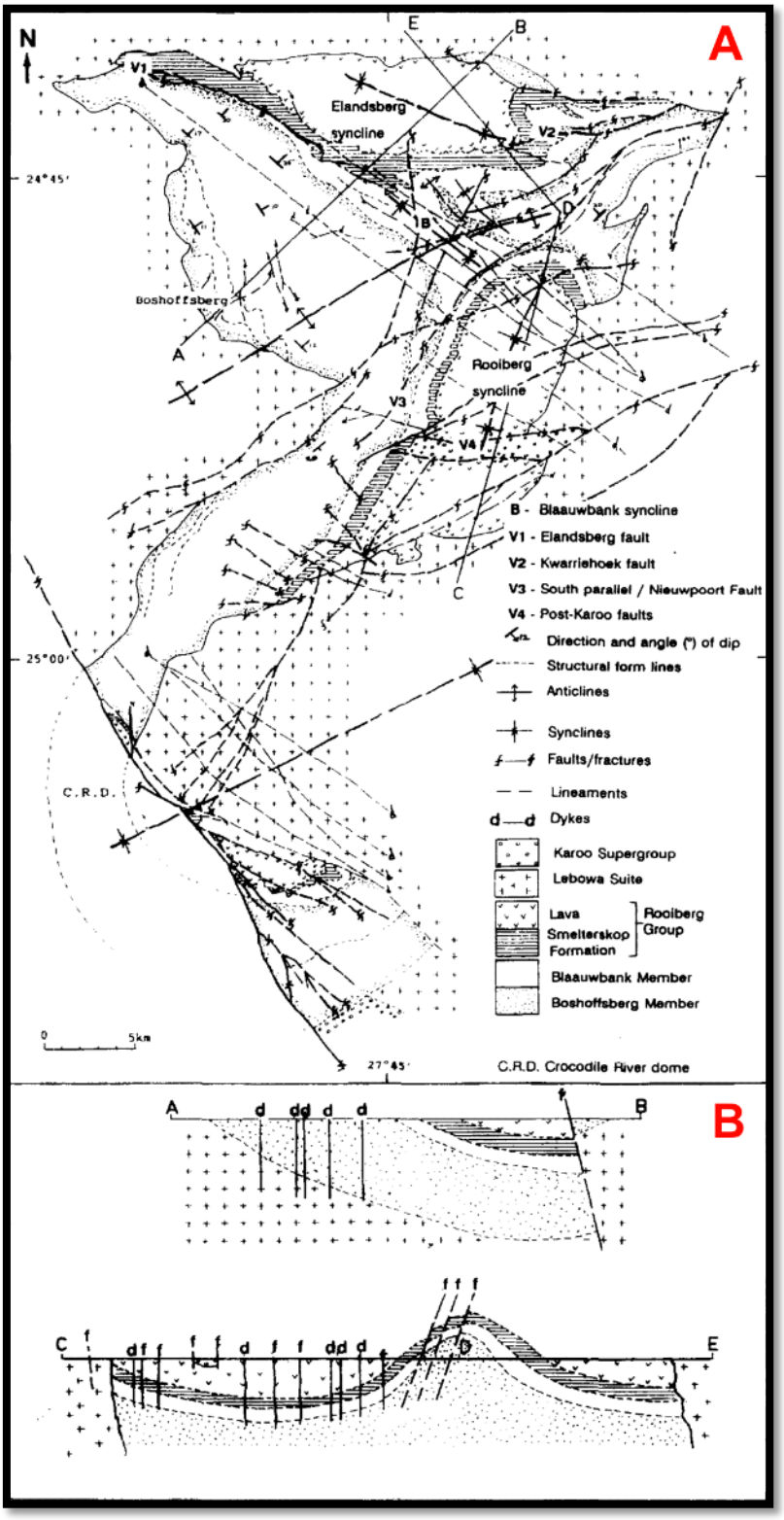

Figure 6: A) Geological map of the Rooiberg Fragment indicating structures, lineaments, dikes, synclines, anticlines and direction and angle of dip. B) Cross-section A-B and C-E through the Rooiberg Fragment indicating the synformal structure of the fragment.

The steep dip fractures are the product of brittle deformation which can be closely related to the Rooiberg mineralization. The formation of the Bushveld Complex caused vertical to sub-vertical tectonics, and led to brittle deformation, as well as the subsequent formation of a prominent three-way fracture direction (065-085°, 120-130° and 350-010°) (Hartzer, 1995; Rozendaal et al., 1995a).

2.4. Mineralization of the Rooiberg tin field

The tin-bearing deposits of Rooiberg consist of hydrothermally altered mineralizations that can be related to tectonic activity. The two largest stanniferous deposits on the Rooiberg Fragment are located at Leeuwpoort (C-Mine) and Rooiberg Village (A-Mine) (Crocker et al., 2001; Labuschagne, 2004; Rozendaal et al., 1995a; Rozendaal et al., 1986). Smaller stanniferous deposits are located and exploited at Vellefontein, Nieuwpoort (B-Mine), and Blaauwbank (D-Mine). These deposits are located approximately at the same stratigraphic position that can be found in a sector below the transition zone of the arkose foot wall and the overlying shale (Leube and Stumpfl, 1963; Rozendaal et al., 1995a). This feature formed a laterally continuous strata bound tin zone. Each individual deposit is similar, however, they do display different styles of mineralization.

The Rooiberg deposits have been classified as being both replacement and open space-filling type, or depending on the geometric relationship with the surrounding bedding, as conformable or unconformable (Crocker et al., 2001; Labuschagne, 2004; Rozendaal et al., 1995a; Phillips, 1982; Rozendaal et al., 1986). At A-Mine pocket-type mineralization is prevalent and consists of cassiterite-bearing, annular or orbicular nodules that are developed and controlled by bedding planes. Tourmaline-rich replacement bodies are associated with faults, fractures, and hairline fissures, and are ellipsoidal or elongated in shape. These tourmaline bodies occur parallel to the bedding of the grey-pinkish arkose host rock (Crocker et al., 2001; Rozendaal et al., 1995a). Bedding plane mineralizations are spatially contrasted with pocket-type mineralizations, and are characterised by fine grained cassiterite and disseminated schorl tourmaline, pyrite, chalcopyrite, carbonates (dolomite-ankerite), sericite and minor chlorite. The ore body at A-Mine is sheet-like and is generally limited by lateral dimensions (Rozendaal et al., 1995a).

At Leeuwpoort Mine, two types of mineralization occur: bedded lodes, and fissure and faulted lodes (Phillips, 1982). The bedded lodes are the most significant contributors to the total tin production. Bedded lodes are flat-dipping vein deposits that have an approximate thickness of 10 to 15 cm, an average dip of 15 degrees, are laterally extensive, and form parallel to sub-parallel to the sedimentary bedding (Leube and Stumpfl, 1963; Rozendaal et al., 1995a;

Phillips, 1982). Pyrite, ankerite, red potash feldspar and chalcopyrite can all be associated with coarse-grained cassiterite. Both shallow dipping and steeply dipping fissure and faulted lodes are present at Leeuwpoort Mine (Rozendaal et al., 1995a; Phillips, 1982). The mineralogy of the fissure and faulted lodes, and the bedded ores are similar. The depth of the tin continuation extends beyond the limits of the mining operation, however, the grade of the tin decreases drastically with increasing distance away from the tin zone (Labuschagne, 2004; Rozendaal et al., 1995a).

Gap Lower, which is a bedded lode, is a continuous lode, and is one of the greatest tin producers in the mine's history. The bedded lodes were mined using an updip stoping method (Leube and Stumpfl, 1963; Falcon, 1989). Mineralization also occurs on the major unconformable units, and has a strike that is parallel to the strike of the strata, and a dip direction opposite to the dip of the strata. Another set has a strike approximated in the dip direction of the strata and have lodes that are very steep to vertical. The fissure and faulted lodes were predominantly mined using the shrinkage method (Hartzer, 1995) (Lenthall, 1974) (Falcon, 1989). In some places the mineralization is scattered and erratic and expert geological interpretation is required.

2.5. The tin zone

Rozendaal et al. (1995a) theorised that a continuous stanniferous zone is present in the mines on the Rooiberg Fragment. He suggested that the mineralization was structurally controlled, which produced several distinct localities at approximately similar stratigraphic elevation (Labuschagne, 2004; Rozendaal et al., 1995a). An impermeable caprock, such as the overlying shale, prevented hydrothermal fluids from ascending further and led to the formation of distinct localities at similar stratigraphic elevation (Phillips, 1982). However, some authors also suggested that the distinct sections were of syngenetic, pre-Bushveld origin due to the stratabound distribution of the sections (Labuschagne, 2004; Crocker et al., 2001).

The tin zone was first identified on the basis of visual discrimination parameters, such as colour, mineralogy, pocket or orbicular concentration, and the presence of significant cassiterite. Mining of the tin ore was successful when using these parameters as guidelines and by restricted the mining to the tin zone (Leube and Stumpfl, 1963; Rozendaal et al., 1995a). The tin zone was considered to be a feature aerially restricted to the replacement deposit of A-Mine, however, exploration within the rest of the Rooiberg Fragment was limited despite the fact that B-, C- and D-Mine as well as Vellefontein, had similar stratigraphic positions (Rozendaal et al., 1995a).

Whole rock geochemical surveys were done at A-Mine, with the aim of characterising the tin zone. During the period of 1984 to 1987, an exploration program was launched at A-Mine where several cores of diamond drill holes were collected and petrologically and geochemically analysed. A total of 9 representative boreholes were selected on the premises of hanging wall and footwall intersection and not on the basis of tin grades (Labuschagne, 2004; Crocker et al., 2001; Rozendaal et al., 1995a). The chemical analysis included elemental presence and includes SiO_2, TiO_2, Al_2O_3, Fe_2O_3, MnO, MgO, CaO, Na_2O, P_2O_5, CO_2 S, H_2O, Cl, Cu, Pb, Zn, Ni, Ba, Sn, Sr, Rb, Mo, Sb, Cr, and W.

2.6. Distribution and petrology of tin

The theorised tin zone present at A-Mine, was confirmed with mineralogical and textural characteristics of the rocks investigated. The tin zone was also confirmed to be present at the other mining regions regardless of their different mineralization styles (Rozendaal et al., 1995a). Table 3 describes the distinguishing features of the footwall, hanging wall and tin zone. The tin zone at B- and C-Mine is not continuous, and the discontinuity is noted when the tin zone intersects the shaly arkoses (Rozendaal et al., 1995a). The laterally continuous zone was confidently indicated on a fragment scale for Vellefontein, A- and B-Mine, however, sufficient conclusive evidence is not available to confirm the theorised 10 km continuity to C-Mine.

Table 3: Geological features and distinguishing characteristics of the arkosic footwall, tin zone and hanging wall. Sourced from Rozendaal et al. (1995).

	FW	TZ	HW
Colour	Pale grey to greenish grey	Pink-grey	Red to pink-red
Host	Altered k-spar, quartz, plag arkose	Altered quartz, k-spar, plag arkose	Altered quartz, k-spar, plag arkose
Textures	Ankerite mottling, chlorite zones, poorly banded, fine-grained	Ankerite, tourmaline mottling, medium-grained	Hematite speckling, fine-grained
Structures, sedimentary	Bedding, cross-bedding	Bedding, cross-bedding	Bedding, cross-bedding
Pockets (not all mineralized)	Some, increase towards upper contact (mainly A Mine, some at B, Vellefontein)	Maximum pockets/orbicules at A Mine (some at B, vellefontein)	Some, decrease rapidly away from contact (mainly A Mine, some at B, C, Vellefontein)
Bedded lodes (mineralized)	Some, numbers decrease into FW	Maximum, vertically stacked mostly C Mine, some at B, Vellefontein and A Mine	Some, particularly C Mine up to shales
Steep lodes	Present but poorly mineralized	Payably mineralized	Present with limited vertical extent and poorly mineralized
Specular hematite	Low to none	Low to none	Maximum
Sulphides (py, cpy) and cassiterite	Some to none, disseminated	Maximum dissem. and fracture filling	Some to none disseminated
Tourmaline	Moderate to none, decrease with depth	Maximum, particularly A Mine	Moderate to none
Sericite	Moderate to low	Maximum dissem. and in pockets A Mine	Moderate
Chlorite	Moderate	Low	Low
Carbonates (Ca, Mg, Fe)	Moderate to low	Maximum, dissem and in lodes, pockets	Moderate to low
Potash feldspar	Low	Moderate	Maximum
Albite-oligoclase	Maximum	Moderate	Moderate but less than TZ

The total vertical extent of the grey-green albite-rich arkose, that forms part of the wall rock, was not established due to the 350 m depth limitations of the boreholes. The surface studies conducted at A-Mine, indicated an irregular gradational contact between the footwall and the white orthoquartzite, that consist of interbedded small pebble conglomerate bands (Rozendaal et al., 1995a). The studies showed that the albite-rich footwall had a minimum thickness of 300 to 350 m, with an approximate thickness of 500 m approaching C-Mine. The thickness of the red potash-feldspar-rich hanging wall is limited by the overlying shaly arkose. Consequently, the hanging wall has a variable thickness at C-Mine and a maximum thickness of 80 m at A-Mine. Visual identification and delineation of the grey-pinkish sericite tin zone was not as conclusive at A-Mine, as at the rest of the mining regions (Leube and Stumpfl, 1963; Hartzer, 1995; Rozendaal et al., 1995a).

The tin zone and the adjacent wall rock constitute the upper 500 to 600 m of the Boschoffsberg Quartzite Member. These rocks were classified previously as arkosites but mineralogical and textural features indicated that the superimposed processes that occurred at a later stage altered the original rocks (Rozendaal et al., 1995a). Sedimentary structures, which include planar- and trough cross-bedding, were preserved and subsequently replaced by minerals such as tourmaline, hematite, pyrite, chalcopyrite, and cassiterite. Most of the rocks analysed were fine-grained, however, mineral grains of the tin zone were found to be more coarse-grained.

2.7. Microscopy of the Rooiberg tin field

The quartz grains are rounded, and the boundaries are enclosed due to the replacement of quartz with albite-oligoclase, sericite, carbonate, chlorite and tourmaline (Crocker et al., 2001; Rozendaal et al., 1995a; Phillips, 1982). Generally, the fine-grained groundmass is densely intergrown with silicates or carbonates, and has replaced the original mineral assemblage, except for minor quartz and feldspar relics. The primary structures are completely destroyed indicating replacement that is unrelated to digenesis and low-grade metamorphism (Rozendaal et al., 1995a). Replacement texture includes hematite speckling, carbonate mottling, and tourmaline-rich pockets or orbicules. The original mineralogy is difficult to deduce due to the pervasive alteration that produced, not only a new mineral assemblage, but changed the original mineral textures and features as well.

2.8. Geochemistry of the Rooiberg tin field

The rocks within the Rooiberg Fragment can be divided into three chemically distinct groups (Table 3). This subdivision confirmed to a large extent the visual and mineralogical subdivision of the lithotypes into the hanging wall, footwall and tin zone (Figure 7). The three groups display some overlap, however, this is not unusual, as the contact relationships are gradual (Labuschagne, 2004; Rozendaal et al., 1995a; Phillips, 1982). The most distinguishing feature of the footwall, is the presence of high amounts of sodium as opposed to the presence of potassium in the hanging wall. This phenomenon can be explained mineralogically by the substantial concentrations of albite-oligoclase and potash-feldspar in the footwall and hanging wall respectively (Rozendaal et al., 1995a). The chemical contrast between the hanging wall and footwall is enhanced by K-feldspar substituting trace elements such as rubidium (Rb) and barium (Ba), as well as the Rb/Sr ratio.

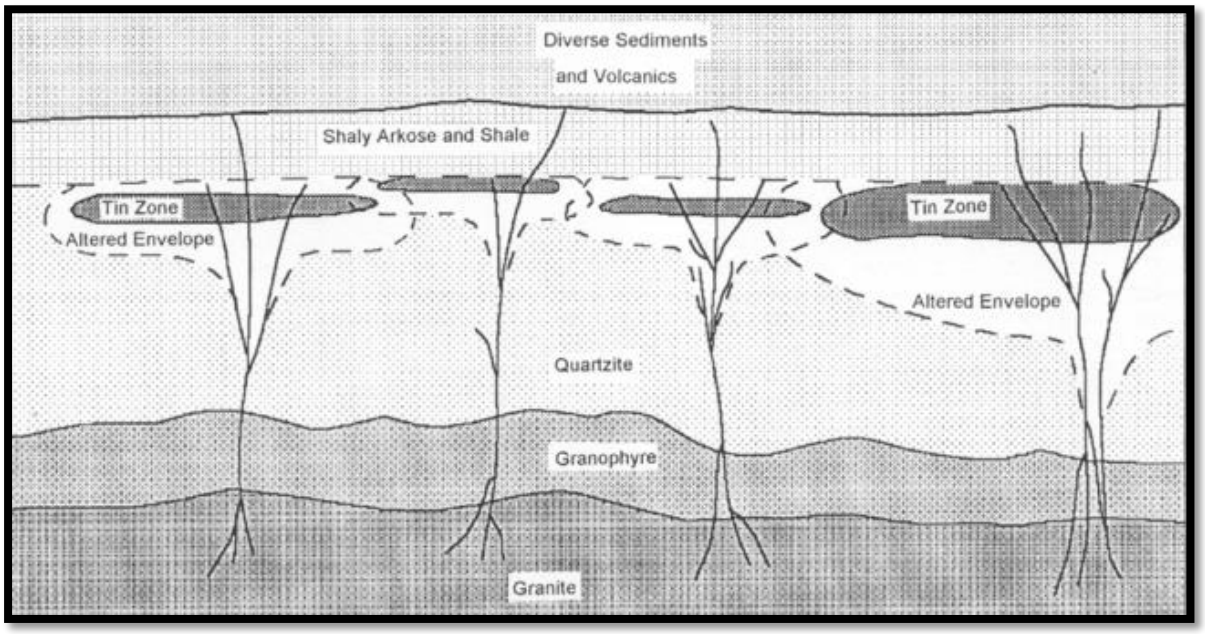

Figure 7: Schematic depiction of the relationship between the granites of the Bushveld Complex as the origin for the hydrothermal fluid, the subsequent fracture system and the wall rock alteration and halo envelope of the Rooiberg tin zone. Sourced from Rozendaal et al. (1995a).

The hanging wall-tin zone contact in the Rooiberg Fragment is characterised by a very sharp increase in the Rb/Sr ratio, along with an elevated Ba and K_2O concentration that serves as an upper-limit chemical marker. The tin zone clearly acts as a marker and thus confirms the geochemically distinct transition between the footwall and hanging wall sections (Rozendaal et al., 1995a). The maximum cassiterite concentrations can be obtained in the tin zone (Rozendaal et al., 1995a). Several smaller stanniferous lodes and pockets are present outside

the predefined parameters, however, these deposits have never contributed significantly to the total metal production.

The wall rock adjacent to the tin zone contains tin values exceeding the global averages for clastic sedimentary rocks by a great magnitude. The tin zone is characterised by the presence of sulphide minerals, in particular, chalcopyrite and pyrite (Rozendaal et al., 1995a). A general increase in the sulphur, copper, cobalt, nickel, and molybdenum content relative to the values of the wall rock, is also indicative of the tin zone. A higher carbonate content is also a characteristic feature of the tin zone and can be supported by the elevated CaO, MgO, Sr, CO_2, and Mn, as well as anomalous sericite by a higher content of Al_2O_3, TiO_2, and H_2O (Rozendaal et al., 1995a; Leube and Stumpfl, 1963). In certain portions of the Rooiberg Fragment, several intersections displayed a sharp increase in the oxidation ratio (Fe_2O_3/Fe_2O_3+FeO) from the reduced sulphide rich tin zone (0.25-0.40), towards the slightly rich hematitic hanging wall (0.40-0.70) and acts as an additional chemical criteria (Schreiber et al., 1991; Crocker et al., 2001).

The upper Boschoffsberg Quartzite Member is composed of highly altered arkosites, however, the alteration was so severe that the original composition could not be determined with certainty. Preserved primary structures suggest that the rocks were originally composed of coarse clastic sediment from a high energy environment, even though sorting and maturity remained unknown.

A study was done by Schreiber (1990) and Schreiber et al. (1991) on the possible correlations of the Rooiberg clastic rocks and the Pretoria Group sediments. The study did not reveal any sediment chemistry analogous to the local lithotypes. Geochemical data obtained by Rozendaal et al. (1994) supported these findings and indicated that extensive sodic, potassic and sericite alteration has changed the constituents of the upper 500 to 600 m portion of the clastic sedimentary sequence. If the immobility of aluminium and mobility of sodium, potassium, and silica during metamorphism is assumed, then the original rock of the upper Boschoffsberg Quartzite Member could have been arkosic (Labuschagne, 2004; Rozendaal et al., 1995a).

The alteration patterns within the stratified hydrothermal altered zone are also stratified and marked by a distinguishing zonal distribution of a highly albitized footwall, sericitized-tourmalinized tin zone, and red potash hanging wall. All the tin mines of the Rooiberg Fragment are located within the sericite stanniferous zone, which can be classified as the transition between the sodic and potassic envelope (Figure 7). The distribution of economically

significant cassiterite and subsequent zonal alteration pattern is related to the evolutionary path of the metalliferous hydrothermal fluids (Crocker et al., 2001; Rozendaal et al., 1995a).

Hydrothermal fluids were formed by high temperatures and were enriched in Na, K, Sn, CO_2, H_2O, and B and to a lesser extent Cu, Rb, Ba, Sr, S, Cl and F. Literature suggest that the fluids were related to the granitic intrusions of the Bushveld Complex, more specifically the Lebowa Granite Suite. However, no evidence is available to support this theory and further studies need to be done (Falcon, 1989; Rozendaal et al., 1995a). The Zaaiplaats tin field hosts metallization and alteration in the endo-granite and may suggest that a similar fluid source for the Rooiberg manto-style deposits are possible.

The formation of tin deposits in the form of veins, breccias, and replacement bodies can be accredited to saline hydrothermal fluids that originated from felsic magmas. A range of experiments, including fluid inclusion and isotope studies, have been done and indicated that the hydrothermal fluids were enriched in SnO_2. The hydrothermal fluids that originated from the magmatic activity are acidic, moderately reduced, alkali-and chlorite-rich and have a low oxygen fugacity (Crocker et al., 2001; Labuschagne, 2004; Rozendaal et al., 1995a). Formation conditions for these magmatic hydrothermal fluids are most favourable when the temperatures range from 250 to 500 °C (Taylor and Wall, 1992). The solubility of tin is not greatly enhanced by the presence of fluorine in the melt or the fluids, nor do fluid temperatures greater than 500°C have an effect on the tin solubility. However, a high K/Na ratio does increase the tin solubility (Rozendaal et al., 1995a; Taylor and Wall, 1992).

The steep dipping fractures acted as conduits for the fluids and essentially created the plumbing system needed to form the distal exogranitic deposits. Mining and exploration tends to be more successful in areas of intense fracturing which mark structural focal points were Al_2O_3 alteration and cassiterite precipitation is abundant (Leube and Stumpfl, 1963; Hartzer, 1995; Rozendaal et al., 1995a; Phillips, 1982). Stanniferous hydrothermal fluids generated by magmatic activity ascended along these fractures until it came in contact with the wall rock. The K/Na ratio of the aqueous fluid phase is dependent on temperature. Sodium precipitation will initiate if the temperature decreases, and the reaction of the ascending fluids with the wall rock occur (Labuschagne, 2004; Rozendaal et al., 1995a). Albitization is the process of sodium precipitation and explains the sodic footwall of the tin zone. Potassium and SnO_2 remain in solution and continues its ascent until retardant factors such as equilibration of fluid, lithostatic pressure, limited fracture evolution and impermeable rocks (shaly arkose) decrease or stop the fluids' ascent (Leube and Stumpfl, 1963; Rozendaal et al., 1995a).

Continuous fluid supply led to the accumulation and lateral spreading of hydrothermal fluids updip along micro-fractures, mineral grain boundaries, and planar sedimentary structures and subsequently formed a broad front, stratified parallel to the lithology. Hydrothermal brecciation and precipitation of cassiterite and sulphides occured when the fluid temperature were lowered. Oxygen fugacity and acidity, as well as compositional changes, took place due to wall rock interaction, fluid boiling and local CO_2 overpressure (Rozendaal et al., 1995a). These changes also led to potassic alteration, sericitization, and tourmalinization along with continuous albitization.

As the evolving, cooler fluids continued their slow ascent upward, the hanging wall was extensively changed by the potassic alteration which ultimately led to the formation of red hematitic arkose (Rozendaal et al., 1995a). The final stage of stanniferous deposit formation was the formation of a potassium-rich cupola with a greisen correlated endogranite. The hydrothermal fluid evolution was not a single event, but rather a continuum of fluid pulses over a period of time within the same plumbing system. This continuum resulted in a complex system of superimposed prevalent alteration and metallization (Rozendaal et al., 1995a). This complex system is present at both A-Mine and C-Mine as contrasting processes of tourmalinization, chloritization, silicification, albitization, and sericitization.

The fluids were subjected to the same physio-chemical constraints, as indicated by the similar zonal alteration and mineralization at the various mines and prospects. This resulted in a series of deposits located at approximately the same stratigraphic elevation, with a similar extent of alteration haloes and minerals that are indicative of a magmatic source (Figure 7). The vertical and lateral extent of wall rock alteration is dependent on the amount of fluid available as well as the extent of faulting and fracture intensity (Leube and Stumpfl, 1963) (Rozendaal et al., 1995a). The systems at A-Mine and C-Mine were so extensive that they produced laterally continuous tin zones and alteration haloes that overlapped with the mineralizations at B-, D-Mine, and Vellefontein (Figure 7). This overlap at the various mines created the impression of a continuous stratabound tin zone with variable thickness (Labuschagne, 2004; Rozendaal et al., 1995a; Phillips, 1982). Quantifying the parameters that characterise the tin zone and adjacent envelope will aid in further Greenfield and Brownfield exploration. Exploration should be focused on areas of intense fracturing along with geochemical identifiers and parameters to laterally delineate the tin zone (Rozendaal et al., 1995a).

3. LITERATURE REVIEW

Geological models allow the user to have a better understanding of the geological environment in which mining is taking place. Three dimensional (3D) geological, ore deposit, and mining models are therefore becoming increasingly important in the mining industry. 3D modelling software is preferred to manual hand-written or hand-drawn models of geological environments, because the use of modelling software reduces the time consumed when developing the models (Cowan et al., 2002; Reid, 2017). The technological advancements in (3D) models has allowed users to effectively store, manage, process and display large quantities of obtained geological information (Wu et al., 2005). 3D models are being used more frequently for mineral potential targeting, as well as resource assessment, because good quality geological models allow the user to determine grade domains within mineralized environments (Wang et al., 2011). This section of the thesis will discuss the different statistical methods used to determine grade domains, as well as the different methods used to determine grade-tonnage models. The influence of cut-off grade in quantitative resource assessments will be discussed in detail. In addition, the importance of conducting a statistical analysis, using a specific method, for resource assessment models will be discussed.

When conducting a quantitative resource assessment of mineral deposits, grade-tonnage models form a fundamental part in the estimation and prediction process. Grade and tonnage models are used during quantitative resource assessment to predict the values of the known deposits for a specific type, and can also be used to determine the potential value of undiscovered deposits in a specific area. If sufficient geological data is available, the tonnage of mineralized bodies can be calculated and a grade-tonnage model can be created form the 3D geological model. The uncertainty associated with estimating undiscovered deposits are presented as a probability factor (Singer, 2010; Scott and Dimitrakopoulos, 2001; Singer, 1993). The estimation of grade-tonnage models, for a number of undiscovered deposits, must be consistent and comparable in order for the assessments to be realistic.

The process of quantifying resources can be described in a three-part assessment; 1) the mineralization is delineated according to the specific type of deposit and associated geology, 2) grade and tonnage models are used to estimate the amount of metal and associated characteristics, and 3) estimation of the undiscovered deposits (Singer, 1993; Scott and Dimitrakopoulos, 2001). This three-part assessment is dependent on two types of models: descriptive models and grade-tonnage models.

Descriptive models can be divided into two main steps, the first step is to describe the geological environment and subsequent formation of mineral deposit; and the second step is to define the characteristics of the mineral deposit (Singer, 1993; Singer, 2010). The first step is achieved by identifying and describing the general setting of the mineral deposit. The second step is achieved by classifying the mineral occurrences of the deposit, and ultimately the delineation of the mineral deposit. Grade and tonnage models are usually displayed in the form of frequency distributions of tonnage and average grade of the mineral deposit. Descriptive statistics, such as mean and standard deviation, are used to provide a best-fit lognormal curve of the data along with the cumulative frequency graphs (Singer, 1993; Singer, 2007a). The first step in a grade-tonnage model, is to compare the attributes of each deposit to the descriptive model, in order to determine if the various mineralizations formed by the same geological process. Data for the deposits include average grade, tonnage based on production rates, as well as reserve and resource estimates based on cut-off grades (Singer, 1993; Scott and Dimitrakopoulos, 2001; Singer and Kouda, 2011).

The most fundamental part of the exploration phase is to estimate the size of the undiscovered deposit. The major cause of variation in the size of unknown deposits, is due to the different types of mineralizations within a deposit (Singer, 1993; Singer, 2010). Grade and tonnage models are used during quantitative resource assessment to identify the known deposits in a region, therefore, delineating this area. Grade and tonnage models can also be used to determine the potential value of undiscovered deposits in a specific area. The most important rule of grade and tonnage models is: never remove any low-grade or low-tonnage deposits from the data, as this will result in a negative correlation in the data set (Singer, 1993; Singer, 2007a). Low-grade deposits are important as they may have large tonnages, and future low-cost mining techniques might make these deposits more economical. Estimating cut-off grades from a grade-tonnage model, created from insufficient data can lead to over- and under estimation of the grade values for undiscovered deposits (Singer, 1993; Cox and Singer, 1986).

The cut-off grade is the minimum grade at which the ore can still be economically extracted (Thompson and Barr, 2014; Rendu, 2014). The selection of lower cut-off grade results in larger volumes of material being processed, however, this also results in a lower average quantity of contained metal. An increase in the cut-off grade results in a decrease in waste production (Krautkraemer, 1988; Thompson and Barr, 2014). The influence of predicted values of future metal prices led to the development of traditional cut-off grade models. The cut-off grade selected for the current mining period, not only influences the rate of metal production, but the amount of resource depletion and associated mining costs. The cut-off grade is continuously

monitored and adjusted during price fluctuations, indicating that cut-off grade is directly dependent on market price variability.

The profitability and life of mine is dependent on the cut-off grade value. Available technology, extraction capacity, mining method, the capacity of milling, geometry and geology of the ore body and smelter requirements are all factors that need to be considered when determining cut-off grade (Cairns and Shinkuma, 2003). Krautkraemer (1988) stated that a general increase in price should also lead to a decrease in the cut-off grade value. Cairns (1986) suggested that cut-off grade decreases as the price increases. Therefore cut-off grade is inversely proportional to price increase.

Cut-off optimization is the term that is used when the mine adjusts the production rates as a result of changing production costs due to price changes (Scott and Dimitrakopoulos, 2001; Rendu, 2014; Thompson and Barr, 2014). Johnson et al. (2010) proposed the method where fluctuating prices and geological models were combined. The mining surface was divided into equal blocks (similar to the geometric block method), and a subsequent partial differential equation (PDE) was derived to estimate the relative value of each block. This method allowed the mine to determine whether the specific block could be classified as economic or waste (Rendu, 2014; Krautkraemer, 1988; Thompson and Barr, 2014). However, uncertainty exists within this block ordering method, due to the high uncertainty level of the exact mineral content within each block. Without this knowledge a feasible block ordering cannot be made.

3.1. Geometric block method (GBM) and tonnage estimation

The spatial representation of the ore-body is referred to as the resource model. The resource model can be determined with various methods, although the most common is the geometric block method, which is the three-dimensional array of blocks (Thompson and Barr, 2014; Annels, 2012; Sinclair and Blackwell, 2002; Rossi and Deutsch, 2013). Block grade estimation is a common method used, where the deposit is divided into equal blocks and the respective grade for each block is determined. Grade and tonnage curves generated from this data is generally smoother and less selective than normal averaging techniques, such as inverse distance weighting (IDW) or nearest neighbour approach (Annels, 2012; Sinclair and Blackwell, 2002; Dominy et al., 2002).

With the use of kriging and multivariate statistics, the importance of each block can be assigned by using grade and density. The distribution of the grade within each block can be determined by referring back to the established resource model, and comparing the distribution of the grades. The exact mineral content within each block is highly uncertain prior

to excavation. However, when combining all the blocks into a mining section, a relative grade distribution of the section can be determined with a high degree of accuracy (Thompson and Barr, 2014; Rossi and Deutsch, 2013). A strategy to estimate the cut-off grade can be determined once the long-term mine excavation schedule has been established. The cut-off grade strategy used to schedule the production of the mining operation is flexible, and is continuously adjusted according to market prices.

Traditionally, geometric and geostatistical methods are used to estimate ore tonnage and average grade values for a single ore deposit. These methods use the principle of orebody thickness and the grade over a given thickness, located within a grid system, to estimate the reserve (Wang et al., 2010b) . Once the cut-off grade is determined the correlating ore tonnage and average grade of the orebody and deposit can be determined.

Lasky (1950) proposed that the ore tonnage of a deposit generally follows a fractal distribution. He identified a trend where the grade and the logarithms of the cumulative ore tonnage, above a certain cut-off value, tend to have a linear relationship. Matheron (1962) and Matheron (1963) realised the importance of the tonnage and cut-off relationship, and suggested that Lasky's model was derived from the lognormal distribution of the ore grades. DeYoung (1981) established that Lasky's equation had mathematical limitations. It became evident that a maximum point was reached when plotting cumulative metal tonnage against log cumulative ore tonnage, which implies that the grade becomes negative beyond the maximum allocated point.

The orebody thickness and grade of each exploration intersection can be calculated based on a predetermined cut-off grade value (Figure 8). The exploration area is projected horizontally onto a vertical plane (vertical longitudinal projection, VLP) if the orebody dips more than 45°, or the exploration area is projected vertically onto a horizontal plane (horizontal longitudinal projection, HLP) if the orebody dip is less than 45° (Daneshvar Saein et al., 2013; Wang et al., 2010b; Agterberg, 1995). When using the GBM, the first step is to identify the orebody range with area (A) in the VLP and HLP. The orebody can then be separated into various blocks in the vertices of the VLP or HLP, where the inside of the block consists of the average grade, horizontal or vertical thickness of the respective orebody as well as the value of the local reserve. The final step is estimating the global reserve for the deposit by summing all the local reserves in each block (Wang et al., 2012; Wang et al., 2010b).

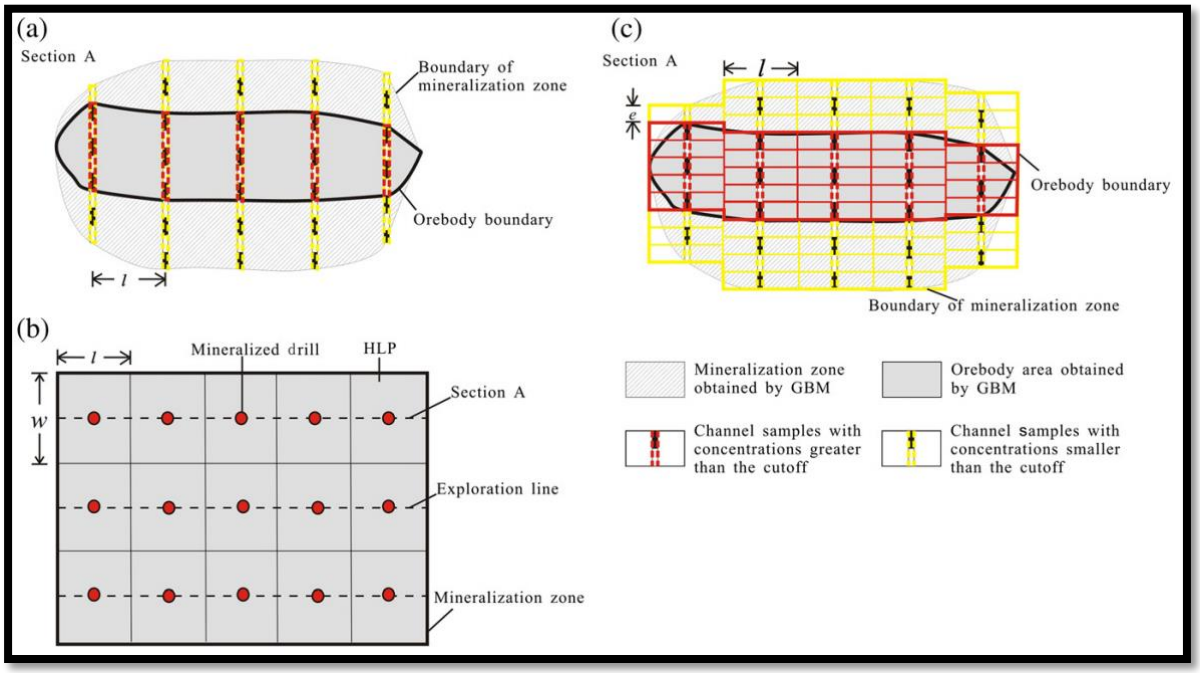

Figure 8: Representation of the ore tonnage and tonnage-cut-off calculation model. A) Geometric block method applied in a section in order to accurately delimitate the mineralized zone. B) Calculation of the mineralized zone mass with the use of horizontal longitudinal projection of the delimitated mineralized zone. C) Tonnage-cut-off model of the delimitated mineralized zone and orebody. (*e* is the length, l and w respectively represent the intervals that are parallel and perpendicular to the exploration line). Sourced from Wang et al. (2010b).

3.2. Fractal Models

The mathematician Benoit Mandelbrot developed the fractal, i.e. a mathematical formula, which can be used to represent seemingly irregular shapes of objects often found in nature (Mandelbrot and Blumen, 1989). He coined the term “fractal” to describe complex geometric shapes that, when magnified, continue to resemble the shape’s larger structure. In this way, fractal formulae can be repeated over and over to produce increased levels of details. The repeating property of fractal models is called self-similarity (Mandelbrot and Blumen, 1989). Figure 9 provides examples of basic shapes, modified by fractal formula, that eventually represent shapes and forms often found in nature (Sadeghi et al., 2015). This ability of fractal modelling is used in various fields of study to model patterns in nature, including geology (Mandelbrot and Blumen, 1989).

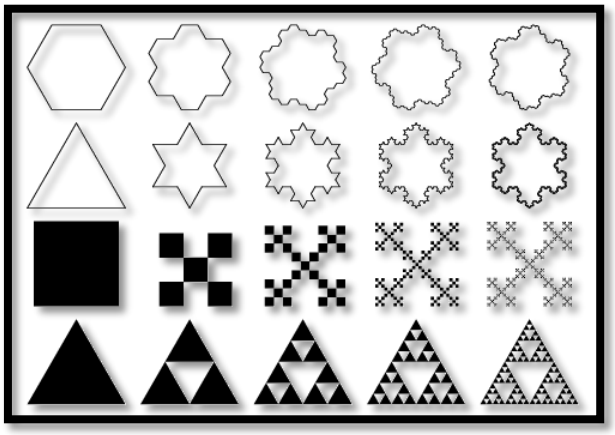

Figure 9: Example geometric shapes created by fractal modelling (Mandelbrot and Blumen, 1989)

Geological objects and features usually have irregular, heterogeneous and skewed characteristics that can be described by a fractal model. Fractal models can be used to describe the spatial attributes of mineral deposits or specific geochemical features (Wang et al., 2010a; Sadeghi et al., 2015). The spatial distribution of chemical elements can be modelled using fractal models, because they have “self-similar” properties on various scales, one of the core properties of a fractal model. Fractal geometry considers frequency as well as spatial distribution of data (Wang et al., 2010a; Sadeghi et al., 2015).

The number-size fractal model is the most widely applied fractal model and can be used to model orebody thickness and grade thickness in the exploration phase of a single deposit (Wang et al., 2010b; Osanloo and Ataei, 2003; Taylor, 1985). Concentrations of precious and base metals are also models with the number-size fractal model.

Fractal models were developed specifically for the determination of the relationship between geometric and spatial attributes for geographical and geochemical properties (Agterberg, 1995; Sadeghi et al., 2015). Fractal models can be used to describe the spatial distribution of mineralized zones and areas based on the variation in geochemical and geological features. In addition, fractal analysis allows for the identification of populations in spatial data within mineral deposits which can be used to define zones (Sadeghi et al., 2015)

Volumes of the mineralized zones can thus be approximated more accurately with the use of fractal models than by the use of traditional statistical methods. This use of fractal models is especially important when 3D models are developed as part of the quantitative assessment and prediction of mineral resources (Scott and Dimitrakopoulos, 2001; Singer, 2007a; Krautkraemer, 1988; Sadeghi et al., 2015). Geological, geochemical, and geophysical data have different spatial distributions and attributes that can to be used to delineate and properly

explore the mineral deposit. Semi-variograms are geostatistical tools that can be used for spatial analysis of element distribution in mineral deposits, and identifies parameters that can be used to interpolate, estimate, and simulate 3D models (Rossi and Deutsch, 2013; Sadeghi et al., 2015).

Fractal models are combined with geostatistical simulations to provide a mineral resource classification. The first step is to use Gaussian geostatistical simulation to model the spatial distribution and variability of the data (Rossi and Deutsch, 2013; Sadeghi et al., 2015). Secondly, the boundaries of the mineralized zones are determined with the use of a simulated size-number (SS-N) fractal which forms an essential part of the mine planning and mineral resource classification phase. Fluctuations in ore grade can be reliably modelled when combining Gaussian geostatistical simulations with SS-N fractal models (Daneshvar Saein et al., 2013; Sadeghi et al., 2015). Mineral resource classifications become more reliable when geostatistical simulation is used to determine the estimates. Reliable information of the zones can be obtained with the use of the SS-N method as it produces grade distribution that are more accurate when data is declustered to produce histograms. Mineralized zones can then be categorized according to the measured, indicated and inferred sections along with the tonnage-cut-off curves (Daneshvar Saein et al., 2013; Sadeghi et al., 2015; Wang et al., 2012).

The number-size (N-S) fractal model was developed by Mandelbrot (1983) with the purpose of describing the distribution of geochemical data, with specific relevance to the relationship between the number and size parameters for a given database. A concentration-size multifractal was developed by Agterberg (1995) based on the N-S model, and can be used to model geochemical data. These N-S models describe relative enrichment of minerals by replacement due to metasomatic processes that resulted from hydrothermal activity (Daneshvar Saein et al., 2013; Sadeghi et al., 2015). The power-law frequency model was developed based on the N-S model and measures the frequency distribution of mineral concentration based on the amount of samples present. Sadeghi et al. (2012) developed the first 3D model based on the N-S fractal model in order to separate the mineralized zones and wall rocks. The model was proven to have great precision when compared to the concentration-volume (C-V) model (Figure 10). The most beneficial advantage of this model is that there was no need to pre-process or pre-estimate the data before the modelling (Sadeghi et al., 2015).

Ideally, the mineralized zone thickness in each exploration work correlates with the number-size model leading to the estimation of the mineralized zone mass. If the element concentration of the samples in the mineralized zone is properly exposed by exploration or

mining activity, and correlates sufficiently with the number-size model, then the model can be used to calculate both the zone mass and ore tonnage (Agterberg, 1995; Wang et al., 2010b). A general trend was identified when comparing the different models: as the cut-off increases the tonnage decreases proportionally (Rendu, 2014; Krautkraemer, 1988; Wang et al., 2010b).

Lasky's model was discounted, and instead Cargill et al. (1980) plotted cumulative tonnage against the grade in order to determine a fractal relationship for tonnage and average grade. By using the geological ore-forming processes for specific ore deposits, Turcotte (1997), developed a tonnage-grade model with specific relevance to the fractal relationship between tonnage and grade. The fractal model is considered to be more effective in describing the relationship between tonnage and grade than the lognormal model at a regional scale (Wang et al., 2010b; Agterberg, 1995).

The information obtained from the number-size model for element concentrations can be used to create cut-off grade models from which the ore tonnage and average grade curve can be calculated. The relationship between ore tonnage, cut-off grade and average grade can be calculated due to the fact that element concentration can either be randomly or evenly distributed in the mineralized zone (Rendu, 2014; Wang et al., 2010b). The results obtained from the abovementioned models, and the traditional geometric block model are similar, indicating that the mathematical modelling is reliable enough to be used in the study of tonnage-cut-off relationships. However, the number-size fractal model still fails to determine local reserves and traditional estimation methods still need to be used to calculate the reserves (Daneshvar Saein et al., 2013; Wang et al., 2010a).

Characterization, delineation, and separation of the mineralized zone can be achieved with the use of fractal models and can be applied to 3D modelling. When compared to traditional statistical methods, fractal models have the advantage of separating individual mineral zones from one another without normalizing the data. Fractal models can determine the vertical distribution of elements in boreholes and can accurately determine the shape of the deposit.

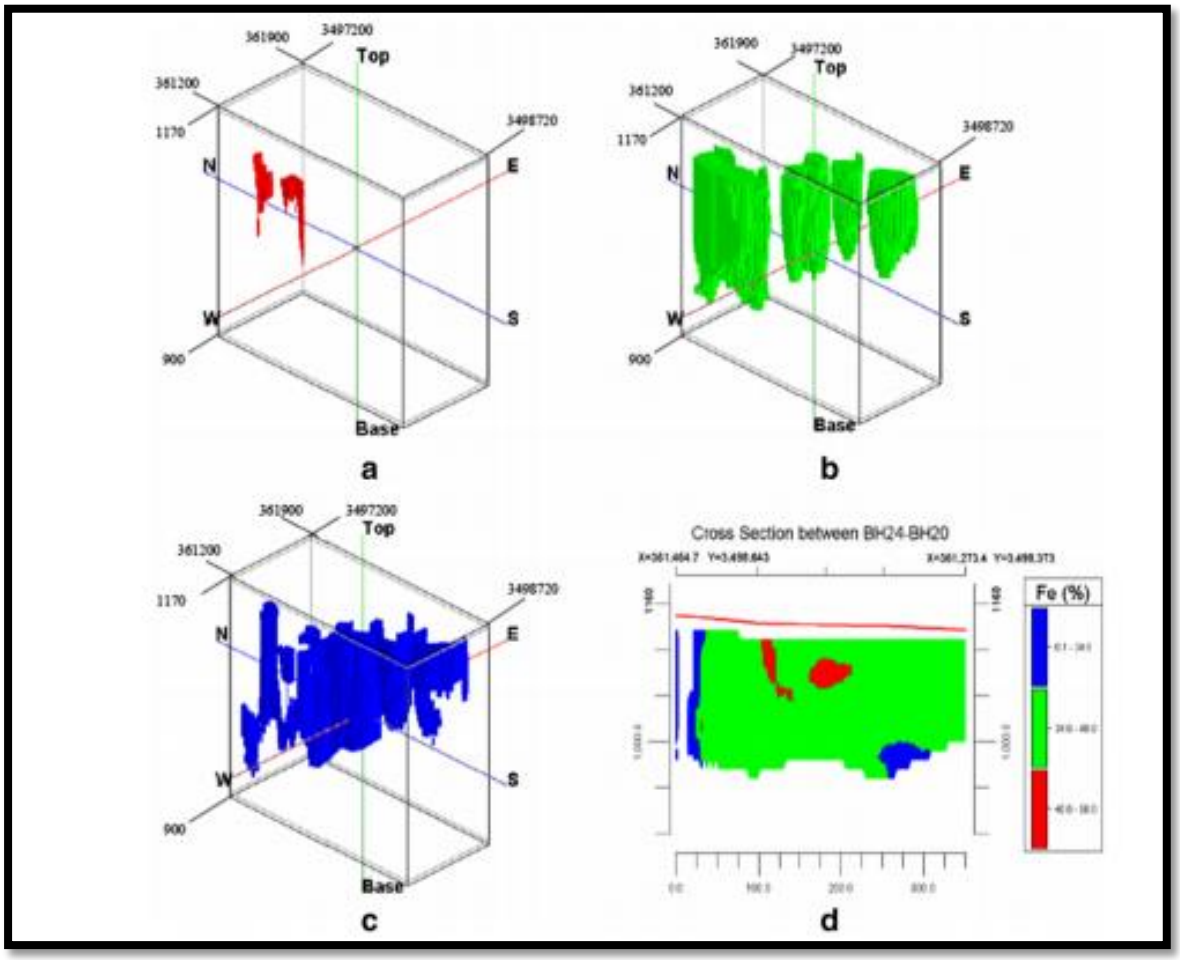

Figure 10: The results obtained from the 3D model developed by Sadeghi et al., (2012). A) The highly mineralized zone modelled in 3D. B) The moderately mineralized zone modelled in 3D. C) The weak mineralized zone modelled in 3D. D) A cross-section of the three zones. Sourced from Sadeghi et al. (2012).

3.3. Continuity and grade domains

Data analysis is dependent on the clustering of the data as it effects not only the statistical application, but can also lead to bias of the variography. Generally, a higher concentration of boreholes will be drilled in sections where a higher grade proportion of the mineralization is noted, leading to clustered and unrepresentative samples (Rossi and Deutsch, 2013; Sinclair and Blackwell, 2002; Glacken and Snowden, 2001). The data should thus be declustered with the use of various techniques such as moving averages or IDW before modelling is done with the data. If the data is not declustered it may lead to bias and unrepresentative results. Geostatistical analysis should identify any trends, as well as the spatial continuity and anisotropy of the mineralization. Anisotropy can be defined as the same amount of variation but occurring in different directions at different ranges (geometric anisotropy) or as different magnitudes in varying direction (zonal anisotropy) (Singer, 2007b; Sinclair and Blackwell,

2002; Glacken and Snowden, 2001). Anisotropy is most notable in grade analysis where the orientation of high grade veins is different to the orientation of the bulk mineralization.

Continuity can be defined as the measure of geological properties, or characteristics, against distance, which can become variable with anisotropy, meaning there is more continuity in one direction than another (Sinclair and Blackwell, 2002; Sadeghi et al., 2015). Continuity allows for the determination of the different types of boundaries between lithological or mineralized units, and thus subsequently provide a comprehension of the different grade distributions and domains throughout the mineral deposit. The behaviour and characteristics of grade domains can be established with the use of continuity. This allows for the identification of variability, spatial directions, orientations and anisotropy within the deposit (Rossi and Deutsch, 2013) (Dominy et al., 2002).

Two types of continuity can be defined and used for resource estimation:

1. Geological continuity which is a 3D feature that describes the geometry of the geological structures and zones that host the various mineralizations, this includes thickness and dip;
2. Grade continuity, also known as value continuity, describes the grade within a specific geological zone or unit.

It is important to note that both grade and geological continuity are scale-sensitive features. Geological continuity generally effects tonnage estimations, with specific relevance to the spatial orientation of the orebody (Scott and Dimitrakopoulos, 2001; Dominy et al., 2002).

A common process in the construction of geological models is to contour the grade within the mineralized zones in order to generate grade shells (see Section 4.3.6.). Each shell is considered to be homogeneous in order for the cells to be interpreted as a stationary random function, which allows the cells to be modelled with variograms, kriging or conditional simulation (Emery and Ortiz, 2005; Singer, 2007b; Annels, 2012). Characteristic mineralizations within the deposit are used to determine grade domains or grade zones, for instance, the high-grade, medium-grade, and low-grade domains of each mineralized unit are defined. Grade domains, also known as grade interpolants in 3D models, are determined from the interpretations of the deposit from the available exploration information, such as borehole data, and thus contain interpretation and analytical error (Emery and Ortiz, 2005) (Sadeghi et al., 2015).

The different grade domains are caused by the variation in the spatial continuity within the deposit. The defined boundaries are generally soft, meaning that there is a spatial correlation between the grades on either side of the boundary. The implication of soft boundary interpretation means that the estimations are not as precise, especially along the boundaries (Emery and Ortiz, 2005). These boundaries are then interpreted separately in order to minimise the error. These independent, individual entities create geological boundaries that are incorrect because it identifies a relationship between grade distribution and spatial continuity that is non-existent. The grade zone approach does not account for the uncertainty and miscalculation of unsampled locations within the shell boundaries.

Ideally, the geology should be used as the main feature during resource estimation, however, if this is not possible then other forms of the domain boundaries needs to be considered. This boundary is usually a grade boundary that is defined by the cut-off grade values that can be correlated to the current economic conditions (Rendu, 2014; Glacken and Snowden, 2001). Geostatistical methods can be used to define grade domains as well. Determination of domain boundaries on the basis of grade alone can become problematic especially when a cut-off grade is used that is too similar to the overall economic cut-off grade. This may cause an overestimation of grades within the domain and a subsequent underestimation of grades outside of the domain boundaries (Glacken and Snowden, 2001). Deposits that were formed in structurally complex regions consist of both hard and soft boundaries. A hard boundary is, for example, a hanging wall that has a definitively identifiable contact with the footwall. A soft boundary is the gradational transition from the surrounding geology to the footwall and associated stockwork mineralization.

Grade domains can be used along with continuous grade intervals in order to predetermine grade-tonnage curves (Sinclair and Blackwell, 2002; Emery and Ortiz, 2005). The predetermination process occurs before any geostatistical modelling, such as kriging, is used to estimate the grades. However, this approach is not advised when estimating ore reserves. The spatial extensions of high-grade domains are generally overestimated and waste rock may be wrongfully classified as ore causing the total amount of recoverable reserves to be overstated (Emery and Ortiz, 2005). Grade domaining is considered to be a common practice for grade calculation, however, this approach increases estimation errors and causes conditional bias in the resource estimates. This is due to the uncertainty of domain boundary location and unsampled location estimation (Sinclair and Blackwell, 2002; Emery and Ortiz, 2005).

Defining geological domains that differ in mineralogy, alteration, and lithology is an imperative step for mineral resource estimation. The first step is to identify similar geological domains within the mineral deposit and to identify the spatial continuity of the grade. Unique geological features are used to classify the grade zone. However, three main problems can hinder the classification process (Emery, 2007; Ortiz and Emery, 2006):

1. The identification of grade domains is subjective to the interpretation of the mining geologist and his/her general understanding of the geological processes that form the mineralization. Thus various interpretations possible can introduce uncertainty.
2. The drill hole data is the primary source for information and a certain amount of error is always associated with the drilling process. The delineation of the geological domains is thus subject to the unavoidable error of the drilling data.
3. Contacts between geological domains are seldom hard and the measured grades are not independent, for example, boundaries can be defined by a gradual change in the local mean rather than an abrupt change.

Two assumptions are made when grades are estimated for geological domain (Emery, 2007; Sinclair and Blackwell, 2002; Ortiz and Emery, 2006):

1. Information across the boundaries cannot influence the grade estimation within a geological domain. This implies that there is no spatial correlation of grades between the boundaries.
2. Within each domain, the grades are assumed to be stationary and do not show any significant change in the local mean as the boundary is approached.

A change between two geological domains, whether it be alteration, mineralogy, or lithology, is considered to be a hard boundary if no transition over a certain distance within the orebody is notable. Structural features such as faulting generally prevent a soft boundary between geological domains (Osanloo and Ataei, 2003; Ortiz and Emery, 2006). Petrophysical features, such as porosity, is considered to be a hard boundary especially if mineral bearing fluids are heterogeneous between domains. However, change in grade behaviour is generally a transitional process, which indicate a correlation between data on either side of a boundary. Estimation techniques, such as ordinary kriging, is used to calculate the local mean for every location where the grade is estimated (Emery, 2007; Ortiz and Emery, 2006).

3.4. Uncertainty during grade determination

Any suitable modelling technique has two sources of error when applied to grade estimation: sampling error and estimation error (Stanley, 2007; Dominy et al., 2002).

3.4.1. Sampling error

Whenever sampling error occurs, it immediately introduces bias and unpredictable random errors into the data. Sampling errors are usually reported in the nugget variance model and during geostatistical analysis. Potential sources of sampling error can be generated from sampling representation, sample bias, sample preparation, analytical error and transcription errors (Dominy et al., 2002; Annels, 2012). If the grade is less continuous and less selective than expected, it indicates that the nugget effect is artificially high. If core loss occurs during the drilling process the borehole as a whole is ignored, or an assumption is made that the grade of the missing sample is the same as the recovered core. This poses a risk for the grade estimations, because these values are assumed and not representative and may lead to the overestimation or underestimation of grade (Sinclair and Blackwell, 2002; Dominy et al., 2002).

3.4.1.1. The nugget effect

The nugget effect can be described as a measure of the randomness (Rossi and Deutsch, 2013) or as the variation between samples at small separation distances (Dominy et al., 2002). A high nugget effect is indicative of insufficient and bias sampling techniques. The randomness that is introduced into the data makes the prediction of unsampled areas more difficult. The reduction and understanding of the nugget effect is thus of the utmost economic importance, as improper data leads to inaccurate grade estimation and evaluation (Dominy et al., 2002; Rossi and Deutsch, 2013)

3.4.2. Estimation errors

The most common error during the construction phase of a grade-tonnage model, is to mix old production data from different deposits within the same mineralization or to mix data from different sections, areas and districts of the mine (Singer, 1993). Mixing of data may lead to a skewed distribution and result in correlations among variables that are consequences of mixed units of sampling. An inconsistent database, incorrect data, geological modelling, estimation methods, and analytical procedures are all components that can introduce errors during resource estimation. The resource database consists of the collected, recorded, stored, and processed data. Data validation is essential for any modelling process due to numerous errors

that can occur during the database construction phase such as (Stanley, 2007; Dominy et al., 2002):

- data transcription,
- data compilation,
- typing errors,
- location errors (true north and magnetic north),
- coordinate transformation between program systems,
- survey errors,
- inconsistent stratigraphy and lithology,
- missing intervals,
- correct interpretation of “below level of detection values”,
- interpretation of null or void (does not exist) values,
- reporting figures and scales,
- correct assay values,
- drillhole interpretation,
- data subdivision and reworking,
- grade weighting techniques,
- data correction,
- the inclusion of incompatible sample sets.

3.4.2.1. Grade continuity errors

As mentioned previously, grade and geological continuity are linked to the respective spacing and density of the drill holes. Poor continuity resolution is caused by error and uncertainty of resource estimates. The question to ask is thus: what is the optimum spacing required that would give the best continuity results? Increased drillhole density may resolve the problem of poor continuity, however, the potential cost of the drill holes will increase drastically. Logically one has to consider that the grid and drillhole spacing will be different for different deposit types. If drill spacing and density does not solve the problem of poor geological continuity of the mineralization, a potential data gap may be the reason. Data density also controls

continuity and a large data gap will thus result in poor continuity resolution influencing the grade-tonnage estimation (Dominy et al., 2002; Sinclair and Blackwell, 2002; Annels, 2012).

Post-mineralization, folding, and faulting also influence the continuity of an orebody. The fault location, orientation, intersection, separation, and estimated magnitude are all characteristics that need to be known in order to make reliable estimates. Fault locations may remain unknown if the drilling space is too wide or the drillhole inclination is unsuitable for detecting the fault (Sinclair and Blackwell, 2002; Dominy et al., 2002). Folding duplicates lithological horizons within a specific mineralized zone. This may result in incomplete intersections and various errors in true thickness estimates of the lithologies near the fold axes. Errors in true thickness estimates may result in over- or underestimation of the importance of specific lithologies.

3.4.2.2. Boundary and domain errors

Defining the orebody domains depend on the ability to detect the assay contacts. Assay contacts can be hard, gradational, or soft boundaries between drill holes. If the assay contact is highly irregular and the mineralization is variable, then the construction of the orebody boundaries are subjected to discrepancy and correlation errors that can be caused by geological interpretation (Emery and Ortiz, 2005; Dominy et al., 2002). Specific emphasis should be placed on accurate boundary definition in order to prevent smearing and grade dilution during grade estimation. Defining structural features, such as faults and folds, as well as defining the boundaries between low and high-grade mineralization zones for different lithologies and host rocks is of utmost importance. When estimation modelling is done different mining methods should be tested for the same resource. Different mining methods will have different economic cut-off grades and tonnage values (Emery, 2007; Dominy et al., 2002).

3.5. Geostatistical methods used to determine grade estimates

Geostatistical methods are becoming increasingly valuable tools needed to accurately predict spatial attributes. Geostatistical methods can be used to predict the uncertainty associated with unsampled locations. Geostatistical techniques, such as kriging, are able to provide the best estimation results provided that the dataset is large enough. When global estimation of the orebody is calculated methods such as kriging and uniform conditioning (UC) are used in order to make initial estimates of the total recoverable reserve in the individual resource block (Rossi and Deutsch, 2013; Chiles and Delfiner, 2009; Dominy et al., 2002). Grade control and reserve estimations are done during production and the final decision on whether or not to mine a block is based on these estimates. An acceptable error in grade estimation is 10% and

can be considered a common error for an underground operation. Geological boundaries may not always be clearly defined due to a lack of sufficient structural information, such as faults or en echelon, which inevitably results in uncertainty during estimation calculations (Sinclair and Blackwell, 2002; Dominy et al., 2002; Singer, 2007b).

Disseminated orebodies have poorly defined boundaries and are usually determined by mineral grades rather than geological features and properties. Tonnage is dependent on the chosen cut-off grade and indirectly on economical parameters when the geological boundaries are gradational. Bulk density influences grade-tonnage estimates as well. Bulk density can be described as the density of the material including any natural voids and can be used for estimation calculations. However, it is important to note whether dry bulk density or wet bulk density (bulk density that includes water content) is used (Sinclair and Blackwell, 2002; Dominy et al., 2002).

Inaccurate bulk density assumptions and calculations can lead to order-of-magnitude errors when grade and tonnage values are estimated. This can significantly influences the economic viability of the mining project. Even is the geometry of the ore body is well known the tonnage will inevitably depend on the ore bulk density (Sinclair and Blackwell, 2002; Dominy et al., 2002). Bulk density is not homogeneous throughout the orebody and varies with change in geology, faults, fractures, weathering, porosity and mineralization. Ideally dry bulk density values are modelled along grade to establish resource estimations.

3.5.1. Common geostatistical methods

This section will describe some of the most common geostatistical methods.

3.5.1.1. Polygon and nearest-neighbour approach

Polygon, area of influence and nearest-neighbour approach are the simplest techniques used in resource estimation as they assign a clearly define area of influence to an orebody intersection (Rossi and Deutsch, 2013; Glacken and Snowden, 2001). Polygons are developed in the plane of the mineralization or they can be projected onto a horizontal or vertical plane with proper geometric transformation techniques. The sectional area of influence method is another polygon approach. This method is based on the principle of defining a section perpendicular to the mineralization that extends orthogonally halfway to a section of the plane in the adjacent section (Glacken and Snowden, 2001; Rossi and Deutsch, 2013; Annels, 2012).

Polygons of influence are considered to be the easiest way to determine the grades. Polygons are generated by constructing perpendicular bisecting lines between adjacent samples on two-dimensional composite intersections (Glacken and Snowden, 2001). When the polygon approach is applied in block modelling, the results are obtained with the use of nearest neighbours that assumes the grade of the closest sample to the block or cell to be estimated is similar. The simplicity of the polygon and nearest neighbour approach along with the theoretical ease of the application of these methods can be seen as advantages (Annels, 2012; Glacken and Snowden, 2001). Other advantages of the polygon estimation method include fast results as well as providing a reproducible technique for declustering irregular data. However, as expected, this method also has some disadvantages which includes the wrongful assumption of grade variation and the ineffectiveness of the method when applied to thick, non-tabular orebodies.

3.5.1.2. Triangulation

An uncommon method used today to determine the average grade, is with the use of a triangulation technique. Triangles are constructed at the mid-point of the intersection where the arithmetic mean of the grades are represented at each of the corresponding vertices. Another method that can be used is to average the grade values at the corner of other regular shapes or with the help of grade contours (Annels, 2012; Glacken and Snowden, 2001). More complex methods surrounding grade estimation include attaching weighting functions to grades surrounding a point or a block that has to be estimated. This method is especially helpful in instances where regular points or blocks has to be estimated in 2D or 3D for either manipulation purposes or mine planning phase (Glacken and Snowden, 2001).

3.5.1.3. Inverse distance weighting (IDW) method

The inverse distance weighting method is the most common weighting function, and was created on the basis of the inverse of the distance of the sample from the point that has to be estimated that is the subsequently raised to the second power (Glacken and Snowden, 2001). However, the inverse distance method may produce issues such as declustering decisions and only works efficiently for the use of block estimation of a specifically defined size as well as point estimates (Annels, 2012; Glacken and Snowden, 2001).

IDW ultimately describes the relationship where a certain point is more influenced by the nearest measurement than by a distant measurement (Figure 11). The prediction at an unknown point is therefore inversely proportional to the distance of a known (measured) point.

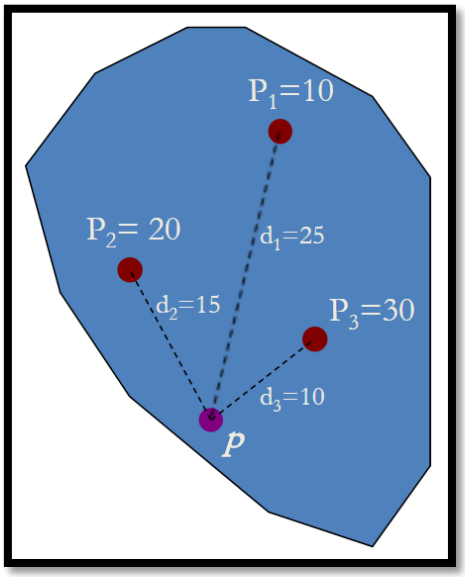

Figure 11: Inverse distance weighting method. The estimation of point p using the known values and distances of P1, P2 and P3. Sourced from Rossi and Deutsch (2013).

3.5.1.4. Kriging

More complex calculations were developed by French mathematician Matheron (1963), to identify the spatial relationship between the samples that has been quantified by the semi-variogram. These calculations determine the specific weights for unknown points or blocks in the estimate. The most standard geostatistical technique was named kriging by Matheron, in the honour of Danie Krige, a mining engineer from South Africa. The most commonly used kriging technique is the varieties of ordinary kriging, more specifically the linear kriging technique (Chiles and Delfiner, 2009; Rossi and Deutsch, 2013; Glacken and Snowden, 2001). Kriging is the most widely used interpolation method and is known as being a linear and robust estimator, however kriging is also known for the unavoidable disadvantages such as the smoothing effect especially in highly skewed data (Chiles and Delfiner, 2009; Sadeghi et al., 2015). When non-Gaussian datasets are used with accordance to kriging methods, spatial heterogeneity characteristic of each dataset is lost due to the smoothing effect. Kriging is not able to produce interpolated data with similar spatial variability of the original data unless the data has a strict Gaussian distribution (Rossi and Deutsch, 2013; Sadeghi et al., 2015). Continuous variables of the datasets can be simulated by transforming the data sets to a Gaussian (multi-Gaussian) distribution and by then applying Gaussian simulation as an alternative method to kriging which produces more precise results.

Non-linear kriging techniques and transformation of grade methods were developed in the last decade and includes techniques such as indicator kriging, uniform conditioning, and

disjunctive kriging. The main aim of non-linear kriging is to estimate the distribution of grade into points or blocks providing each section with a certain measure of uncertainty. A full measure of uncertainty can theoretically be achieved when a random sampling approach is used in a conditional simulation which is an extension of kriging. The conditional simulation uses the data values at a set location and overcomes numerous limitations of the ordinary kriging method (Rossi and Deutsch, 2013; Glacken and Snowden, 2001). The most pronounced limitation to this approach is the lack of simplicity of the method that make it very difficult to computationally determine. Although kriging techniques initial had a bad reputation, the non-linear approaches is increasingly being used as an estimation method (Chiles and Delfiner, 2009; Glacken and Snowden, 2001). If the geological units and the mineralization domains are similar, the grade modelling will be dependent on the geological model and the resource grade will be a correct representation of the geology. However, for structurally-controlled mineralization, the geological units do not correlate entirely with the mineralization.

Grade interpolation forms part of geostatistical analysis and rely on kriging methods, where specific weights are assign to a sample based on the semi-variogram model. This allows for the identification of the continuity of grades in two- and three-dimensions (Chiles and Delfiner, 2009; Glacken and Snowden, 2001). Linear kriging, non-linear kriging and simulation are all various methods that can be applied in geostatistical analysis.

3.5.1.4.1. Linear kriging method

Linear kriging methods are by far the easiest to use, and was developed from simple or ordinary kriging and their variants. Linear kriging specifically relies on classic parametric statistics that are dependent on the distribution of the grade population of the data. Ordinary kriging is optimally used when the data has a normal or Gaussian distribution and does not depend solely on the assumption of stationarity (Chiles and Delfiner, 2009; Rossi and Deutsch, 2013; Glacken and Snowden, 2001).

3.5.1.4.2. Non-linear kriging method

Non-linear kriging techniques have been used more in the last decade to handle the disadvantages of linear techniques. Non-linear kriging techniques are based on the non-linear transformation of data with the use of the natural logarithm, Gaussian transform function or with indicator transformation (Rossi and Deutsch, 2013; Glacken and Snowden, 2001). Some of the main advantages of non-linear kriging techniques are the ability to process highly-skewed or mixed distributions of data as well as determine the distribution and spatial relationship of uncertainty data. This gives a practical estimation of resources above a certain

portion of cut-off grade. These estimated resources are known as recoverable resources and subsequently form part of the reserve process (Chiles and Delfiner, 2009; Glacken and Snowden, 2001).

3.5.1.4.3. Indicator kriging method

Indicator kriging is commonly used in ore reserve estimations, where the distribution of a regional attribute, at an unsampled location, is determined. Indicator kriging is known for being a non-parametric method, which means that the data does not need to fit a Gaussian distribution and mostly uses ordinal data (ranking or ordered) (Chiles and Delfiner, 2009; Emery and Ortiz, 2004). Indicator kriging allows the user to identify structurally complex areas that are present in different magnitudes and occur as soft information. However, even successful geostatistical methods have limitations. Indicator kriging is known to cause conditional bias, meaning that the truly recoverable reserves located in high-value areas are overestimated (Annels, 2012). When an unsampled location is highly correlated to one datum the indicator kriging estimates become imprecise especially when a fine-scale simulation is used.

The indicator kriging method is unable to predict any occurrences of values outside the predetermined range of the neighbouring data, and causes understated variability of the unknown data. Indicator kriging is only recommended when parametric assumptions are not applicable, such as in the case of multi-Gaussian distribution, and the quantification of the continuity becomes an essential part of the estimation process (Chiles and Delfiner, 2009; Rossi and Deutsch, 2013)Emery and Ortiz, 2004).

3.5.1.5. Volume-variance model

Volume-variance models have a known trend: grades that were determined with the use of sample support are more variable than grades that were estimated with the use of block support (Rossi and Deutsch, 2013). This trend can be extended and includes the relationship between larger blocks, which are less variable, and allows for smoother grade distribution curves. These relationships implies that representative distributions of grade-tonnage relationships can only be achieved when the correct block size is chosen (Annels, 2012; Glacken and Snowden, 2001). All estimation techniques aim to convert grades into block estimates in order to add weighting to each subsequent block to establish a relationship between adjacent blocks.

Block sizes are ideally chosen with mining equipment in mind, and is referred to as the selective mining unit (SMU). SMU is defined as the smallest area of ground on which mining can take place in terms of waste or ore (Annels, 2012; Glacken and Snowden, 2001). The block dimensions should be even and equal in size, because blocks that are too small in size will result in over smoothing of the sample data during geostatistical analysis and subsequently lowers the precision results. Conditional bias results from over smoothing, and leads to high-grade blocks being underestimated and low-grade blocks being overestimated (Annels, 2012) (Glacken and Snowden, 2001). The importance and influence of data clustering should again be noted, and causes bias especially if populations are skewed, and needs to be corrected accordingly.

3.5.1.6. Radial basis function (RBF)

Radial basis function (RBF) is a statistical method commonly used for implicit modelling. Implicit modelling was describes by Cowan et al. (2003) as the geological approach for spatial modelling, where the data and specified parametric controls identified by the user define a unique mathematical volume function. The RBF, in essence, is the weighted sum of functions positioned on each point data (Krishnamurthy, 2005; Cowan et al., 2003). Linear equations are used to derive the weights and underlying coefficients of the drift model. Once the mathematical equation has been derive, RBF can be used to estimate the average grade of an unsampled point. RBF can also be used to estimate block grades. RBF is now widely used in most 3D modelling software, for example, Leapfrog Geo (Cowan et al., 2002; Cowan et al., 2003). For this thesis, Leapfrog Geo was used to create the geological model, ore deposit model, and interpolant models, which implies that all the estimation and results obtained was through the RBF statistical method.

4. METHODOLOGY

At the time each of the mines of Rooiberg Tin Limited were closed down, all the mine related data of the specific mine were transferred to the closest operational mine for safe keeping. During the final stages of mine closure of Rooiberg Tin Limited all the data from A-Mine (Rooiberg), NAD, B-Mine (Nieuwpoort), Vellefontein, and D-Mine (Blaauwbank) were transferred to C-Mine. Due to the vast quantity of data, most of the information of the different mines were not stored separately and created administrative chaos, because document preservation was not a priority. This resulted in important information being lost due to insect activity and fading of documentation due to sunlight exposure.

The various processes of digitizing, management, and processing of the data for a historical mine will be referred to as a “post-mortem study”. This entails a detailed search and organisation process of the historical data, as well as the establishment of effective systems and protocols for data management and processing. A post-mortem study of a closed down mine is a time consuming process and proper planning is needed to conduct the study. Due to the lack of proper administrative systems some important information, such as lithological data, survey- and collar information, often was not evident and despite extensive search could not be found. This section of the report will discuss the numerous validation and verification procedures that were implemented in order to conduct a post-mortem study of Leeuwpoort (C-Mine). In addition, this section will also include the processes implemented in order to generate the various grade interpolant models (Section 4.3.6.) as well as a three dimensional (3D) geological model for Leeuwpoort Mine.

4.1. Historical database

When Rooiberg Tin Limited closed down Leeuwpoort Mine in 1993, the only available electronic media was a 5” floppy disk with the map catalogue on it. The major task for this thesis was to digitize the historical data of Leeuwpoort Mine whilst minimizing typing and digitization errors. Leeuwpoort Mine produced tin for approximately 87 years. During this period the mine was owned by different mining companies and had different geologists, mining engineers, and surveyors collecting data. This lead to inconsistency when data was transferred to new administrative systems between the different mining companies. Data was duplicated and mislabelled, or in some cases different versions of the same borehole is available. Data for boreholes that were deepened were not always correctly recorded for the different versions of borehole logs leading to variation of important collar and survey information.

The historical borehole data used for this thesis were digitized from three different data sources:

1. Old handwritten borehole logs that were stored in files.
2. The data of the borehole logs stored in the files were recorded using the Imperial System. 16 log summary books are available where some of the data has been converted to the Metric System.
3. Surface, underground, regional, geological, civil, and surveying maps.

4.2. Data processing and data management

4.2.1. Historical data background

The database for this thesis consists of 476 surface boreholes and 2402 underground boreholes that were digitized from the historical borehole data of Leeuwpoort Mine. The data for each borehole includes a very detailed description of the rock type, orientation (inclination and azimuth), spatial location (coordinates), position (within the mine section), tin content (assay values) and additional borehole information, such as fracture type, mineralization, and formation. Of the 2878 boreholes in the database only 1509 boreholes could be used for this thesis. 1396 boreholes were excluded from this thesis because essential information such as coordinates, collar elevation and survey information (dip, azimuth and depth) are missing. However, these 1396 boreholes did contain descriptive- and grade assay information that was not removed from the database. The database was subsequently split into two groups: usable and unusable data. It is important to emphasise that historical borehole information for the unusable data could still be uncovered in the future and should thus never be completely removed from the database.

Precompiled data files of lithological information for the 169 surface boreholes were provided by Mr Jaco Delport for this thesis. The lithological data is a key component for the 3D geological model generated in Leapfrog Geo. Currently, the only historical lithological information available for Leeuwpoort Mine is from the precompiled lithological data. The lithological data for the underground boreholes are not available at present, but could be recovered as the post-mortem study of Leeuwpoort Mine progresses.

The borehole data was primarily gathered from six different mining sectors, as labelled by the mine: C-Mine Surface (CMS), C-Mine Waggon drilling (CMW), C-Mine Underground (CMU), C-Mine Kempe (CK), C-Mine Kemp Boreholes (CKB) and C-Mine Leeuwpoort Underground (CLU). These boreholes differ in location and spatial orientation as well. The surface boreholes include CMS and CMW, whereas the underground boreholes include CMU, CK, CKB, and

CLU. The historical log sheets for the underground boreholes followed a consistent scheme and could easily be compared with one another. The historical log sheet for the surface boreholes were different from the log sheet for the historical underground boreholes and had to be reworked in order to compare the different sections of the mine with one another.

4.2.2. Historical data digitization process

4.2.2.1. Establishing an effective data capturing system

Set spread sheet templates were created in order for the underground log sheets and surface log sheets to achieve internal consistency. The borehole data of the 16 log summary books were captured according to:

1) Borehole identification
2) Location
3) Target (specific section mined)
4) X coordinate
5) Y coordinate
6) Collar elevation (Z coordinate)
7) Dip
8) Azimuth (direction)
9) Total depth
10) Tin intersection (core intersection)
    - 10.1) From (m)
    - 10.2) To (m)
    - 10.3) Over (cm)
    - 10.4) Core Value (wt. - % Sn)
11) Sludge intersection
    - 11.1) From (m)
    - 11.2) To (m)
    - 11.3) Over (cm)
    - 11.4) Sludge value (wt. - % Sn)
12) Remarks and additional information

A manual system for data capturing was used when the mine was still operational, resulting in duplication some of borehole data in the 16 log summary books. The duplication of borehole data occurred because the information was written down manually by various geologists and more than one book was available for use. If the current log summary book that was used could not be found, a new book would be used or the borehole information was added to an old book. The log summary books were also written down for different purposes. The log summary books for the mining office was not as detailed as the log summary books used in the geology Department. The log summary books of the geology Department were more detailed and care was taken to meticulously note significant figures. This led to inconsistencies in the data because the information was written down from various books resulting in data transfer errors.

Keeping track of the different versions of the borehole data became difficult during the digitization process. In order to reference back to the specific log summary book where the borehole data was captured from an additional column was added. This column is referred to as Book Record. This column contains the name of the specific log summary book with the corresponding page number where the information for the specific borehole was captured from. By adding the Book Record column a QA/QC (quality assure/quality control) process for the digitized data can be assured.

4.2.2.2. Data processing

The following processes were applied to the digitized historical borehole data in order to remove any errors and inconsistencies from the data set. These processes were necessary to ensure that good quality data would be used in the 3D modelling program, Leapfrog Geo.

1. One of the most important validation steps followed was to ensure that each borehole had a unique borehole identification number (BH ID). No duplications are allowed to ensure a valid 3D model. If any uncertainty or questions arise for a specific borehole, the original data can be searched with the unique borehole identification.
2. The next validation step was to ensure that each borehole had X-, Y- and Z-coordinates. Leapfrog Geo was used to create the 3D geological and ore deposit model as well as the various Interpolant models. This program uses coordinates to accurately plot the location of the boreholes in the program. Data points that did not have corresponding coordinates were removed from the data set and stored with the unusable data. If a borehole does not have coordinates, Leapfrog Geo will identify this

borehole and you as user are able to ignore the borehole. This means that the borehole will not form part of the generated 3D model.

3. ArcMap was the program used to spatially validate the boreholes. This validates that the borehole data is correct and corresponds spatially with the known location of Leeuwpoort Mine. The original coordinates for the boreholes were recorded as easting-northing coordinates. However, in order for the data set to be compatible with the ArcMap program the coordinates were converted to the Cape Lo27-coordinate system using a Transverse Mercator Projection (Bolstad, 2005). The converted borehole coordinates were used in Leapfrog Geo as well.
4. The historical borehole information obtained for Leeuwpoort Mine prior to September 1972 was recorded using the Imperial System. At the end of September 1972, Leeuwpoort Mine started to use the Metric System to record all borehole information. This meant that all borehole data prior to September 1972 had to be converted from Imperial measurements to Metric measurements.
5. Borehole coordinates prior to September 1972 were recorded in an unknown coordinate system. To date, documentation has not yet been obtained to specify what coordinate system was used. Boreholes prior to September 1972 were thus not used for this thesis and subsequently forms part of the unusable data.
6. Null values (a value with no data or amount) were not used or imported into either Leapfrog Geo or ArcMap.
7. Tin assay values that recorded 0 wt. - % Sn were not used or imported into either Leapfrog Geo or ArcMap.
8. The historical borehole data of Leeuwpoort Mine includes core assay values as well as sludge assay values. The sludge assay values were imported into Leapfrog Geo but were not used to create the 3D geological or Interpolant models.
9. Leapfrog Geo has a build in function that identifies any overlaps in the imported assay information. The user is also able to fix any overlap within the program. In order for the core assay values to be acceptable in Leapfrog Geo, the core sections are not allowed to overlap. The core from and core to values are not allowed to overlap the next core section. The overlap values identified were caused by typing errors and could easily be rectified.

4.2.3. Historical borehole validation process for the log summary books

The data was subjected to a thorough validation process in which the historical borehole data for all 16 log summary books were checked and correctly recorded. A colour coding system was implemented for the validation process of the typed log summary books. The colour coding system was used to identify discrepancies of information, missing values, different measurement units, additional information and missing records. The complete colour coding system implemented for the log summary books is summarized in Table 4.

Table 4: The colour coding system used for the validation process of the data typed from the log summary books.

Colour	Code description
Yellow	Error/uncertain. Data needs to be checked in the other log summary books.
Blue	Different values for a borehole in different log summary books.
Green	A measurement unit other than meters were used. These values need to be converted to meter values.
Purple	These values were marked as errors/uncertain when checked in log summary books. Error/uncertain data (yellow code) was then checked in file records but were not found (checked in books and files).
Orange	Different values for a borehole in the log summary books and files.
Pink	This borehole has a peg. The data needs to be validated in the peg index.
Grey	No record of a borehole in file (file Validation).
Dark Red	A record of a borehole is in the file, but no is information written down (file Validation).

As mentioned in Section 4.2.1., the historical borehole data for this thesis was digitized from three data sources: log summary books, data written on logs and stored in files, and lastly maps. A distinct age relationship exists between these three data sources. The information written on logs that was stored in files are the oldest data records. The file data was written down in the log summary books. File information was corrected in the log summary books. The maps correlate well with both the files and the log summary books. The oldest maps corresponds well with the information in the file, whereas the younger maps match the log summary books. The youngest information is more reliable than the older information because these data records include the corrections made of the older file information.

The more recent maps are especially useful because they are an updated version of the mining activity just before mine closure. If information of old maps are used for a study the user must bear in mind that borehole information shown could include planned and unsurveyed boreholes. Planned boreholes are not always executed and sometimes rejected due to financial constraints, especially in the case of Leeuwpoort Mine, where the mine closed due to the crash of the continued depressed tin market. Boreholes can also be deepened,

resulting in old maps not indicating the new total depth of boreholes. Using historical maps thus increases the risk of working with outdated, incorrect survey information.

If the assumed age relationship of the historical borehole data is correct, it means that younger data are more reliable. The reason for less confidence in the accuracy of the older data is that there is no proper documentation and record for the data capturing phase of the information. There is no proper indication of who logged the borehole, what the adherence to sampling procedure was, no records from the surveyors, multiple people handling the documentation, and lastly unreliable collar elevation on borehole coordinate information.

The colour coding system for the validation of the historical borehole data also indicates an increasing level of confidence in the accuracy of the historical borehole information. The borehole data in the log summary books were summarized from the filed log sheets. Because the log summary books are just a summary of the data in the files, some detailed information might be missing.

The log summary books were the first data source to be digitized. Any errors and inconsistencies noticed whilst capturing the data were marked in a *yellow colour*. In the 16 log summary books different handwriting styles, some of which are difficult to read, resulted in the values or information being transferred incorrectly. Some of the styles were difficult to read and resulted in the values or information being written down incorrectly. Duplicated boreholes would thus have conflicting information in the different log summary books. Different values for a borehole in different books were marked in a *blue colour*. Boreholes information (coordinates, assay, depth etc.) recorded in Imperial Units were marked in a *green colour*. These measurements were converted to the Metric system as mentioned in Section 4.2.2.2.

After the log summary books had been digitized some essential collar and survey information was still missing. The survey and collar data are required in order to import information into Leapfrog Geo. The survey data (dip, azimuth and total depth) provides information on the orientation of a borehole, whereas the collar data (x-, y- and z coordinates and collar elevation) provides information on the spatial location of a borehole. The next validation step was to go back to the original logs. A lot of borehole information was lost due to animal interaction. Unfortunately, when conducting a post mortem study of a closed down mine, rigorous cleaning will be part of the process.

After the document preservation was complete a file catalogue was created. It was noted that each file had a specific number which were used as a unique identifier for the catalogue. The file catalogue thus consists of a unique number for each file with an accompanying file name.

Files that did not have original file numbers were given a new number. The allocated numbers were chosen to avoid any overlap with pre-existing numbers.

The historical borehole data can now be validated with the files. In order to know where the original data in the files can be found for each borehole, a new column was added in the set spread sheet called: File Record. The File Record consists of the unique file number linking back to the file catalogue and file name. The data marked in a yellow and blue colour was then searched for in the files. If the data marked in the yellow colour was not found in the files it was changed to a *purple colour*. The purple colour means that the data was searched for in the original log sheets located in the files, but could not be validated. If the marked data could not be validated or found in the files then the yellow/blue colour was changed to a purple colour.

If a difference in the data for the log summary books and the files were noted, the data was marked in an *orange colour.* The digitized boreholes where validated with the files. If no record for a borehole was available in the files a *grey colour* was assigned in the File Record column. If a record was available for a borehole but no information was available i.e. borehole name but no data information, the data was marked a *dark red colour*. Some boreholes included peg numbers in the locality description. These peg numbers correspond with the pre-compiled peg index provided for this thesis. The peg index was used to search for missing collar elevation values of the historical boreholes. If a borehole locality description included a peg number, the borehole was marked in a *pink colour*.

A Map Record column was added to the set spread sheet (Section 4.2.2.1.) in order to properly record the source of the maps. The Map Record includes the corresponding unique file number where the map can be found, file name, as well as the map name. This means that borehole information was validated by three different data sources: log summary books, original log sheets stored in files, and maps. The three validation processes ensures that a good QA/QC process was applied to the data resulting in a high level of confidence in the accuracy of the data can be expected.

Failure to validate the data will result in poor, inconsistent modelling results. The old saying holds true: garbage in, garbage out (Griffith, 2007). Proper validation processes are time consuming and strenuous but necessary to get the best possible results. The processes followed ensures the maximum level of confidence in the data.

4.3. Generating a three dimensional geological model of the Leeuwpoort Mine

This section of the report discusses in detail the steps followed to generate a 3D geological model for Leeuwpoort Mine. The section will also discuss the methods used to model the lodes found at Leeuwpoort Mine, and using these lodes for exploration purposes. Leapfrog Geo was the program used to generate the geological model which resulted in the ore zone analysis and probability predictions.

4.3.1. Importing the data into Leapfrog Geo

In order to import borehole data into Leapfrog Geo, the data must be in the correct file format. The borehole data is defined by three main data files: the collar file, the survey file, and at least one interval file (LeapfrogGeo, 2016). Leapfrog Geo assumes no default unit and values imported are assumed to all be of the same unit and scale.

The collar file consists of a unique borehole identification number, x- and y coordinate, collar elevation (z coordinate), and maximum depth. The maximum depth is used to validate the interval tables with the collar files. The survey file contains of a unique borehole identification, dip, azimuth, and depth. The interval file provides the program with segment information down a borehole (LeapfrogGeo, 2016). In this thesis the interval data is lithological information and assay data. The lithological data for the boreholes, a unique borehole identification, “from and to” depth with a corresponding lithological description make up the lithological file. In the case of the assay file, the data consists of a unique borehole identification number along with to and from depth with corresponding assay values.

Overlapping assay segments, “from and to” values exceeding maximum depth, missing collar or survey information, and duplicated information will automatically be flagged by Leapfrog Geo. The user is thus able to make changes to the data in the program and set certain rules or functions for the inconsistent data. The changed data can be exported and added to the newly digitized database of the historical borehole data.

After the collar, survey, lithology, and assay files for all the usable boreholes of Leeuwpoort Mine were imported to Leapfrog Geo, the spatial position (Figure 12), orientation (Figure 13) and assay values (Figure 14) for each borehole can be visually examined. The only lithological data obtained from the post-mortem was from the 169 surface boreholes (CMS) (Figure 15) and was used to generate the geological model. The lithological data consists of five main lithological units as identified by the mine: Quartzite, Shaly Quartzite/Shaly Arkose, Shale, Gritty Quartzite/Arenite and Soil. The lithological data corresponds to the CMS borehole positions (Figure 15).

4.3.2. Creating a topography

A 3D topographic surface of Leeuwpoort Mine was created in Leapfrog Geo. A set of 20m interval contour lines were provided by Mr Jaco Delport, for the purpose of creating the topography. These contour lines were digitally created in ArcMap from two maps: map C716 and map C467. These maps can be viewed in Appendix 1. Map C716 is a 1:5000 map of Leeuwpoort Mine that represents geology, lodes, and structure and surface boreholes (Misiewicz, 1989). Map C467 is a 1:20000 map of the farm Leeuwpoort 554 KQ indicating main roads and power lines (Warmbad-Munisipaliteit, 1989).

The contour lines were created as a shape file in ArcMap. In order for the contour lines to be imported into Leapfrog Geo with the corresponding elevation, the shape file has to be converted to a DXF file. The DXF file is then exported from ArcMap and imported into Leapfrog Geo as polylines (Figure 16). For viewing purposes of the imported contour lines, the vertical exaggeration of the model was set to a value of 3. The polylines (contour lines) where then extracted as GIS lines and could thus subsequently be used to create the topography (Figure 17).

The extent of the topography was set at the same boundary as the geological model. The topography was thus enclosed by the geological model. The boundary of the geological model was chosen based on the location of the boreholes in the prospecting area of Leeuwpoort Mine. The prospecting area of consists of two neighbouring farms: Leeuwpoort 554 KQ and Rietfontein 536 KQ (Delport, 2017) (Figure 18).

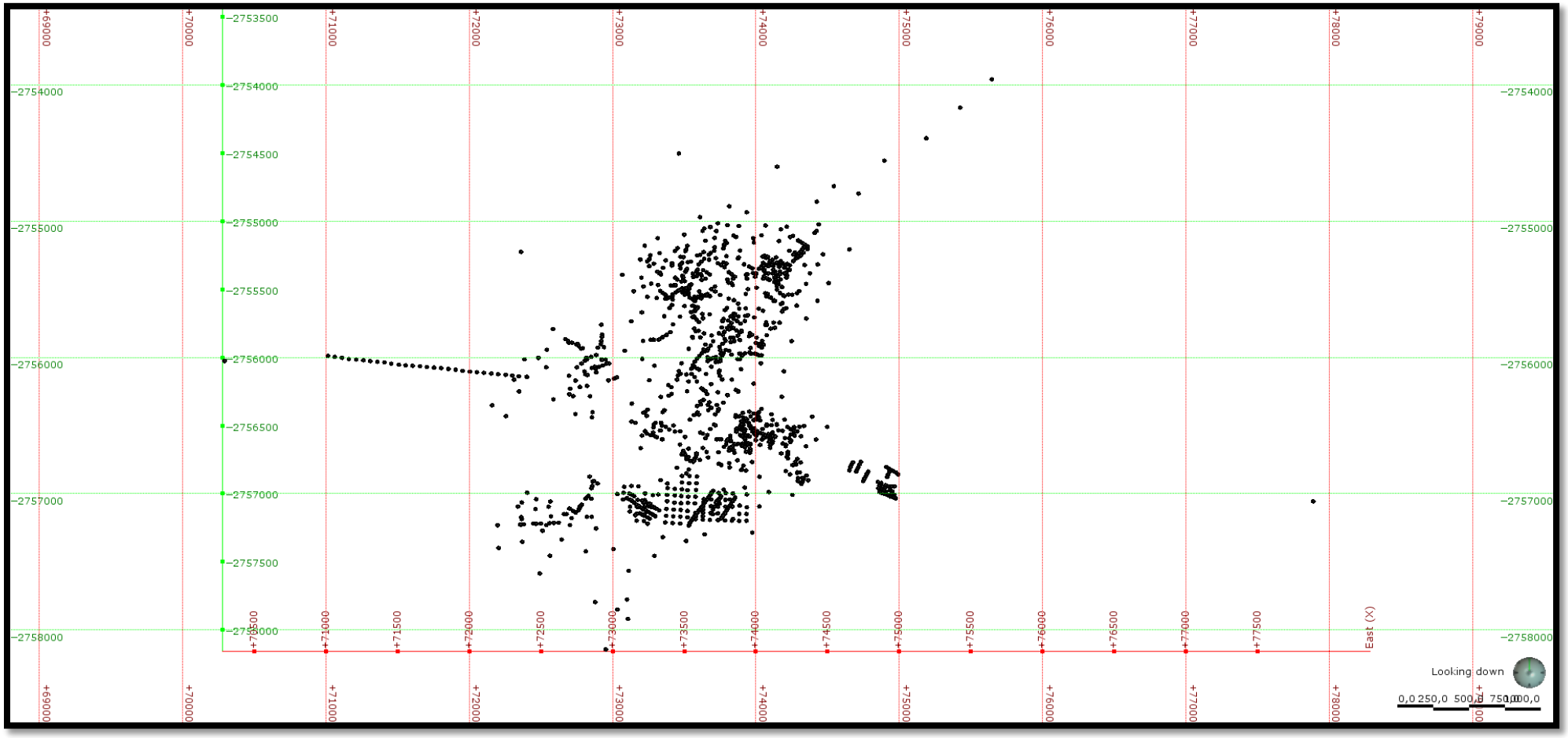

Figure 12: Spatial position (collar elevation) of all the boreholes used for this thesis. This figure depicts the spatial position of all the boreholes: CMS, CMW, CMU, CK, CLU and CKB.

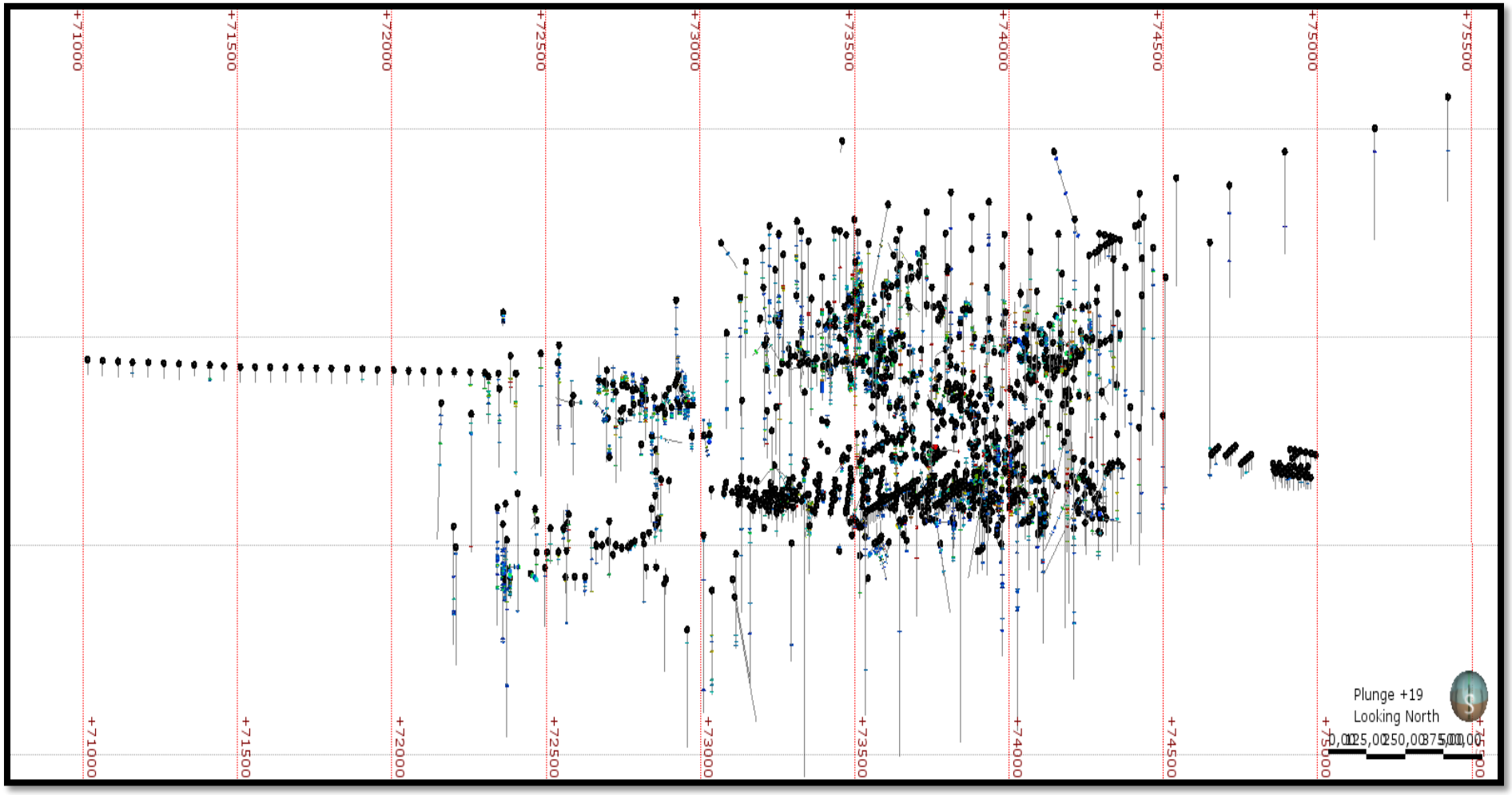

Figure 13: Spatial orientation (survey) of all the boreholes used for this thesis. This figure depicts the spatial orientation of all the boreholes: CMS, CMW, CMU, CK, CLU and CKB. The disks indicate the position where assay data is available.

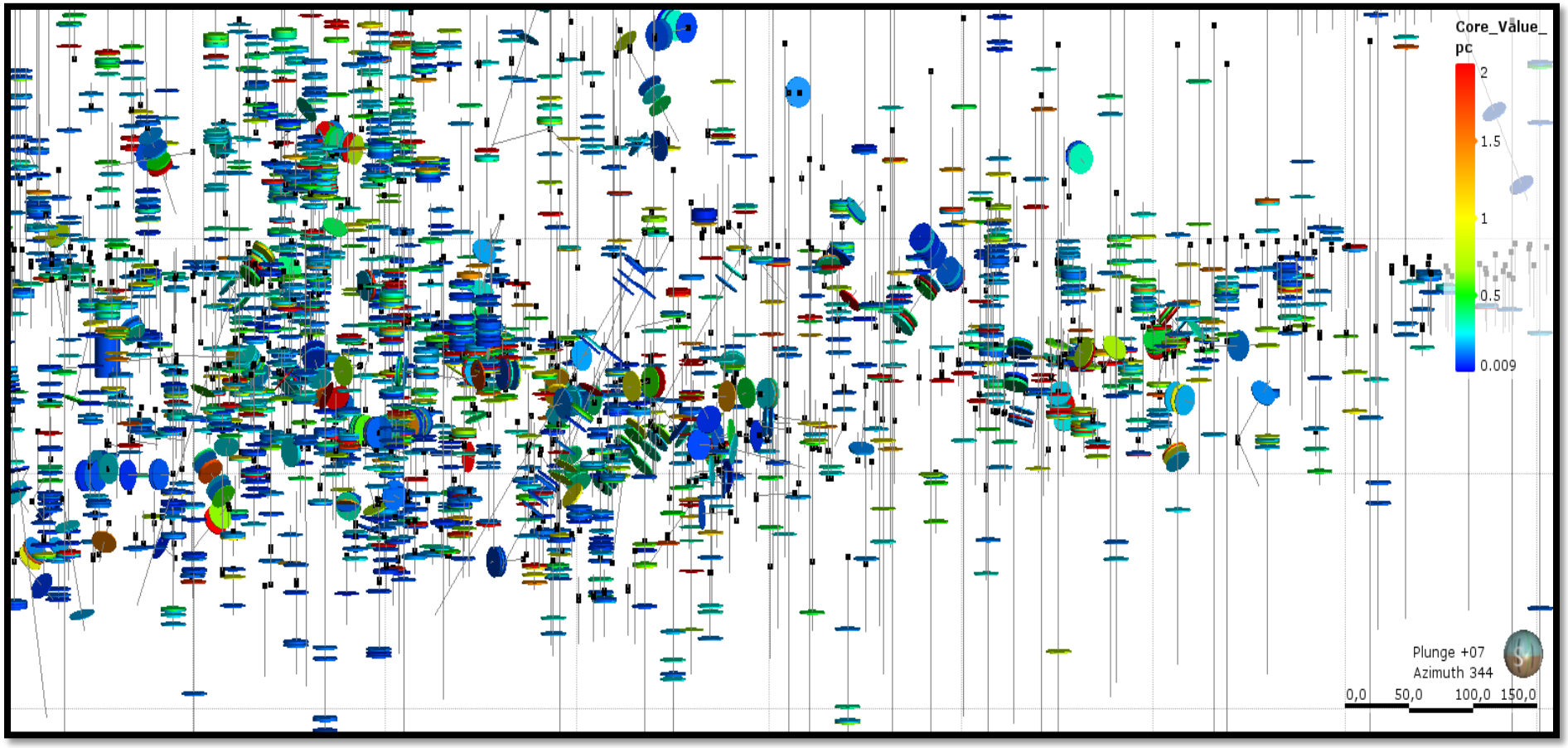

Figure 14: Assay data of all the boreholes used for this thesis. This image depicts the assay data as disks relating to the thickness of the sample, each corresponding to the specific Sn weight % at a certain depth. This figure includes the assay data of all the boreholes: CMS, CMW, CMU, CK, CLU and CKB.

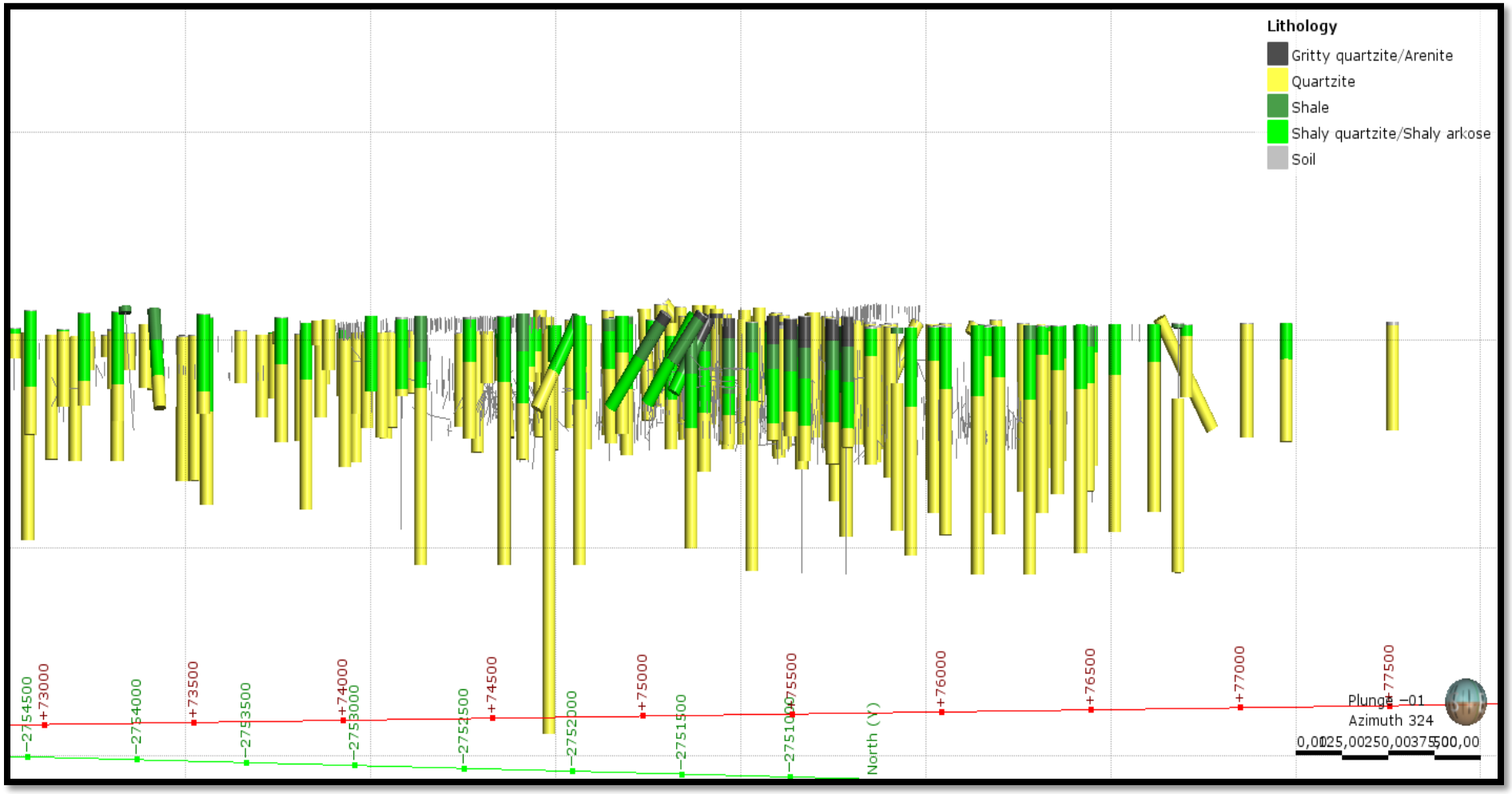

Figure 15: Lithological data for the CMS boreholes. Lithological data for only the surface boreholes (CMS) is currently available and was thus the only lithological information used to generate the 3D geological model

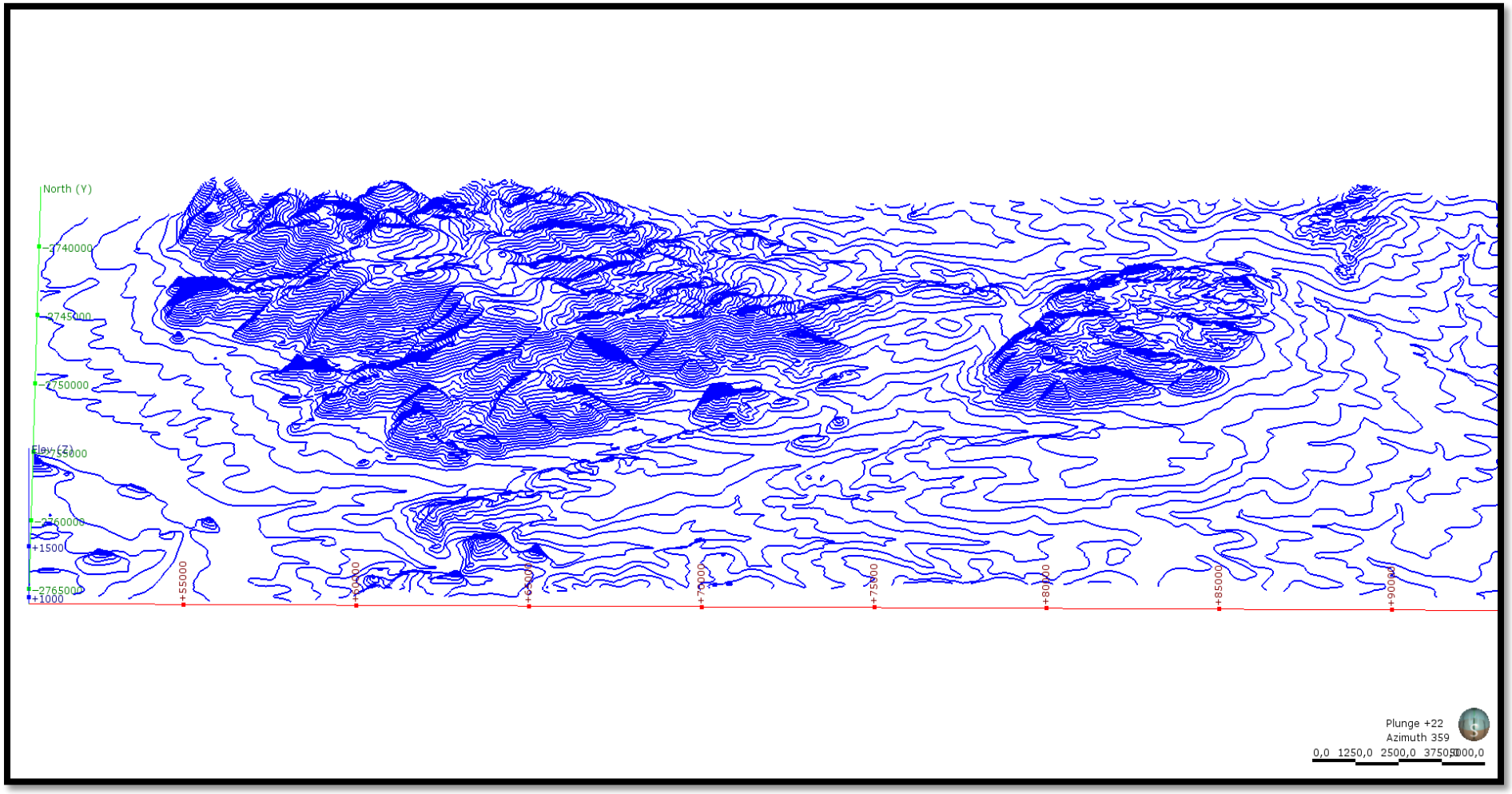

Figure 16: Digitized 20m contour lines imported into Leapfrog Geo. These contour lines were used to generate the topography of Leeuwpoort Mine. For viewing purposes, the vertical exaggeration was set to a value of 3.

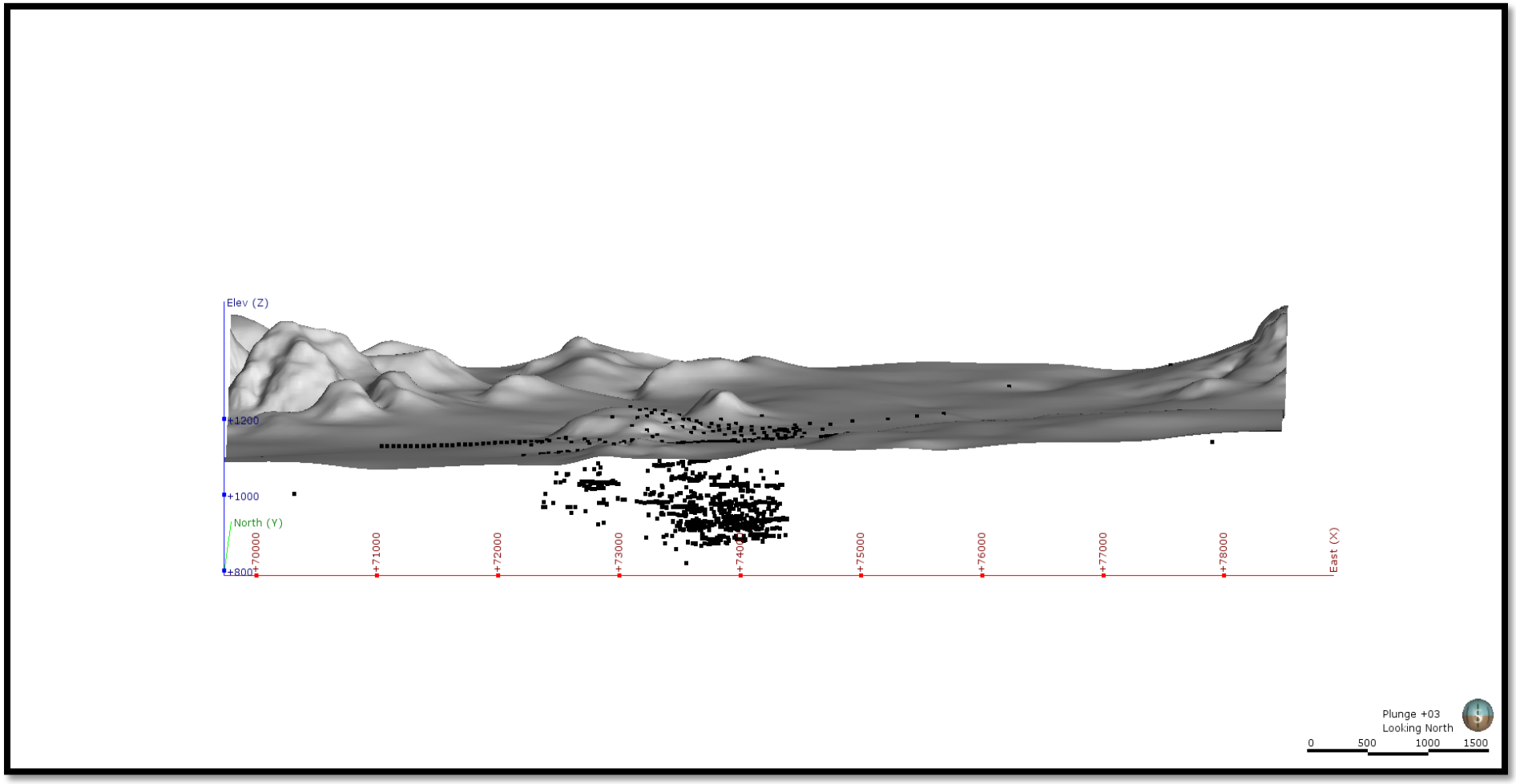

Figure 17: Topography of Leeuwpoort Mine. The topography was created from the digitized contour lines. For viewing purposes of the topography, the vertical exaggeration was set to a value of 3. The black points indicate the collars of the usable boreholes.

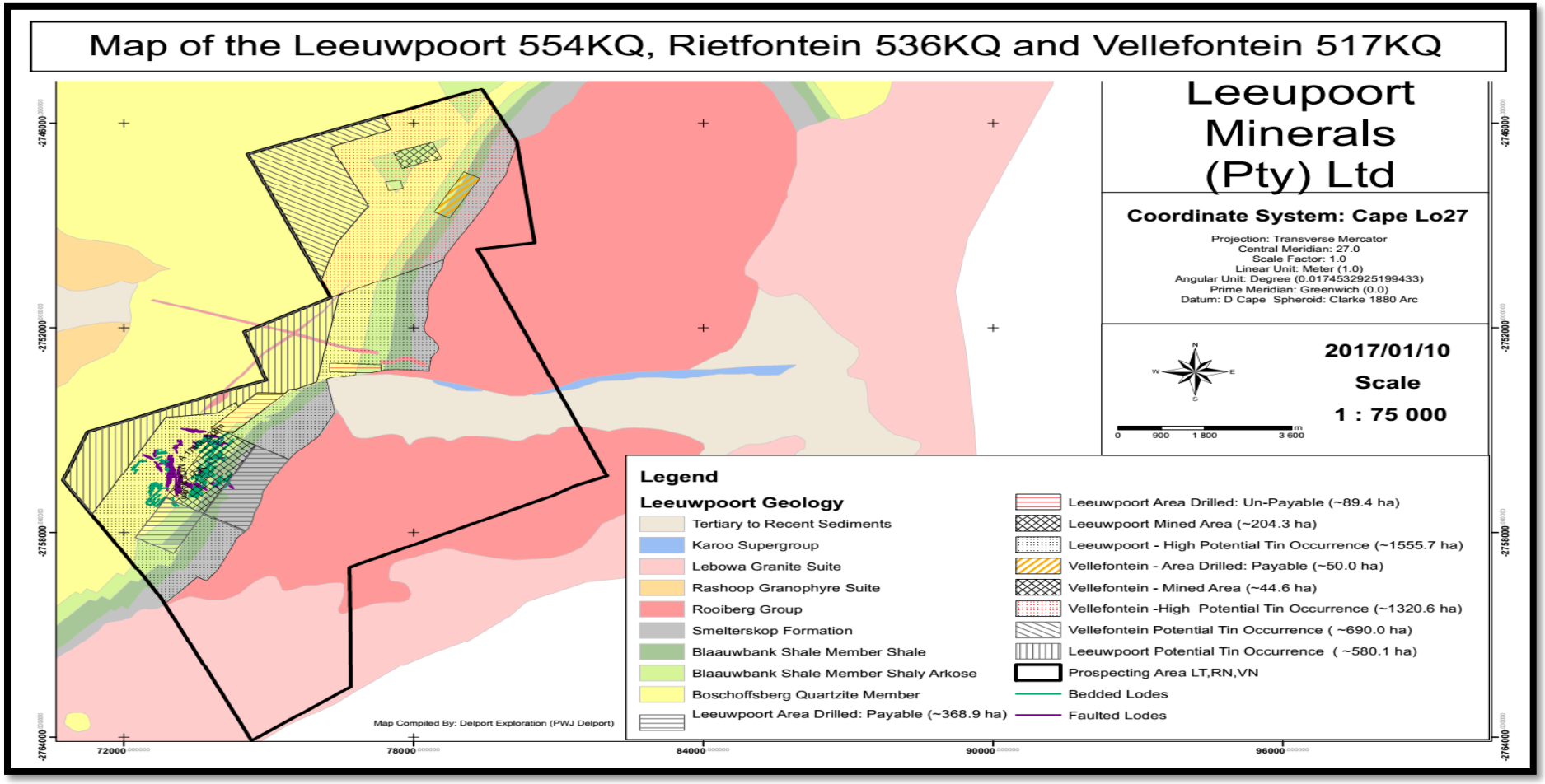

Figure 18: Map depicting the regional geology of the prospecting area (solid black line) of Leeuwpoort Mine. The prospecting area consists of two neighbouring farms: Leeuwpoort 554 KQ and Rietfontein 536 KQ. The boundary for both the geological model and topography was confined by the borehole location (Delport, 2017).

4.3.3. Importing GIS data, maps and photos

During the post-mortem study of Leeuwpoort Mine, a large number of maps, majority of which were underground mine maps, were scanned and digitally stored. A 5” floppy disk with the complete map catalogue was uncovered prior to the post-mortem study. This resulted in the creation of a validation system where the maps where cross-referenced with the original map catalogue. A new digital map catalogue was created indicating which maps where missing or damaged. The maps were also subdivided according to the specific mine. The map catalogue thus includes maps for A-Mine, NAD, B-Mine, C-Mine, D-Mine and Vellefontein. Each map consists of a unique map identification number and a corresponding map title. The map catalogue noted 777 maps for Leeuwpoort Mine. All 777 maps were found, scanned and digitally stored.

Different types of maps are available for each mine: surface, underground, regional, geological, resource and reserve, civil, and surveying maps. For this thesis only the maps for Leeuwpoort Mine (C-Mine) were used. The map coordinates were recorded in Easting-Northing, whereas the borehole coordinates were converted to Cape Lo27 to facilitate usage in Leapfrog Geo.

These maps were georeferenced in Leapfrog Geo. The program has a built-in application where maps can easily be georeferenced. The requirement for georeferencing is that three points with corresponding coordinates be identified. Once the map has been correctly georeferenced in Leapfrog Geo the map can then be draped onto topography. This is an essential part in ensuring that the digitized borehole data is consistent. The easiest way to confirm the spatial position of boreholes is to use a map with borehole locations, drape the map onto the topography and validate the collars of the boreholes with the collars on the map. This results are shown in Figure 19. Map C57 is a surface map indicating the position of the surface boreholes, along with the outer limits of the Gap Lower Lode mineralization, and is used to illustrate the results (H.C.B., 1982).

GIS data such as surface features (roads, rivers, power lines) and underground features (tunnels, shaft openings, underground workings) were also imported into Leapfrog Geo. Specific positions of lodes at each of the different levels of the mine were digitized from maps and used to create geological surfaces. This process will be discussed later in the thesis.

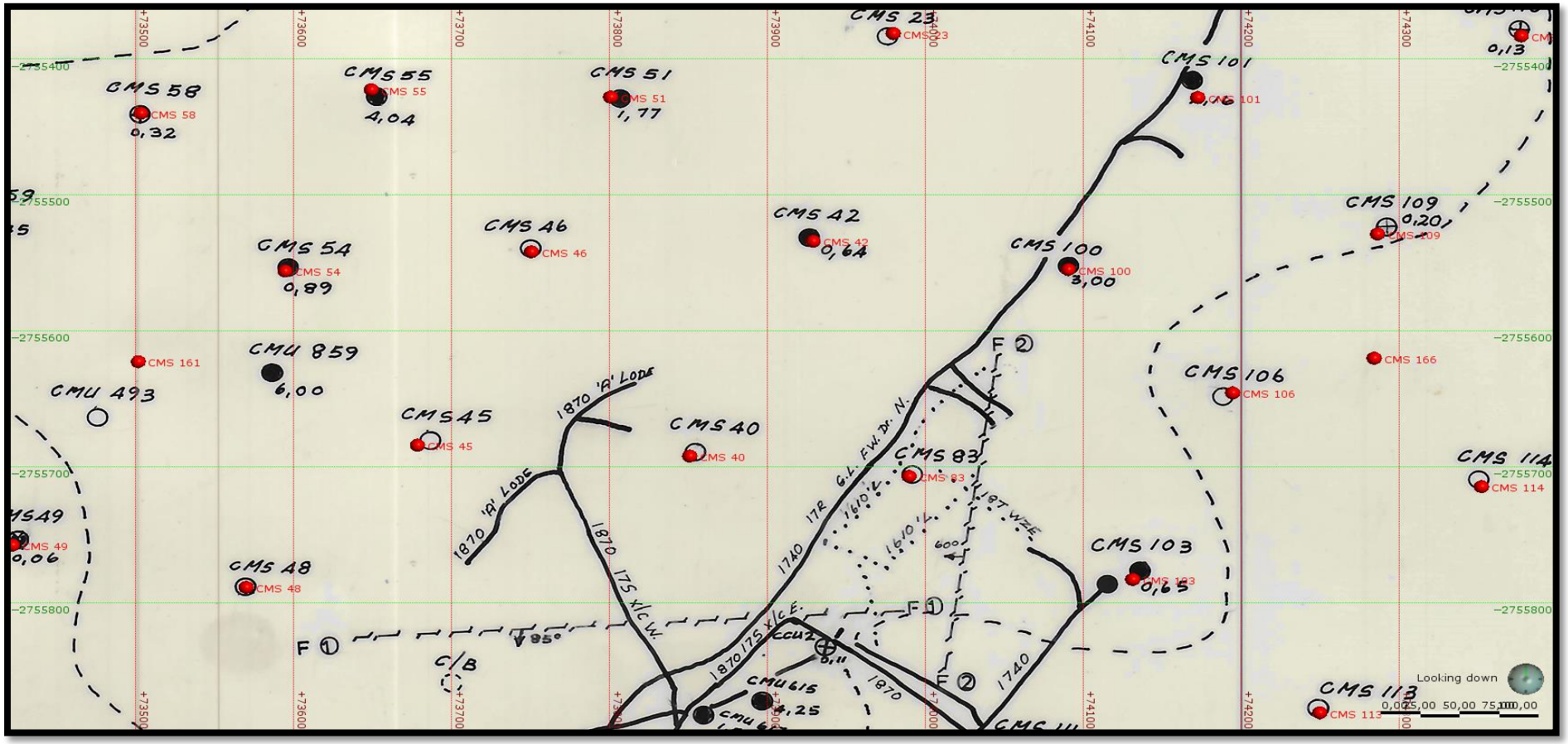

Figure 19: Map C57 (H.C.B., 1982) was imported into Leapfrog Geo and georeferenced. The map was draped onto the topography and the map features are indicated in the black colour. The borehole locations are indicated by the black circles. Coloured circles indicate drilled and surveyed boreholes, whereas the non-coloured circles indicate planned boreholes. The collars of the boreholes imported into Leapfrog Geo are indicated by the red dots. The spatial position of both the boreholes indicated on map C57 and the imported boreholes accurately correlates with one another, and indicates that the digitized borehole information is consistent.

4.3.4. Using point data in Leapfrog Geo

A precompiled digital peg index, provided by Mr Jaco Delport, consisting of 14106 peg positions of Leeuwpoort Mine was provided for this thesis. The complete peg index was imported into Leapfrog Geo as point data. The peg index is composed of the Number Series, B-Series, C-Series and D-Series, as used by the mine. (Figure 20). These different peg series' represent different sections and survey periods of the mine. Each peg includes the following information: peg number, location, x-, y- and z coordinate, distance to the closest peg, description, and source of the peg data.

Once the peg index was imported according to the specific requirements of Leapfrog Geo, it became evident that some of the pegs were located outside the defined geological boundary. These pegs had incorrect x-, y- and z coordinates and they were subsequently removed using the interval selection tool of Leapfrog Geo. An Excel spread sheet of the incorrect pegs was made and a record of the spread sheet was properly stored. As the post-mortem study progresses and more information is obtained, these incorrect values can be searched for and corrected. The corrected pegs can later be added into Leapfrog Geo to either support the existing model, or to supply additional information.

The peg index supplies crucial missing information of the mining activity. Due to limited structural and lithological data, the spatial location of the lodes can be determined with the use of the peg index. 39 lodes were distinguished between when Leeuwpoort Mine closed down in 1993. The lodes are subdivided into two different types: fissure and faulted lodes, and bedded lodes. The presence of these lodes can be noted when viewing the imported peg index. A detailed study of the lodes can be found in Section 4.3.5.2.

In addition, the peg index can also be used to indicate the different mining levels. Leeuwpoort Mine has a total of six mining levels. These levels are all horizontal and parallel to one another. The information for these mining levels is summarized in Table 5. The pegs were used to verify the spatial location and position of the mining levels at Leeuwpoort Mine (Figure 21). The peg index can be used in conjunction with the digitized underground workings of the mining levels (Figure 22) to build a mining model for Leeuwpoort Mine at a future stage.

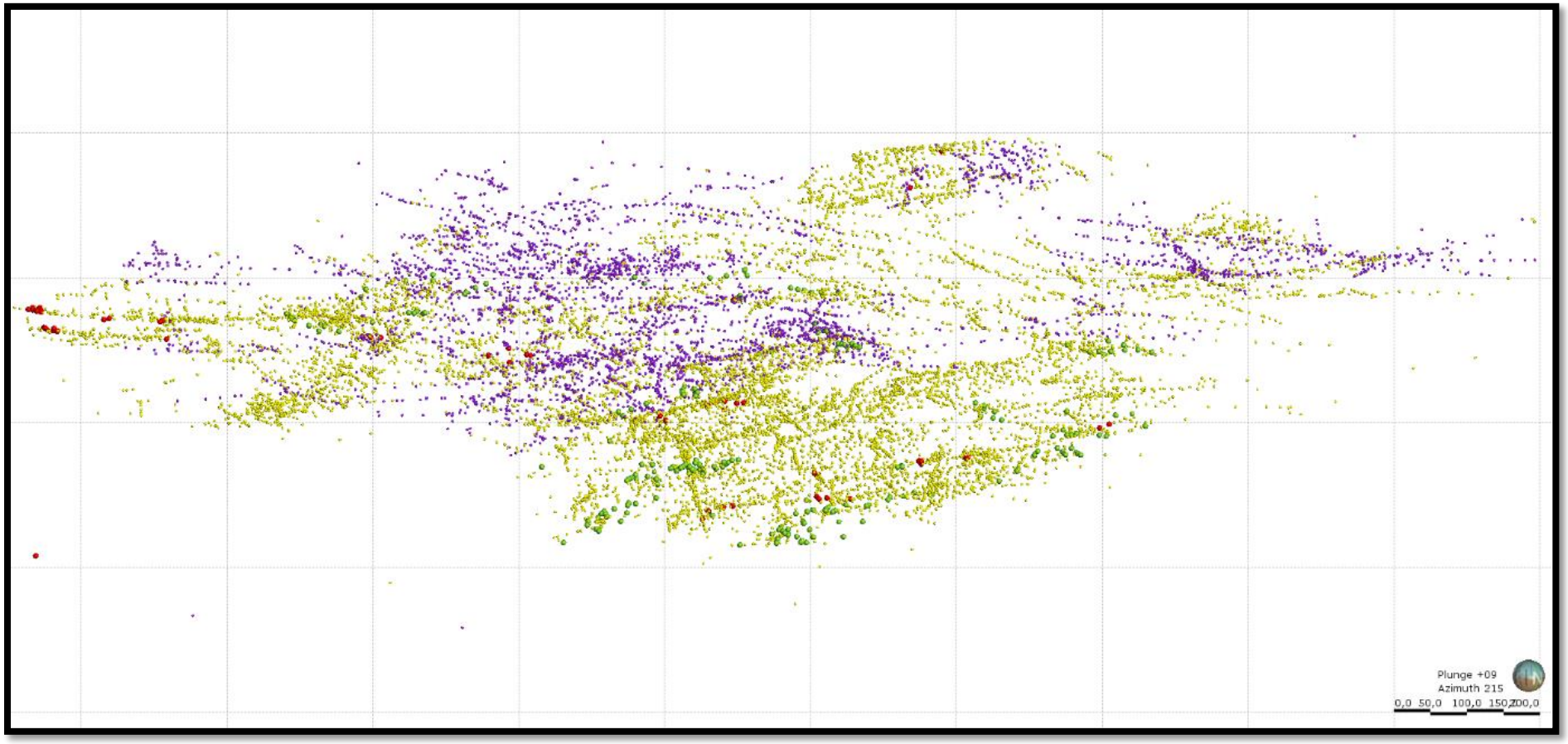

Figure 20: Tilted view of the mine peg locations of Leeuwpoort Mine. The different peg Series' represents different mining periods of Leeuwpoort Mine. The red points represent the B-Series, the yellow points represent the C-Series, the green represent the D-Series and purple points represent the Number-Series.

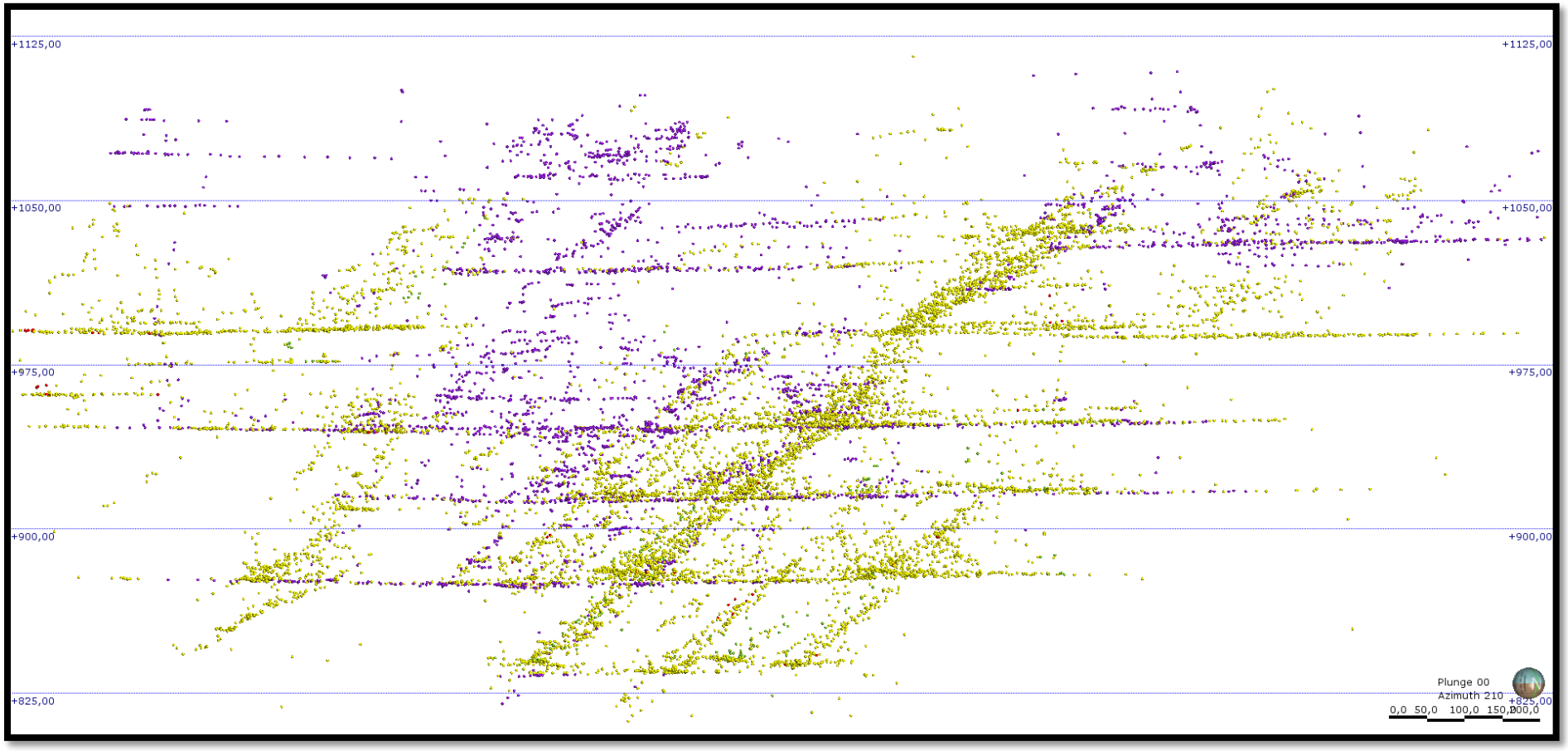

Figure 21: Side view of peg index imported into Leapfrog Geo. The peg index reflects the mining levels for Leeuwpoort Mine, as indicated by the horizontal levels of the peg index. The peg index thus confirms the spatial position of the mining levels. The peg index also notes the presence of the lodes. The steeply dipping features are the fissure and faulted lodes, whereas the shallow dipping features indicate the bedded lodes

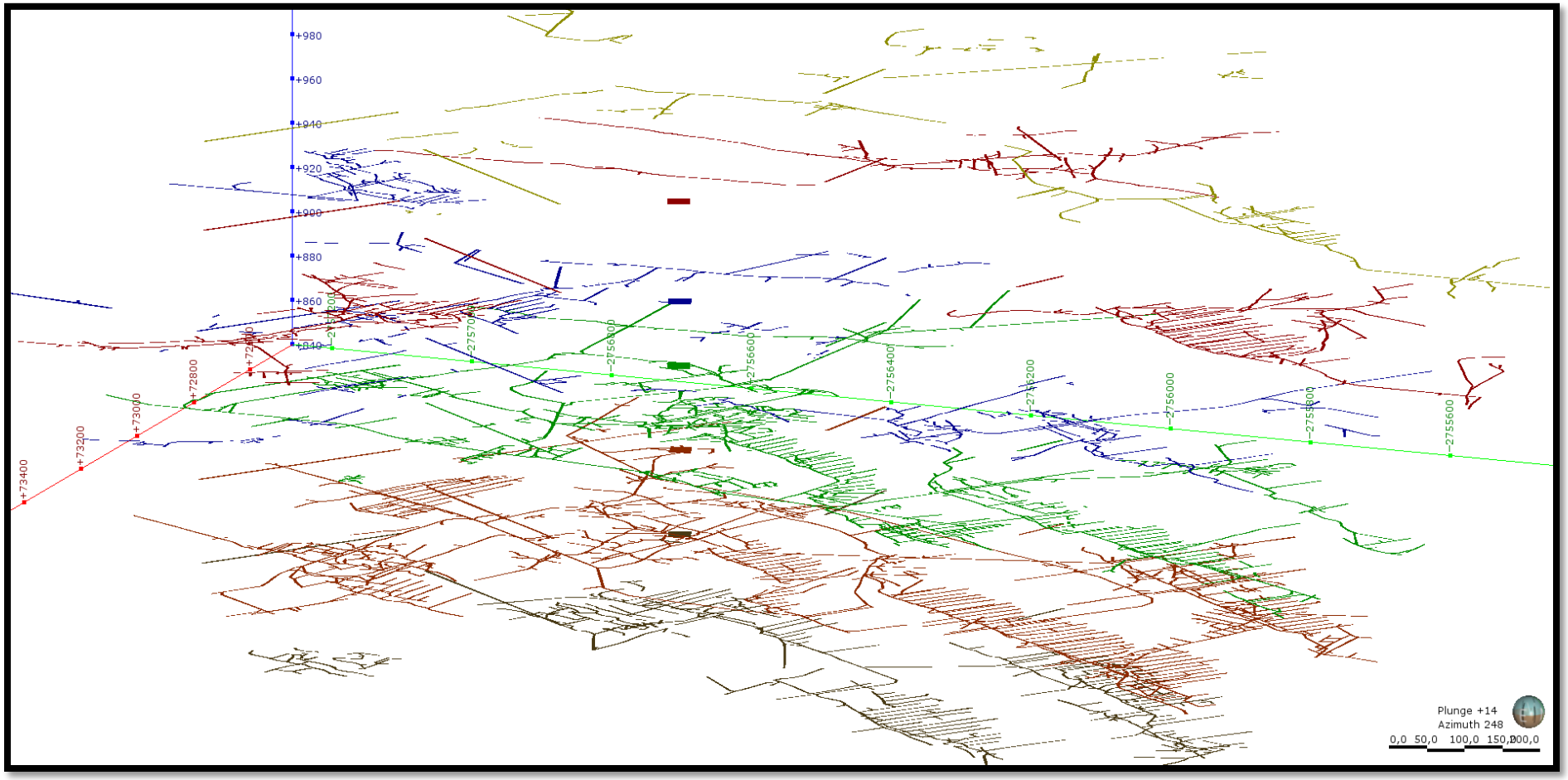

Figure 22: Underground workings for each mining level. The mining levels are represented by the following colours: yellow (1250 Level), red (1350 Level), blue (1510 Level), green (1610 Level), orange (1740 Level) and brown (1870 Level). Coloured blocks indicate the position of the C-Shaft station at the different mining levels.

Table 5: The six mining levels of Leeuwpoort Mine with the corresponding mean average mean sea level elevation (m.a.m.s.l.) of each mining level

Name of mining level	Elevation of mining level (m.a.m.s.l.)
1250 Level	1030
1350 Level	990
1510 Level	945
1610 Level	916
1740 Level	878
1870 Level	840

4.3.5. Creating a 3D geological model for Leeuwpoort Mine

As mentioned in Section 4.3.1., the only lithological data obtained from the post-mortem study was for the 169 CMS surface boreholes. The lithological data consists of five main lithological units: Quartzite, Shaly Quartzite/Shaly Arkose, Shale, Gritty Quartzite/Arenite, and Soil (Figure 15). However, as seen in Figure 18, the rhyolites of the Rooiberg Group are also part of the prospecting area. The rhyolites where not intersected in the CMS boreholes because the boreholes were mainly drilled on Leeuwpoort Farm 554 KQ. The rhyolites of the Rooiberg Group also needs to be included in the geological model, as future exploration drilling at Leeuwpoort Mine might be carried out on Rietfontein Farm 536 KQ.

The CMS lithological data does not identify any lodes that where intersected. From looking at underground maps as well as old mining reports, it becomes evident that they distinguished between 39 tin lodes at Leeuwpoort Mine. These lodes needed to be created and combined with the original lithological data in order to create a representative geological model of Leeuwpoort Mine.

4.3.5.1. Using the lithological data

The lithological data was used to create the first geological model for Leeuwpoort Mine because this data is known and can be assumed to be the basic geology of the area. Then the lodes and Rooiberg Group were added to the geological model. Similar to the log summary books, the lithological record was also re-written and re-typed numerous times during the mine operation. The information was adjusted continuously as more information became apparent.

The biggest concern with regards to working with pre-compiled data is the accuracy of the data. How many people before you handled the data? Are there any typing errors? Does the data represent the latest version or is it an older version? Outdated data will result in out of date and incomplete geological models. It is thus important to emphasise that the quality of

the geological model will rely on the quality of the data and the competence of the geologist creating the model.

The first step in creating a geological model in Leapfrog Geo is to choose the correct base lithology file and to set the boundary of the geological model. The boundary can be defined as the lateral extent of the model (LeapfrogGeo, 2016). In the case of Leeuwpoort Mine, the boundary for the geological model was set as the extent of the drilling. Because the lithological data is based on the CMS surface boreholes.

Once the boundary has been defined, the modelling process can begin. There are no set rules for the sequence to create geological models. However, some guidelines can be used to make the modelling process easier. Geological areas, where the geological environment is predominantly depositional, the steps in which you model the lithology does not matter. In geological areas, where lithological units cross-cut one another, it is important to build the lithological surfaces from the youngest to oldest. This will ensure that the rule of cross-cutting relationships is followed.

In the case of Leeuwpoort Mine, the Gritty Quartzite/Arenite, Shale, Shaly Quartzite/Shaly Arkose, and Quartzite lithological units were all considered to be “depositional surfaces” whereas the Soil contact was considered to be an “erosional surface”. The “depositional” and “erosional surfaces” are created in the same manner in Leapfrog Geo. The only difference is in the way the surfaces are created to define a volume. The contacts between the lithological units need to be modelled first. When creating contact surfaces, a rule of thumb is to create one less contact surface than there are lithological units (output volumes).

The Soil contact was modelled first because it is the youngest. The Gritty Quartzite/Arenite-Shale contact surface was modelled next, followed by the Shale-Shaly Quartzite/Shaly arkose surface and Shaly Quartzite surface (Figure 23). The type of “surface” (deposition, erosion, vein or intrusion, as defined by Leapfrog Geo) chosen to create the contact surfaces will determine how the lithological data is used to model these contact surfaces. If the quality of the lithological data is inconsistent and irregular unrealistic geological surfaces might be created. Any irregularities that does not conform to the geological conditions, are an artefact of the contact surfaces modelled.

The Gritty Quartzite/ Arenite contact surface represented as an A-symmetrical fold when created, however, based on known geological information this representation is not geologically accurate. The folding in this instance was an artefact of the contact surface that was created from the lithological data. In order to remove the folding artefact, the Gritty Quartzite/Arenite portions of the following boreholes were “ignored”: CMS 34, CMS 97 and

CMS 99. Because these Gritty Quartzite/ Arenite portions were removed, the contact surface conforms to the expected geology. The contact surface between the Quartzite and Shaly Quartzite/Shaly Arkose lithologies was not modelled because the Quartzite lithology was considered to be the basement. Basement is considered to be the oldest lithology and the lithological unit that includes “everything else” (LeapfrogGeo, 2016).

Once the surfaces have been created, output volumes must be created. This is done by activating the surfaces under “Surface Chronology” in Leapfrog Geo. This creates four surfaces representing four out of the five lithologies. The final lithology (Quartzite) is the “Basement” and a contact surface is thus not required for the Quartzite lithology. In order to create output volumes the age relationships of the lithologies are needed.

The contact surface chronology was specified as follows, listed from youngest to oldest: Soil, Gritty Quartzite/Arenite, Shale, and Shaly Quartzite/Shaly Arkose. The Quartzite lithology was set as the background lithology by default, specifying that the Quartzite lithology is the oldest. The cross-cutting relationships of the lithological units become especially important when modelling veins or intrusions, which will be discussed in the next section.

4.3.5.2. Modelling the lodes of Leeuwpoort Mine

Leeuwpoort Mine distinguished between 39 lodes that can be defined as the ore zone of the mine. The word lode is a synonym for ore bodies and is a Cornish term that was commonly used on tin mines (Phillips, 1982). As mentioned in the Geology Section (Section 2), Leeuwpoort Mine has two major types of lodes: bedded lodes and fissure- and faulted lodes. There are 22 bedded lodes and 17 fissure- and faulted lodes. Table 6 summarizes all 39 lodes of Leeuwpoort Mine subdivided by the lode type. Displacement of the lodes occurred due to the development of a structurally complex area. Whenever a new lode was discovered during the mining period it was given a unique name. However, because Leeuwpoort Mine is situated in such a structurally complex area, the newly discovered lode was sometimes a displaced extension of an already known lode.

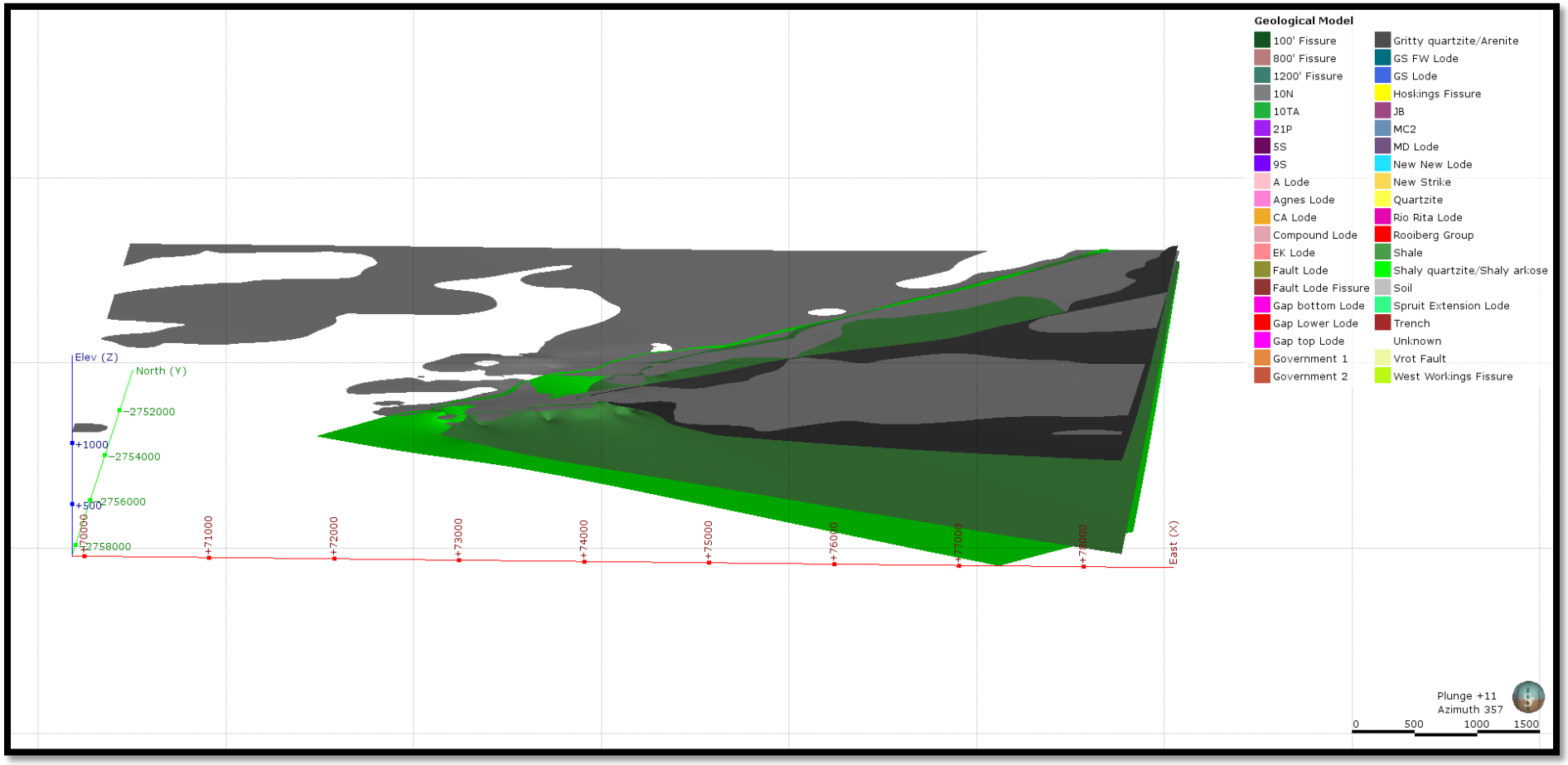

Figure 23: The contact surfaces created in Leapfrog Geo. The light green colour represents the Quartzite-Shaly Quartzite/Shaly arkose contact surface. The dark green colour represents the Shaly Quartzite/Shaly Arkose-Shale contact surface. The dark grey colour represents the Shaly-Gritty Quartzite/Arenite contact surface. The light grey colour represents the Soil contact surface.

Table 6: The tin lodes of Leeuwpoort Mine subdivided according to lode type.

Lodes of Leeuwpoort Mine	
Bedded Lodes	**Fissure and Faulted Lodes**
10N Lode	100' Fissure
10TA Lode	800' Fissure
1A Lode	1200' Fissure
5S Lode	21P Lode
9S Lode	Fault Lode
A Lode	Fault Lode Fissure
Agnes Lode	Government 1 Lode
CA Lode	Government 2 Lode
Cemetery Lode	HG Workings
CNS Lode	Hoskings Fissure
Compound Lode	JB Lode
EK Lode	MC2 Lode
Gap Bottom Lode	Nek Fracture
Gap Top Lode	New Strike Lode
Gap Lower Lode	Trench Lode
GS Lode	Twin Lode
GS FW Lode	West Workings Fissure
MD Lode	
New Lode	
New New Lode	
Rio Rita Lode	
Spruit Extension Lode	

4.3.5.2.1. Using point data to identify areas of possible mineralisation

The lithological data does not include information regarding the intersection of tin lodes for the boreholes. The peg index indicates where mining activity took place in the mine. The pegs that were inserted at Leeuwpoort Mine were all roof pegs, meaning the pegs can be found on the roof portion of the mine tunnels (Figure 20 and Figure 21). Because the peg index is so extensive, it can be used to locate structural features as well as areas of tin mineralization. The peg index was thus used in conjunction with map information of the tin lodes to model a tin ore zone for Leeuwpoort Mine.

4.3.5.2.2. Digitization of the lodes from historical maps

Aside from the peg index, historical maps of the tin lodes and structure were used to model the tin mineralization at Leeuwpoort Mine. Two maps that will be discussed can be found in Appendix 1. Map C716 is a 1:5000 map of Leeuwpoort Mine that represents geology, position of the lodes, structure, and surface boreholes (Misiewicz, 1989). This map was drawn in 1989

and is one of the most recent completed maps drawn of the lodes. Map C696 is a 1:5000 map of Leeuwpoort Mine that represents surface boreholes and structural contours (Walker, 1985). This map was used in conjunction with map C716 because it also indicates the position of the lodes. Map C696 indicates where the lodes were intersected at the different mining levels, and were subsequently projected onto surface. Each identified lode has a specific elevation that can be linked back to the level where it was intersected at. The lodes where modelled from maps C716 and C696. This means that any new lodes discovered after 1989 will not be part of the geological model (see Section 4.3.5.2.3.).

The maps were imported into Leapfrog Geo and accurately geo-referenced. Each individual lode on Map C696 was digitized using the “polyline tool” in Leapfrog Geo. The lodes were then adjusted according to the specified elevation on Map C696 (Figure 24). This means that for all 39 known lodes the position of the lode at different levels can be viewed in 3D.

4.3.5.2.3. The process of lode modelling

In order to model the 39 lodes distinguished between at Leeuwpoort Mine, the peg index was used to identify the location of the lodes. The digitized lode polylines were used to constrain the boundaries of the lodes. In order to accurately model the lodes the following processes were followed:

1) Each peg has a specific location which can be grouped together based on the location to form a point cloud for the roof portion of a specific lode. A separate spread sheet for the grouped pegs for a specific lode was created in Excel. Each point cloud thus consist of points with the same location name, for example, Figure 25 is a point cloud of pegs for Rio Rita Lode.
2) For each individual lode a new “vein surface” was generated form the grouped pegs in Leapfrog Geo. In order to use the “vein surface tool”, the user has to specify the hanging wall and footwall of the vein. Each peg is located on the roof portion of a stope. This means that the identified point cloud would be the hanging wall portion of the vein. In order to define the footwall portion of the vein a new point cloud had to be generated. The stoping width of Leeuwpoort Mine was 1.2m. The assumption was made that the thickness of each lode is 1m. In order to generate a corresponding footwall point, 1m was subtracted from hanging wall point.
3) For the bedded lodes a rules were implemented that the X- and Y coordinate of the footwall peg is the same as the X- and Y coordinate of the known peg (hanging wall peg). The Z coordinate of the footwall peg was calculated by subtracting one meter

from the Z coordinate of the known peg. The calculation for the Z coordinate of the footwall point is illustrated below:

Z coordinate of footwall point= (Z coordinate of known peg) – 1m

4) The fissure and faulted lodes have an omnidirectional dip. The exact dip for each fissure and faulted lode is not known due to limited structural data. In order to generate the footwall points for the fissure and faulted lodes, the following rules were implemented: the Z coordinate of the footwall peg is the same as the known peg (hanging wall peg). Depending on the dipping direction of the fissure and faulted lode, 1m was either added to the X coordinate of Y coordinate. If the fissure and faulted lode generally dips in the X-direction, 1m was subsequently added to the X coordinate of the known point and the Y coordinate was kept constant. If the fissure and faulted lode generally dips in the Y-direction, 1m was subsequently added to the Y coordinate of the known point. And the X coordinate was kept constant. The calculations for the X and Y coordinates of the footwall points are illustrated below:

Dipping in X-direction:

X coordinate of footwall point= (X coordinate of known peg) +1m

Dipping in Y-direction:

Y coordinate of footwall point= (Y coordinate of known peg) +1m

5) The hanging wall points and footwall points were imported into Leapfrog Geo. In order to validate that the grouped pegs for each lode are correct, the hanging wall points were checked against the lode polylines (Figure 25). The lode polylines was used to further constrain the hanging wall and footwall points that was used to build the vein surface. The lode polylines can be seen as the boundary that confine the points. The hanging wall and footwall points that were not within the lode boundary were removed using the new category selection tool in Leapfrog Geo.
6) Before the vein surfaces could be created in Leapfrog Geo, the 39 lodes had to be added as new lithologies. In order for the vein surfaces to be created the program needs to know what lithology will be inside the vein, i.e. the vein lithology, and what the vein surface will be in contact with on the outside of the vein (older lithology). For the lodes at Leeuwpoort Mine, the vein lithology was the individual lodes and the outside lithology was selected as Unknown.
7) Once the hanging wall and footwall points had been constrained by the lode, the vein surface was created in Leapfrog Geo (Figure 26). The veins surfaces was created

using the hanging wall and footwall pegs for each lode and the lithologies were selected as described above.

For the bedded lodes the Z coordinate of the footwall point is perpendicular to the position of the hanging wall points. Because the bedded lodes are stratiform, the assumed 1m thickness will be constant throughout each of the bedded lodes. For the fissure and faulted lodes the X- and Y coordinates were adjusted, however, the coordinates were not adjusted to be perpendicular to the hanging wall points. Each of the fissure and faulted lodes have a unique orientation and dip the assumed 1m thickness is not correct. Because a perpendicular coordinate was not calculated the thickness for each of the fissure and faulted lodes will not be the same. The modelled volumes are not the same because the lodes dip at different angles. At present, the fissure and faulted lodes do not have a constant thickness, but due to limited data of the lodes at Leeuwpoort Mine, the actual thickness of the lodes cannot be calculated. The volumes created for the fissure and faulted lodes are artificial and not representative of the actual volumes. The volumes for the flat lying lodes will be underestimated, whereas the volumes of the steeply lodes will be overestimated.

During the modelling phase of the lodes it became apparent that some of the lodes identified on the C696 and C716 maps did not have corresponding pegs. This is most likely the result of lodes being identified and indicated on the underground maps but not having been mined yet. The following lodes could not be modelled due to a lack of peg information (Figure 27): New Lode, 1A Lode, HG Workings, Twin Lode, Cemetery Lode, CNS Lode and Nek Fracture. This means that from the 39 lodes identified on the C696 and C716 maps only 32 lodes had sufficient information to be modelled.

Each of the 32 lodes of Leeuwpoort Mine were created using the abovementioned processes. All of the modelled lodes were constrained using the digitized lodes as the boundaries. The modelled vein, hanging wall and footwall points, as well as the digitized mineral lodes for each of the 32 lodes at Leeuwpoort Mine can be viewed in Appendix 2.

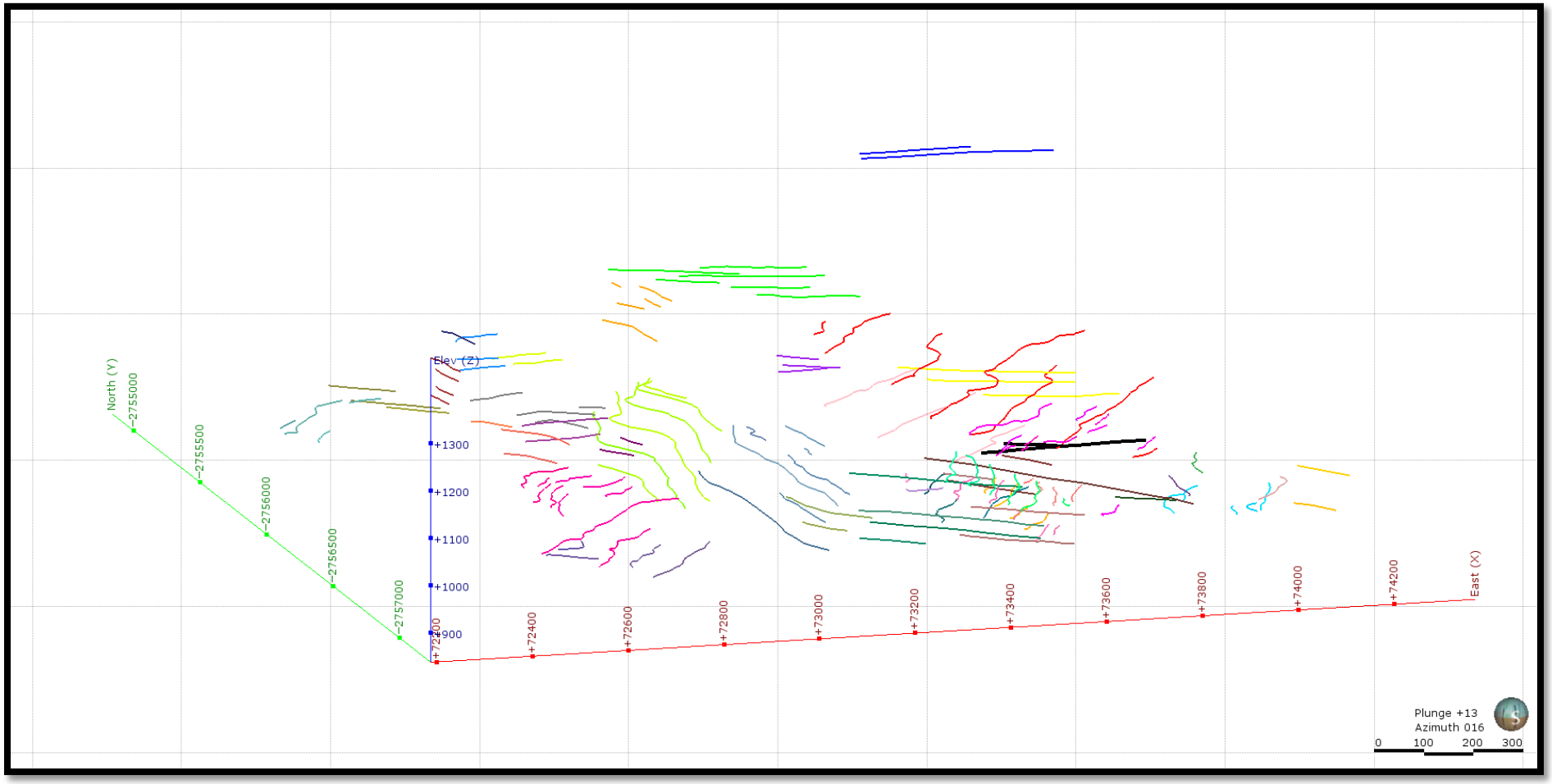

Figure 24: The digitized lodes of Leeuwpoort Mine. The polyline of each lode is at a specific elevation of where the lode was intersected at a specific level.

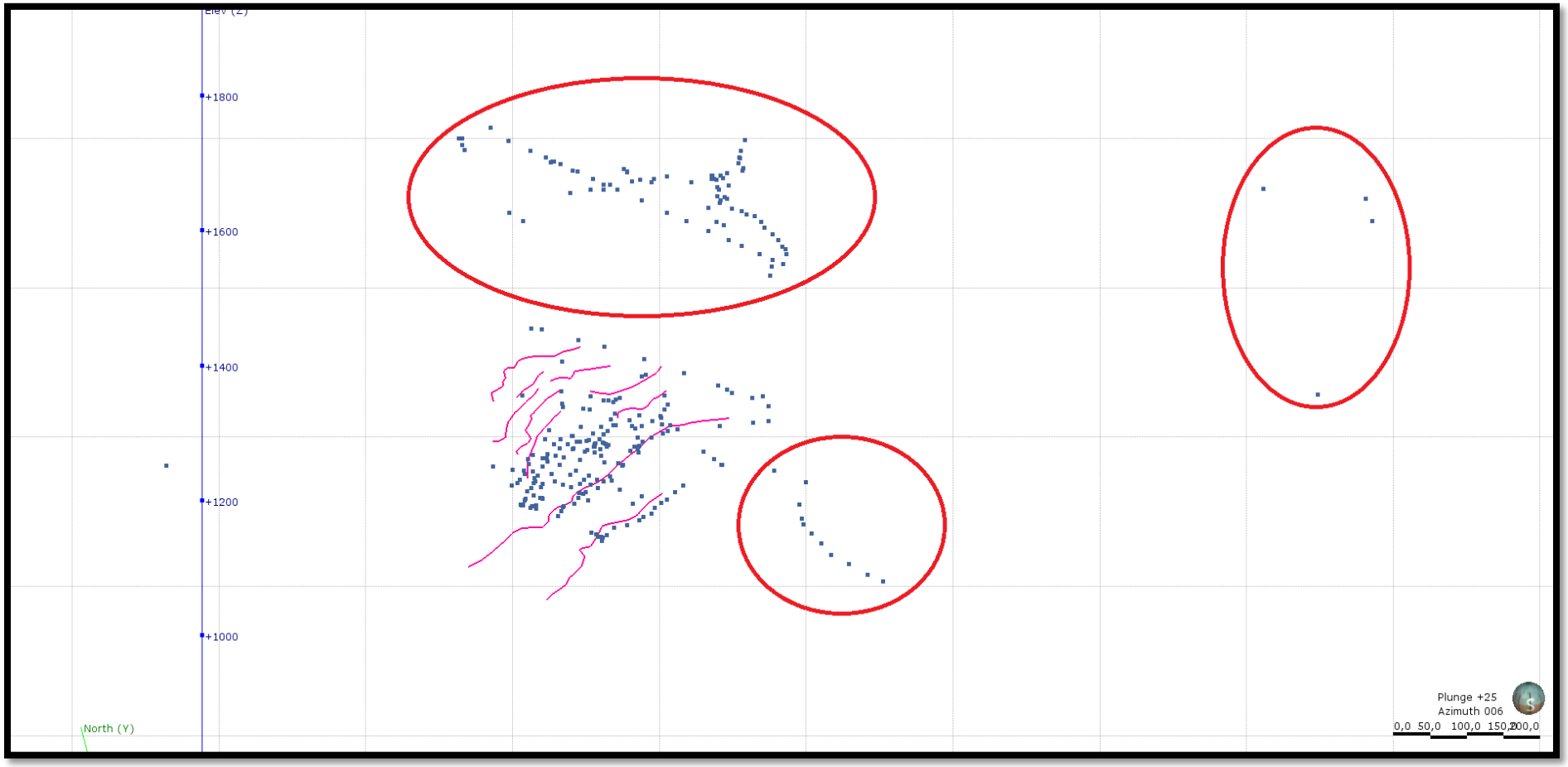

Figure 25: The hanging wall points (blue dots) defined from the grouped peg point cloud for Rio Rita location. The pink lines are the digitized lodes for Rio Rita. As seen on the figure, some of the hanging wall points (circled in red) fall outside the boundary of the lodes.

4.3.5.2.4. Adding the lodes to the geological model

Once all the lode surfaces were created, they had to be added into the existing geological model. This was done by activating the surfaces in the same manner as the surfaces of the base geology, under “Surface Chronology” in Leapfrog Geo. The cross-cutting relationship of the lodes now become important.

Let’s consider the lithostratigraphy of the Rooiberg Fragment. The Quartzite lithology is part of the Boschoffsberg Quartzite Member. The Shaly Quartzite/ Shaly Arkose and Shale units form part of the lower and upper portion of the Blaauwbank Shale Member and the Gritty Quartzite/Arenite forms part of the lower Smelterkop Quartzite Formation (see Table 7 for a summary of the lithostratigraphy of the Rooiberg Fragment). The full geological study can be reviewed in Section 1. We also know that the lodes formed later as structurally and stratigraphically controlled exogranitic hydrothermal ore deposits (Phillips, 1982).

Table 7: Summary of the lithostratigraphy of the Rooiberg Fragment. Sourced from Rozendaal et al. (1986).

Superficial deposits — Alluvium, eluvium, chemical and residual deposits and scree Karoo Sequence — Ecca Group — Buff sandstone		
Bushveld Complex	Lebowa Granite Suite Rashoop Granophyre Suite	Nebo Granite; a grey to red, coarse, equigranular, in places porphyritic granite. Mineralogy: quartz, feldspar, biotite, amphibole. Red to grey granophyric quartz-feldspar rocks, medium- to coarse-grained, locally with country rock xenoliths.
Rooiberg Group	(258–1 100 m)	Quartz porphyry at the top, banded felsite (flow banding), porphyritic felsite, massive fine-grained felsite at the base. Agglomerate occurs locally towards the base. Primary features; flow banding.
Pretoria Group	Smelterskop Quartzite Formation (275–550 m)	Lenticular pink to red feldspathic quartzites and tuffaceous shales with interbedded andesitic volcanics. Local development of conglomerates, pebble bands, grits and agglomerates. Primary features; trough cross-bedding, tabular cross-bedding, ripple bedding, mud flake layers, slump structures. Andesites show amygdales, flow banding, pillow structures.
	Leeuwpoort Formation (1 510–1 700 m)	*Blaauwbank Shale Member (190–300 m)* Thinly bedded shales and sandstones with facies variation to massive mudstones and siltstones. Shaly-arkose; a transition zone typified by lenticular arkoses and sandstones interbedded with shales and siltstones, upward fining. Primary features; ripple marks, flaser bedding, scour channels, slump and ball-and-pillow structures, clay-pellet conglomerates, mud cracks, cross-bedding (tabular, trough), ripple laminations. *Boschoffsberg Quartzite Member (1 320–1 400 m)* Cross-bedded feldspathic quartzites and arkoses, upward-fining sequence. Coarse-grained units with interbedded conglomerate and pebble bands at the base grade to trough cross-bedded arkoses with shale layers in places towards the top. Primary features; trough and planar cross-bedding; slumping diapiric structures, load casts, ball-and-pillow structures, clay pellets, current lineation, mud cracks, shale-flake conglomerates, ripple marks (asymmetrical and symmetrical).

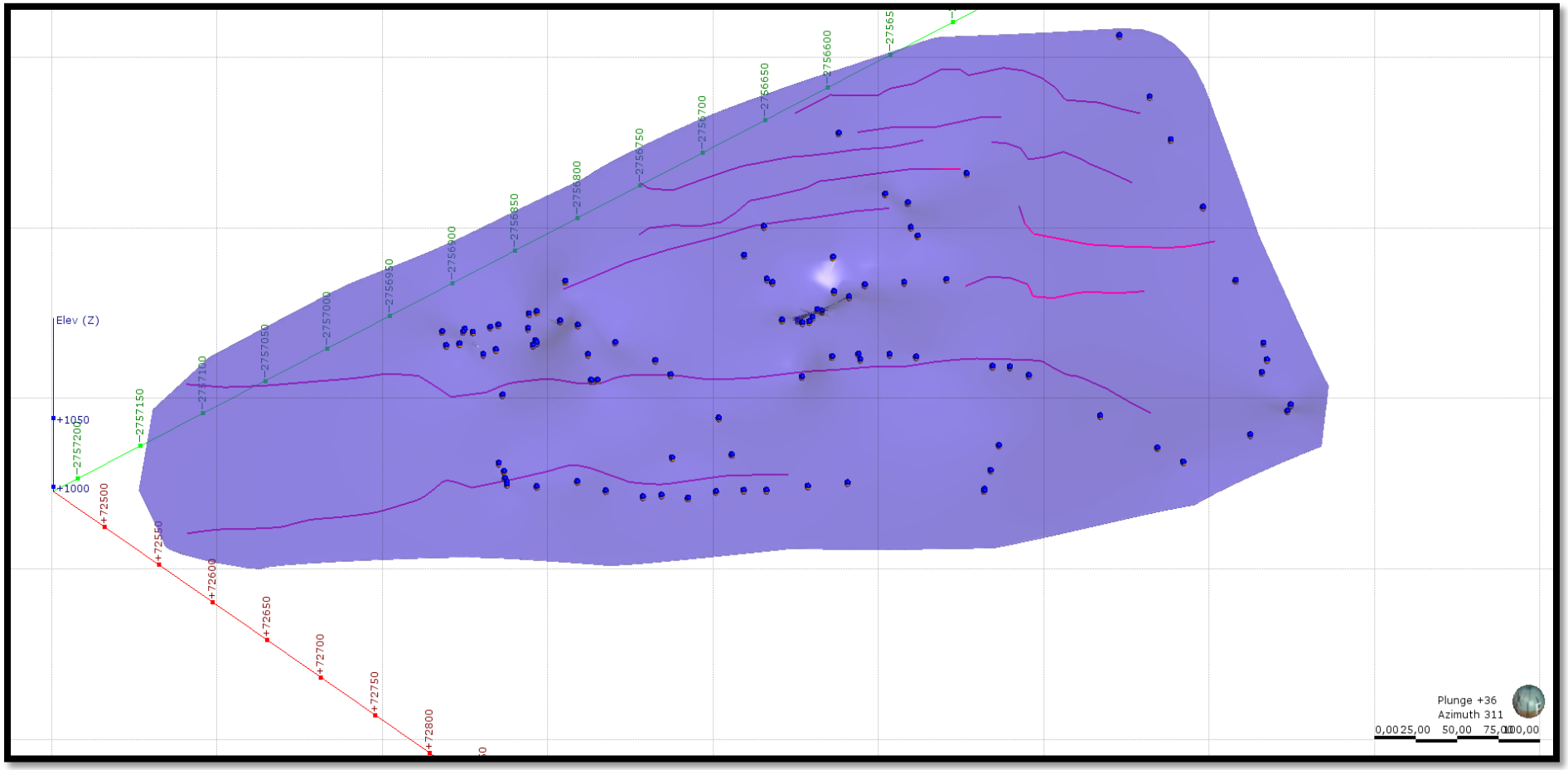

Figure 26: Side view of the modelled bedded lode for Rio Rita (purple). The hanging wall points (blue points) and footwall points (orange points) that were used to generate the "vein surface" can be seen in this figure. The points were constrained by the digitized lodes of Rio Rita (pink polylines), which also acts as the boundary for the "vein surface".

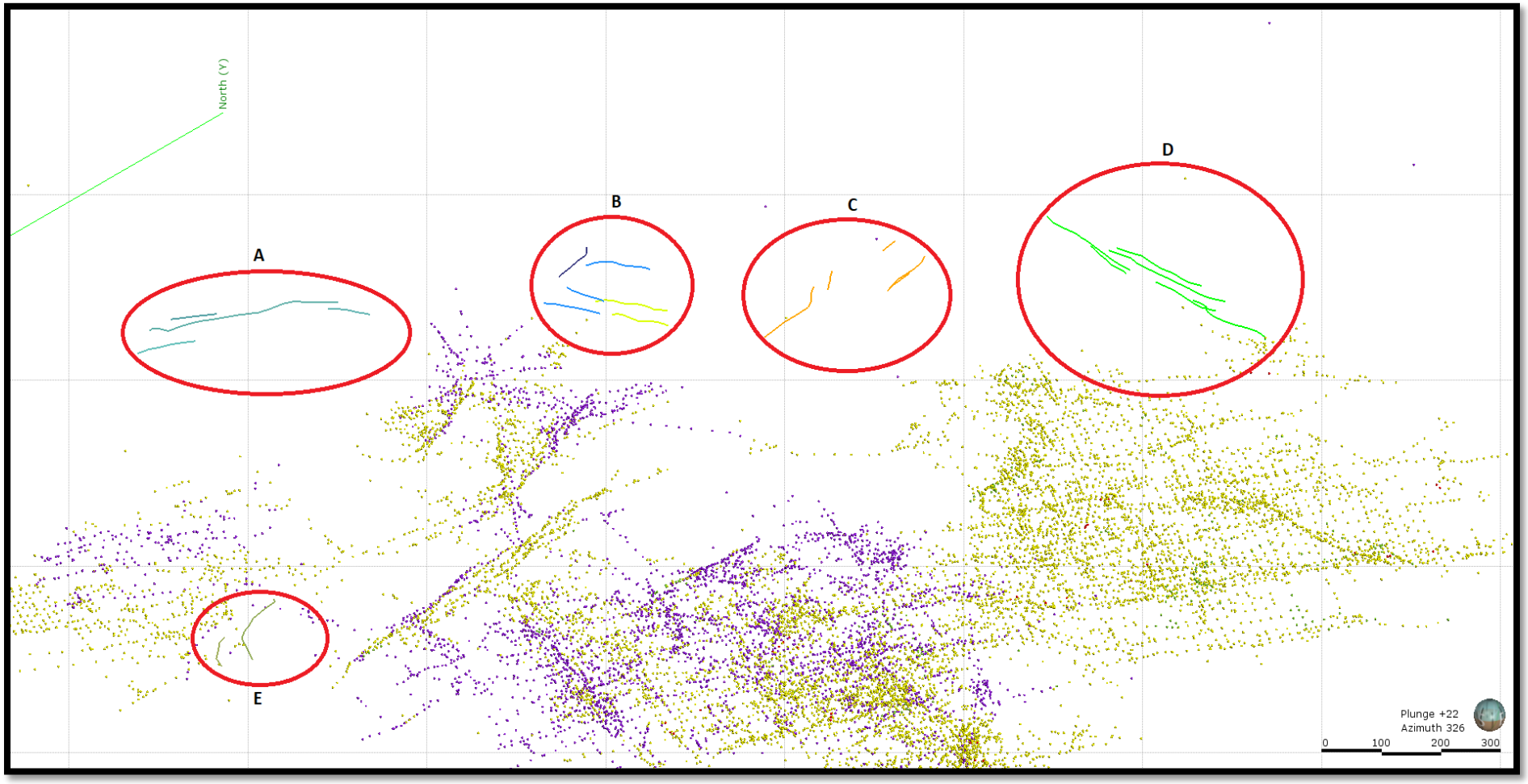

Figure 27: The seven lodes that could not be modelled due to a lack of peg points to generate the hanging wall and footwall surfaces. A: Cemetery. B: Twin Lode (brown), 1A Lode (blue) and New Lode (lime green). C: HG Workings. D: Nek Fracture. E: CNS Lode.

The lodes are mainly constrained to the Quartzite lithology. because the Shaly Quartzite/Shaly Arkose acted as a “cap rock” for ascending fluid, effectively constraining the mineralization to the Quartzite lithology (Rozendaal et al., 1995a). The exact age relationships between the bedded lodes and the fissure and faulted lodes are not know. No age dating of the tin mineralization at Leeuwpoort Mine has yet been done.

For the purpose of establishing the surface chronology of the lodes, the assumption was made that the bedded lodes were formed first and the fissure and faulted lodes were formed later. This consequently means that the bedded lodes are older than the fissure and faulted lodes. Even though this assumption might be incorrect, the cross-cutting relationships established for the surface chronology of the lodes is required to add the surfaces into the geological model. Until the exact age relationships are determined this assumption holds true for the geological model given in this thesis. Once the lodes were activated in the correct “chronology”, they were added to the geological model.

4.3.5.3. Modelling the Rooiberg Group

As mentioned in the beginning of this section, the Rooiberg Group lithology was not noted in the CMS lithology data because the majority of the drilling done on Leeuwpoort Mine was on the Leeuwpoort Farm 554 KQ. However, Rietfontein Farm 536 KQ is also part of the prospecting area and future drilling projects might be focused on this farm. For this reason, the Rooiberg Group lithology was added to the geological model. Because no actual data is available for the Rooiberg Group the map indicated in Figure 18 was used to digitize the contact surface of the Rooiberg Group. A new GIS line was created in Leapfrog Geo. The contact surface of the Rooiberg Group was digitized using the 3D polyline drawing tool. The “draw on slicer” tool was used to adjust the dip of the lithology.

The Rooiberg Group was then added as a new lithology. The Rooiberg Group was created as an “erosional surface”, however this does not refer to the actual geological process of erosion but rather the type of surface that was modelled in Leapfrog Geo (Figure 28) in order to represent an unconformity. We know that the Rooiberg Group is younger than the Pretoria Group (Table 7). The age relationship of the unit was set accordingly when the surface was activated under Surface Chronology. The Rooiberg Group was thus subsequently added to the geological model.

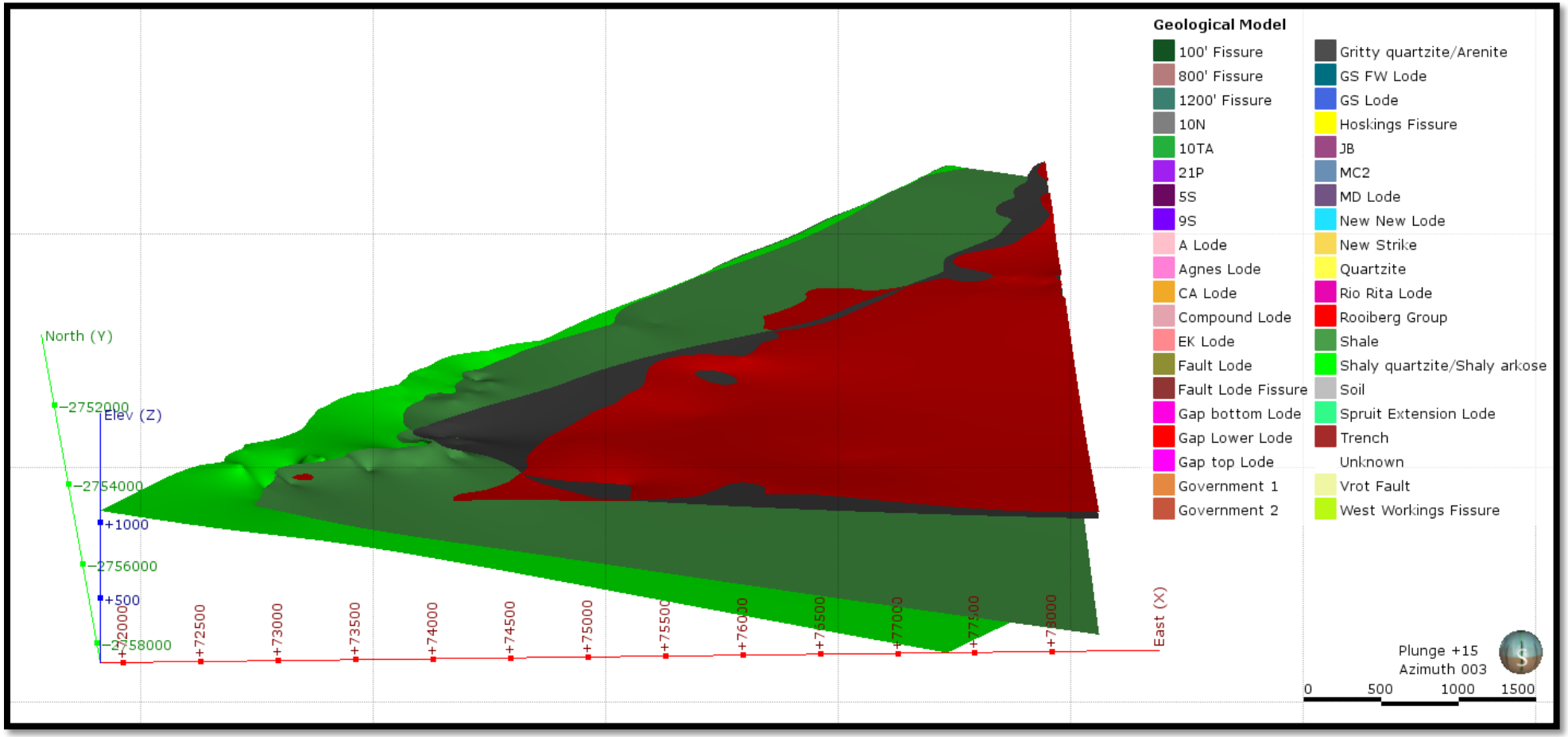

Figure 28: The Rooiberg Group contact surface (red) created in Leapfrog Geo.

4.3.6. Interpolant Models

Interpolation can be defined as a curve estimation statistical method (non-linear regression) (Griffith, 2007). If we have, for example, a set of data point in a 2D or 3D space, each having a certain numeric value (temperature, assay, height etc.) a mathematical expression has to be derived which represents the data relationships The missing points or unknown points can then be calculated using the equation of the curve. Interpolation is one of the method by which these unknown points are derived (Griffith, 2007).

Interpolant models, also known as numerical models, can be generated from any type of data that consists of points with an X-, Y-, and Z coordinate that has a related numerical values (LeapfrogGeo, 2016). The data has to be distributed across a 3D space in order for an interpolation to be generated. One of the many advantages of using Leapfrog Geo is that the shells (domains of similar value) that are created from the Interpolance are smoother and more reproducible than using the more traditional method of hand drawn meshes (LeapfrogGeo, 2016).

The general modelling approach that is followed when creating an interpolant model is as follows (LeapfrogGeo, 2016):

1. The first step is to ensure that the numerical data that will be used has been sufficiently cleaned and is error free. The quality of any model will depend on the quality of the underlying data.
2. Select the specific type of numerical data that the interpolant model will be created with. Add the specific parameters for the type of data you use. Interpolant models are created from known values. Leapfrog Geo uses these numeric values and estimates the values in between the known data points.
3. The last step is to apply a trend to the interpolant model. If assay data are used, as in the case of Leeuwpoort Mine, a trend allows to control the “strength” (ellipsoid ration) of mineralization in a specific direction. This is especially useful when dealing with structurally or stratigraphically controlled mineralization. Global or structural trends can be added to ensure that the Interpolance model is created according to the expected mineralization pattern.

4.3.6.1. Creating an overall interpolant model for Leeuwpoort Mine

The numerical values used to create an interpolant model of Leeuwpoort Mine was obtained from the log summary books. The assay data obtained from the log summary books recorded a specific tin percentage (Sn wt.-%) at a corresponding depth in a borehole. The data went through a thorough cleaning and validation process as described in Section 4.2.3. As seen in Figure 14, the assay data for the total length of the boreholes are not available, however, partial assay data for the boreholes are available.

A recommended practice to follow when creating interpolant models is to first create a quick, rough interpolant in order to see how the isosurfaces interact with one another (LeapfrogGeo, 2016). Isosurfaces can be defined as shells that confine areas or regions of similar value (in this instance assay data). Leapfrog Geo creates three isosurfaces values by default. These values are the lower quartile, median and upper quartile values of the data used (LeapfrogGeo, 2016). However, these isosurfaces values can be changed to fit the specific need of the data being used. In the case of assay data, the isosurfaces could be changed to fit certain cut-off values.

Once a rough interpolant model has been created, a complete interpolant model of the area can be built using all the aspects of the available data (LeapfrogGeo, 2016). Interpolants can be created in Leapfrog Geo, under the “Interpolants folder”. The new interpolant has to be defined by a set of numeric values, which in the case of Leeuwpoort Mine, are the assay data was used. Next a boundary or volume has to be selected to model. The boundary for the interpolant model of Leeuwpoort Mine was chosen as the existing geological boundary. The partial assay data are essentially 3D points that are sparsely distributed throughout the geological boundary and can thus be used to interpolate across the region.

The interpolant has now been created for the whole geological area, but no structural trends have been added to the interpolant yet (Figure 29). This means that the strength of the mineralization has not yet been defined. Without changing any of the important parameters, the interpolant model looks unrealistic.

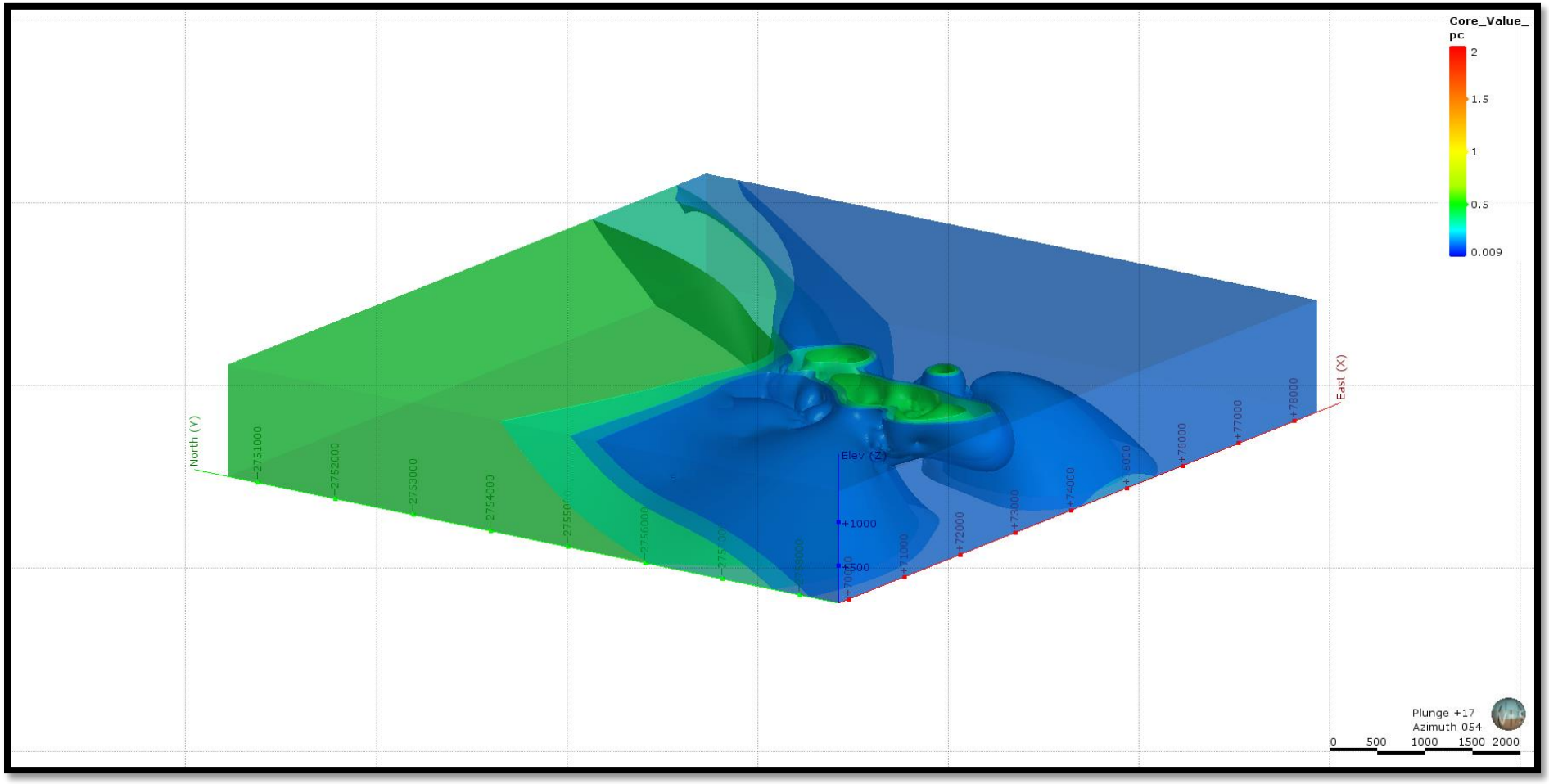

Figure 29: Interpolant created for the whole geological area. This interpolant was created to view the interaction of the isosurfaces. No structural trend where added in this interpolant. A grade scale (Sn wt.-%) can be viewed in the right-hand corner of the figure (core value pc).

4.3.6.2. Creating a refined interpolant model

4.3.6.2.1. Choosing the type of interpolant model

Leapfrog Geo currently has two different types of interpolant models that can be created: “linear interpolant” or “spheroidal interpolant”. Linear interpolant models are ideal for lithological data and for quick trend visualization (LeapfrogGeo, 2016). However, linear interpolants are not ideal for cases where a finite range of influence can be defined (geological reality). Linear interpolants assumes that the influence of a certain distance away from a known point will be greater for a distance closer to the known point than a distance further away. Using spheroidal interpolants, on the other hand, assumes that there is a finite range beyond which the influence of a certain distance from a known point will become zero. Therefore there is a finite distance where two point will not influence one another (LeapfrogGeo, 2016)

In order to refine the interpolant model for Leeuwpoort Mine the type of interpolant model to be used has to be determined. There are three important aspects to consider before creating a refined interpolant model of Leeuwpoort Mine:

1. Majority of the mineralization at Leeuwpoort Mine is confined to the Quartzite lithology.
2. The lodes are structurally and stratigraphically controlled.
3. Only partial assay data for each borehole is available.

As discussed in the previous Sections, the lodes were formed by the infilling of fractures caused by a complex shear system (Phillips, 1982). The shear system itself consists of varying shears of different ages, orientation, and magnitudes. The size and magnitude at which these shear events took place resulted in the formation of varying types of omnidirectional mineralization. The formation of the structurally complex shear system and the source of the mineralization is considered to be due to the intrusion of different granitic magmas surrounding the Rooiberg Fragment (Phillips, 1982).

Geological interpretation implies that the metasomatic fluid ascended from the magmatic intrusions and the fluids where mobilized throughout the cracks and fractures of the complex shear system, as illustrated in Map C893. Map C893 is a 1:9000 cross-sectional map of Leeuwpoort Mine, and can be viewed in Appendix 1. The inferred contact between the Quartzite lithology and the Bushveld Granites is indicated on this map. The complex shear system could have acted as feeders to form the lodes. Different pulses of fluids would have had different compositions and intrinsic characteristics, temperatures, and pH.

It stands to reason that that the concentration of the tin bearing fluid would decrease away from the feeder. If multiple feeders are located in close proximity to one another these mineralizations will overlap. These assumptions were made and accepted and it was determined that the best type of interpolant model, at present, is the linear model.

4.3.6.2.2. Creating an interpolant for the Quartzite domain

We know that the mineralization at Leeuwpoort Mine was constrained to the Quartzite lithology. An interpolant model can be created for the Quartzite lithology by "clipping" (restraining) the interpolant to the geological domain. Two interpolant models were created: the first being the interpolant model for the whole geological boundary and the second being the Quartzite interpolant model. By "clipping" the interpolant to an economical lithological domain, a reasonable volume result can be created.

In the new Quartzite interpolant model, the boundary was adjusted by changing the "lateral extent" of the interpolant as the Quartzite output volume. This means that the interpolant model will re-run and create an interpolant model for only the Quartzite domain (Figure 30). The interpolant model has changed in two different ways when compared to the original interpolant model for the geological boundary. 1) The isosurfaces have been clipped to the Quartzite boundary. 2) The assay data has been clipped to the Quartzite boundary (LeapfrogGeo, 2016). When the 0.4 wt.-% Sn isosurfaces of the linear interpolant model for the Quartzite domain is viewed, the structure of the lodes become evident (Figure 31 and Figure 32).

4.3.6.2.3. Adding structural data to the interpolant model

During the post-mortem study of Leeuwpoort Mine, very limited structural data had been recovered. The lodes at Leeuwpoort Mine were formed by stratigraphically and structurally controlled open space filling processes. The lodes where modelled using the peg index and reflect the spatial orientation and position of the lodes.

Global or structural trends can be used to refine interpolant models. Global trends are usually used when minimum structural data is available and an overall view of the mineralization in a specific direction is required. Structural trends can refine the interpolant models the best as multiple trends can be identified and used. Multiple structural trends, each with varying "ranges" and "strengths", can be used to refine mineralizations. Structural trends are especially useful when working with multiple zone of varying grade (LeapfrogGeo, 2016).

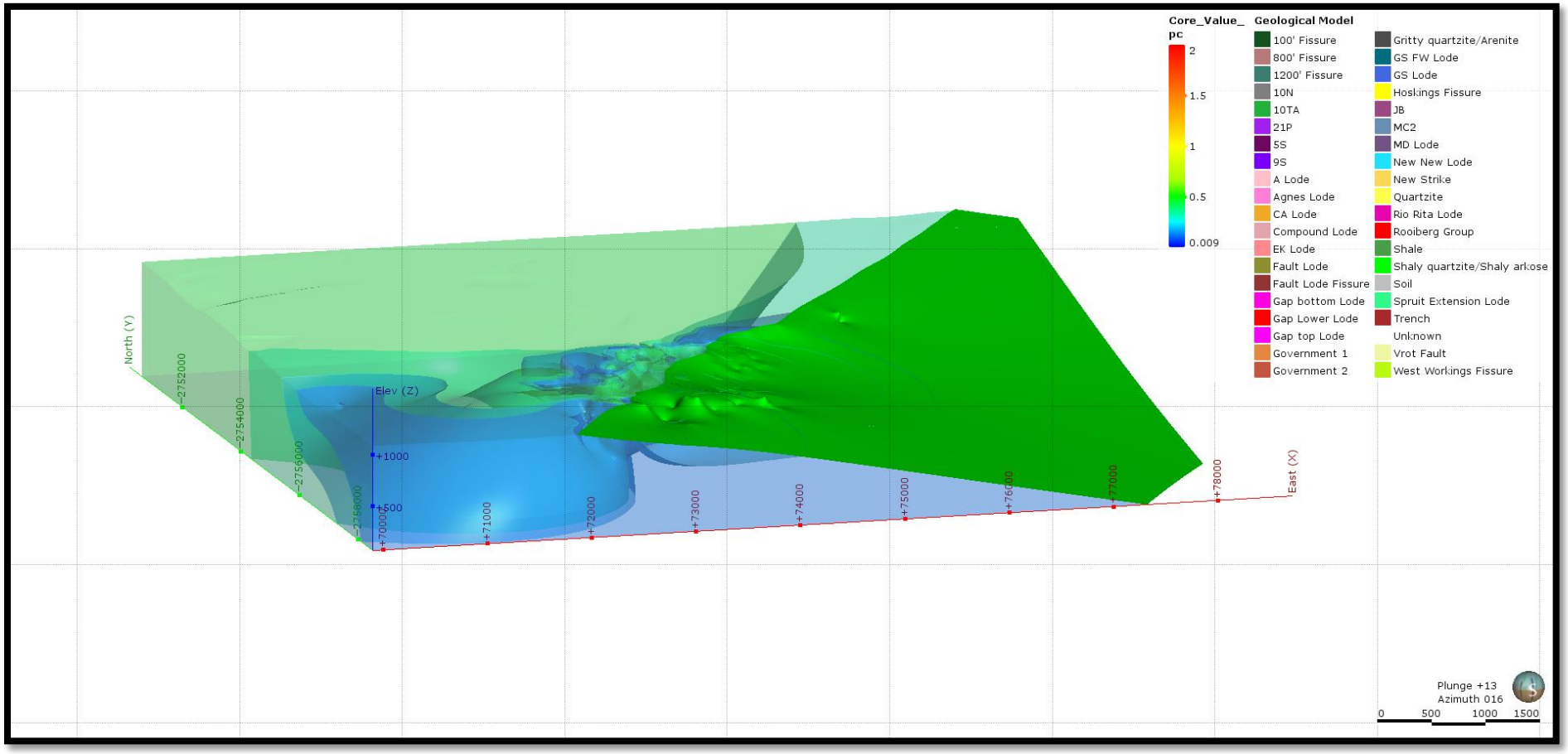

Figure 30: Linear interpolant model for the Quartzite lithological domain. The green surface indicates the contact surface between the Quartzite lithology and the Shaly Quartzite/ Shaly Arkose lithology. A grade scale (Sn wt.-%) is present (core value pc) in the right-hand corner of the figure, next to the legend of the geological model

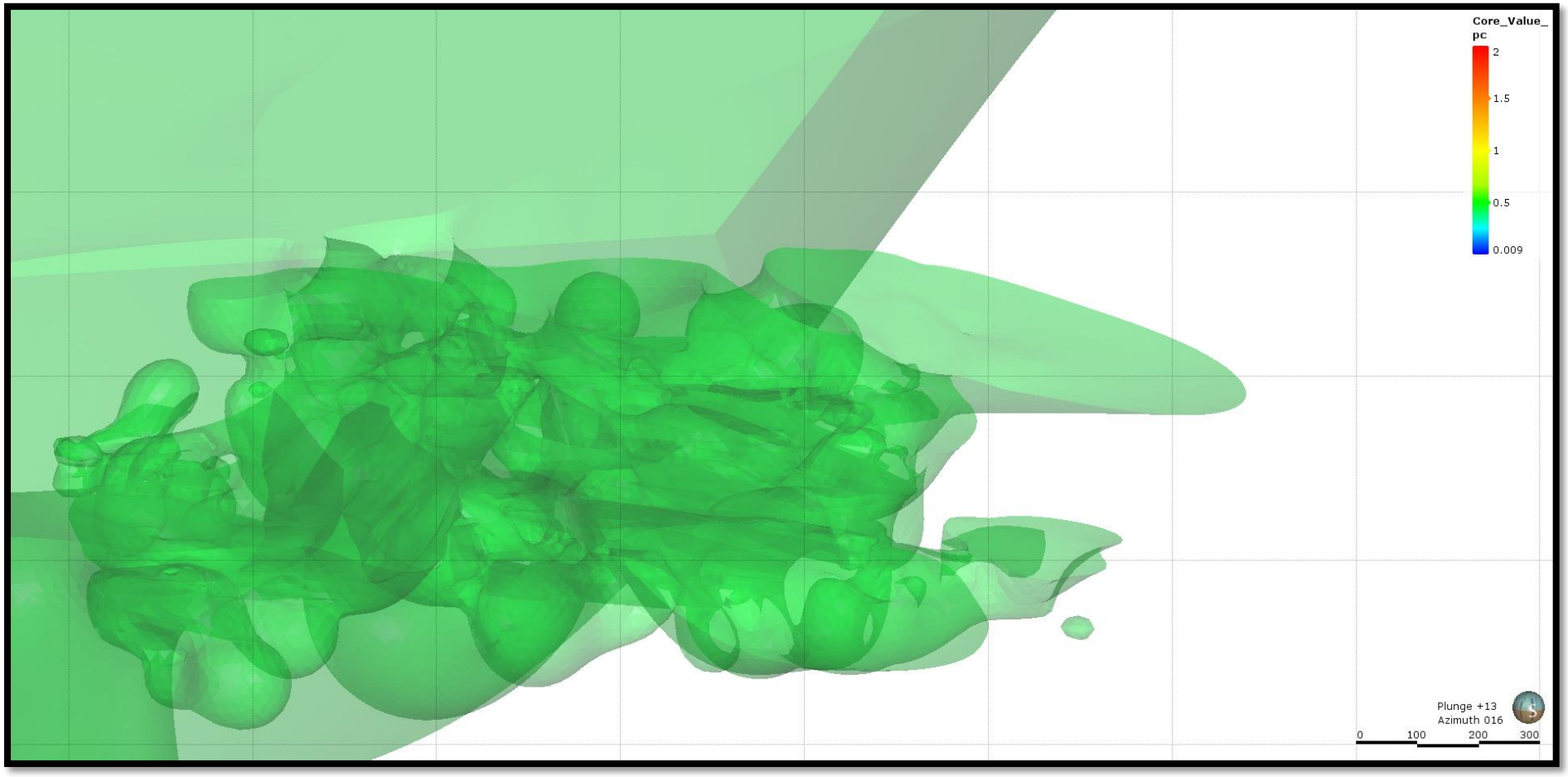

Figure 31: When viewing the 0.4 wt.-% Sn isosurfaces of the linear interpolant model for the Quartzite domain is viewed, the lode structures become evident in the interpolant. A grade scale (Sn wt.-%) is present (core value pc) in the right-hand corner of the figure, next to the legend of the geological model.

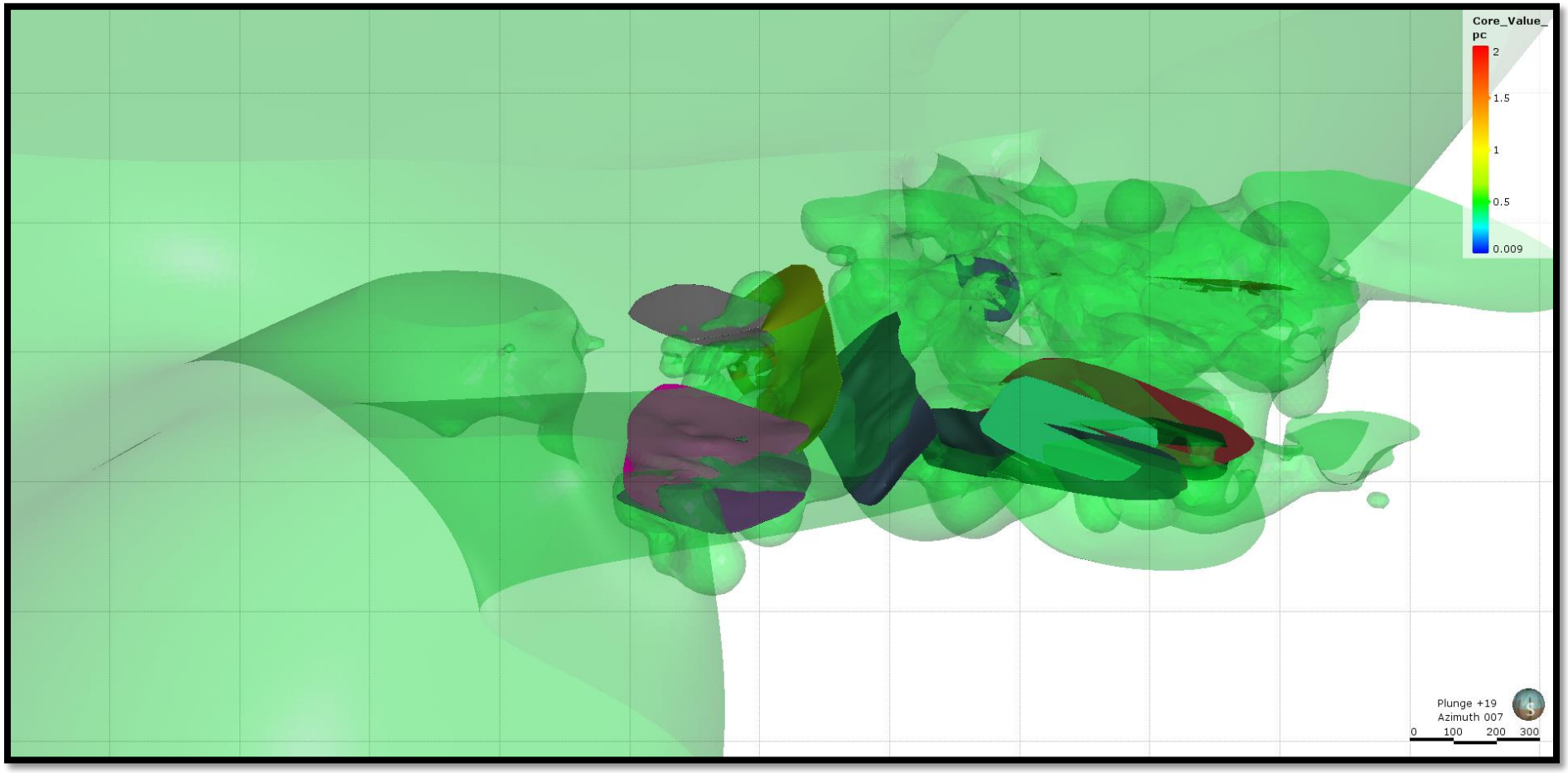

Figure 32: When viewing the 0.4 wt.-% Sn isosurfaces of the linear interpolant model for the Quartzite domain is viewed, the lode structures become evident in the interpolant. The lodes have been highlighted in order to better view them. A grade scale (Sn wt.-%) is present (core value pc) in the right-hand corner of the figure, next to the legend of the geological model.

Because the linear interpolant type was chosen to model the interpolants at Leeuwpoort Mine, a global trend can be used to refine the interpolants. Structural trends cannot be used in Leapfrog Geo in conjunction with linear interpolant models but only with spheroidal interpolants. Majority of the ore at Leeuwpoort Mine is found in the bedded lodes. The bedded lodes strike east of north and have a dip of approximately 20 degrees to the east-southeast and conform closely to the bedding planes of the Quartzite lithology (Phillips, 1982). However, the mineralization is not constrained to one bedding plane, but rather occurs on multiple planes. Lode transgression took place mainly due to the lenticular nature of the sandstone body in which the lodes where formed (Phillips, 1982).

In Figure 33 the bedded lodes of Leeuwpoort Mine are shown in conjunction with the contact surface between the Quartzite and Shaly Quartzite/Shaly Arkose lithologies. A global trend for the bedded lodes was derived: dip: 16.1, azimuth: 126.5, pitch: 92.6. When this global trend is applied to the linear interpolant for the Quartzite lithological domain a significant change in the interpolant can be seen (Figure 34).

A global trend refines an interpolant model to some extent. However, in order to have an interpolant model that does not contradict geological knowledge, structural information is needed. Sufficient structural information will allow us to use structural trends to build a refined interpolant model, however, at present this information is not available.

4.3.6.2.4. Creating interpolant models for the lodes

Just as an interpolant model of the Quartzite lithology was created, interpolant models can be built for all the lodes. By creating the interpolant models for the lodes we are able to identify the areas of economic interest. The interpolant model could also be used to identify specific portions of a lode that will be minable depending on the cut-off grade, providing the information is available. The isosurfaces could be changed to specific cut-off grades.

Because assay data are used to build the interpolant models, we are dependent on the quality and quantity of the assay data. In Figure 14 we can see that only partial assay data for each borehole is available to create interpolants. When we created the overall interpolant model for the whole geological boundary as well as the interpolant model for the Quartzite lithology, the partial assay data was used. Because these interpolants cover a large spatial extent, the partial assay data was intersected by the interpolant boundaries. However, when considering that each of the lodes are modeled to be only one meter thick and covers a significantly smaller spatial extent than the other boundaries, the incomplete assay data becomes problematic.

A significant amount of assay data intersections per modelled lode is needed to create an interpolant that represents the assay distribution. If no assay data is available for the lodes volumes, it will not be possible to create an interpolant for that lode. Leapfrog Geo will inform you that you have insufficient values to create the interpolant. In Figure 35 the example of Spruit Extension Lode (bedded lode) is used to show that no assay data is available for the lode volume. The complete assay data must have been produced during the life of mine in either the preproduction or the quality control on the production, but the data has not been found. An interpolant for Spruit Extension Lode could thus not be modelled.

An interpolant can also not be created if only one assay value is available for the lode volume. In this case, Leapfrog Geo will generate an “empty” interpolant. Only 9 out of the 32 lodes have sufficient assay information to create interpolants with. The interpolant models that were created in Leapfrog Geo are used in the following sections to determine the applicability of 3D modelling for exploration purposes.

4.3.7. 3D models and its application to exploration predictions

3D models and their application in the mining industry are becoming increasingly important. Mining models, geological models, ore deposit models, financial models, and grade-tonnage models all have a symbiotic relationship and form a key component in any mining related environment. The technological advancements made in the last decade have enhanced the practical visualization of complex geological environments. This has allowed geologists and non-geologists alike to conceptually grasp complicated scenarios by viewing the problems in a 3D environment (Cowan et al., 2002; Wu et al., 2005; Singer, 1993).

The development of implicit modelling software, as opposed to explicit modelling, has allowed geologist the comfort of using user-friendly software. These technological advancements have minimized a previous time-consuming process. The effectiveness and accuracy of any geological model depends on the competence of the person responsible for creating these 3D models (Reid, 2017). Competency of the creator goes hand in hand with the completeness and accuracy of the data used to create these models.

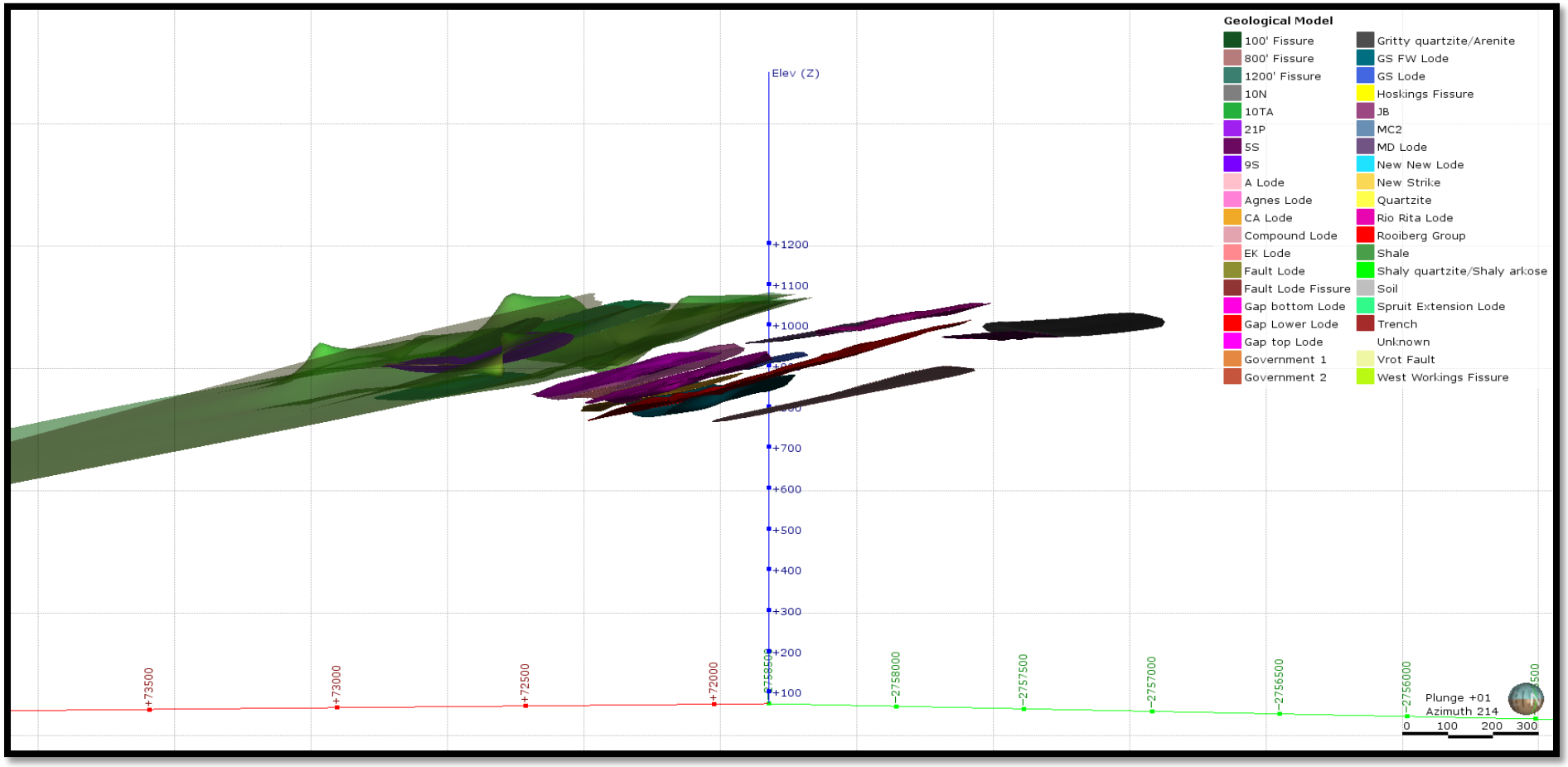

Figure 33: Bedded lodes of Leeuwpoort Mine in conjunction with the contact surface of the Quartzite and Shaly Quartzite/Shaly Arkose lithologies (green surface). The bedded lodes strike east of north and have a dip of approximately 20 degrees to the east-southeast. The bedded lodes conform closely to the bedding planes of the Quartzite lithology.

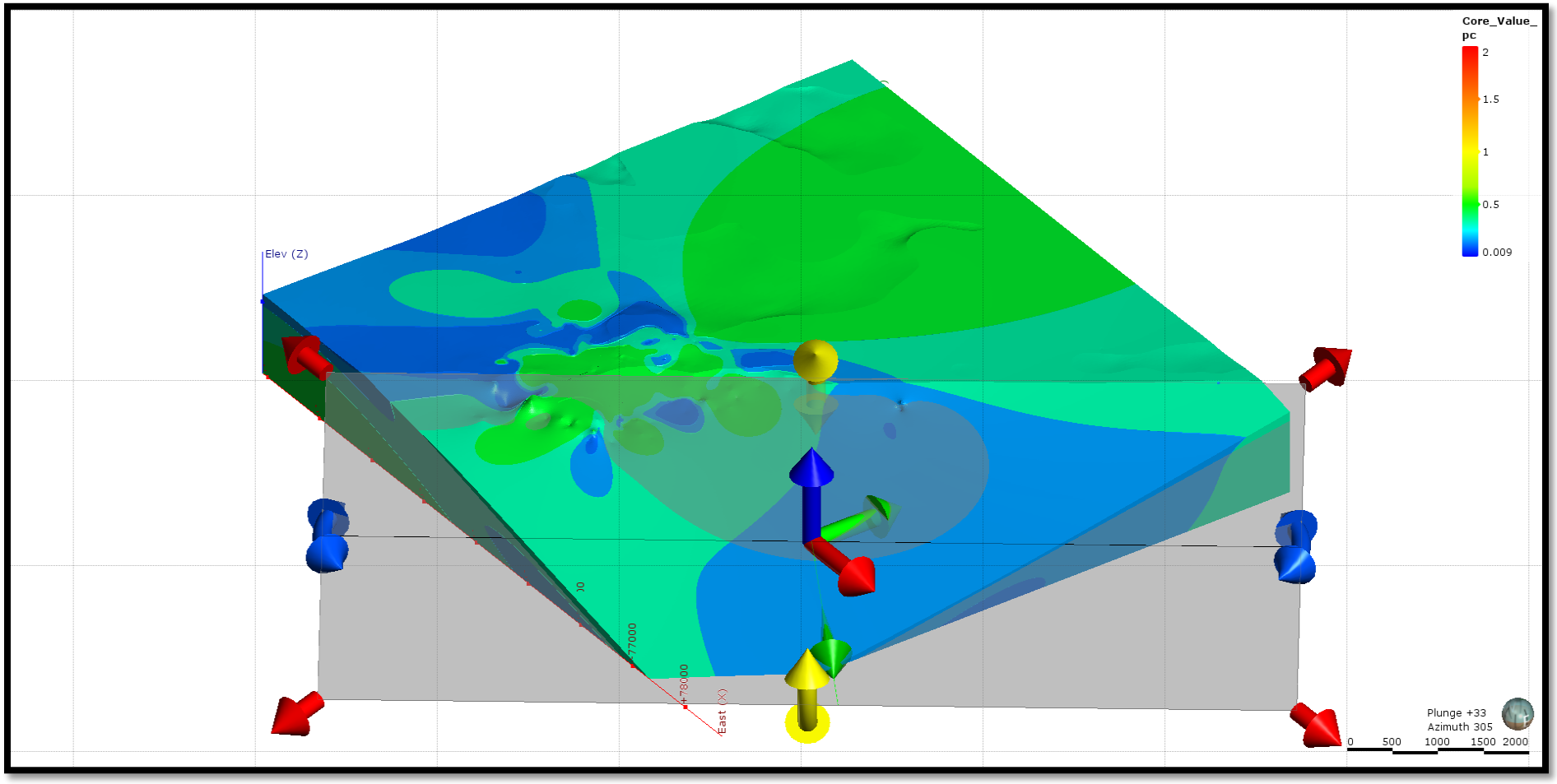

Figure 34: A global trend for the bedded lodes (dip: 16.1, azimuth: 126.5, pitch: 92.6) was applied to the linear interpolant for the Quartzite lithological domain. The global trend is represented as a plane for viewing purposes.

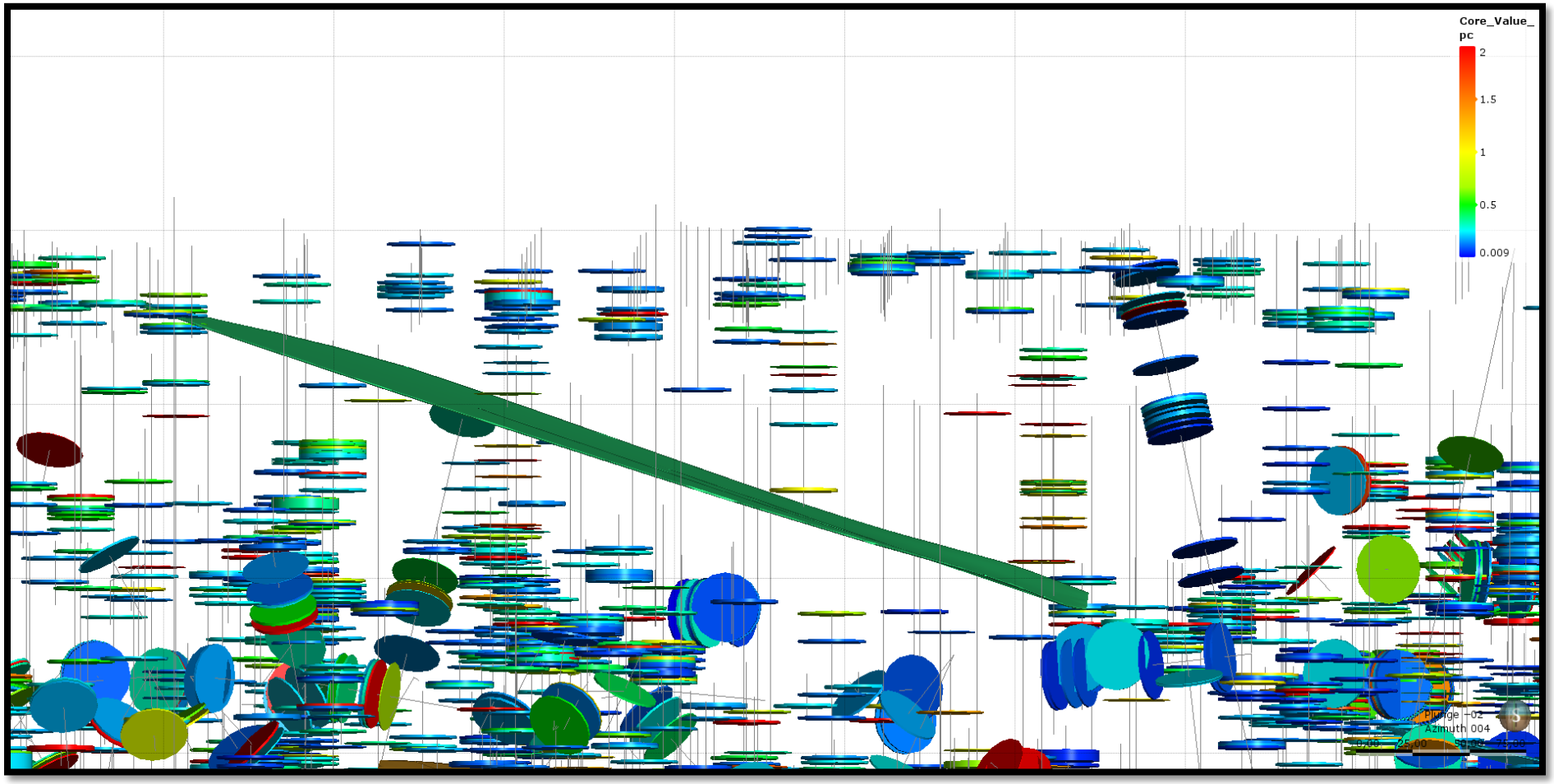

Figure 35: Spruit Extension Lode (green surface volume) with the available assay data (disks). No assay data is available for the lode surface. Due to insufficient assay information an interpolant cannot be generated for Spruit Extension Lode. A grade scale (Sn wt.-%) is present (core value pc) in the right-hand corner of the figure, next to the legend of the geological model

3D models are not just used to visualize geological environments, but can also be used as a tool for prediction and planning of future drillholes. They are updated regularly to fit current mining condition especially for resource and reserve estimation purposes, as well as to determine the best spatial location to add more drillholes. They can also be used to determine the best possible mining location to optimize ore extraction when the cut-off grade is changed.

This section discusses the processes followed to determine what the probability for intersecting a lode of economic interest is. This section includes the process of drillhole planning in Leapfrog Geo, as well as the evaluation of these planned drillholes against estimated assay values. The use of bootstrapping as a statistical method to determine the probability of economic intersection is discussed. Finally, using the 3D models created for Leeuwpoort Mine to estimate volumes of the lodes to determine the minimum contained metal for each of the individual lodes.

4.3.7.1. Planned drillholes and the probability of lode intersection

The main goal of the exploration prediction is to determine the probability of successful exploration drilling. Before starting the process of drillhole planning in Leapfrog Geo, the following assumptions are made:

1) We assume that exploration is required in a tin field that was formed by the same conditions as Leeuwpoort Mine. A stratigraphically and structurally controlled exogranitic hydrothermal processes formed this tin field. This area is as structurally complex as Leeuwpoort Mine.
2) We assume that Greenfield exploration is taking place and no prior exploration knowledge is available for this prospecting area.
3) 500 random drillholes/boreholes will be planned in a defined spatial boundary. These boreholes are planned to be drilled from surface at a 90 degree dip to a depth of 300m.
4) The planned drillholes and all related information obtained from these planned drillholes are based on the 3D geological model. Assay data and interpolant models are used to estimate the new values created for the planned drillholes.

Planned drillholes can easily be done in Leapfrog Geo. The output of the planned drillholes includes estimated grade data as well as expected lithology based on existing models and survey data.

4.3.7.1.1. Determining the boundary of the planned drillholes

The “planned drillhole” function in Leapfrog Geo uses the assay and lithological files of the 3D geological model. It is thus important to confine the boundary of the planned drillholes to an area where sufficient information is available. The defined spatial boundary coincides with the current drillhole boundaries of the CMS surface boreholes (Figure 36). Anything outside the current drillhole boundary is an estimated value and will have a high level of uncertainty.

CMS 6 and CMS 7 were excluded from this boundary as they are located at the Northern portion of the prospecting area. The majority of the CMS boreholes are located in the central area of Leeuwpoort Farm 554 KQ. The spatial distance between the central boreholes and CMS 6 and CMS 7 is too large and any correlation between these sets of borehole data will not lead to meaningful estimates.

4.3.7.1.2. Generating data for the planned drillholes

In order for the probability predictions to be unbiased, the location (spatial coordinates) of the planned drillholes must randomly selected. The random coordinate selection was achieved using “random functions” in Excel. The boundary limits were used as maximum and minimum coordinate values in order for the selected random coordinates to fall inside the boundary. The first step was to give a unique borehole identification number to each of the 500 planned drillholes. The planned drillholes were named Planned Borehole (PB) 1-500 respectively.

Once the unique borehole identifications were created, the collar file for the planned drillholes could be generated. The collar file consists of randomly generated X-, Y- and Z coordinates (for adjustment of the Z coordinates see Section 4.3.7.1.3). The random function in Excel generates a random value between 1 and 0. Because the planned drillholes needs to be constrained to specific boundary we need to specify the minimum and maximum lateral extent of the boundary within the random function needs to be specified. This will ensure that no randomly generated borehole coordinates will fall outside the boundary

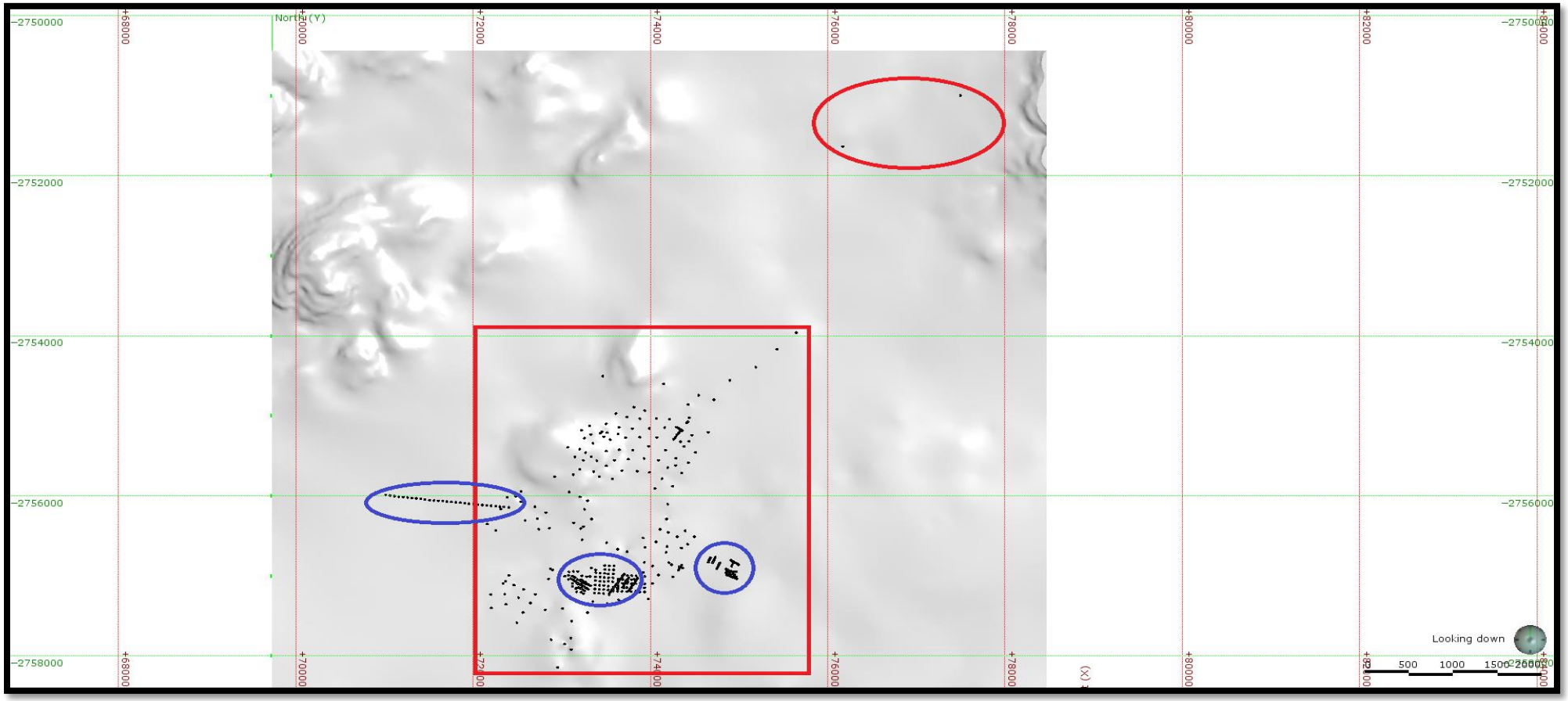

Figure 36: Boundary (red block) selected for the planned drillholes. The CMS surface boreholes were used to constrain the boundary. CMS 6 and CMS 7 are located in the top right hand corner of figure (red circle). The spatial distance between the central boreholes and CMS 6 and CMS 7 is too large and any correlation between these sets of borehole data will not lead to meaningful estimates. The CMW surface boreholes (blue circles) were not considered for the boundary because information for these boreholes are limited.

The start value that was used to generate the random coordinates are the minimum X-, Y- and Z coordinates of the defined boundary (Figure 36). The lateral extent was defined as follow:

(X- or Y- or Z) START= (X- or Y- or Z) MINIMUM

The maximum was calculated by subtracting the minimum coordinate value from the maximum coordinate value (Table 8). The maximum is the amount that needs to be added to the START value to ensure the random coordinate selection is constrained to the boundary.

(X- or Y- or Z) MAX= Maximum (X- or Y- or Z coordinate) – Minimum (X- or Y- or Z coordinate)

Table 8: Minimum (X, Y and Z) coordinates, Maximum (X, Y and Z) coordinates of the boundary used to constrain the random drillholes (PB 1-PB 500). The start and maximum values where used in random function to calculate the collar coordinates for the planned drillholes. The start and maximum values ensure that the randomly generated collars are constrained in the boundary.

	X	Y	Z
Maximum coordinate	75645.945	2753961	1176.972
Minimum coordinate	72158.97	2758143	1079.422
(X, Y, Z) Start	72158.97	2758143	1079.422
(X, Y, Z) Maximum	3486.975	4182.148	97.55

The random function used to create the collar coordinates for the planned drillholes is:

RAND()*(X, Y, Z) Maximum+ (X, Y, Z) Start

4.3.7.1.3. Adjusting the collar elevations of the planned drillholes

The randomly generated Z-coordinate (collar elevation) does not fit the topography. Because it is assumed that the planned drillholes will be drilled from surface, the collars of the boreholes must accurately conforms to the topography. A new collar elevation has to be created that represents the conformed collar on the topography. The easiest way to ensure that the collar elevation conforms to the topography is to use Leapfrog Geo to set the collars to the topographical surface. Table 9 is an extract of the data for the randomly planned drillholes (see Appendix 3 for the complete list of the planned drillholes).

Table 9: Extract of the randomly generated data for the planned boreholes (PB). The collar elevation in this table does not conform to the topographic surface. The data was imported into Leapfrog Geo as point data to generate new collar elevations for each planned borehole. The complete table with the data for all 500 planned boreholes can be viewed in Appendix 3.

BH id	X-Coordinate	Y-Coordinate	Collar Elevation
PB1	73861.09	-2754409.88	1104.86
PB2	72693.26	-2755625.48	1145.51
PB3	73779.89	-2755221.78	1110.31
PB4	73493.08	-2756222.55	1172.44
PB5	75537.12	-2756130.80	1170.40
PB6	73171.23	-2755074.81	1153.20
PB7	72868.76	-2754678.89	1118.95
PB8	75153.22	-2757044.63	1082.86
PB9	73884.54	-2755274.23	1159.72
PB10	75473.31	-2754371.37	1117.57
PB11	73058.79	-2756672.33	1161.32
PB12	72993.57	-2754487.07	1164.14
PB13	73832.16	-2754946.32	1083.83
PB14	75198.62	-2754498.57	1165.03
PB15	72344.83	-2757322.97	1110.73
PB16	74286.02	-2754948.66	1114.69
PB17	73559.47	-2756892.89	1119.54
PB18	74048.43	-2755180.88	1100.07

The planned boreholes were imported as points into Leapfrog Geo. Once the points have been correctly imported the elevation of the points could be changed. The “set elevation” function overrides the current collar elevation and gives each point a new elevation depending on the elevation surface selected. The topography was selected as the surface for which the points needed to be set. The new planned borehole data was exported from Leapfrog Geo. The collar file now contained the correct data for each planned borehole: X and Y coordinate with a collar elevation that conforms to the topography.

4.3.7.1.4. Creating planned drillholes in Leapfrog Geo

Leapfrog Geo has a folder in which planned drillholes can be created or bulk imported. The “planned drillhole” function allows the user to choose whether to start a planned drillhole at a collar or a specific target. The path of the drillhole can also be controlled by changing the lift (vertical movement), drift (horizontal movement), total depth, and specific distance past target. Specific drilling phases can be specified to allow easy planning for future exploration.

In order to do a bulk import of planned drillholes in Leapfrog Geo the following information is needed in a csv spread sheet: Drillhole name (borehole ID), easting (X coordinate), northing

(Y coordinate), Elevation (collar elevation), azimuth, dip, lift rate, dip rate, distance, extension and target depth (LeapfrogGeo, 2016). The planned drillholes start at surface at a 90 degree dip to a depth of 300m. The lift rate, drift rate, distance and extension was entered as 0 in the import table. Table 10 is an extract of the import table for the planned boreholes (see Appendix 4 for the complete list of the import table of the planned drillholes).

4.3.7.1.5. Viewing the drilling prognosis of the planned drillholes

All 500 planned boreholes were imported and can be subsequently viewed in Leapfrog Geo (Figure 37). A prognosis was created for all 500 planned boreholes and indicates the expected grade and lithology at depth for each planned borehole based on the 3D geological and interpolant model. The planned drillhole folder includes a “drilling prognosis” option from which the geological model was selected to evaluate the lithology for the planned drillholes. The linear interpolant model for the whole geological area (Figure 29) was used to determine the expected grade down hole. The drilling prognosis of the expected grades where manually exported to create a new database for the grade data of the planned boreholes. An extract of the expected grade data can be viewed in Table 11.

However, the tin is constrained to the lodes in the Quartzite lithology. We thus assume that anything outside the tin mineralization will be barren (not containing any tin). The drilling prognosis for the grade data has to be evaluated against the tin mineralizations in order to determine what the expected grade will be if a lode is intersected. From this we will be able to determine what the probability is of intersecting a specific grade as well as the probability of intersecting a certain number of lodes.

Table 10: Extract of the import table for the planned boreholes. The complete table with the import data for all 500 planned boreholes can be viewed in Appendix 4.

Drillhole Name	Easting	Northing	Elevation	Azimuth	Dip	Lift Rate	Drift Rate	Distance	Extension	Depth
PB1	73861.09	-2754409.88	1202.56	0	90	0	0	0	0	300
PB2	72693.26	-2755625.48	1158.91	0	90	0	0	0	0	300
PB3	73779.89	-2755221.78	1119.88	0	90	0	0	0	0	300
PB4	73493.08	-2756222.55	1098.11	0	90	0	0	0	0	300
PB5	75537.12	-2756130.80	1142.79	0	90	0	0	0	0	300
PB6	73171.23	-2755074.81	1140.74	0	90	0	0	0	0	300
PB7	72868.76	-2754678.89	1101.84	0	90	0	0	0	0	300
PB8	75153.22	-2757044.63	1138.85	0	90	0	0	0	0	300
PB9	73884.54	-2755274.23	1117.83	0	90	0	0	0	0	300
PB10	75473.31	-2754371.37	1126.53	0	90	0	0	0	0	300
PB11	73058.79	-2756672.33	1087.67	0	90	0	0	0	0	300
PB12	72993.57	-2754487.07	1111.24	0	90	0	0	0	0	300
PB13	73832.16	-2754946.32	1130.29	0	90	0	0	0	0	300
PB14	75198.62	-2754498.57	1125.49	0	90	0	0	0	0	300
PB15	72344.83	-2757322.97	1084.34	0	90	0	0	0	0	300
PB16	74286.02	-2754948.66	1119.23	0	90	0	0	0	0	300
PB17	73559.47	-2756892.89	1103.43	0	90	0	0	0	0	300
PB18	74048.43	-2755180.88	1117.01	0	90	0	0	0	0	300
PB19	73834.7	-2754346.04	1202.78	0	90	0	0	0	0	300
PB20	73387.27	-2755488.93	1158.46	0	90	0	0	0	0	300

Table 11: An extract of the expected grade data as determined from the drilling prognosis of the planned boreholes.

Hole ID	From	To	Expected grade (Sn wt. - %)
PB1	0.00	1.00	1.0904
PB1	1.00	2.00	1.0903
PB1	2.00	3.00	1.0902
PB1	3.00	4.00	1.0901
PB1	4.00	5.00	1.0900
PB1	5.00	6.00	1.0899
PB1	6.00	7.00	1.0898
PB1	7.00	8.00	1.0896
PB1	8.00	9.00	1.0895
PB1	9.00	10.00	1.0894
PB1	10.00	11.00	1.0893
PB1	11.00	12.00	1.0891
PB1	12.00	13.00	1.0890
PB1	13.00	14.00	1.0889
PB1	14.00	15.00	1.0887
PB1	15.00	16.00	1.0886
PB1	16.00	17.00	1.0884
PB1	17.00	18.00	1.0883
PB1	18.00	19.00	1.0881
PB1	19.00	20.00	1.0880
PB1	20.00	21.00	1.0878

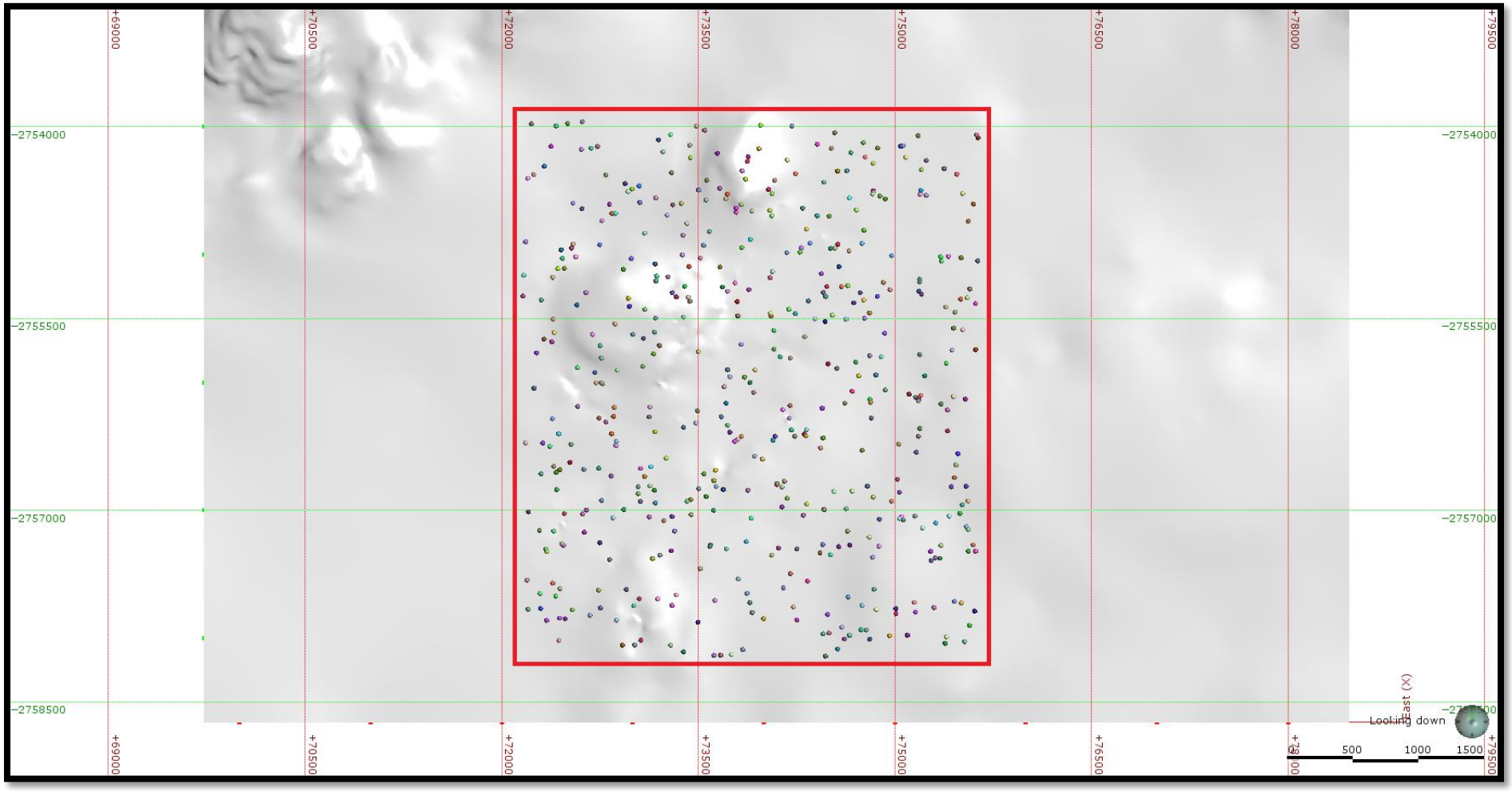

Figure 37: The collars of the 500 planned boreholes constrained within the selected boundary.

4.3.7.2. Evaluating the expected grade against the modelled lodes

In order to evaluate the expected grade data obtained from the drilling prognoses against the lodes created for the geological model. The easiest way to do evaluation is to create a new project in Leapfrog Geo. The data of the planned drillholes were imported according to the required files: collar file, survey file and interval file. The specific requirements for each file was described earlier in this section. The grade data was imported as the interval file. In order to import the lodes into a thesis the lodes have to be converted to “mesh parts”. These “meshes” were exported and imported into the new thesis.

A new geological model was created from these mesh parts as follow:

1) The lodes were added as new lithologies.
2) For each of the lodes a new surface had to be created. The “intrusion surface” was the easiest surface to use to create the lodes. The intrusion surfaces were created from the meshes. During the creation of the lodes, the first lithology was always set as the lode and the second lithology as the “unknown”. The “unknown surface” in this case refers to the barren geology containing no or insignificant quantities of tin.
3) Once all the lode surfaces had been created they were activated in the “surface chronology”. The same contact surface chronology sequence was used for the lodes as defined in the geological model of Leeuwpoort Mine

The intersection of the planned boreholes and the lodes can be viewed in Figure 38 and Figure 39. Evaluations of drillhole data were performed in Leapfrog Geo under the “Drillhole Data” folder. The first evaluation that was done was to determine the specific depth at which specific lithologies are intersected. The geological model only consists of the lodes and the “Unknown” lithology.

In Table 11 we can see that the expected grade was indicated significant tin intersections for the whole planned borehole, however, we know that tin is constrained to the lodes. In order to compensate the overestimation of the grade data a small insignificant tin percentage (0.0001 Sn %) was used to replace Unknown lithology estimations. A merged table was created from the geological evaluation and the grade data of the planned drillholes. The merged table will from now be called the exploration results. An extract of the exploration results can be viewed in Table 12.

4.3.7.3. Determining the number of lodes intersected

The exploration results were used to determine the number of lodes intersected per planned borehole (Table 13). The complete table of the lodes intersected per planned borehole can be viewed in Appendix 5. The number of lodes intersected form the bases of the exploration study. The aim is to determine the following:

1) What is the probability of intersecting a lode of economic interest
2) What is the probability of intersecting a certain number of lodes

Table 12: Exploration results obtained from the drilling prognoses and evaluations done in Leapfrog Geo.

Hole ID	From	To	Estimated grade (Sn wt. - %)	Geological Unit
PB4	164.844	165	0.5326	GS Lode
PB4	165	165.84	0.5491	GS Lode
PB4	165.84	166	0.0001	Unknown
PB4	166	167	0.0001	Unknown
PB4	167	168	0.0001	Unknown
PB4	168	169	0.0001	Unknown
PB4	169	170	0.0001	Unknown
PB4	170	171	0.0001	Unknown
PB4	171	172	0.0001	Unknown
PB4	172	173	0.0001	Unknown
PB4	173	174	0.0001	Unknown
PB4	174	175	0.0001	Unknown
PB4	175	176	0.0001	Unknown
PB4	176	177	0.0001	Unknown
PB4	177	177.489	0.0001	Unknown
PB4	177.489	178	0.7558	CA Lode
PB4	178	178.494	0.7732	CA Lode

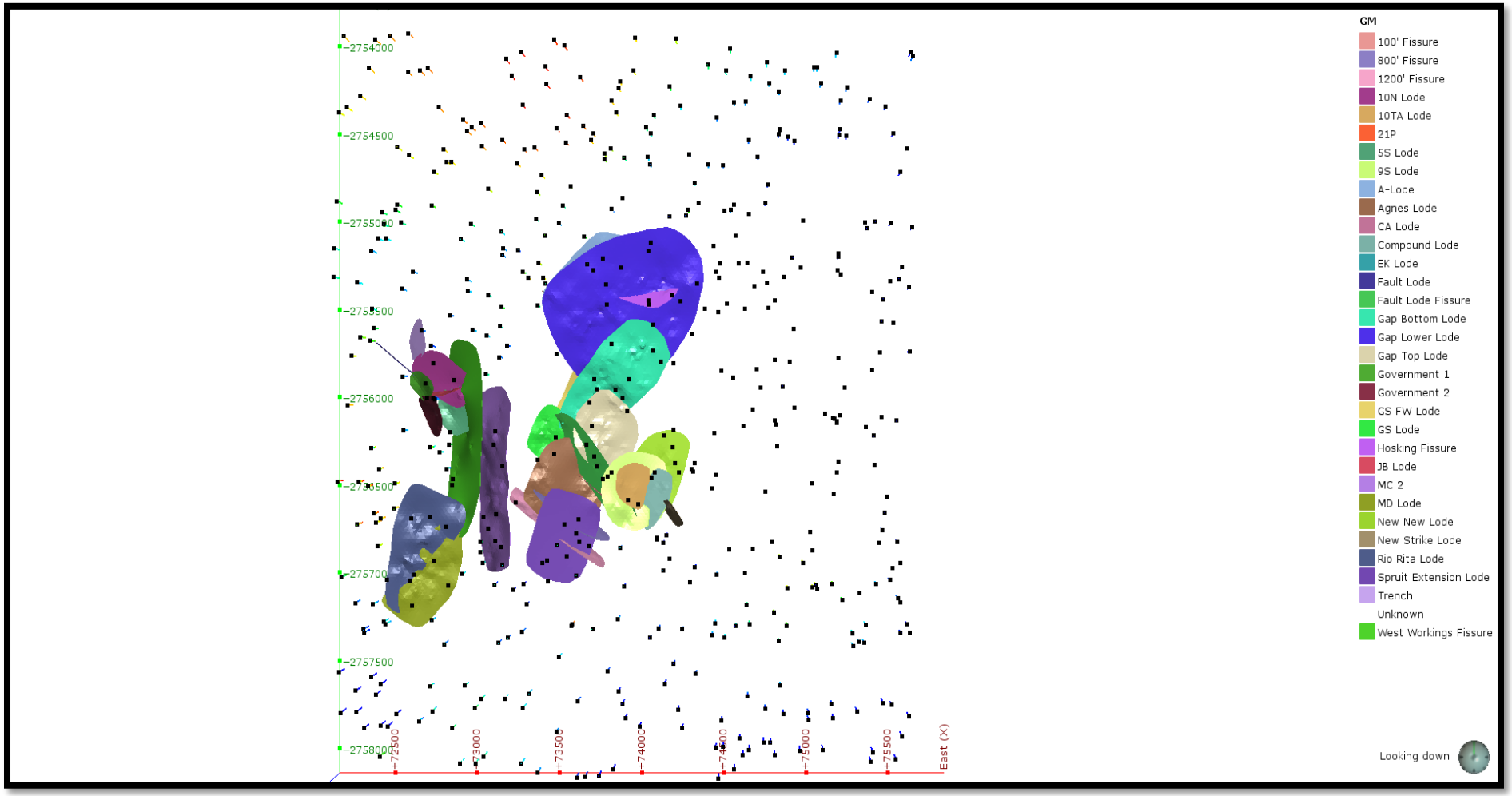

Figure 38: Plan view of the intersection between the planned boreholes and the lodes.

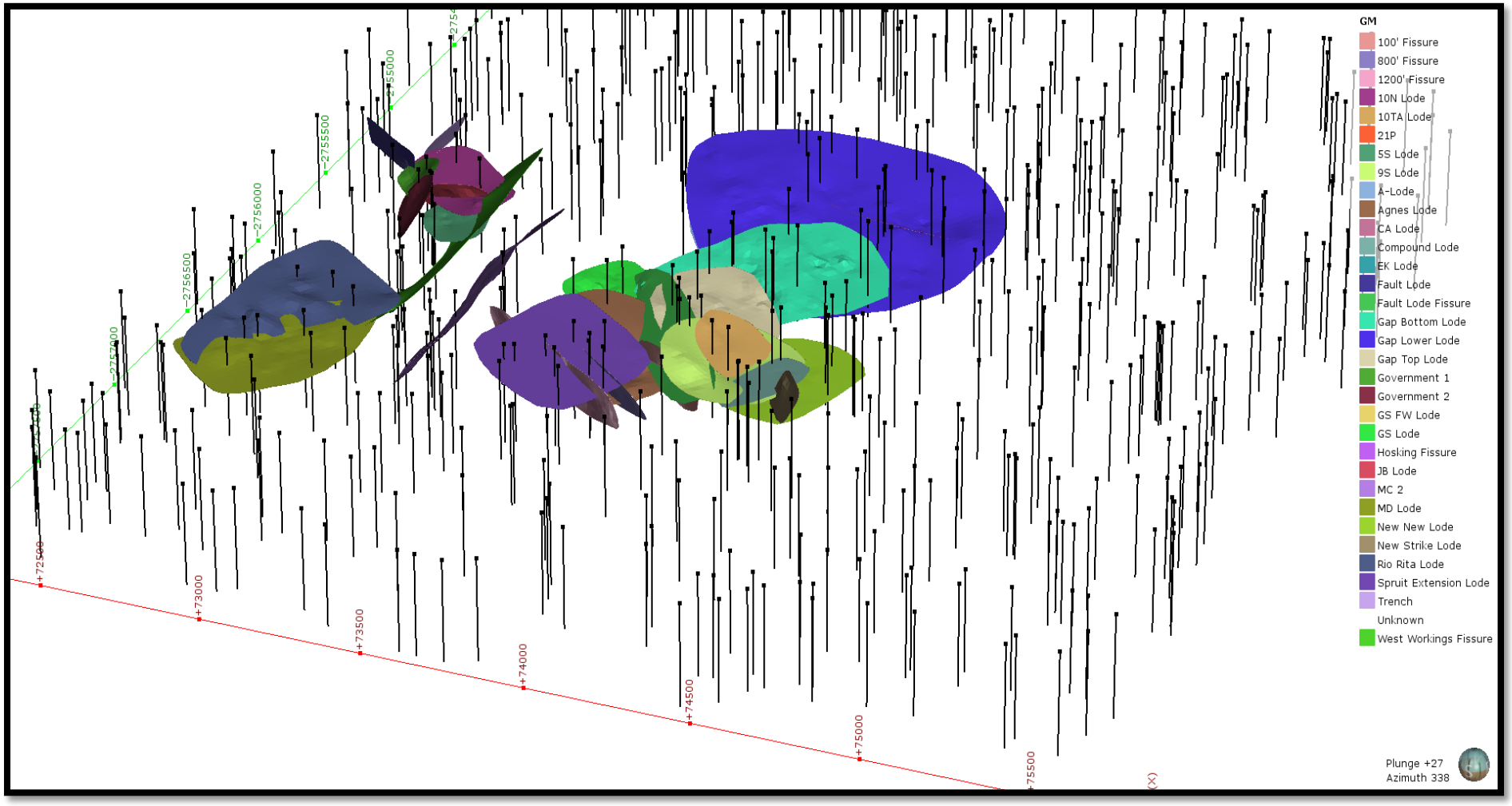

Figure 39: Side view of the intersection between the planned boreholes and the lodes.

Table 13: Extract of the number of lodes intersected per borehole. The complete table can be viewed in Appendix 5.

Hole Id	Number of lodes intersected
PB1	0
PB2	1
PB3	2
PB4	4
PB5	0
PB6	0
PB7	0
PB8	0
PB9	3
PB10	0
PB11	1
PB12	0
PB13	0
PB14	0
PB15	0
PB16	0
PB17	1
PB18	2
PB19	0
PB20	0

The results in the data are now sufficient to perform a statistical analysis of the lodes. The program IBM SPSS Statistics 23 was used to generate a frequency table (Table 14), pie diagram (Figure 40) and histogram (Figure 41) for the number of lodes intersected per planned borehole. From Figure 40 we can see that if exploration were to take place with the 500 planned drillholes there would be a 16.6% chance of intersecting a lode of economic interest.

Table 14: Frequency table created in IBM SPSS Statistics 23 for the number of lodes intersected per planned borehole

Number of Lodes intersected

		Frequency	Percent	Valid Percent	Cumulative Percent
Valid	0	417	83.4	83.4	83.4
	1	43	8.6	8.6	92.0
	2	18	3.6	3.6	95.6
	3	14	2.8	2.8	98.4
	4	4	.8	.8	99.2
	5	3	.6	.6	99.8
	6	1	.2	.2	100.0
	Total	500	100.0	100.0	

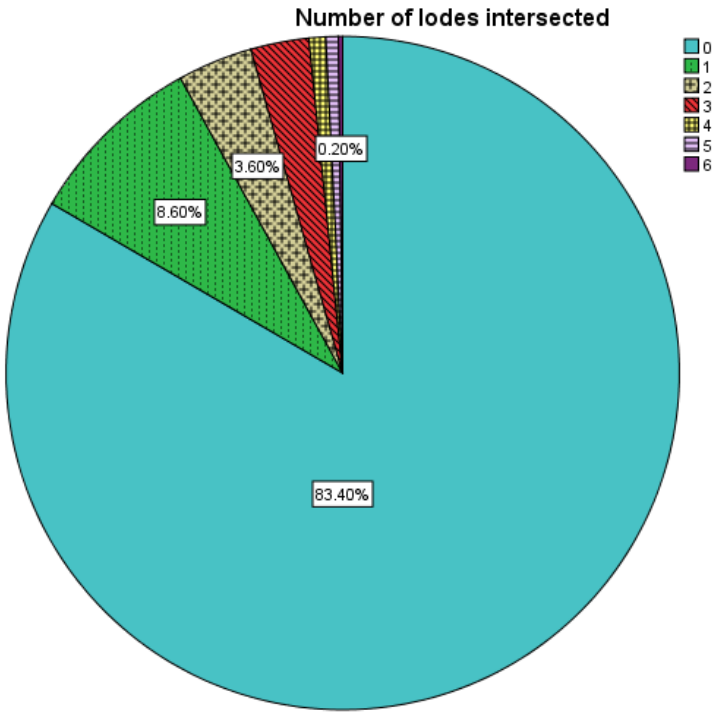

Figure 40: Pie diagram indicating the probability of intersecting a certain number of lodes for a population of 500 planned boreholes. There is a 16.6% chance of intersecting one or more lodes of economic interest.

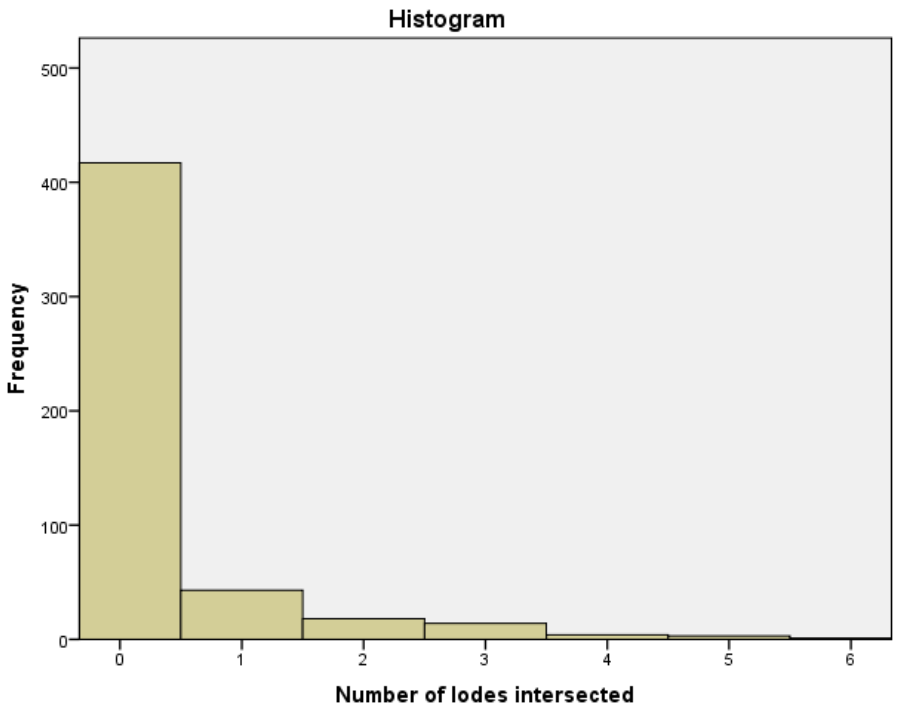

Figure 41: Histogram indicating the frequency distribution of the number of lodes intersected for 500 planned boreholes

4.3.7.4. Resampling the intersected lodes using bootstrapping

Figure 41 shows that the distribution is positively skewed. This can be expected as 417 out of the 500 planned drillholes (83.40 %) intersect only barren geology. What would be the effect on the probability if the sample population changed? In this section we will discuss conducting a resampling analysis on the 500 planned drillholes. If 20, 40 and 80 boreholes were randomly selected from the 500 planned drillhole, how will the probability of intersecting a mineralized lode change? Because the distribution is positively skewed the best statistical method to use is bootstrapping

4.3.7.4.1. Explaining the concept of bootstrapping

Bootstrapping is a statistical resampling technique that is based on the random selection of data that is statistically recalculated. The concept of “bootstrapping” can be explained as what variation can be expected during the analysis due to chance. The process is repeated 1000s of times to build a distribution of that will most likely be Gaussian (Rossi and Deutsch, 2013). The basic procedure is to randomly select a certain amount of samples from the original data, recalculate the statistics for the selected samples. The process of repetition removes any bias from the data. Uncertainty in the data generally decreases with an increase in the number of resamples (Rossi and Deutsch, 2013). It is generally assumed that the input distribution is representative of the overall distribution. Simon (1997) stated that by re-using the original data numerous times, we should be able to make inferences about the population from which the data came.

4.3.7.4.2. Bootstrapping the number of lodes

In Excel, random function were used to conduct the bootstrap analysis. The aim of this analysis was to determine whether the probability of intersecting a lode of economic interest will differ for the different sample sizes. The number of lodes intersected dataset was used to conduct the bootstrap analysis. Three different sample sizes were used: 20, 40 and 80. These samples were randomly selected from the 500 planned boreholes. The resampling was done for a 1000 iterations. For each of the sample sizes the probability and standard deviations were calculated.

The processes followed to create the bootstrapping analysis in Excel are discussed below:

1) The original number of lodes intersected data was imported into a new Excel workbook. This data is used to conduct the bootstrap analysis and a “VLOOKUP” function was thus implemented throughout the bootstrap analysis.

2) The samples were randomly selected. The “random” (RAND) function in Excel creates a random value between 0 and 1. The planned boreholes start at PB1 and not PB0. In order to compensate for the planned boreholes starting at 1 the random value was multiplied by a value of 499. This means that a random planned borehole has been identified between 0 and 499. A value of 1 was added to the formula to allow the random planned borehole to range between 1 and 500.
3) Random function values are given in decimal places, so the planned borehole number selected in step number 2 will be given as a decimal value. The “ROUND” function was used so that the calculated integer is between 1 and 500.
4) 20 samples were randomly selected using the “VLOOKUP” function. The randomly generated number refers back to the original number of lodes intersected data (step 1).

The complete equation is as follow:

VLOOKUP(ROUND(RAND()*499,0)+1,Data!$A$2:$B$501,2,FALSE)

Data!$A$2:$B$50: refers to the original number of lodes intersected data spread sheet (step 1)

5) Step 4 was repeated a 1000 times and the results were tabulated.
6) Steps 4 and 5 were repeated for the 40 and 80 sample sizes.

Once the bootstrapping data was obtained, the probability graphs and standard deviations of the 20, 40 and 80 sample sizes were determined.

4.3.7.5. Determining the minimum contained metal for the individual lodes

The last exploration application was to determine what the minimum contained metal for each lode will be. The minimum tonnage of each lode can thus be estimated. The volume of each lode can be viewed in Leapfrog Geo. This volume is the same as the "output volumes" created from the lode surfaces.

The lodes are constrained to the Quartzite lithology. In order to determine the minimum contained metal of each lode the following equations were applied:

1) The tonnage of each lode has to be calculated first. The volume of each lode was multiplied by the specific density of quartzite: 2.65 g/cm^3 (Carmichael, 1982; Daly et al., 1966).

   Tonnage for each lode= volume (m^3) * specific density of quartzite (2.65 g/cm^3)

2) The tonnage was multiplied by a constant 0.4 wt. - % Sn. This will give the minimum contained metal. A constant cut-off grade of 0.4 wt. - % Sn is assumed because that was the cut-off grade used in the mine before mine closure.

   Minimum contained metal= tonnage * 0.4 wt. - % Sn

The volume and minimum contained metal for each lode can be viewed in Table 15. The volume and minimum contained metal valued for the lodes are used to generate statistical graphs in IBM SPSS Statistics 23. As mentioned in Section 4.3.5.2.3., each of the fissure and faulted lodes have a unique orientation and dip the assumed 1m thickness is not correct. Because a perpendicular coordinate was not calculated from the hanging wall point to the footwall point, the thickness for each of the fissure and faulted lodes will not be the same. The modelled volumes are not the same because the lodes dip at different angles.

At present, the fissure and faulted lodes do not have a constant thickness, but due to limited data of the lodes at Leeuwpoort Mine, the actual thickness of the lodes cannot be calculated. A large uncertainty exists for the volumes created for the fissure and faulted lodes, these volumes are artificial and not representative of the actual volumes. The volumes for the flat lying lodes will be underestimated, whereas the volumes of the steeply lodes will be overestimated.

4.3.7.5.1. Generating volume and minimum contained metal graphs

The data from Table 15 was imported into IBM SPSS Statistics 23. Frequency tables were calculated for both the volume (Table 16) and minimum contained metal (Table 17). The following graphs were created in IBS SPSS Statistics 23 and can be viewed in the Results section:

1) Scatter plot for volume against lode
2) Scatter plot of volume against cumulative percentage
3) Scatter plot of minimum contained metal against cumulative percentage

Table 15: Volume and minimum contained metal for each of the lodes at Leeuwpoort Mine.

Lodes	Volume (m^3)	Specific density of quartzite (g/cm^3)	Specific density of quartzite (kg/m^3)	Cut-off grade (0.4 wt.-% Sn)	Minimum contained metal (kg)	Minimum contained metal (ton)
Bedded lodes						
10N Lode	75731	2.65	2650	0.4	80274860	80274.86
10TA Lode	19814	2.65	2650	0.4	21002840	21002.84
5S Lode	49585	2.65	2650	0.4	52560100	52560.10
9S Lode	141640	2.65	2650	0.4	150138400	150138.40
A Lode	356440	2.65	2650	0.4	377826400	377826.40
Agnes Lode	193990	2.65	2650	0.4	205629400	205629.40
CA Lode	260790	2.65	2650	0.4	276437400	276437.40
Compound Lode	44846	2.65	2650	0.4	47536760	47536.76
EK Lode	80131	2.65	2650	0.4	84938860	84938.86
Gap Bottom Lode	261010	2.65	2650	0.4	276670600	276670.60
Gap Top Lode	138200	2.65	2650	0.4	146492000	146492.00
Gap Lower Lode	657490	2.65	2650	0.4	696939400	696939.40
GS Lode	92247	2.65	2650	0.4	97781820	97781.82
GS FW Lode	199650	2.65	2650	0.4	211629000	211629.00
MD Lode	341380	2.65	2650	0.4	361862800	361862.80
New New Lode	139950	2.65	2650	0.4	148347000	148347.00
Rio Rita Lode	188180	2.65	2650	0.4	199470800	199470.80
Spruit Extension Lode	168700	2.65	2650	0.4	178822000	178822.00
Fissure and faulted lodes						
100' Fissure	26394	2.65	2650	0.4	27977640	27977.64
800' Fissure	49966	2.65	2650	0.4	52963960	52963.96
1200' Fissure	92826	2.65	2650	0.4	98395560	98395.56
21P Lode	21115	2.65	2650	0.4	22381900	22381.90
Fault Lode	14753	2.65	2650	0.4	15638180	15638.18
Fault Lode Fissure	46216	2.65	2650	0.4	48988960	48988.96
Government 1 Lode	41391	2.65	2650	0.4	43874460	43874.46
Government 2 Lode	27525	2.65	2650	0.4	29176500	29176.50
Hoskings Fissure	51631	2.65	2650	0.4	54728860	54728.86
JB Lode	19499	2.65	2650	0.4	20668940	20668.94
MC2 Lode	202290	2.65	2650	0.4	214427400	214427.40
New Strike Lode	38726	2.65	2650	0.4	41049560	41049.56
Trench Lode	10605	2.65	2650	0.4	11241300	11241.30
West Workings Fissure	207110	2.65	2650	0.4	219536600	219536.60

Table 16: Frequency table for the volumes of the modelled lodes at Leeuwpoort Mine.

Volume (m^3)				
Valid	Frequency	Percent	Valid Percent	Cumulative Percent
10605.0	1	0.9	3.1	3.1
14753.0	1	0.9	3.1	6.3
19499.0	1	0.9	3.1	9.4
19814.0	1	0.9	3.1	12.5
21115.0	1	0.9	3.1	15.6
26394.0	1	0.9	3.1	18.8
27525.0	1	0.9	3.1	21.9
38726.0	1	0.9	3.1	25.0
41391.0	1	0.9	3.1	28.1
44846.0	1	0.9	3.1	31.3
46216.0	1	0.9	3.1	34.4
49585.0	1	0.9	3.1	37.5
49966.0	1	0.9	3.1	40.6
51631.0	1	0.9	3.1	43.8
75731.0	1	0.9	3.1	46.9
80131.0	1	0.9	3.1	50.0
92247.0	1	0.9	3.1	53.1
92826.0	1	0.9	3.1	56.3
138200.0	1	0.9	3.1	59.4
139950.0	1	0.9	3.1	62.5
141640.0	1	0.9	3.1	65.6
168700.0	1	0.9	3.1	68.8
188180.0	1	0.9	3.1	71.9
193990.0	1	0.9	3.1	75.0
199650.0	1	0.9	3.1	78.1
202290.0	1	0.9	3.1	81.3
207110.0	1	0.9	3.1	84.4
260790.0	1	0.9	3.1	87.5
261010.0	1	0.9	3.1	90.6
341380.0	1	0.9	3.1	93.8
356440.0	1	0.9	3.1	96.9
657490.0	1	0.9	3.1	100.0
Total	32	29.6	100.0	

Table 17: Frequency table for the minimum contained metal of the lodes at Leeuwpoort Mine.

Minimum contained metal (ton)				
Valid	Frequency	Percent	Valid Percent	Cumulative Percent
11241.30	1	.9	3.1	3.1
15638.18	1	.9	3.1	6.3
20668.94	1	.9	3.1	9.4
21002.84	1	.9	3.1	12.5
22381.90	1	.9	3.1	15.6
27977.64	1	.9	3.1	18.8
29176.50	1	.9	3.1	21.9
41049.56	1	.9	3.1	25.0
43874.46	1	.9	3.1	28.1
47536.76	1	.9	3.1	31.3
48988.96	1	.9	3.1	34.4
52560.10	1	.9	3.1	37.5
52963.96	1	.9	3.1	40.6
54728.86	1	.9	3.1	43.8
80274.86	1	.9	3.1	46.9
84938.86	1	.9	3.1	50.0
97781.82	1	.9	3.1	53.1
98395.56	1	.9	3.1	56.3
146492.00	1	.9	3.1	59.4
148347.00	1	.9	3.1	62.5
150138.40	1	.9	3.1	65.6
178822.00	1	.9	3.1	68.8
199470.80	1	.9	3.1	71.9
205629.40	1	.9	3.1	75.0
211629.00	1	.9	3.1	78.1
214427.40	1	.9	3.1	81.3
219536.60	1	.9	3.1	84.4
276437.40	1	.9	3.1	87.5
276670.60	1	.9	3.1	90.6
361862.80	1	.9	3.1	93.8
377826.40	1	.9	3.1	96.9
696939.40	1	.9	3.1	100.0
Total	32	29.6	100.0	

5. RESULTS

This section of the thesis discusses the results obtained for this study. The 3D geological model created for Leeuwpoort Mine is included in this section, along with the interpolants of the lodes. The probability graphs for the number of lodes intersected per planned borehole that was created from the 20, 40 and 80 bootstrap analysis will be discussed. In addition, the statistical graphs created of the minimum contained metal and volumes for the lodes are included.

5.1. The geological model of Leeuwpoort Mine

The geological model of Leeuwpoort Mine was created from the 169 CMS surface boreholes, digitized lodes, and digitized polylines of the Rooiberg Group (Section 4.3.5.). The geological model consists of six lithological units, increasing in age: Soil, Rhyolite, Gritty Quartzite/Arenite, Shale, Shaly Quartzite/ Shaly Arenite, Quartzite (Figure 42). Leeuwpoort Mine distinguished between 39 lodes at the time of mine closure. However, due to limited data available, only 32 lodes could be modelled and were subsequently included in the geological model. The 32 modelled lodes of Leeuwpoort Mine can be defined as the orezone of the mine.

5.2. Ore deposit model for Leeuwpoort Mine

The majority of the mineralization at Leeuwpoort Mine is constrained in the upper quartzite of the Boschoffsberg Quartzite Member, below the Blaauwbank Shale Member (Phillips, 1982). The Blaauwbank Shale Member is thought to have acted as a stratigraphic control or “cap rock” for ascending fluids (Rozendaal et al., 1995b). Complex shearing events created steep fractures which allowed mineralized fluids to ascend through the Blaauwbank Shale Member of the Leeuwpoort Formation, as well as into the Smelterkop Formation.

A mineral deposit (ore deposit) can be defined as the occurrence of an economically significant mineral of a sufficient size and grade to be mineable (Rose, 1988; Hogson, 1990). The available assay data can be viewed in conjunction with the geological model, in particular the orezone, to represent a 3D ore deposit model for Leeuwpoort Mine (Figure 43). Each of the geological units can be viewed separately under the “output volume folder” in Leapfrog Geo.

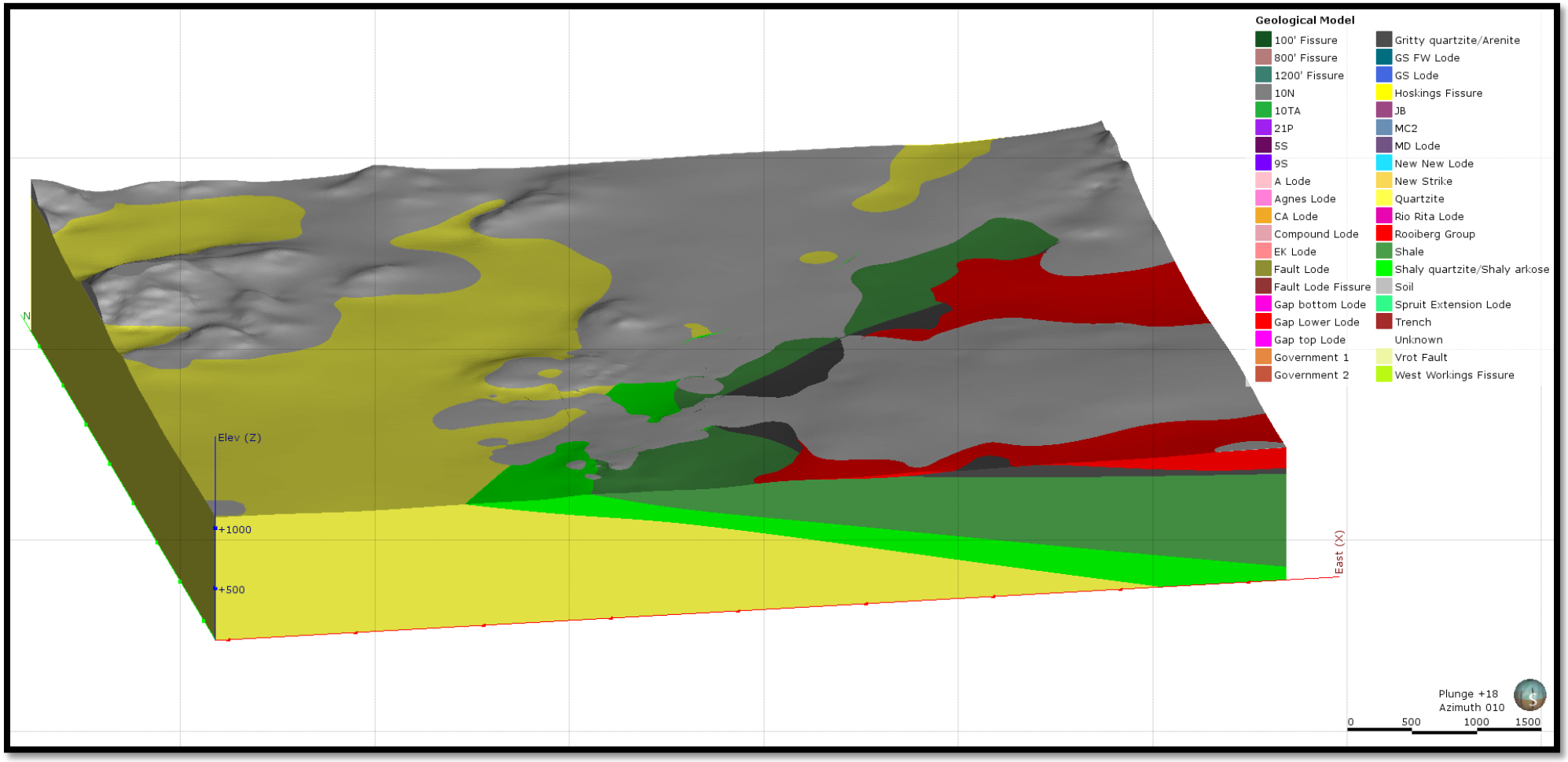

Figure 42: The geological model of Leeuwpoort Mine created with the use of the Leapfrog Geo.

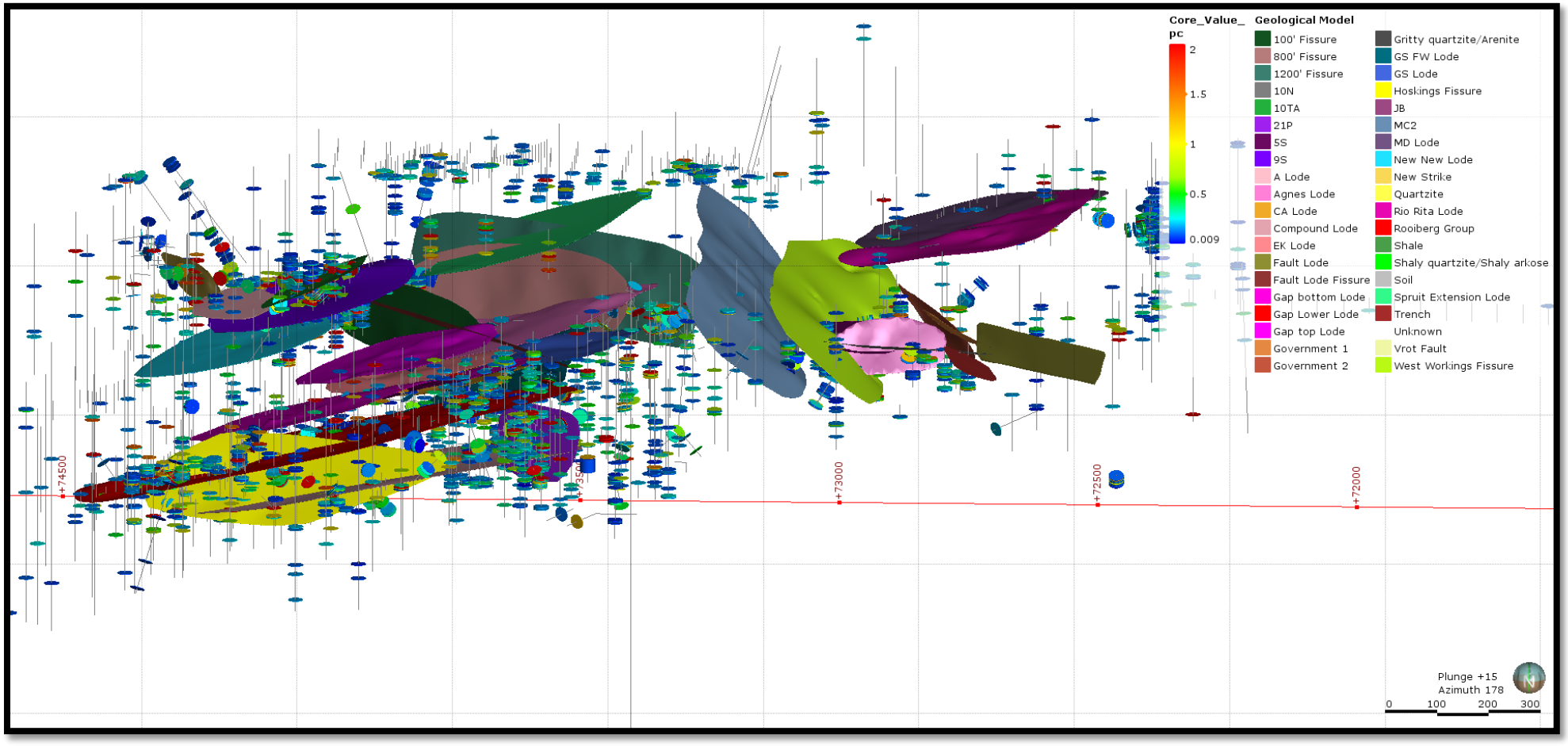

Figure 43: The geological model, in particular the orezone (lodes), can be viewed in conjunction with the assay data to represent a 3D ore deposit model for Leeuwpoort Mine. The grade scale (core value pc) of the assay data (Sn wt.-%) is indicated next to the legend of the geological model.

5.3. Structural surface features

Only limited structural information was uncovered during the post-mortem study of Leeuwpoort Mine. However, the 777 maps discovered during the post-mortem study did include some surface structural features. As mentioned in Section 4.3.3, the maps used in this thesis were imported into Leapfrog Geo and spatially georeferenced. The presence of three major faults were noted on these maps: Sand Fault, Post-Karoo Fault, and the Fault Lode Fracture. These faults were digitized and "draped" on the topography and added to the surface of the geological model (Figure 44). No structural data for these faults are available at present, but the spatial position of the faults on surface can be noted.

The position of underground faults and fractures could not be verified during the post-mortem study. However, we know that the fissure and faulted lodes at Leeuwpoort Mine formed from ascending metasomatic fluids through the complex shear system. The assumption can thus be made that fissure and faulted lodes indicate the position of a structural feature. The bedded lodes are stratigraphically controlled and indicate the position of the bedding planes within the host rocks. Additional structural information might be uncovered as the post-mortem study of Leeuwpoort Mine progresses.

5.4. Interpolant models for the lodes

The modelling process for the linear interpolant model created for the whole geological area, as well as the linear interpolant for the Quartzite lithology was discussed in Section 4.3.6. Limited assay grade data was obtained from the post-mortem study of Leeuwpoort Mine and only 9 interpolant models could be created from the 32 lodes. These linear interpolant models were constrained to the "surfaces" for each of the 9 lodes. The 9 lode surfaces used to create these linear interpolants are: EK Lode (Figure 45), 5S Lode (Figure 46), Agnes Lode (Figure 47), A-Lode (Figure 48), Gap Lower Lode (Figure 49), GS FW Lode (Figure 50), GS Lode (Figure 51), MD Lode (Figure 52), and New New Lode (Figure 53). In each of the linear interpolant models for the lodes the distribution of the grade can be viewed. The grade interpolant is dependent on the type of interpolant model chosen and the structural constraints implemented.

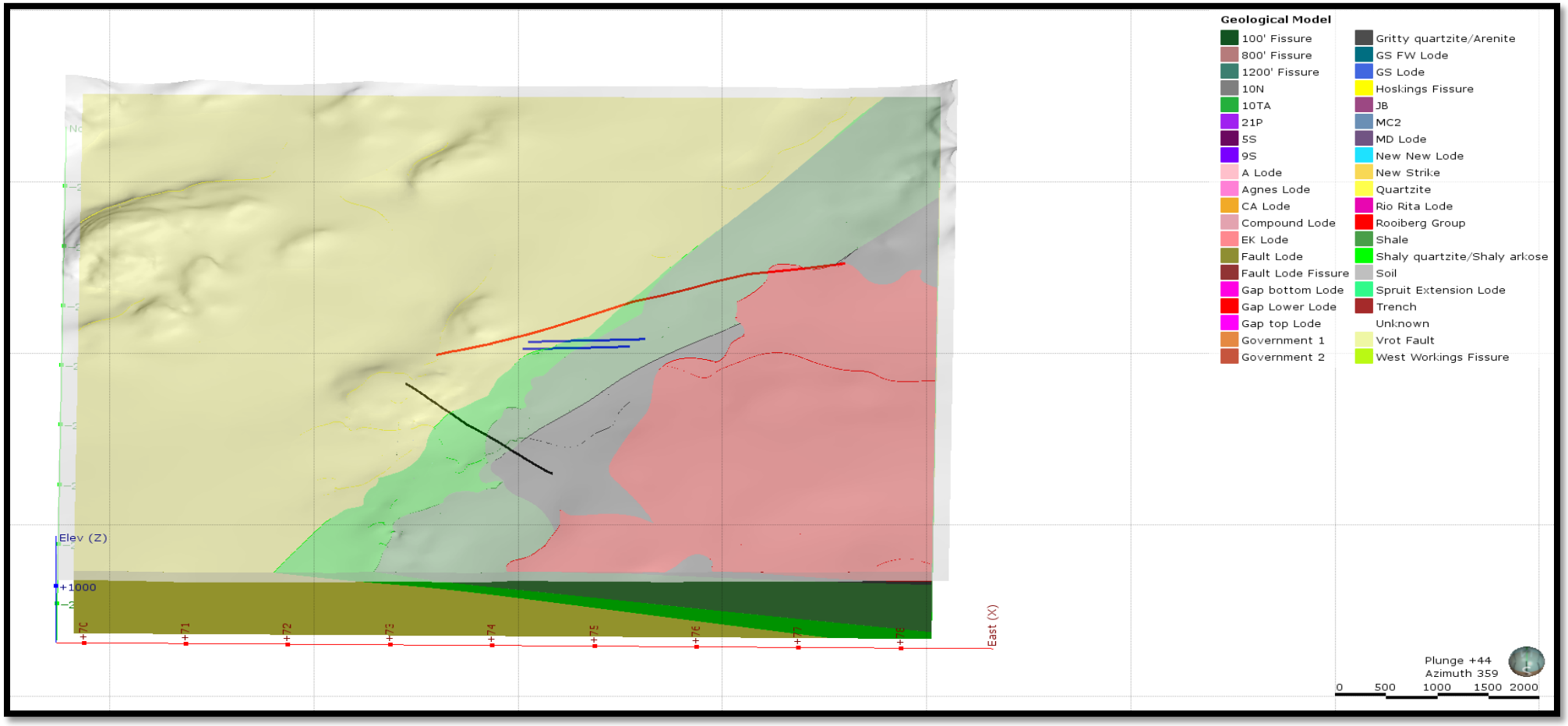

Figure 44: The three major fault present at Leeuwpoort Mine: Fault Lode Fracture (black line), Post-Karoo Fault (red line) and the Sand Fault system (blue lines). These faults were draped onto the surface of the geological model in order to indicate the spatial position of the faults. The Soil lithology was left out for viewing purposes.

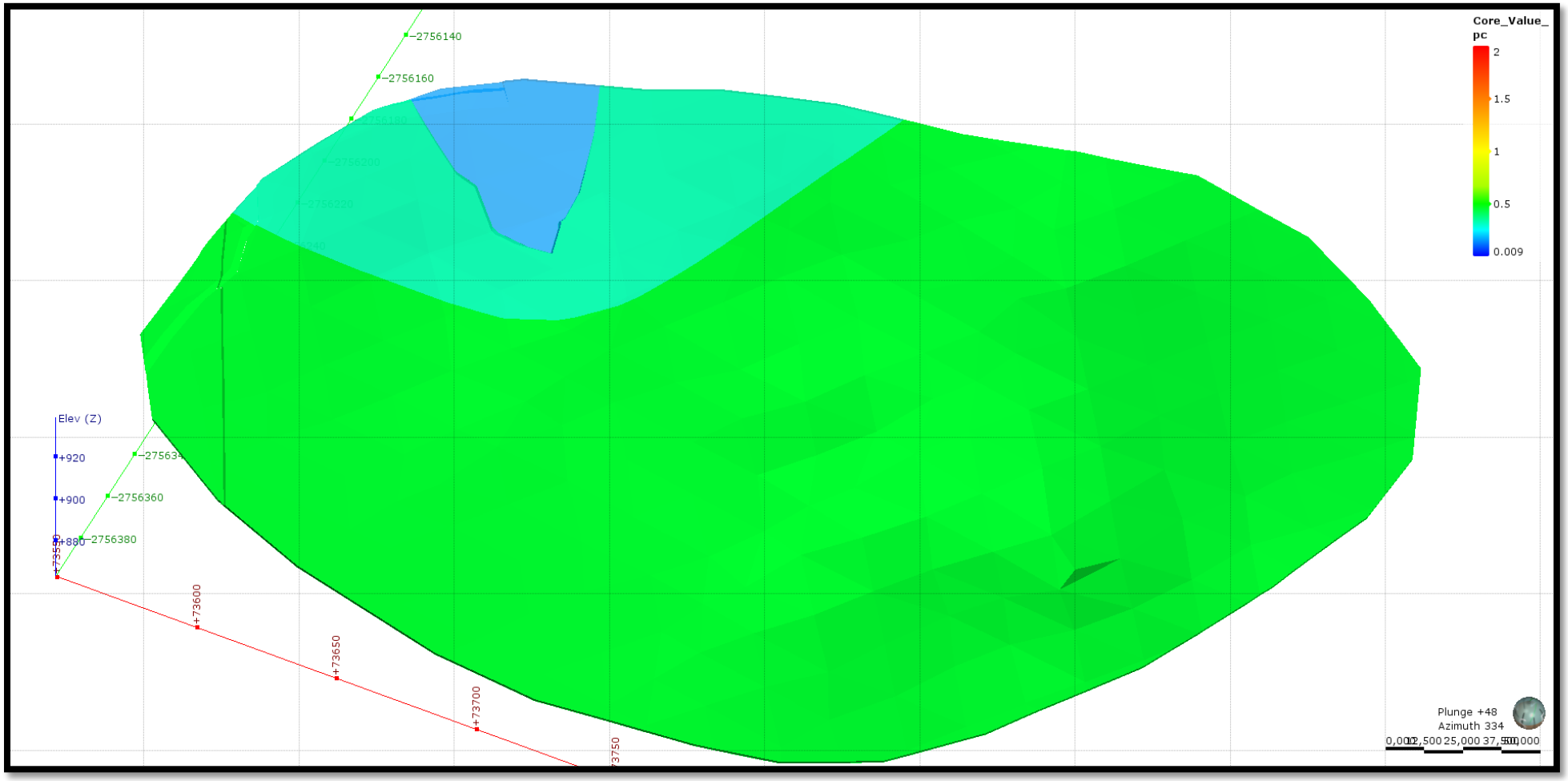

Figure 45: Linear interpolant created for EK Lode. The grade scale wt.-% Sn (core value pc) can be used to view the distribution of the grade within the modelled lode.

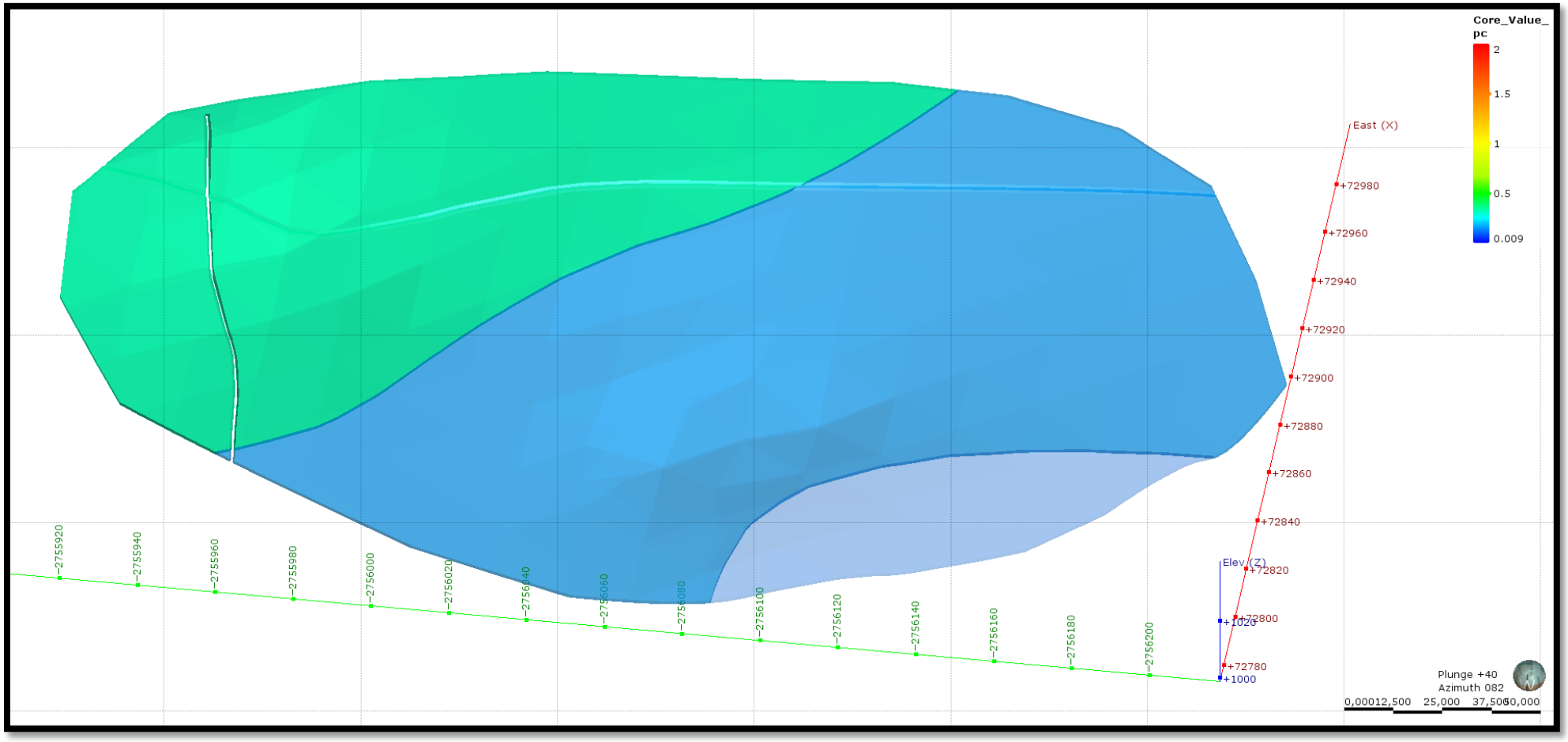

Figure 46: Linear interpolant created for 5S Lode. The grade scale wt.-% Sn (core value pc) can be used to view the distribution of the grade within the modelled lode. The small cut out slivers in the lode is where fissure and faulted lodes cross-cuts 5S Lode.

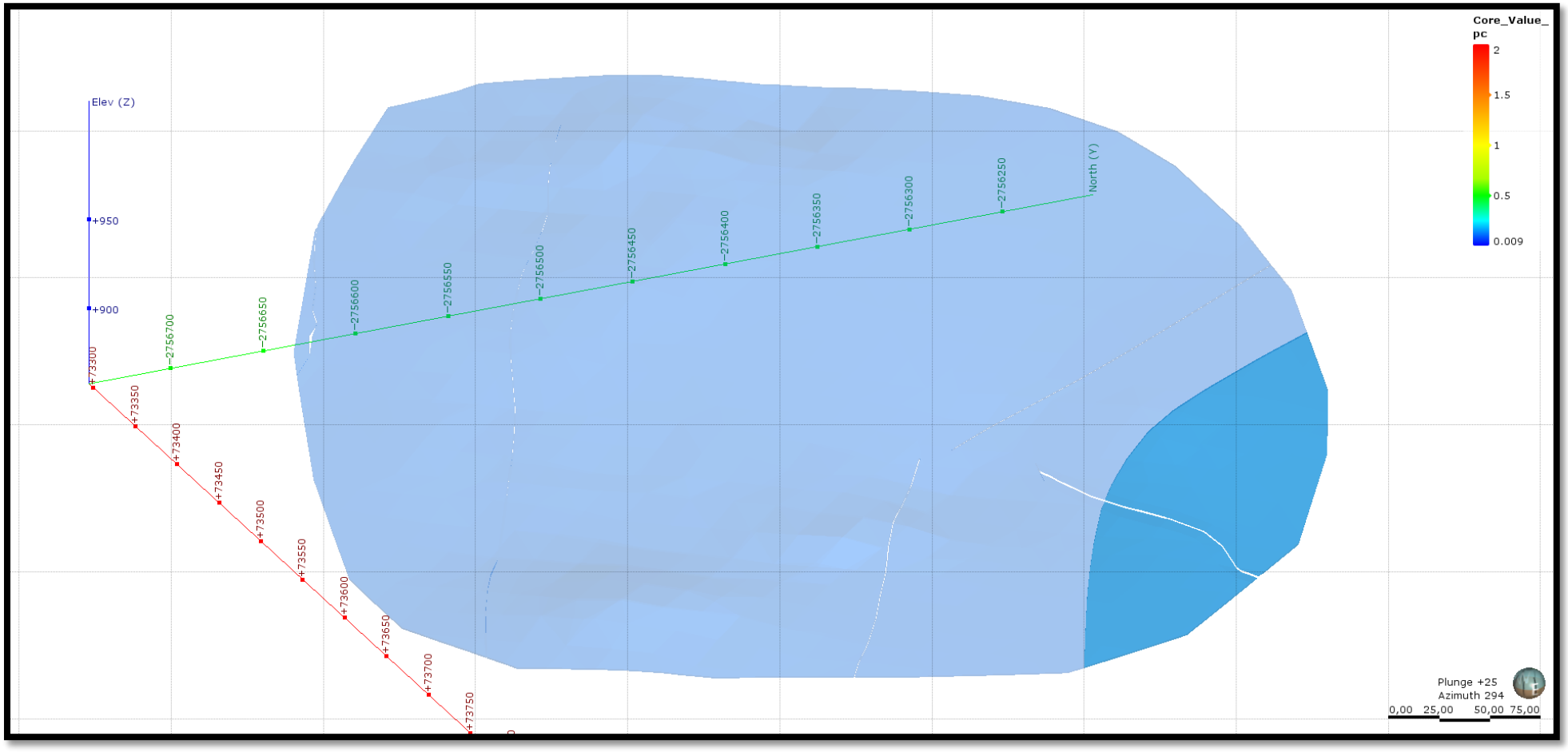

Figure 47: Linear interpolant created for Agnes Lode. The grade scale wt.-% Sn (core value pc) can be used to view the distribution of the grade within the modelled lode. The small cut out slivers in the lode is where another fissure and faulted lodes cross-cuts Agnes Lode.

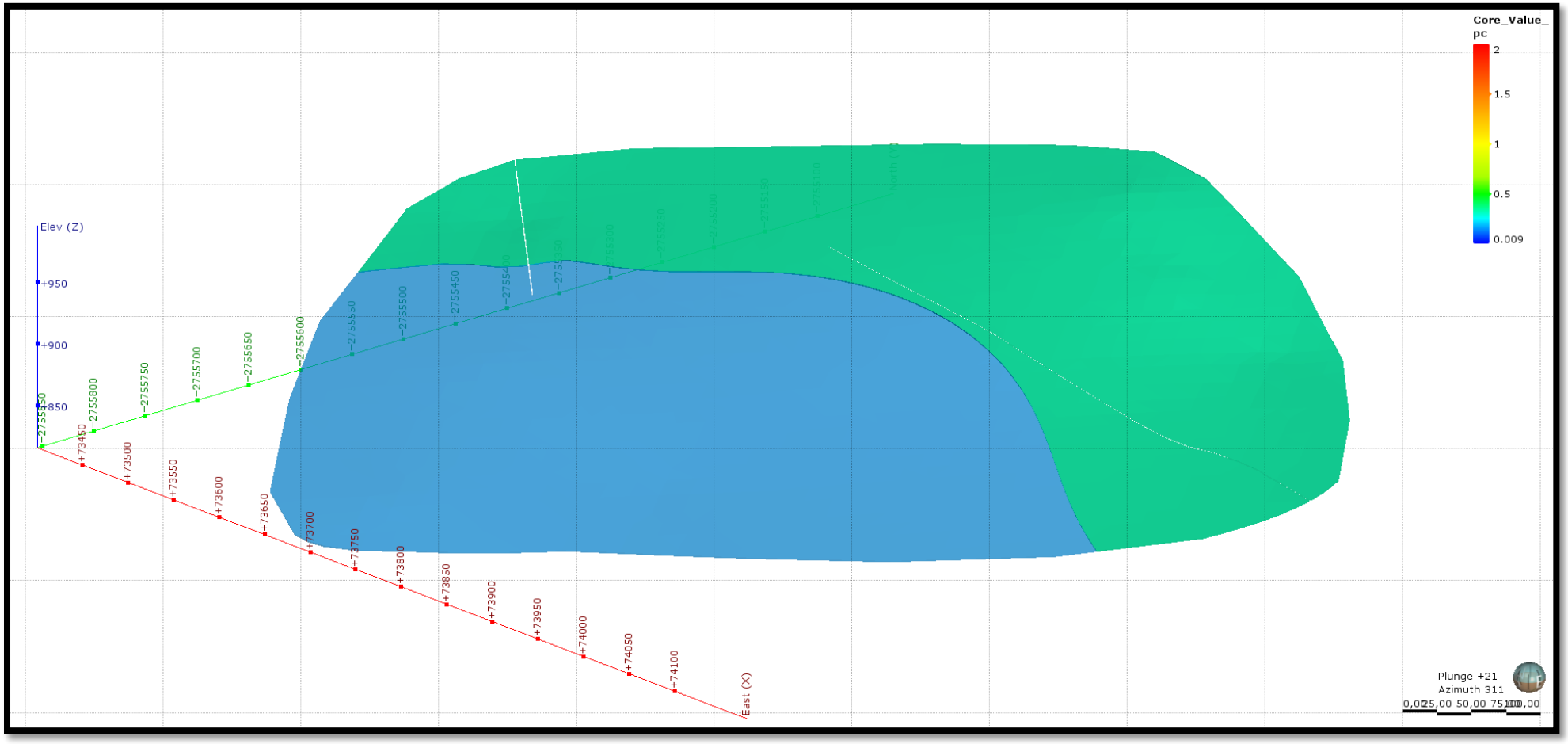

Figure 48: Linear interpolant created for A-Lode. The grade scale wt.-% Sn (core value pc) can be used to view the distribution of the grade within the modelled lode. The small cut out slivers in the lode is where another a fissure and faulted lode cross-cuts A-Lode.

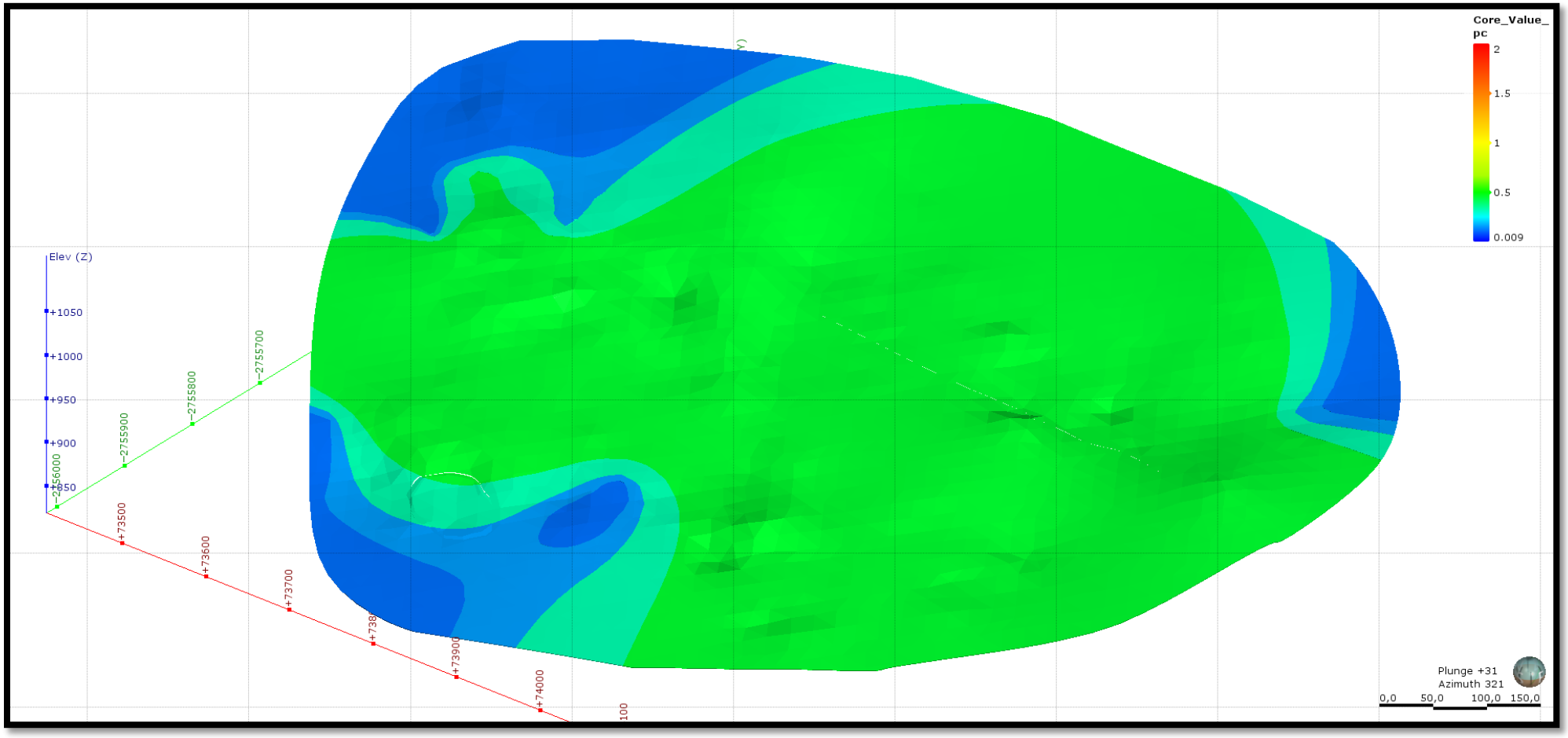

Figure 49: Linear interpolant created for Gap Lower Lode. The grade scale wt.-% Sn (core value pc) can be used to view the distribution of the grade within the modelled lode.

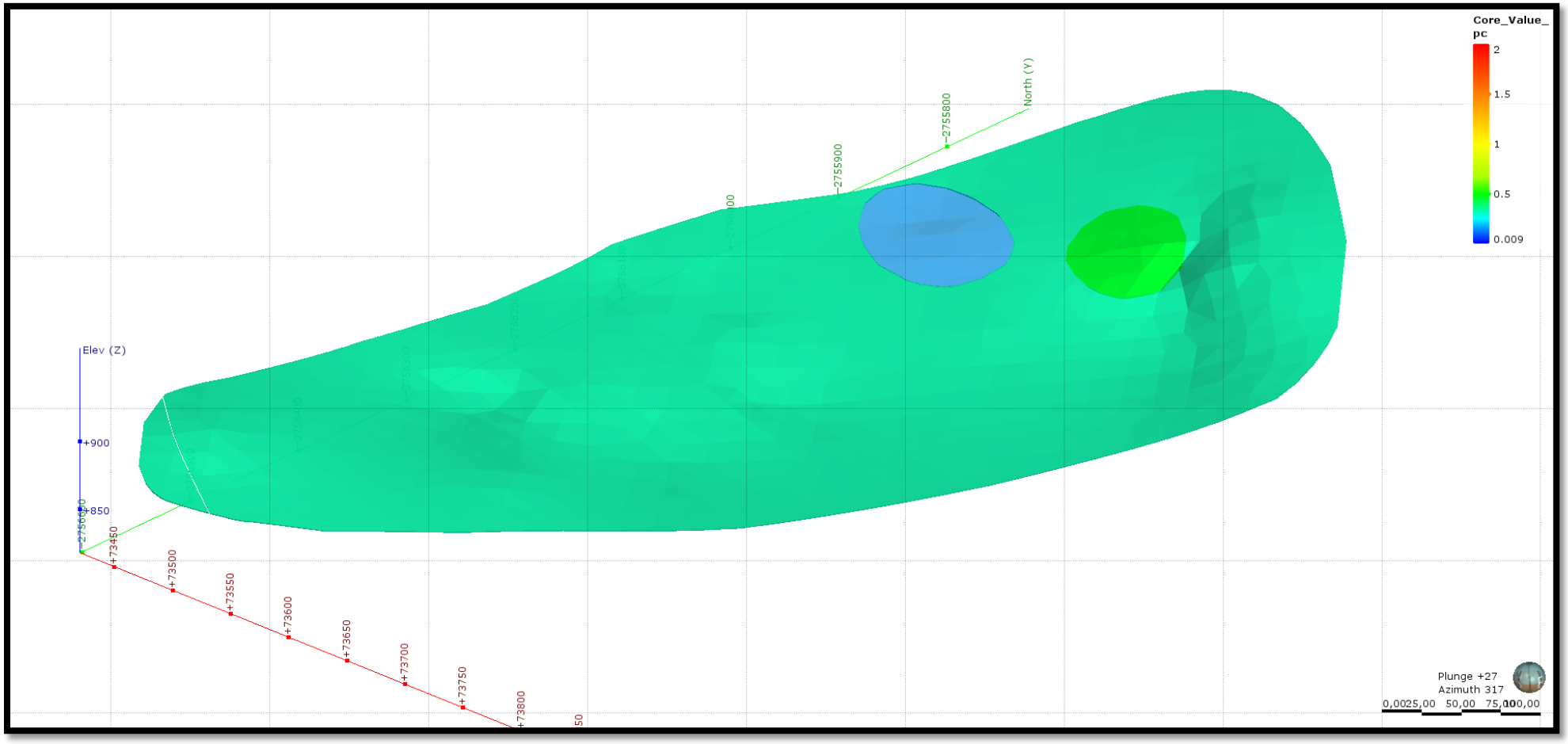

Figure 50: Linear interpolant created for GS FW Lode. The grade scale wt.-% Sn (core value pc) can be used to view the distribution of the grade within the modelled lode.

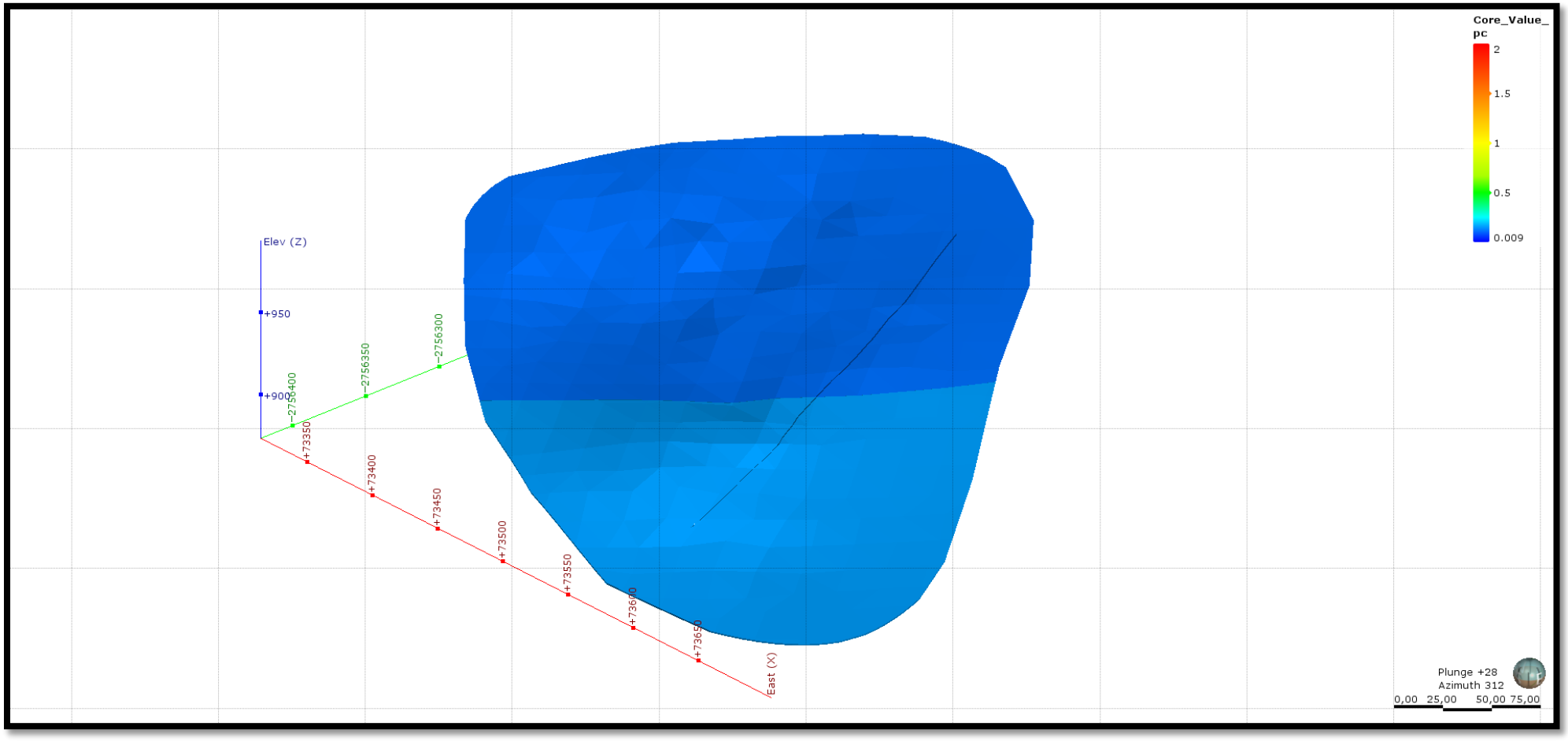

Figure 51: Linear interpolant created for GS Lode. The grade scale wt.-% Sn (core value pc) can be used to view the distribution of the grade within the modelled lode. The small cut out slivers in the lode is where another a fissure and faulted lode cross-cuts GS Lode.

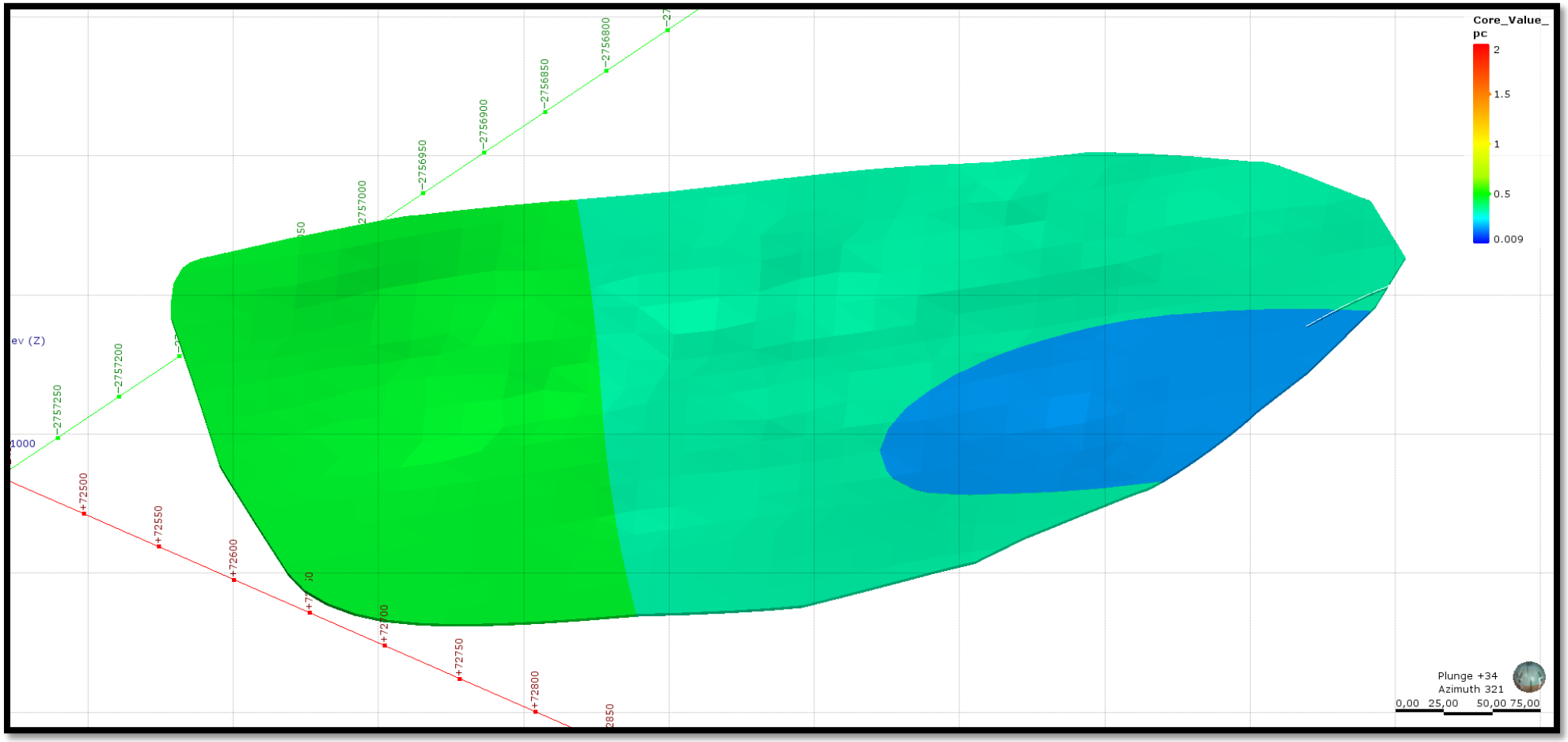

Figure 52: Linear interpolant created for MD Lode. The grade scale wt.-% Sn (core value pc) can be used to view the distribution of the grade within the modelled lode.

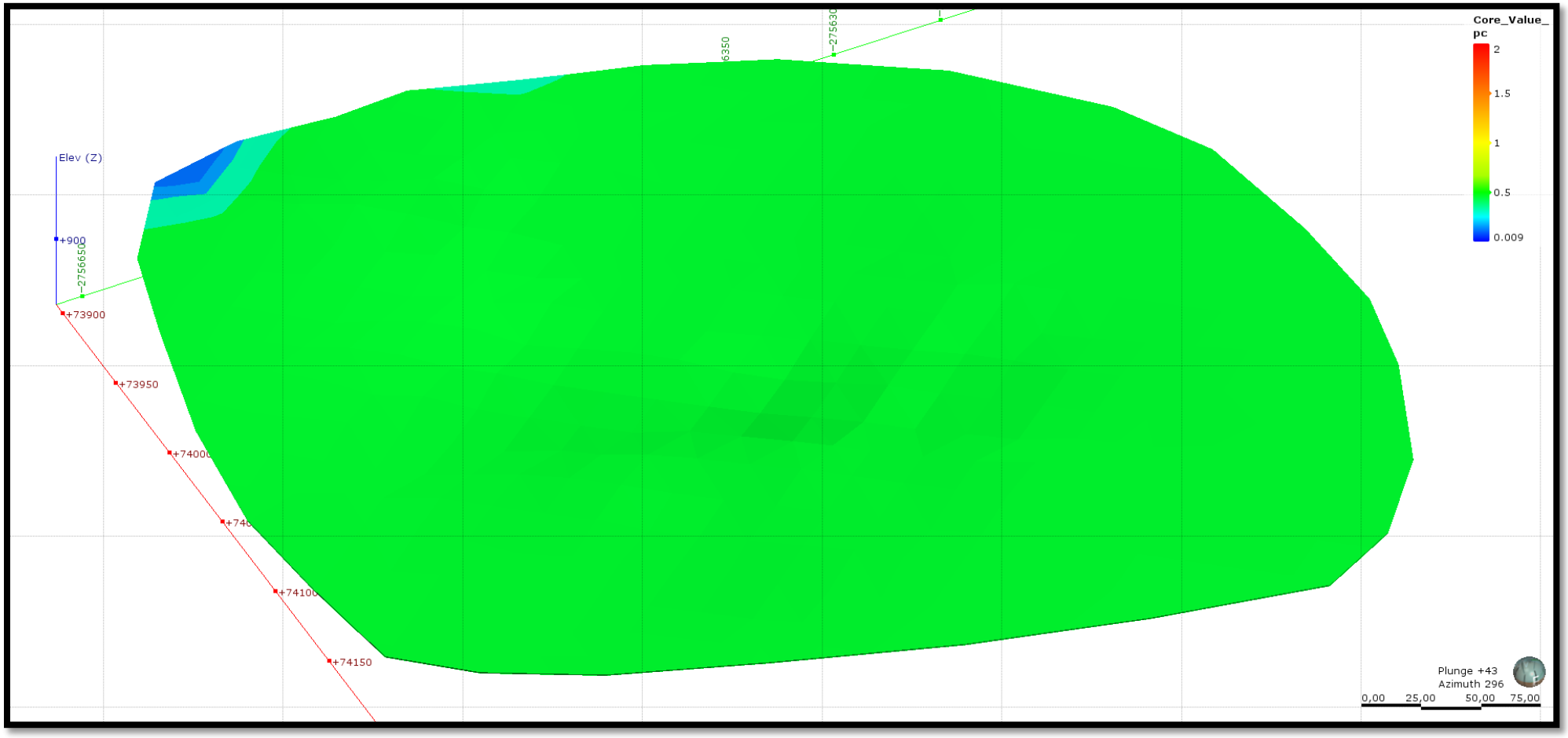

Figure 53: Linear interpolant created for New New Lode. The grade scale wt.-% Sn (core value pc) can be used to view the distribution of the grade within the modelled lode.

5.5. Exploration results

The geological- , ore deposit-, and interpolant models were used to determine the applicability of 3D models for exploration purposes. 500 boreholes were randomly planned in a selected boundary in order to determine the probability of intersect a lode of economic interest (Section 4.3.7). The “drilling prognosis” for these planned boreholes were calculated by Leapfrog Geo from the created models. The volumes of the 32 lodes modelled lodes were extracted and used to calculate the minimum contained metal for each individual lode.

5.5.1. Probability of lode intersection.

The evaluation completed in Leapfrog Geo (Table 12) were used to determine the number of lodes intersected per planned borehole (Table 13). Using the obtained data, statistical analysis indicated that there is a 16.6% probability of intersecting a lode of economic interest (Figure 40). In Figure 42 we can see that the distribution is positively skewed, as can be expected because 417 out of the 500 planned drillholes (83.40 %) intersect only barren geology. A resampling analysis on the 500 planned drillholes was conducted using the Bootstrap method (Section 4.3.7.4.). Sets of 20, 40 and 80 samples were randomly selected from the 500 planned drillholes in order to determine the variation in the probability of intersecting a lode due to chance.

The probability graphs for the 20 (Figure 54), 40 (Figure 55), and 80 (Figure 56) samples used for the bootstrap analyses indicates the probability of intersecting a lode of economic significance. The statistical data for the bootstrap analyses obtained from the 20, 40, and 80 samples are summarized in Table 18, Table 19, and Table 20, respectively.

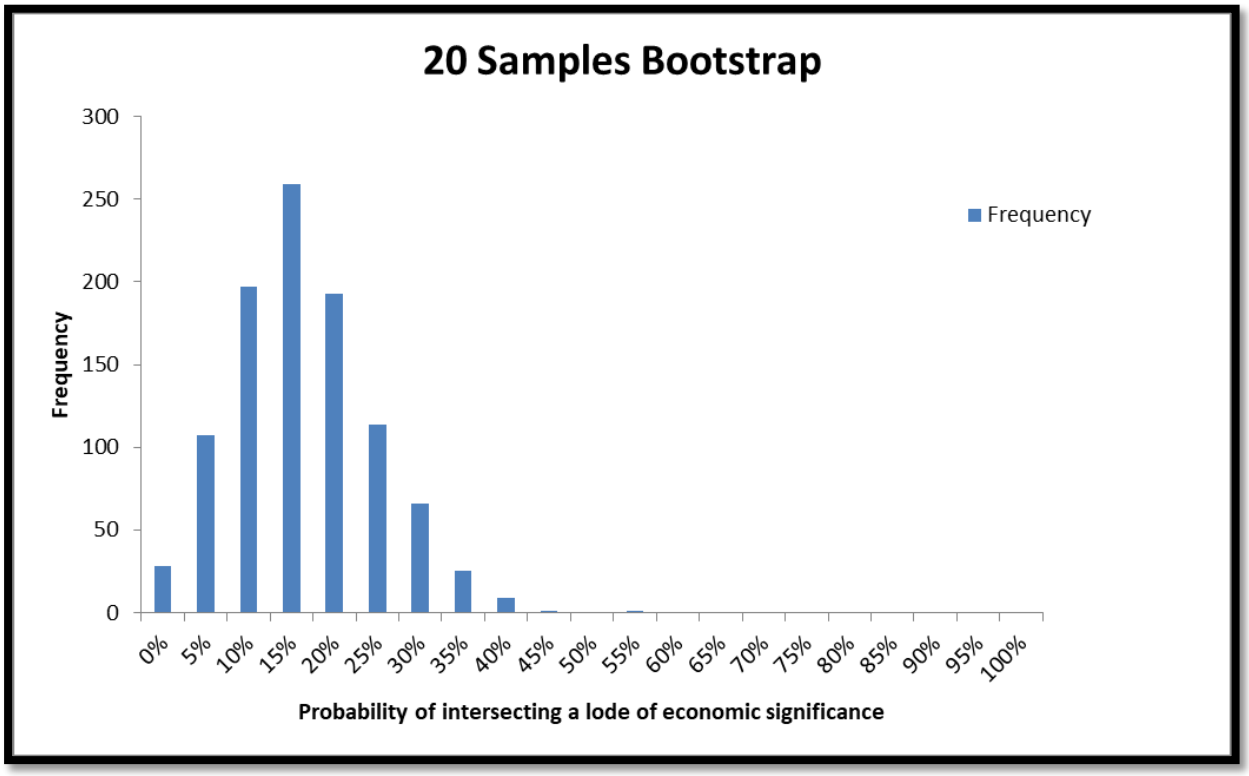

Figure 54: Probability graph for the Bootstrap analysis using 20 random samples in 1000 iterations. This graph indicates the probability of intersecting a lode of economic interest.

Table 18: Statistical data for the 20 sample Bootstrap analysis.

Statistics

Probability of intersecting a lode using 20 samples

N	Valid	1000
	Missing	0
Mean		16.3300
Std. Error of Mean		.26306
Median		15.0000
Mode		15.00
Std. Deviation		8.31867
Variance		69.200
Skewness		.376
Std. Error of Skewness		.077
Kurtosis		.172
Std. Error of Kurtosis		.155
Range		45.00
Minimum		.00
Maximum		45.00
Sum		16330.00

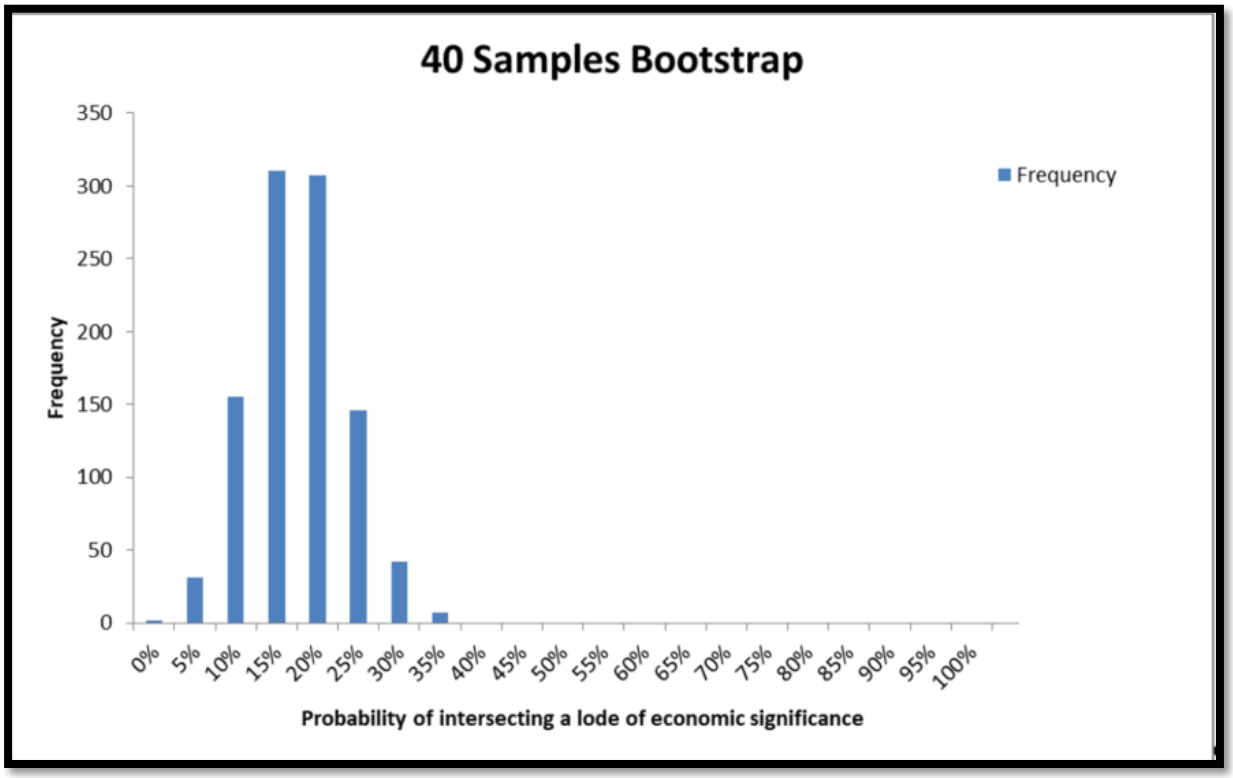

Figure 55: Probability graph for the Bootstrap analysis using 40 random samples in 1000 iterations. This graph indicates the probability of intersecting a lode of economic interest.

Table 19: Statistical data for the 40 sample Bootstrap analysis.

Statistics

Probability of intersecting a lode using 40 samples

N	Valid	1000
	Missing	0
Mean		16.4700
Std. Error of Mean		.18254
Median		17.5000
Mode		17.50
Std. Deviation		5.77256
Variance		33.322
Skewness		.057
Std. Error of Skewness		.077
Kurtosis		-.194
Std. Error of Kurtosis		.155
Range		35.00
Minimum		2.50
Maximum		37.50
Sum		16470.00

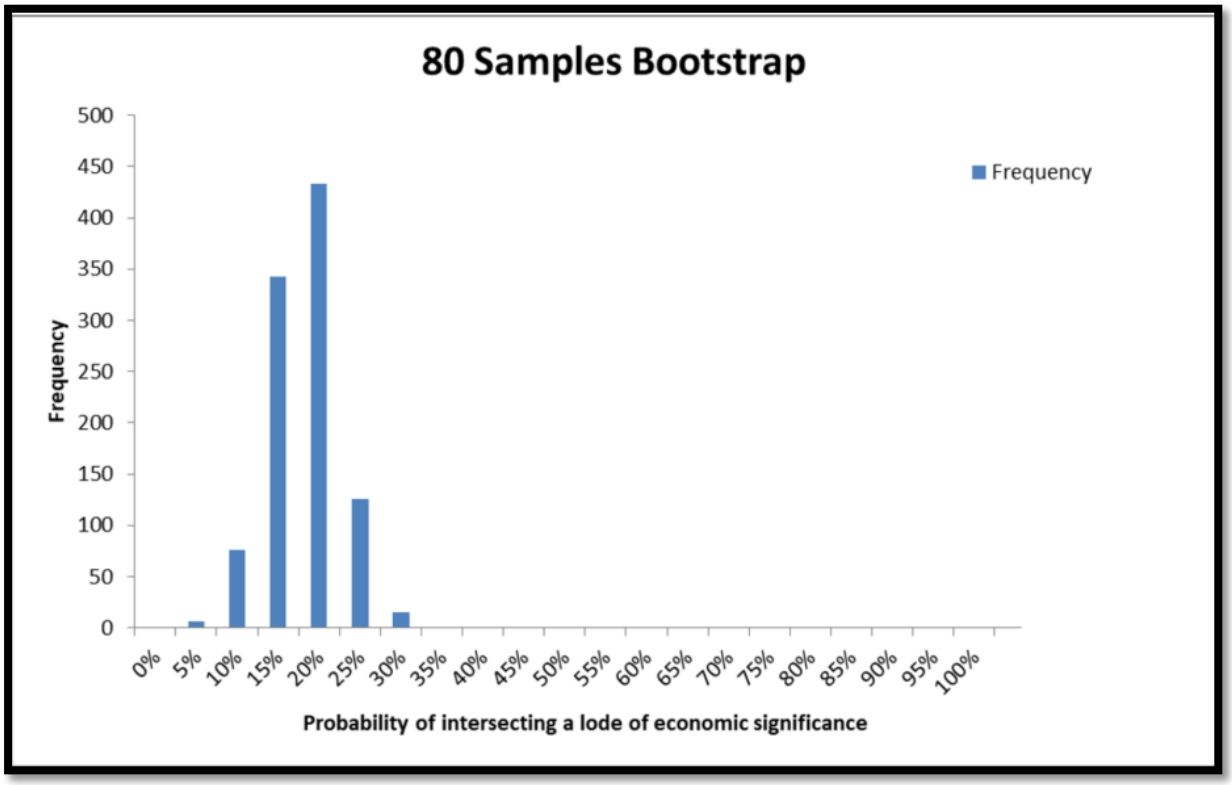

Figure 56: Probability graph for the bootstrap analysis using 80 random samples in 1000 iterations. This graph indicates the probability of intersecting a lode of economic interest.

Table 20: Statistical data for the 80 sample bootstrap analysis.

Statistics

Probability of intersecting a lode using 80 samples

N	Valid	1000
	Missing	0
Mean		16.3425
Std. Error of Mean		.13336
Median		16.2500
Mode		16.25
Std. Deviation		4.21714
Variance		17.784
Skewness		.205
Std. Error of Skewness		.077
Kurtosis		-.113
Std. Error of Kurtosis		.155
Range		26.25
Minimum		5.00
Maximum		31.25
Sum		16342.50

5.5.2. Tonnage and minimum contained metal for the modelled lodes

The volumes created for the 32 modelled lodes distinguished at Leeuwpoort Mine was obtained from the "output volume" in Leapfrog Geo. These volumes were used to calculate the minimum contained metal for each of the individual modelled lodes (Table 15). Figure 57 represents the linear relationship between the volumes (m^3) of the modelled lodes and the calculated minimum contained metal (tonnage) for lodes. The cumulative frequency graph for the volumes of the 32 modelled lodes can be viewed in Figure 58. The cumulative frequency graph for the minimum contained metal (tonnage) of the 32 modelled lodes can be viewed in Figure 59.

Due to a constant grade of 0.4 wt. - % Sn and density of 2.65 g/cm^3 assumed, the function of the graph between the minimum contained metal and volume has to be linear. Due to the linear relationship between minimum contained metal and volume, Figure 58 and Figure 59 is similar, however, the graphs for Figure 58 and Figure 59 is both expressed exponentially (exponential graphs). For drilling purposes, the probability of a certain volume and minimum contained metal can be read from the graphs.

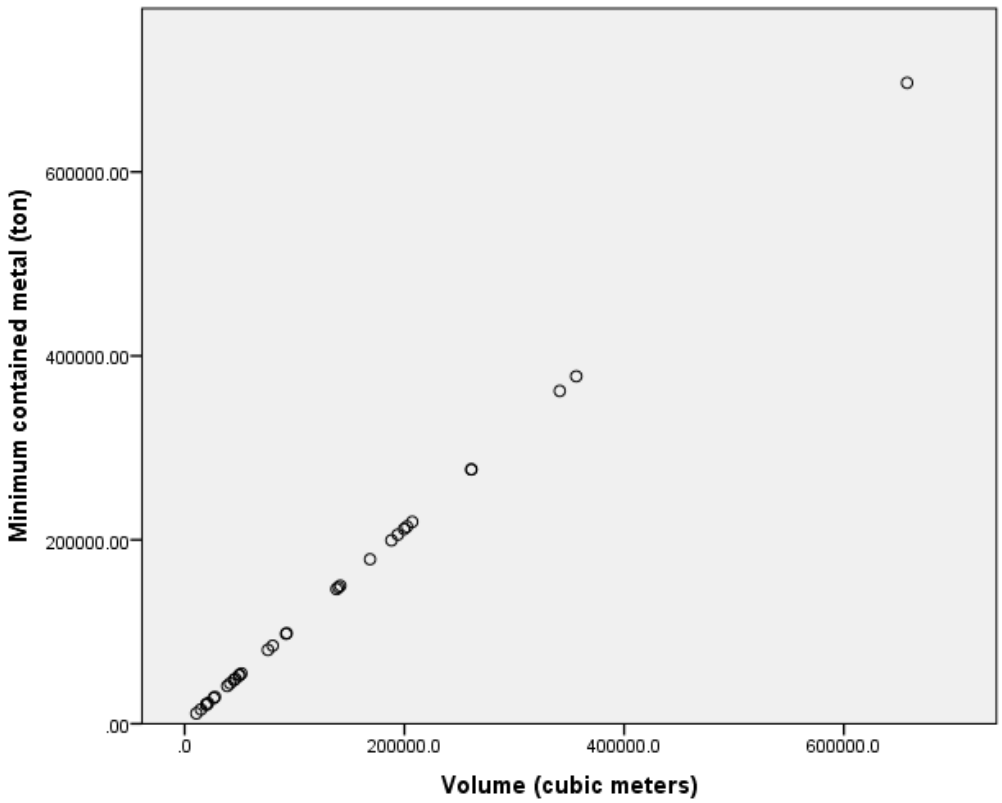

Figure 57: Scatter plot indicating the linear relationship between the volumes (m^3) of the modelled lodes and the calculated minimum contained metal (tonnage) for each lode.

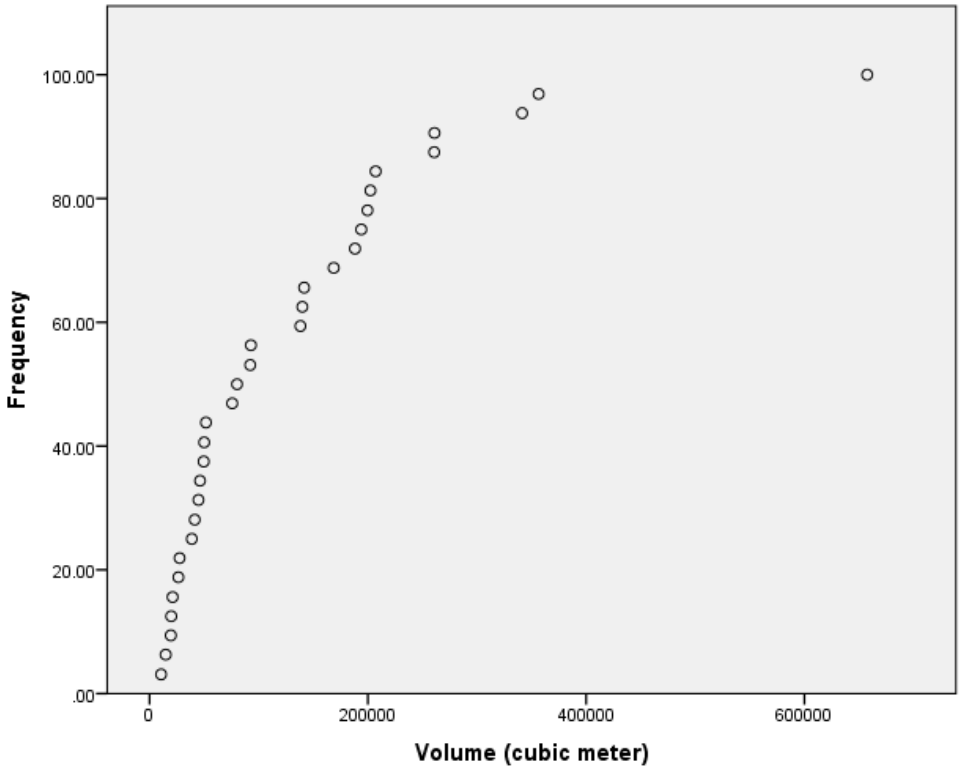

Figure 58: Cumulative frequency graph for the volumes (m^3) of the lodes at Leeuwpoort Mine.

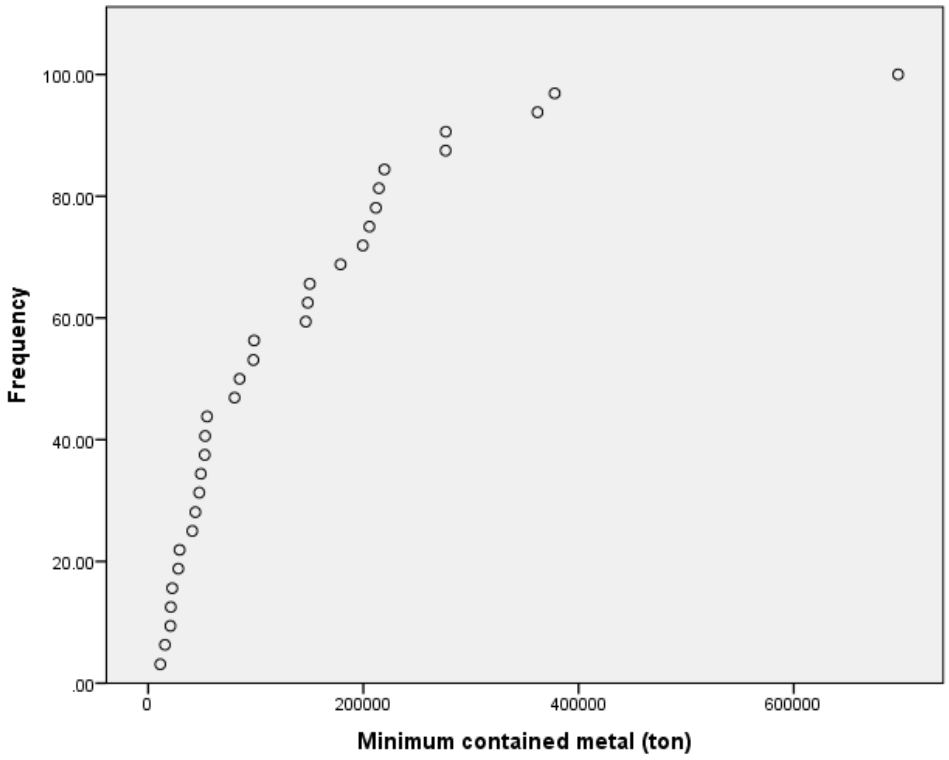

Figure 59: Cumulative frequency graph for the minimum contained metal (tonnage) of the lodes at Leeuwpoort Mine.

6. DISCUSSION

This section discusses in detail the results obtained, and indicate the significance of the results. The limitations of the created geological, ore deposit, and interpolance models are discussed. In addition, the applicability of 3D models for exploration purposes is evaluated.

6.1. The historical data obtained from the post-mortem study of Leeuwpoort Mine

The post-mortem study conducted at Leeuwpoort Mine was a time consuming process, but resulted in the recovery of historical borehole data. The historical data obtained includes hand-written borehole logs that consists of survey, collar, and assay data, as well as summary logs of the borehole data. Various surface, underground, regional, survey, civil, mining, locations of mining pegs, and resource and reserve maps were found. The historical data was thoroughly validated with various implemented QA/QC procedures (Section 4.2.3).

However, the recovered historical borehole data provided only limited information. Production data of the mine, which includes complete assay data for all the borehole data, as well as structural data for the mine are still missing. The geological, ore deposit, and interpolant models created for Leeuwpoort Mine is therefore based on limited historical data. As the post-mortem study for Leeuwpoort Mine progresses, more information might be recovered and will subsequently provide improved information. Production data will result in better quality ore deposit and interpolant models, whereas structural data will refine the interpolant and geological models.

6.2. The geological model of Leeuwpoort Mine

Due to the limited information obtained from the post-mortem study so far, three different modelling techniques had to be used to create the geological model of Leeuwpoort Mine. The base geological units (Soil, Gritty Quartzite/Arenite, Shale, Shaly Quartzite/Shaly Arkose and Quartzite) were modelled using the provided lithological data of the 169 CMS surface boreholes (see Section 4.3.5.1). No lithological data for the CMW surface boreholes, or the underground boreholes (CMU, CLU, CK and CKB) were recovered during the post-mortem study

Leeuwpoort Mine distinguished between 39 lodes at the time of mine closure. The provided lithological data of the 169 CMS surface boreholes did not include the spatial position of the lodes intersected. The peg index, composed of the spatial position of the mining pegs, were used in conjunction with underground mining maps to model the lodes of Leeuwpoort Mine. The stoping width of the mine was 1.2m, an average thickness of 1m was assumed for both

the bedded lodes, and fissure and faulted lodes (see Section 4.3.5.2. for the process followed to create the “output volumes” of the lodes).

For the bedded lodes 1m was subtracted from the elevation of the peg points (hanging wall points) to generate footwall points. Because the bedded lodes conform to the bedding planes of the Quartzite unit, the footwall points are perpendicular to the hanging wall points. This means that the modelled bedded lodes have a constant thickness of 1m. For the fissure and faulted lodes, 1m was added to the X- and Y coordinates, depending on the dipping direction of the fissure and faulted lode. However, the fissure and faulted lodes are omnidirectional and each lode has a unique dip. The generated footwall points are not perpendicular to the hanging wall points, and the modelled fissure and faulted lodes do not have a constant thickness. The thickness, and thus subsequently the “output volume”, depends on the angle of dip of the fissure and faulted lodes. As a result, volumes generated for steeply dipping lodes will be overestimated, whereas volumes for shallow dipping lodes will be underestimated. The peg index only indicates where mining took place within the mine. The modelled lode “volumes” thus only represent the mined portions of the lodes and do not include the possible future mining areas for each of the lodes.

The provided lithological data do not note the occurrence of the rhyolites of the Rooiberg Group. Geological maps indicate the presence of the Rooiberg Group on Rietfontein Farm 536 KQ, and the contact of the Rooiberg Group with the underlying geology was thus created in Leapfrog Geo (see Section 4.3.5.3). The geological model of Leeuwpoort Mine was created based on limited information and inferred contact surfaces, and best represent the present knowledge of the geological environment. The 3D geological model is an estimated representation of the geological environment of Leeuwpoort Mine, this model is subject to change.

6.3. Interpolant models

During the post-mortem study, 16 log summary books were uncovered which contain limited assay data (Section 4.2.). The assay data indicates the spatial position ("to and from") of intersected tin mineralization per borehole. This data was used to generate a 3D ore deposit model (Section 5.2.) as well as interpolant models for Leeuwpoort Mine (Section 4.3.6.). Records of structural data could not be uncovered during the post-mortem study, however, surface maps indicate the surface position of some faults and structural features.

In Section 4.3.6.2.1., it is discussed that geological interpretation implies that the metasomatic fluid ascended from the magmatic intrusions and the fluids where mobilized through the cracks and fractures of the complex shear system, as illustrated in Map C893 (Appendix 1). Different pulses of fluids would have had different compositions and intrinsic characteristics, such as temperatures, and pH. It stands to reason that the concentration of the tin bearing fluid would decrease away from the feeder. If multiple feeders are located in close proximity to one another these mineralizations may overlap. These assumptions were made and accepted, and it was concluded that, at present, the best type of interpolant model, is the linear model.

The majority of the mineralization at Leeuwpoort Mine is constrained to the quartzite lithology, and an interpolance model for this lithology was created. Interpolance models are refined by incorporating structural data. Due to the limited structural information, a "global trend" was used to refine the interpolant model for the geological area (Section 4.3.6.2.2.). The bedded lodes are stratigraphically controlled and conform to the contact surface between the Quartzite unit and Shaly Quartzite/ Shaly Arkose unit. A "global trend" (16.1 dip, 126.5 azimuth, and 92.6 pitch), derived from the contact surface, was used to refine the quartzite interpolant model. Global trends refine interpolant models to some extent, but "structural trend" defines omnidirectional trends and will refine an interpolant model the best. However, large quantities of structural data is needed to define "structural trends".

Out of the 32 lodes modelled for Leeuwpoort Mine, only 9 lode interpolant models could be created. A significant number of assay data needs to be available for a lode "surface" in order to create a representative interpolant of the lodes. If more complete assay data are found, interpolant models for all 32 lodes could be created.

6.4. Application of 3D models for exploration purposes

The aim of this thesis was to create a 3D geological model of Leeuwpoort Mine and to assess the applicability of the 3D model as a possible tool for exploration. The 3D geological model was used to plan 500 random drillholes, and to evaluate the expected grade for the drillholes (Section 4.3.7.1. and Section 4.3.7.2). The results obtained from the planned drillholes were used to determine the number of lodes intersected per drillhole (Section 4.3.7.3). The probability of intersecting a number of lodes were calculated in IBM SPSS 23.

If 500 boreholes are randomly drilled, there is a 16.6% chance of intersecting a lode of economic significance and an 83.4 % chance of intersecting only barren geology. The question arises what the effect on the probability would be if the sample population changed? A resampling analysis on the 500 planned drillhole was conducted using the Bootstrap method. Sample sizes of 20, 40 and 80 boreholes were randomly selected from the 500 planned drillhole to determine how the probability of intersecting a lode would change? In addition, the modelled volumes of the lodes were used to determine the minimum contained metal for each of the individual lodes

6.4.1. 3D models as a future borehole planning tool

One of the main reasons why 3D geological modelling software is becoming increasingly popular is because future exploration projects can easily be planned. Leapfrog Geo has a “planned drillhole” function which allows the user to plan future boreholes for a specific area to reach a target with a specific grade. The “planned drillhole” function was used to create the 500 random drillholes and to evaluate the expected grade for each of the drillholes. The expected grades of the planned drillholes are generated from known assay data in the 3D model.

However, the expected grades of the planned drillholes are only estimated values and depends on the quality of the geological model. If large quantities of assay data is available to complete the evaluation, the expected grades will have a low level of uncertainty. In the case of Leeuwpoort Mine, limited assay data are available. Therefore the planned drillholes were evaluated against the ore zone to give a better geological representation of the grade distribution (Section 4.3.7.2.) The results obtained from this evaluation was used to determine the number of lodes intersected per planned drillhole (Section 4.3.7.3.). The boreholes intersecting the most lodes will thus be more favourable.

6.4.2. Evaluating the change in probability for the bootstrap analysis

In Section 4.3.7.4, the processes followed to conduct a bootstrap analysis for the planned drillholes are explained. Section 5.5 includes the results obtained for the probability of intersecting a lode of economic significance if 20, 40 and 80 boreholes were used respectively. The process was iterated 1000 times.

Table 18, Table 19, and Table 20 summarize the statistical results obtained for the probability of intersecting a lode of economic significance. The probability of intersecting a lode is 16.6% for the 20, 40 and 80 samples. This implies that if boreholes are randomly drilled in the defined boundary (Figure 37), there is a 16.6% chance of intersecting a lode of economic significance, irrespective of the borehole location. The statistical results also indicates that the standard deviation of the probability decreases as the sample size increases. This means that the level of uncertainty in the prediction of intersecting an economically significant lode decreases.

6.4.3. Using 3D models to determine volumes and minimum contained metal for the lodes

The volumes of the lodes were determined in Leapfrog Geo, and were used to determine the minimum contained metal for each of the lodes (Section4.3.7.5.). A constant grade of 0.4 wt. - % Sn (the cut-off grade during mining operation) and density of 2.65 g/cm^3 were assumed for the calculation which inevitably resulted in a the linear relationship between minimum contained metal and volume (Figure 57). If production data are discovered in the future, the volumes and contained metal of each lode can be calculated correctly.

In Section 6.2, the modelling limitations for the lodes were discussed. Because the volumes of the modelled lodes are used to calculate the minimum contained metal, the values for the fissure and faulted lodes (Table 15) are not correct. The minimum contained metal calculate for the fissure and faulted lodes are not representative of the volumes as they may be over- and under estimated, depending on the dip angle of the lodes. Steeper dipping lodes will be overestimated, whereas shallow dipping lodes will be underestimated.

6.4.4. 3D models as a tool for exploration purposes

From the bootstrap analysis it can be seen that it was possible, by the applied method, to quantify the difference in uncertainty as a function of boreholes modelled. The sample of 20 boreholes used for bootstrap analysis has a higher level of uncertainty than the 40 and 80 sample analysis. Large quantities of boreholes are needed to give statistically accurate results. 3D geological models are an essential tool for financial planning of a mine. A good quality 3D geological model will identify possible drilling targets and drillhole planning can be adjusted accordingly.

As can be expected, the more money is invested in the drilling program the statistically reliable information will be obtained. If insufficient money is invested for the drilling program, limited boreholes will be drilled, which, considering the statistical probability to intersect a mineralization of economic interest, give the wrong indication of the potential of the exploration target. When considering Greenfields exploration (virgin exploration), the chances of intersecting a mineralized body is extremely low, and a lot of money has to be invested to obtain significant results. However, if Brownfields exploration (exploration on a known area) takes place, the chances of intersecting a mineralized body is higher, because prior knowledge of the area exists and can be used to make informed decisions on where to drill. Less money needs to be invested for the drilling than for Greenfields exploration. In the case of Leeuwpoort Mine, unfortunately even Brownfields exploration will bear a very limited chance of identifying a mineralized body.

The 3D geological model and interpolant models of Leeuwpoort Mine is based on crude estimations due to limited data. The effectiveness of 3D model as possible tools for understanding geological relationships, aid in exploration and ultimately mining, is limited by the quality of the data. However, 3D models can be used as a summary and visualization tool for where mining occurs, and thus subsequently the geological characteristics of the deposit. The 3D visualization of the deposit gives a much better representation of the orebody than 2D cross-sections from a few drillholes.

7. CONCLUSIONS

3D models can be used as a summary and visualization tool for geological environments. The 3D visualization of deposit give a much better representation of the orebody than 2D cross-sections from a few drillholes. The effectiveness of 3D model, as a possible tool for mining, is limited by the quality and quantity of the data. Poor quality data will result in poor quality models, whereas limited data will result in a higher level of uncertainty of the estimates based from these 3D models. However, even limited data can be used to visualize geological environments.

In the case of Leeuwpoort Mine, limited structural and lithological information for the 32 lodes were obtained from the post-mortem study. However, the provided peg index noted the positions of the mine pegs, and consequently indicate where the lodes were mined. In this instance, with limited mine peg data, the lode “volumes” could be reconstructed. The peg index was used to delineate the mining area in order to model the lodes, as well as interpret geological features. Once the 32 lode “volumes” were created in the 3D model, the specific orezone with the geometric relationship between individual lodes of Leeuwpoort Mine could be defined. In addition, the probability of intersecting a certain number of lodes was derived from these modelled surfaces, resulting in the estimation for the predicted probability of success.

The 3D geological and interpolant models created of Leeuwpoort Mine were used to determine the probability of intersecting a lode of economic interest, if exploration drilling were to be done. The study indicated that if 500 drillholes were randomly selected, there is a 16.6% chance of intersecting a lode of economic significance. Because 83.4% of the random drillholes intersected barren geology, resampling was conducted using the bootstrap method, in order to determine how reliable this prediction is as a function of number of boreholes. Because the standard deviation of the estimated success decreases with increasing number of boreholes, less variation from the average success rate can be expected between individual sets of 20, 40 or 80 boreholes. The results obtained from the bootstrap analysis indicates that the average probability of intersecting a lode of economic significance, for each of the different sample sizes stays the same: 16.6%. This implies that irrespective of the location inside the defined boundary, there is a 16.6% chance of intersecting a lode of economic significance. The results from the bootstrap analysis indicates that the standard deviation of the probability of intersecting a lode, reduces as the statistical sample size increases. This means that the more boreholes are drilled, the lower the uncertainty of the estimates. A higher level of

confidence in the probability of intersecting a lode can thus be assumed for areas that have large quantities of drilling.

The volumes for each of the lodes were calculated in Leapfrog Geo, and was subsequently used to calculate the minimum contained metal (tonnage) for each lode. Due to limited production data a constant grade (0.4 wt. - % Sn) and constant density (2.65 g/cm^3) was assumed for the calculation, which subsequently resulted in a linear relationship between minimum contained metal and volume. However, with the identified limitation the size distribution could be calculated. A linear relationship can be identified from these calculated values, the distribution of the minimum grade (tonnage) indicates the probability of finding a lode or orebody of a specific size.

If a geological environment similar to that of Leeuwpoort Mine is considered for an exploration project, the chances of intersecting an economical orebody or lode during exploration is very low. When considering Greenfields exploration (virgin exploration), the chances of intersecting a mineralized body is extremely low, and a lot of money has to be invested to obtain meaningful results. However, if Brownfields exploration (exploration on a known area) takes place, the chances of intersecting a mineralized body is higher, because prior knowledge of the area exists and can be used to make informed decisions on where to drill. Less money needs to be invested for the drilling than for Greenfields exploration. In the case of Leeuwpoort Mine, unfortunately even Brownfields exploration will bear a very limited chance of identifying a mineralized body, which means that in such a scenario, the information about potential success rate of a drilling program is even more important for drilling and financial planning.

8. REFERENCES

AGTERBERG, F. 1995. Multifractal modeling of the sizes and grades of giant and supergiant deposits. *International Geology Review,* 37**,** 1-8.

ANNELS, A. E. 2012. *Mineral Deposit Evaluation: a practical approach*, Springer Science & Business Media.

BOLSTAD, P. 2005. GIS fundamentals. *A first text on Geographic Information Systems*.

BUCHANAN, P. 2006. The Rooiberg Group. *The Geology of South Africa, Johannesburg: Council for Geoscience, Pretoria: Geological Society of South Africa***,** 283-289.

CAIRNS, R. D. 1986. A model of exhaustible resource exploitation with Ricardian rent. *Journal of Environmental Economics and Management,* 13**,** 313-324.

CAIRNS, R. D. & SHINKUMA, T. 2003. The choice of the cutoff grade in mining. *Resources Policy,* 29**,** 75-81.

CARGILL, S., ROOT, D. & BAILEY, E. 1980. Resource estimation from historical data: Mercury, a test case. *Journal of the International Association for Mathematical Geology,* 12**,** 489-522.

CARMICHAEL, R. S. 1982. *CRC handbook of physical properties of Rocks*, CRC Press. Inc.

CHILES, J.-P. & DELFINER, P. 2009. *Geostatistics: modeling spatial uncertainty*, John Wiley & Sons.

COWAN, E., BEATSON, R., FRIGHT, W., MCLENNAN, T. & MITCHELL, T. 2002. Rapid geological modelling. *App. Structural Geo. for Mining Expl. and Miing*.

COWAN, E., BEATSON, R., ROSS, H., FRIGHT, W., MCLENNAN, T., EVANS, T., CARR, J., LANE, R., BRIGHT, D. & GILLMAN, A. Practical implicit geological modelling. Fifth International Mining Geology Conference, 2003. Australian Institute of Mining and Metallurgy Bendigo, Victoria, 17-19.

COX, D. P. & SINGER, D. A. 1986. *Mineral deposit models*, US Government Printing Office Washington, DC, USA.

CROCKER, I. T., EALES, H. V. & EHLERS, D. L. 2001. The fluorite, cassiterite and sulphide deposits associated with the acid rocks of the Bushveld Complex. *Memoir- geological survey(Pretoria)*.

DALY, R., MANGER, G. E. & CLARK, S. P. 1966. Section 4: Density of rocks. *Geological Society of America Memoirs,* 97**,** 19-26.

DANESHVAR SAEIN, L., RASA, I., RASHIDNEJAD OMRAN, N., MOAREFVAND, P., AFZAL, P. & SADEGHI, B. 2013. Application of Number-Size (NS) Fractal Model to Quantify of the Vertical Distributions of Cu and Mo in Nowchun Porphyry Deposit (Kerman, Se Iran)/Zastosowanie modelu fraktalnego ns (liczba-rozmiar) do ilościowego określenia

pionowego rozkładu Cu i Mo w złożu porfirowym (Kerman, Iran). *Archives of Mining Sciences,* 58**,** 89-105.

DELPORT, P. W. J. 2017. *Map of Leeuwpoort 554KQ, Rietfontein 536KQ and Vellefontein 517KQ*, 1:75000.

DEYOUNG, J. H. 1981. The Lasky cumulative tonnage-grade relationship; a reexamination. *Economic geology,* 76**,** 1067-1080.

DOMINY, S. C., NOPPÉ, M. A. & ANNELS, A. E. 2002. Errors and uncertainty in mineral resource and ore reserve estimation: The importance of getting it right. *Exploration and Mining Geology,* 11**,** 77-98.

DU TOIT, M. & PRINGLE, I. 1998. Tin. *The Mineral Resources of South Africa. Handbook, Council for Geoscience,* 16**,** 613-620.

EMERY, K. 2007. Probabilistic modelling of lithological domains and it application to resource evaluation. *Journal of the Southern African Institute of Mining and Metallurgy,* 107**,** 803-809.

EMERY, X. & ORTIZ, J. 2005. Estimation of mineral resources using grade domains: critical analysis and a suggested methodology. *Journal of the South African Institute of Mining and Metallurgy,* 105**,** 247-255.

EMERY, X. & ORTIZ, J. M. 2004. Shortcomings of multiple indicator kriging for assessing local distributions. *Applied Earth Science,* 113**,** 249-259.

ERIKSSON, P., ALTERMANN, W. & HARTZER, F. 2006. The Transvaal Supergroup and its precursors. *The Geology of South Africa. Geological Society of South Africa, Johannesburg/Council for Geoscience, Pretoria***,** 237-260.

ERIKSSON, P., HATTINGH, P. & ALTERMANN, W. 1995. An overview of the geology of the Transvaal Sequence and Bushveld Complex, South Africa. *Mineralium Deposita,* 30**,** 98-111.

ERIKSSON, P., SCHWEITZER, J., BOSCH, P., SCHEREIBER, U., VAN DEVENTER, J. & HATTON, C. 1993. The Transvaal sequence: an overview. *Journal of African Earth Sciences (and the Middle East),* 16**,** 25-51.

FALCON, L. 1989. Tin in South Africa. *Journal of the South African Institute of Mining and Metallurgy(South Africa)***,** 59-72.

FRIEDE, H. 1976. Tin mining and smelting in the Transvaal during the Iron Age. *Journal of the Southern African Institute of Mining and Metallurgy,* 76**,** 461-470.

GLACKEN, I. & SNOWDEN, D. 2001. Mineral resource estimation. *Mineral Resource and Ore Reserve Estimation–The AusIMM Guide to Good Practice, The Australasian Institute of Mining and Metallurgy: Melbourne. P***,** 189-198.

GODSELL, S. 2011. Rooiberg: The Little Town that Lived. *South African Historical Journal,* 63**,** 61-77.

GRANT, M. R. 1999. The sourcing of Southern African tin artefacts. *Journal of Archaeological Science,* 26**,** 1111-1117.

GRIFFITH, A. 2007. *SPSS for Dummies*, John Wiley & Sons.

H.C.B. 1982. *Plan showing all surface boreholes and anticipated outer mineralization limits on the Gap Lower Lode for the Northern Area*, 1:5000.

HARTZER, F. 1995. Transvaal Supergroup inliers: geology, tectonic development and relationship with the Bushveld Complex, South Africa. *Journal of African Earth Sciences,* 21**,** 521-547.

HOGSON, C. 1990. Uses (and abuses) of ore deposit models in mineral exploration. *Geoscience Canada,* 17.

IVANOV, O. P., EFREMENKO, L. J., SHCHERBAKOVA, M. J., SUKNEV, V. S. & VOROBIEV, I. K. 1980. Features of Varying Composition and Properties of the Natural Crystal of Cassiterite in the Process of Its Growth. *Transactions - Doklady, Russian Academy of Sciences: Earth Science Section,* 251**,** 689-692.

IVANOV, O. P., VOROB'YEV, Y. K., YEFREMENKO, L. Y., SUKNEV, V. S. & SHCHERBAKOVA, M. Y. 1982. Variation in composition and properties of a natural cassiterite crystal during growth. *Transactions - Doklady, Russian Academy of Sciences: Earth Science Section,* 251**,** 153-156.

JOHNSON, P., EVATT, G., DUCK, P. & HOWELL, S. The derivation and impact of an optimal cut-off grade regime upon mine valuations. Proceedings of the World Congress on Engineering, 2010.

KENT, L. & MATTHEWS, P. 1980. Stratigraphy of South Africa. Part1. Lithostratigraphy of the Republic of South Africa, South West Africa/Namibia, and the Republics of Bophuthatswana, Transkei and Venda. *Handbook of the Geological Survey of South Africa,* 8**,** 690.

KRAUTKRAEMER, J. A. 1988. The cut-off grade and the theory of extraction. *Canadian Journal of Economics***,** 146-160.

KRISHNAMURTHY, T. 2005. Comparison of response surface construction methods for derivative estimation using moving least squares, kriging and radial basis functions.

LABUSCHAGNE, L. S. 2004. Evolution of the ore-forming fluids in the Rooiberg tin field, South Africa. *Memoir- Council for Geoscience*.

LASKY, S. 1950. Mineral resource appraisal by the US geological survey. *Colorado School of Mines Quarterly,* 45**,** 1-27.

LEAPFROGGEO 2016. *Leapfrog Geo: Fundamentals training session notes,* Christchurch, New Zealand, ARANZ Geo Limited.

LENTHALL, D. 1974. *Tin production from the Bushveld Complex*, University of the Witwatersrand.

LEUBE, A. & STUMPFL, E. 1963. The Rooiberg and Leeuwpoort tin mines, Transvaal, South Africa. *Economic Geology,* 58**,** 527-557.

MANDELBROT, B. 1983. The fractal geometry of nature WH Freeman San Francisco. CA.

MATHERON, G. 1962. Traité de géostatistique appliquée, tome i: Mémoires du bureau de recherches géologiques et minières. *Editions Technip, Paris,* 14.

MATHERON, G. 1963. Principles of geostatistics. *Economic geology,* 58**,** 1246-1266.

MISIEWICZ, J. E. 1989. *Rooiberg Tin LTD. Leeuwpoort 'C' Mine geology, mineralized lodes, structure and surface boreholes*, 1:5000.

ORTIZ, J. & EMERY, X. 2006. Geostatistical estimation of mineral resources with soft geological boundaries: a comparative study. *JOURNAL-SOUTH AFRICAN INSTITUTE OF MINING AND METALLURGY,* 106**,** 577.

OSANLOO, M. & ATAEI, M. 2003. Using equivalent grade factors to find the optimum cut-off grades of multiple metal deposits. *Minerals Engineering,* 16**,** 771-776.

PHILLIPS, A. H. 1982. The geology of the Leeuwpoort tin deposit and selected aspects of its environs.

REID, R. 2017. Implicit modelling disasters in the making-Part 1. *LinkedIn* [Online]. [Accessed 7 August 2017].

RENDU, J.-M. 2014. *An introduction to cut-off grade estimation*, SME.

ROSE, A. W. 1988. Mineral deposit models: Dennis P. Cox and Donald A. Singer (Editors). Bulletin 1693, US Geological Survey, Washington, DC, USA, 1986, 379 pp., $19.00. *Journal of Geochemical Exploration,* 30**,** 334-335.

ROSSI, M. E. & DEUTSCH, C. V. 2013. *Mineral resource estimation*, Springer Science & Business Media.

ROZENDAAL, A., MISIEWICZ, J. & SCHEEPERS, R. 1995a. The tin zone: sediment-hosted hydrothermal tin mineralization at Rooiberg, South Africa. *Mineralium Deposita,* 30**,** 178-187.

ROZENDAAL, A., MISIEWICZ, J. E. & SCHEEPERS, R. 1995b. Hydrothermal alteration associated with sediment-hosted Rooiberg tin deposits, South Africa. *Trans. Inst. Min. Metall. Sect. B-Appl,* 104**,** B121-B135.

ROZENDAAL, A., TOROS, M. & ANDERSON, J. 1986. The Rooiberg tin deposits, west-central Transvaal. *Mineral deposits of southern Africa,* 2**,** 1307-1328.

SADEGHI, B., MADANI, N. & CARRANZA, E. J. M. 2015. Combination of geostatistical simulation and fractal modeling for mineral resource classification. *Journal of Geochemical Exploration,* 149**,** 59-73.

SADEGHI, B., MOAREFVAND, P., AFZAL, P., YASREBI, A. B. & SAEIN, L. D. 2012. Application of fractal models to outline mineralized zones in the Zaghia iron ore deposit, Central Iran. *Journal of Geochemical Exploration,* 122**,** 9-19.

SCHREIBER, U. 1990. *A palaeoenvironmental study of the Pretoria Group in the eastern Transvaal*, publisher not identified.

SCHREIBER, U., ERIKSSON, P. & SNYMAN, C. 1991. A provenance study of the sandstones of the Pretoria Group, Transvaal Sequence (South Africa): petrography, geochemistry, and palaeocurrent directions. *South African journal of geology,* 94**,** 288-298.

SCOTT, M. & DIMITRAKOPOULOS, R. 2001. Quantitative analysis of mineral resources for strategic planning: implications for Australian Geological Surveys. *Natural Resources Research,* 10**,** 159-177.

SIMON, J. L. 1997. Resampling: The new statistics.

SINCLAIR, A. J. & BLACKWELL, G. H. 2002. *Applied mineral inventory estimation*, Cambridge University Press.

SINGER, D. A. 1993. Basic concepts in three-part quantitative assessments of undiscovered mineral resources. *Nonrenewable Resources,* 2**,** 69-81.

SINGER, D. A. Estimating amounts of undiscovered mineral resources. Proceedings for a Workshop on Deposit Modeling, Mineral Resource Assessment, and Their Role in Sustainable Development: USGS Circular, 2007a. 79-84.

SINGER, D. A. 2007b. *Short course introduction to quantitative mineral resource assessments*, Citeseer.

SINGER, D. A. 2010. Progress in integrated quantitative mineral resource assessments. *Ore Geology Reviews,* 38**,** 242-250.

SINGER, D. A. & KOUDA, R. 2011. Probabilistic estimates of number of undiscovered deposits and their total tonnages in permissive tracts using deposit densities. *Natural Resources Research,* 20**,** 89-93.

STANLEY, C. 2007. The fundamental relationship between sample mass and sampling variance in real geological samples and corresponding statistical models. *Exploration and Mining Geology,* 16**,** 109-123.

STUMPFL, E. 1977. Sediments, ores, and metamorphism: new aspects. *Philosophical Transactions of the Royal Society of London A: Mathematical, Physical and Engineering Sciences,* 286**,** 507-525.

STUMPFL, E. & LEUBE, A. 1963. The Rooiberg and Leeuwpoort tin mines, part 2: Petrology, mineralogy and geochemistry. *Economic Geology,* 58**,** 527-557.

TAYLOR, H. 1985. Cutoff grades-some further reflections. *Institution of Mining and Metallurgy Transactions. Section A. Mining industry,* 94.

TAYLOR, J. R. & WALL, V. J. 1992. The behavior of tin in granitoid magmas. *Economic Geology,* 87**,** 403-420.

THOMPSON, M. & BARR, D. 2014. Cut-off grade: A real options analysis. *Resources Policy,* 42**,** 83-92.

TURCOTTE, D. L. 1997. *Fractals and chaos in geology and geophysics*, Cambridge university press.

WALKER, R. L. 1985. *C-Mine boreholes and structural contours*, 1:5000.

WANG, G., ZHANG, S., YAN, C., SONG, Y., SUN, Y., LI, D. & XU, F. 2011. Mineral potential targeting and resource assessment based on 3D geological modeling in Luanchuan region, China. *Computers & Geosciences,* 37**,** 1976-1988.

WANG, Q., DENG, J., LIU, H., YANG, L., WAN, L. & ZHANG, R. 2010a. Fractal models for ore reserve estimation. *Ore Geology Reviews,* 37**,** 2-14.

WANG, Q., DENG, J., ZHAO, J., LI, N. & WAN, L. 2012. The fractal relationship between orebody tonnage and thickness. *Journal of Geochemical Exploration,* 122**,** 4-8.

WANG, Q., DENG, J., ZHAO, J., LIU, H., WAN, L. & YANG, L. 2010b. Tonnage-cutoff model and average grade-cutoff model for a single ore deposit. *Ore Geology Reviews,* 38**,** 113-120.

WARMBAD-MUNISIPALITEIT. 1989. *Leeuwpoort District Warmbad*, 1:20000.

WU, Q., XU, H. & ZOU, X. 2005. An effective method for 3D geological modeling with multi-source data integration. *Computers & Geosciences,* 31**,** 35-43.

YAN-LIN, S., AI-LING, Z., YOU-BIN, H. & KE-YAN, X. 2011. 3D geological modeling and its application under complex geological conditions. *Procedia Engineering,* 12**,** 41-46.

ZU, X. F., HOU, W. S., ZHANG, B. Y., HUA, W. H. & LUO, J. 2012. Overview of Three-dimensional geological modeling technology. *IERI Procedia,* 2**,** 921-927.

9. APPENDIX 1: MAP C467, MAP C696 , MAP C716 , AND MAP C893

10. APPENDIX 2: THE BOUNDARY, HANGING WALL POINTS, FOOTWALL POINTS AND POLYLINES USED TO CREATE THE LODE SURFACES FOR THE GEOLOGICAL MODEL

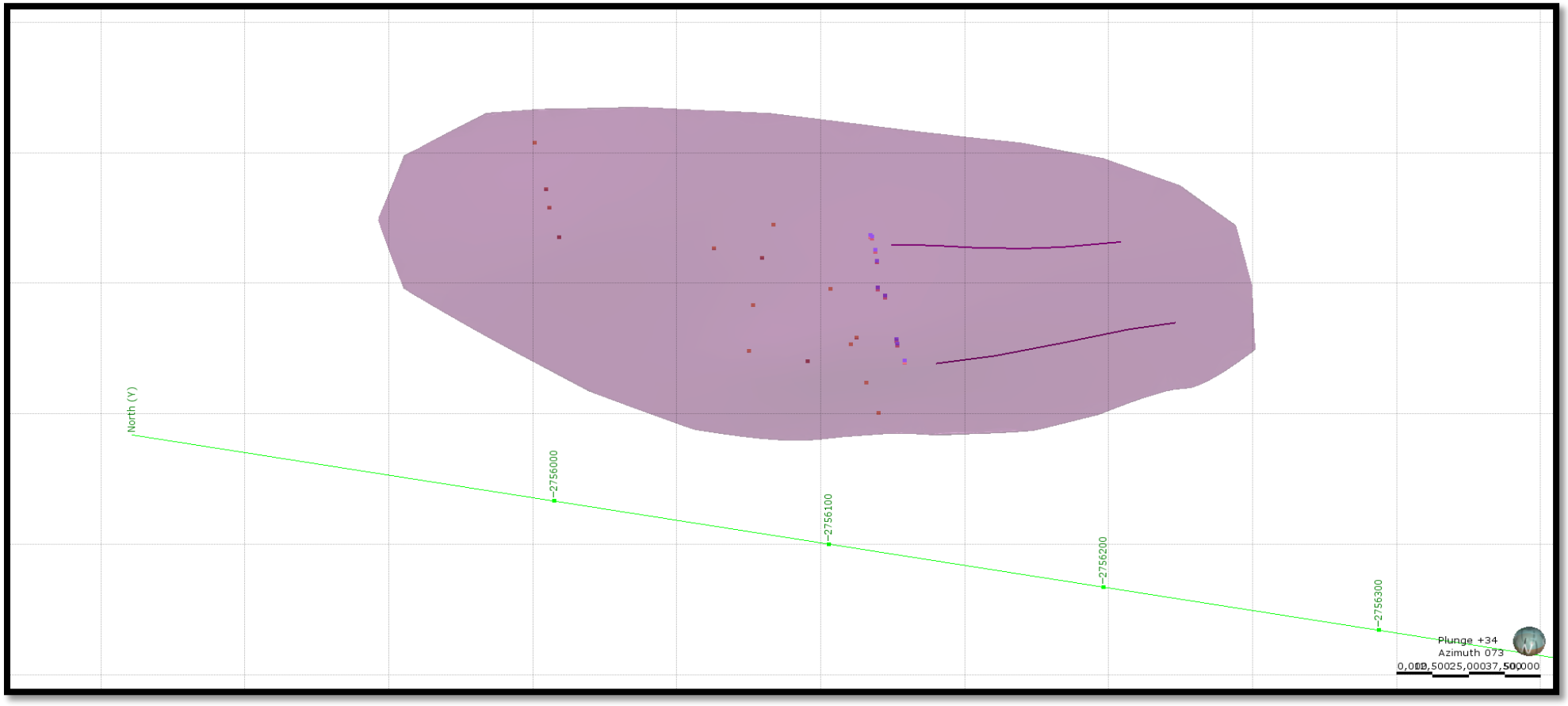

The boundary, hanging wall points, footwall points and polylines used to create the 5S lode surface for the geological model.

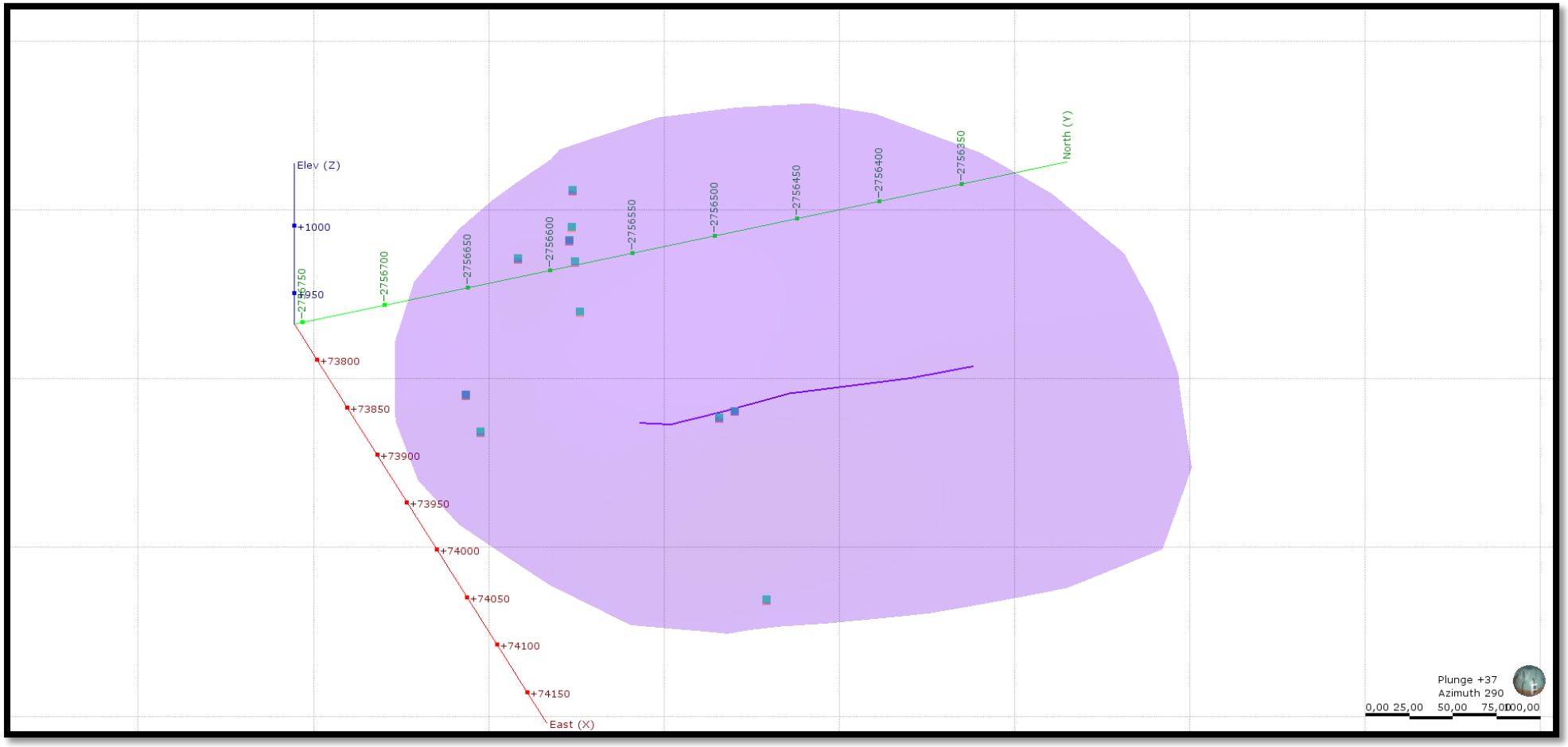

The boundary, hanging wall points, footwall points and polylines used to create the 9S lode surface for the geological model.

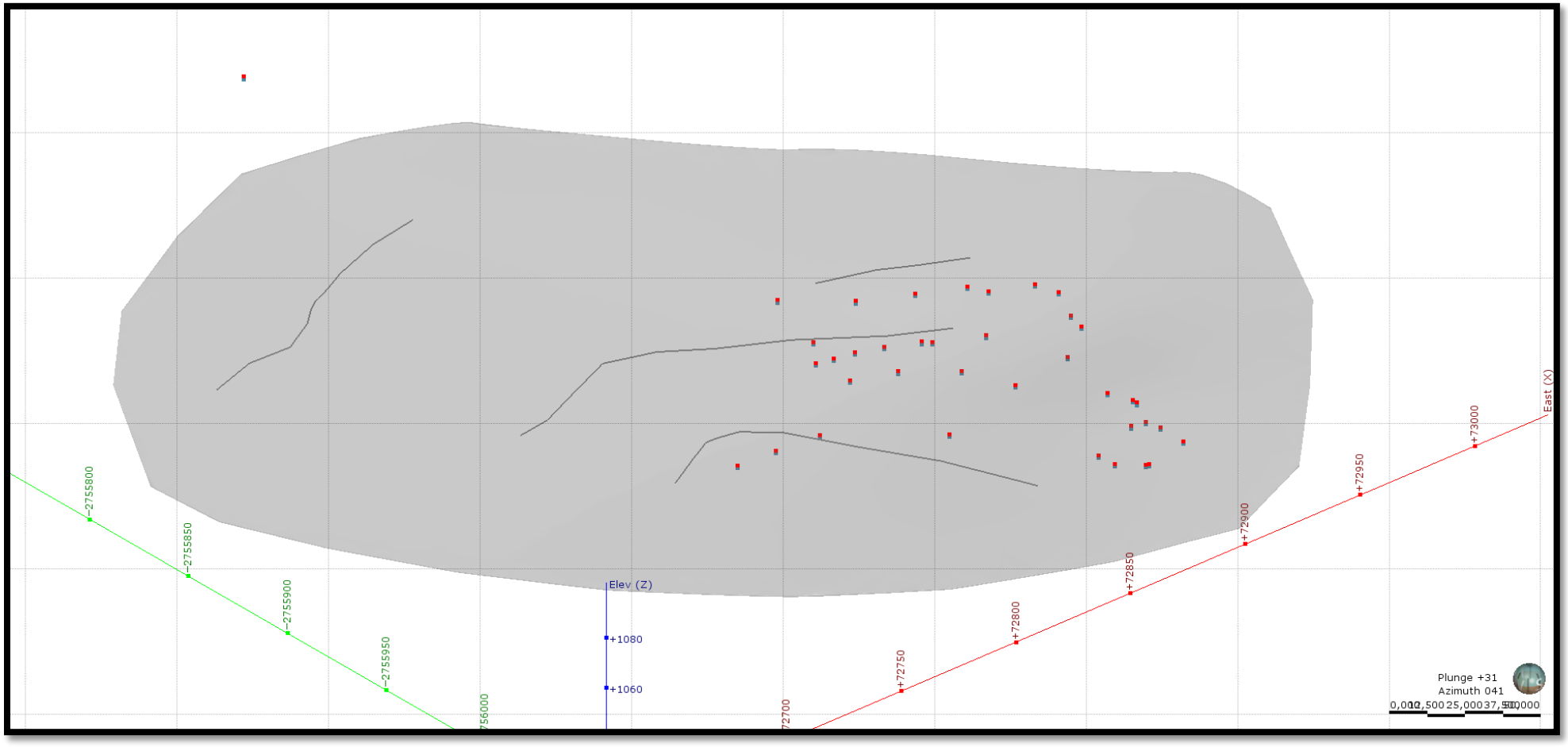

The boundary, hanging wall points, footwall points and polylines used to create the 10N lode surface for the geological model.

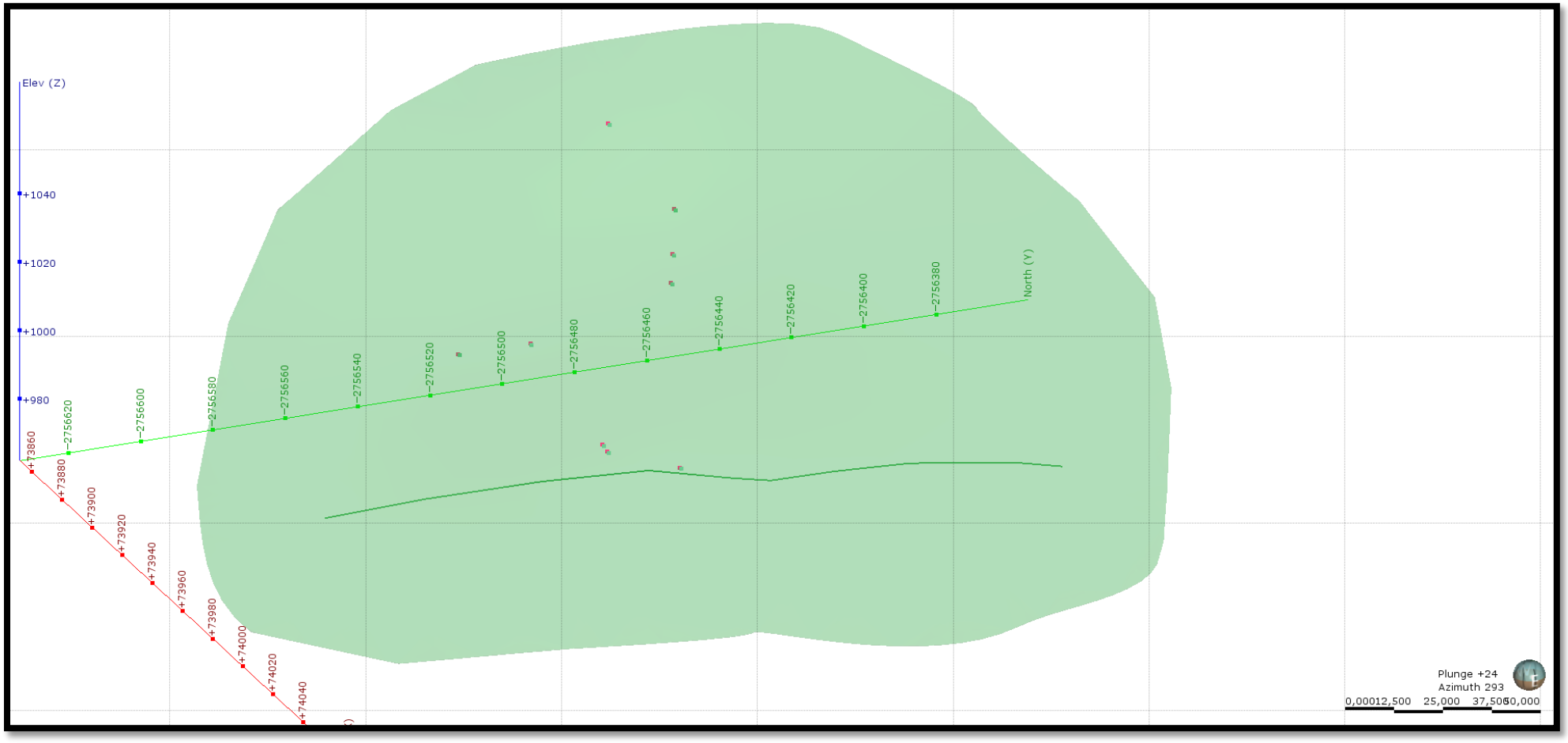

The boundary, hanging wall points, footwall points and polylines used to create the 10TA lode surface for the geological model.

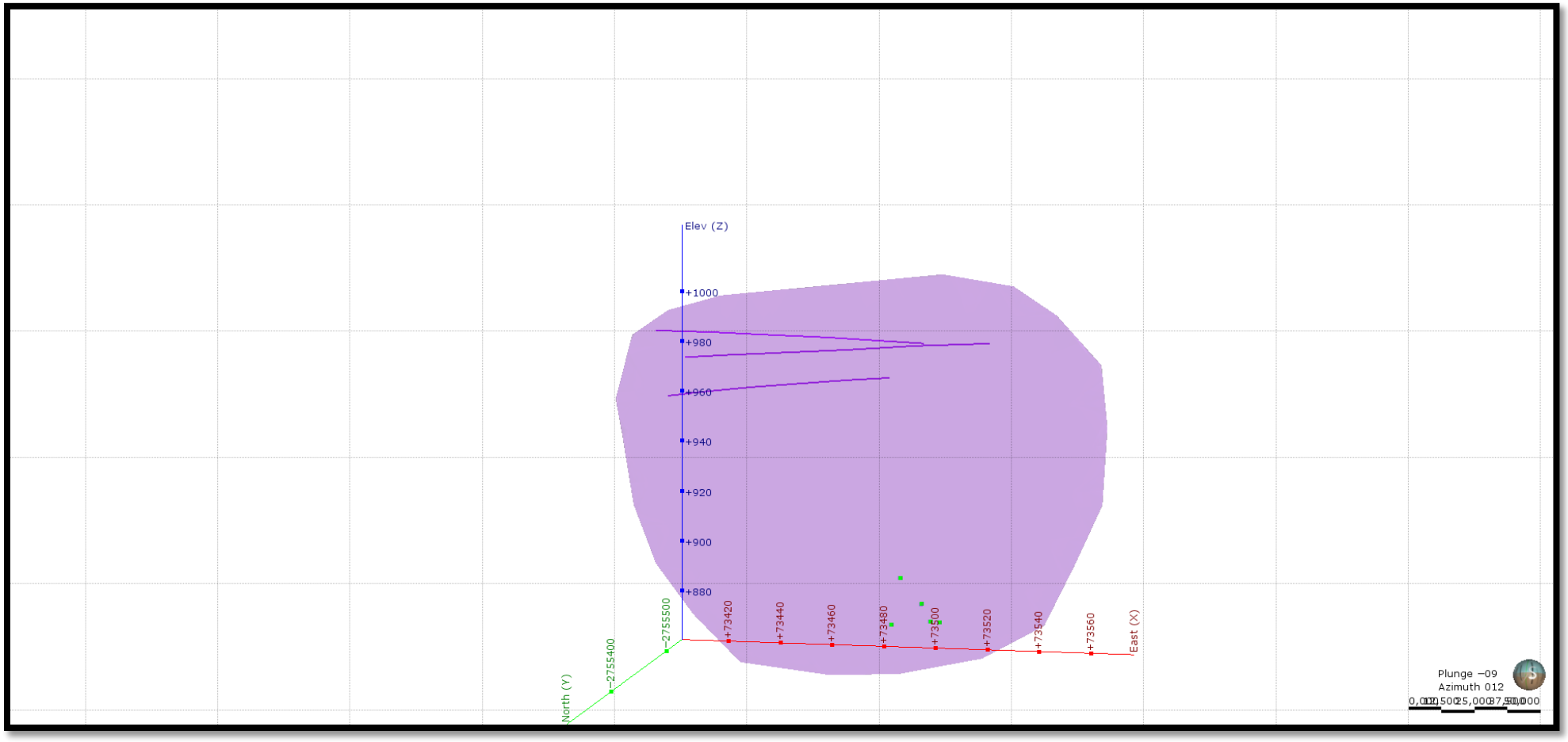

The boundary, hanging wall points, footwall points and polylines used to create the 21P lode surface for the geological model.

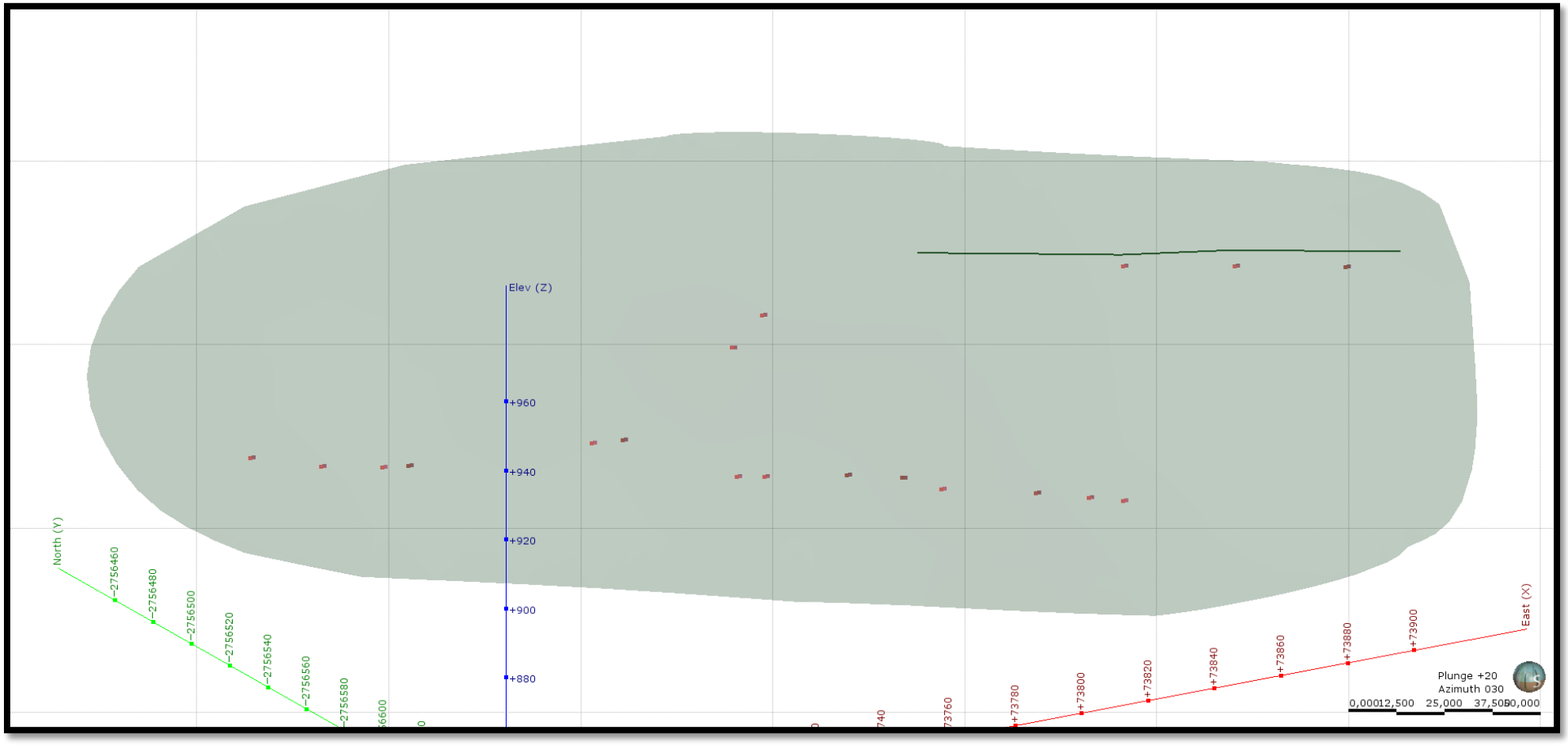

The boundary, hanging wall points, footwall points and polylines used to create the 100’ Fissure lode surface for the geological model.

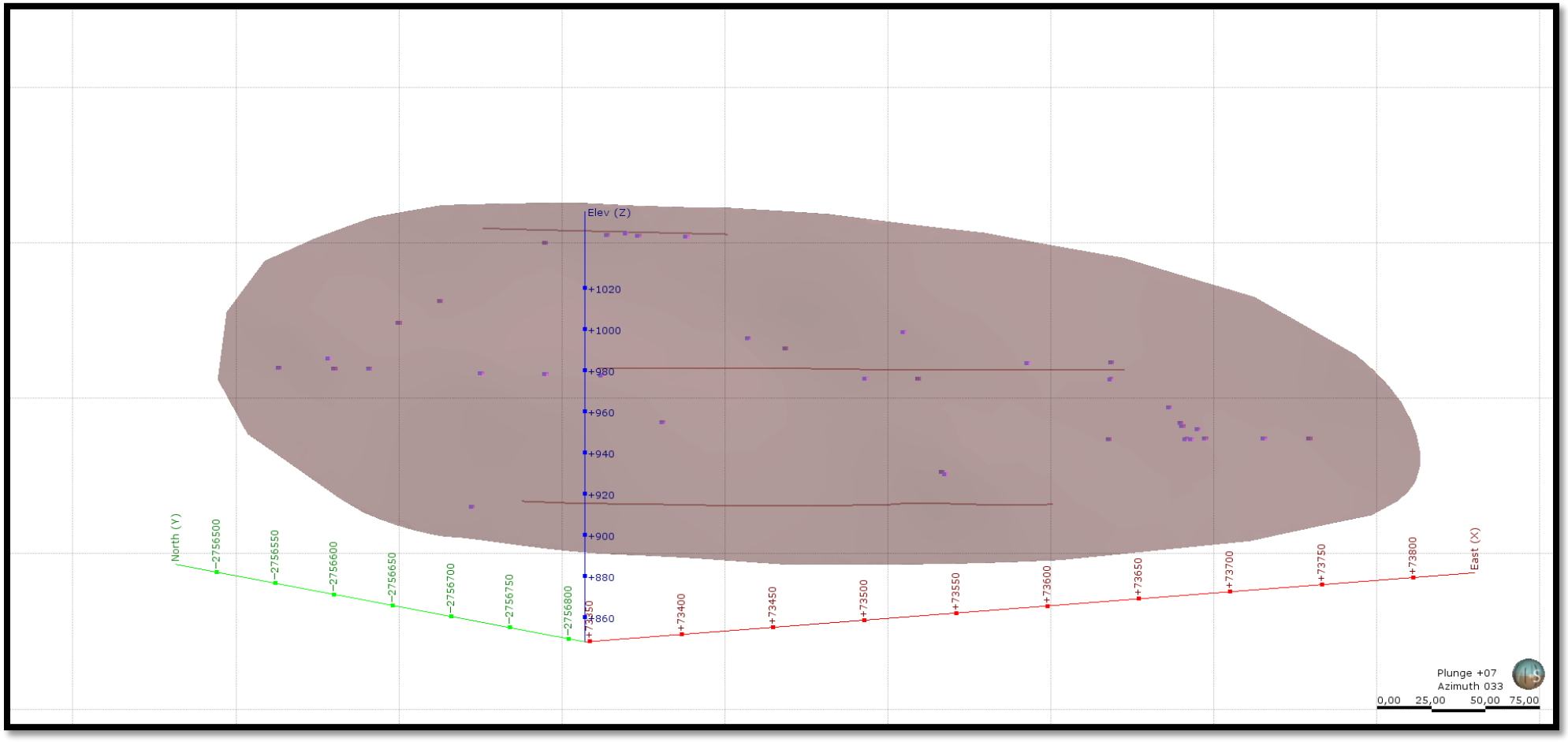

The boundary, hanging wall points, footwall points and polylines used to create the 800’ Fissure lode surface for the geological model.

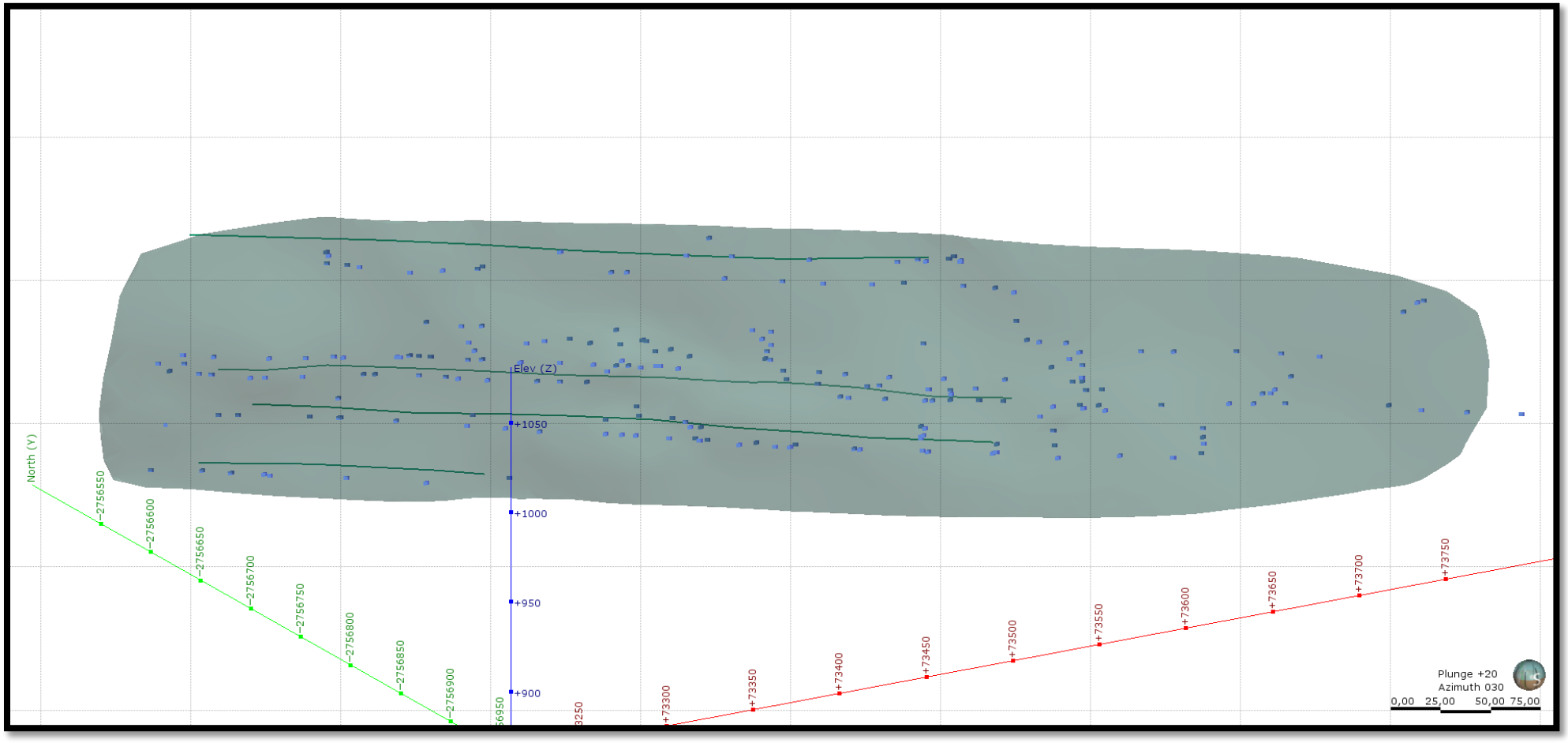

The boundary, hanging wall points, footwall points and polylines used to create the 1200’ Fissure lode surface for the geological model.

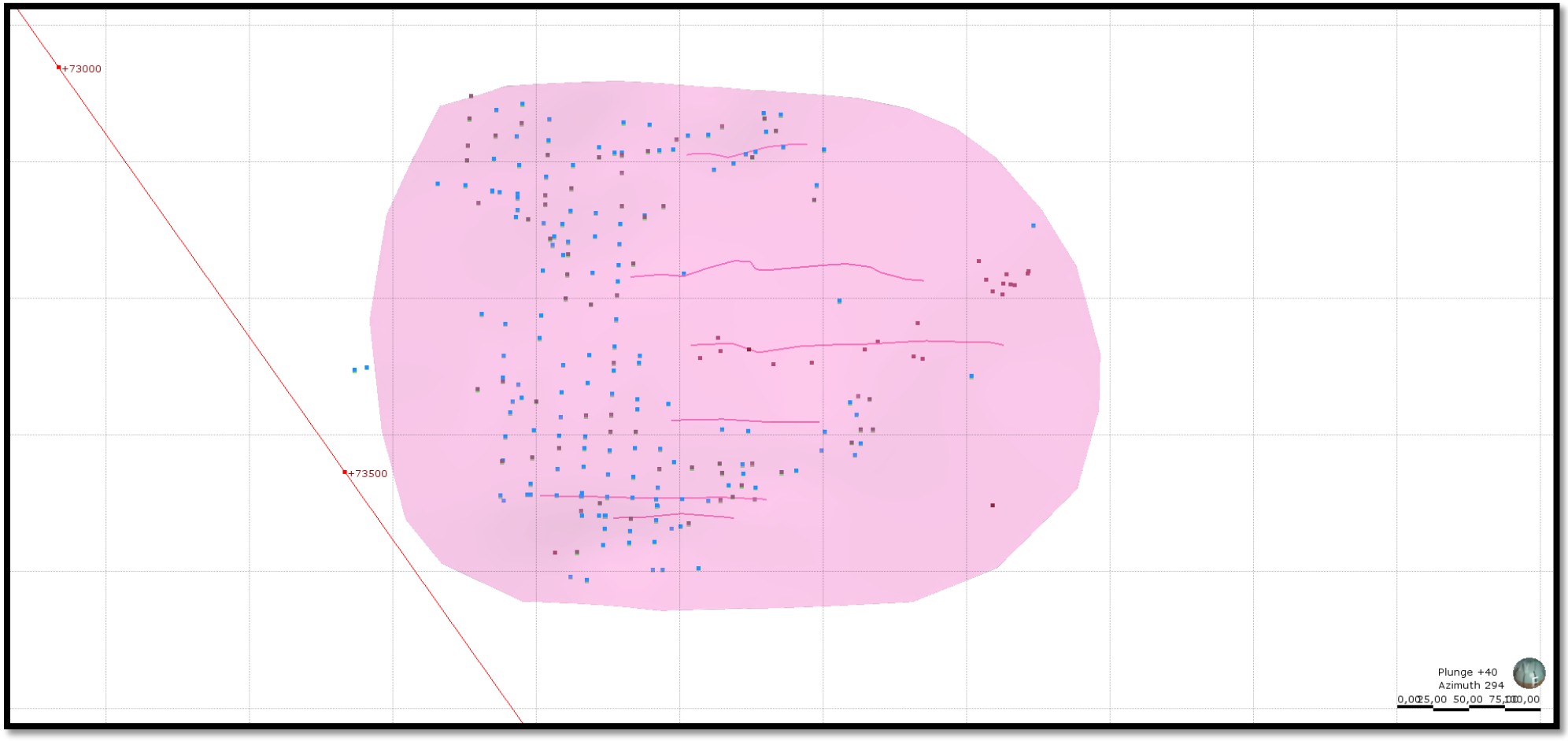

The boundary, hanging wall points, footwall points and polylines used to create the Agnes-Lode lode surface for the geological model.

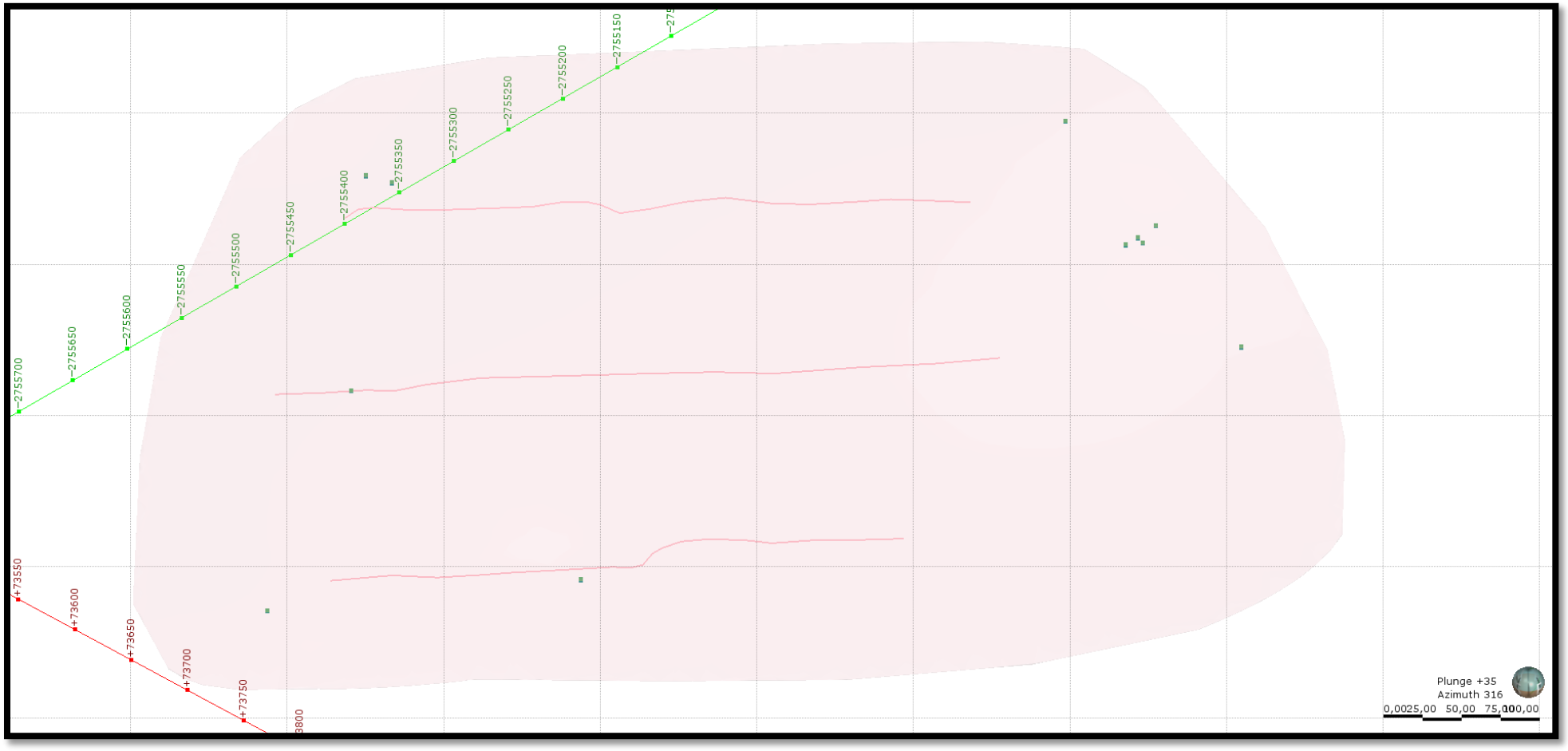

The boundary, hanging wall points, footwall points and polylines used to create the A-Lode lode surface for the geological model.

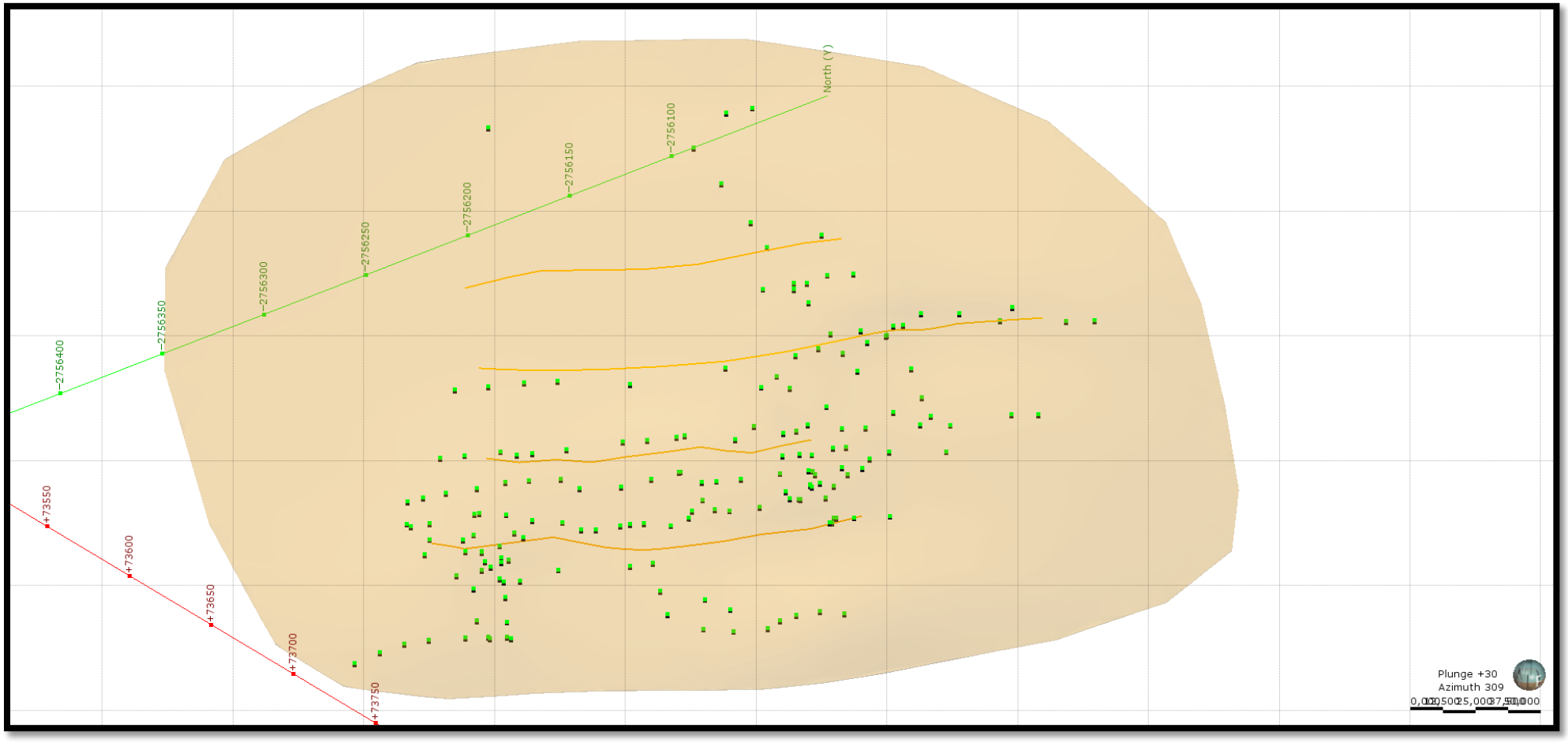

The boundary, hanging wall points, footwall points and polylines used to create the CA-Lode lode surface for the geological model.

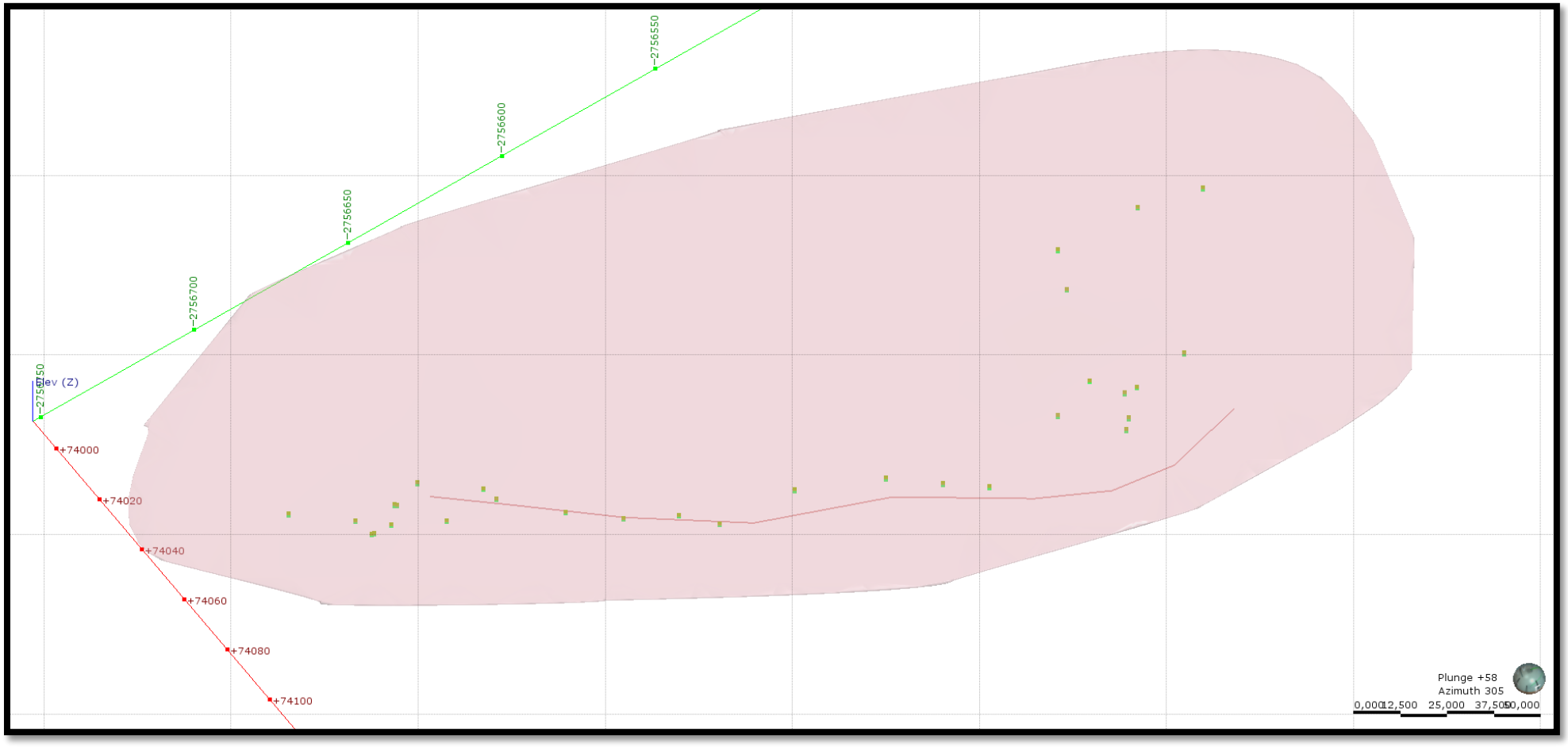

The boundary, hanging wall points, footwall points and polylines used to create the Compound-Lode lode surface for the geological model.

N

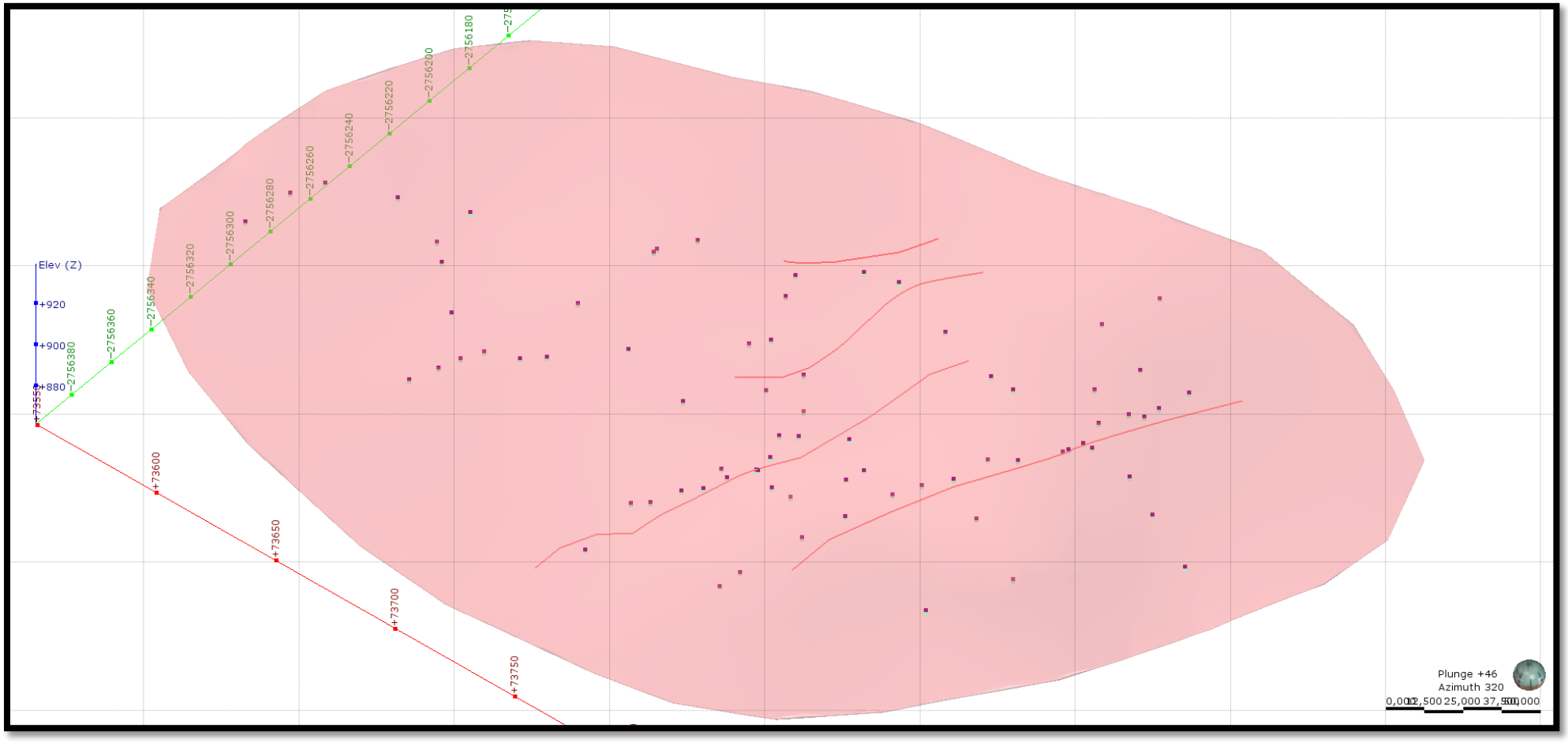

The boundary, hanging wall points, footwall points and polylines used to create the EK-Lode lode surface for the geological model.

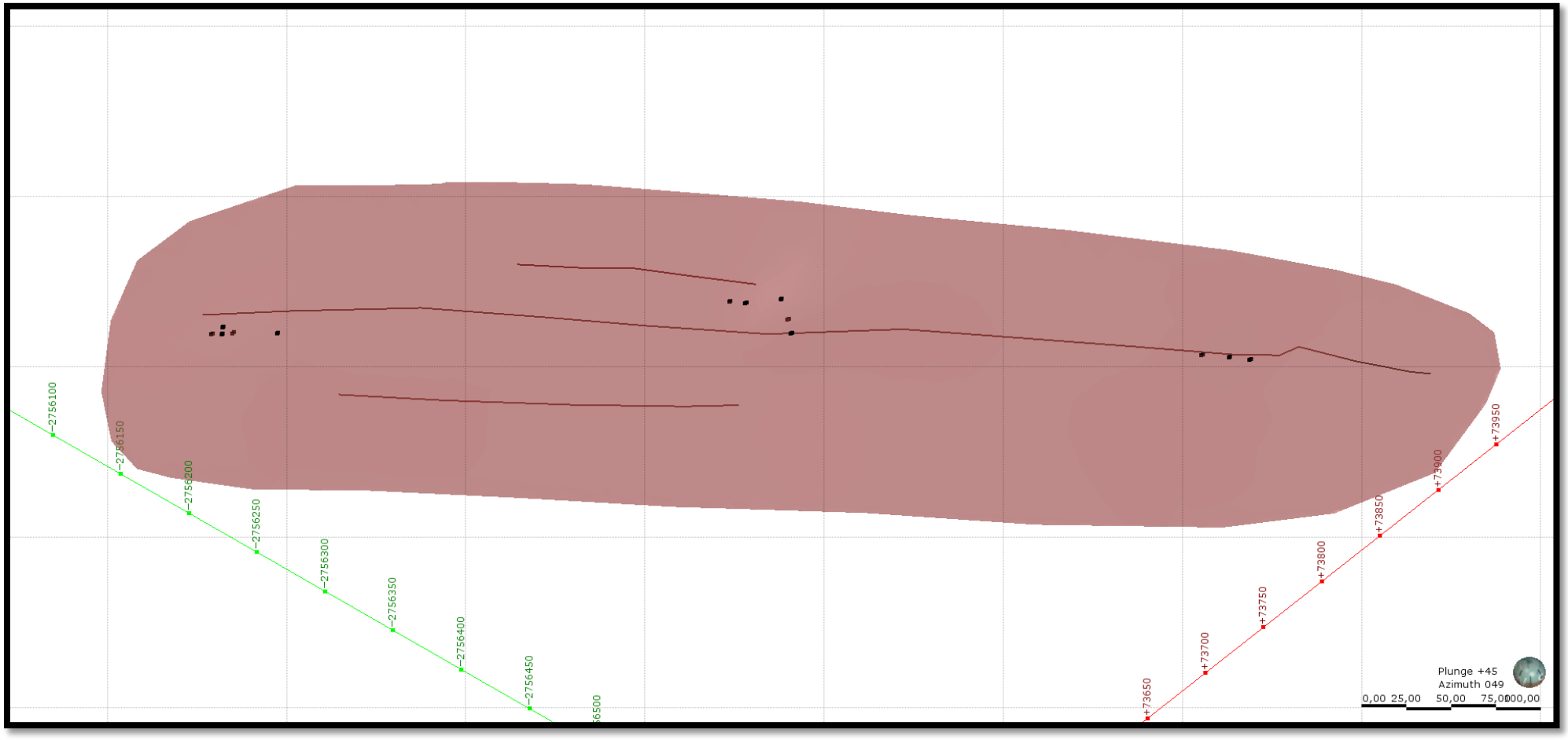

The boundary, hanging wall points, footwall points and polylines used to create the Fault Lode Fissure lode surface for the geological model.

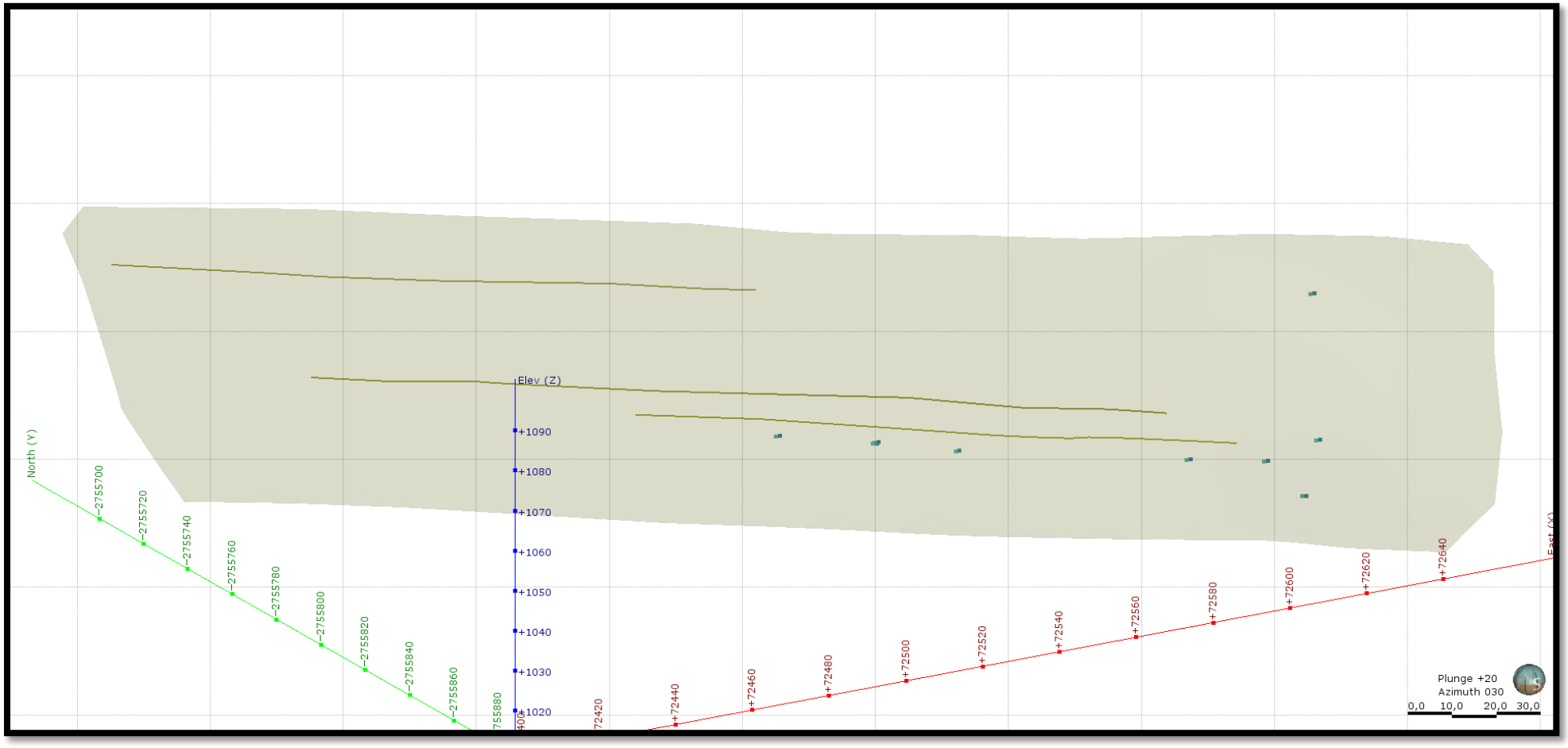

The boundary, hanging wall points, footwall points and polylines used to create the Fault-Lode lode surface for the geological model.

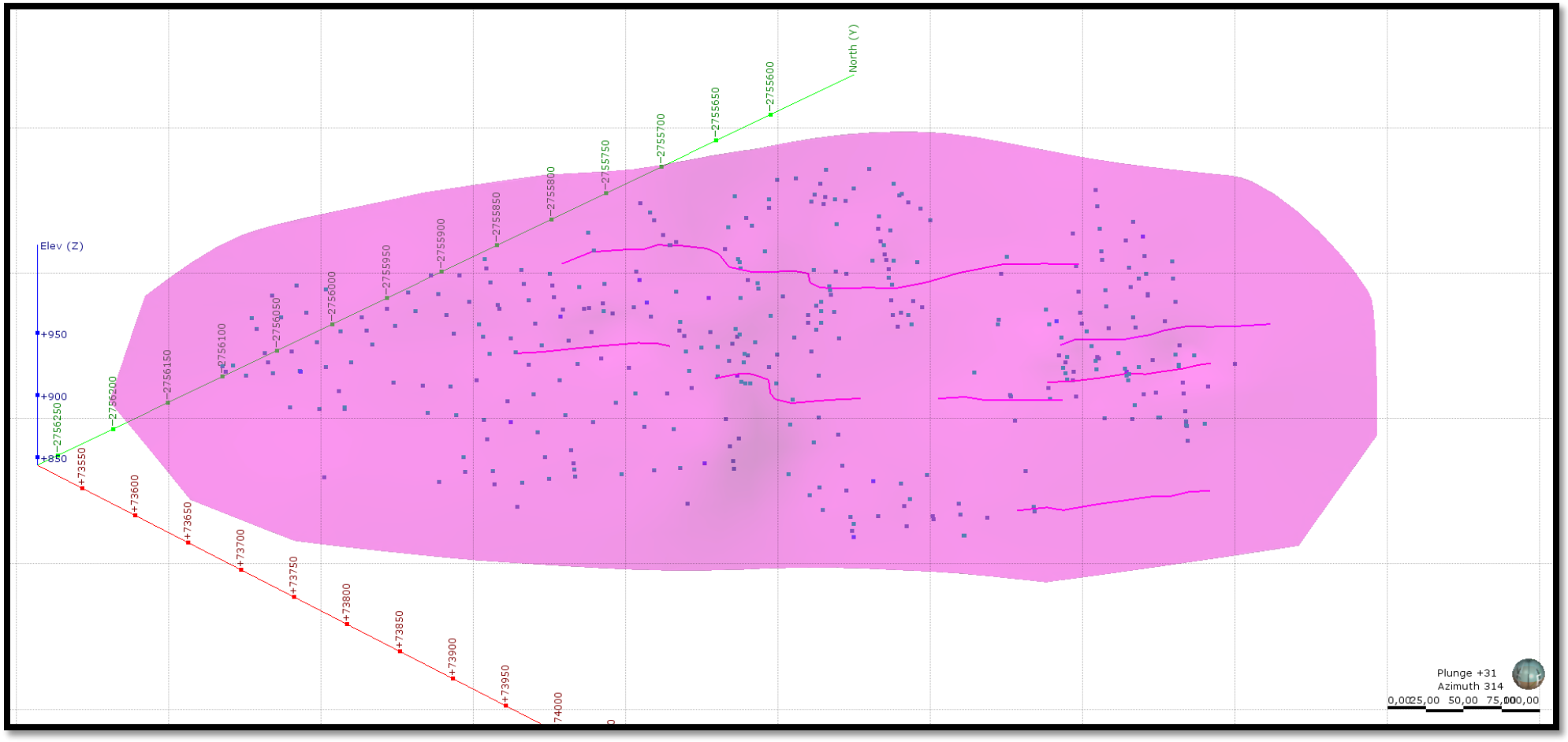

The boundary, hanging wall points, footwall points and polylines used to create the Gap Bottom-Lode lode surface for the geological model.

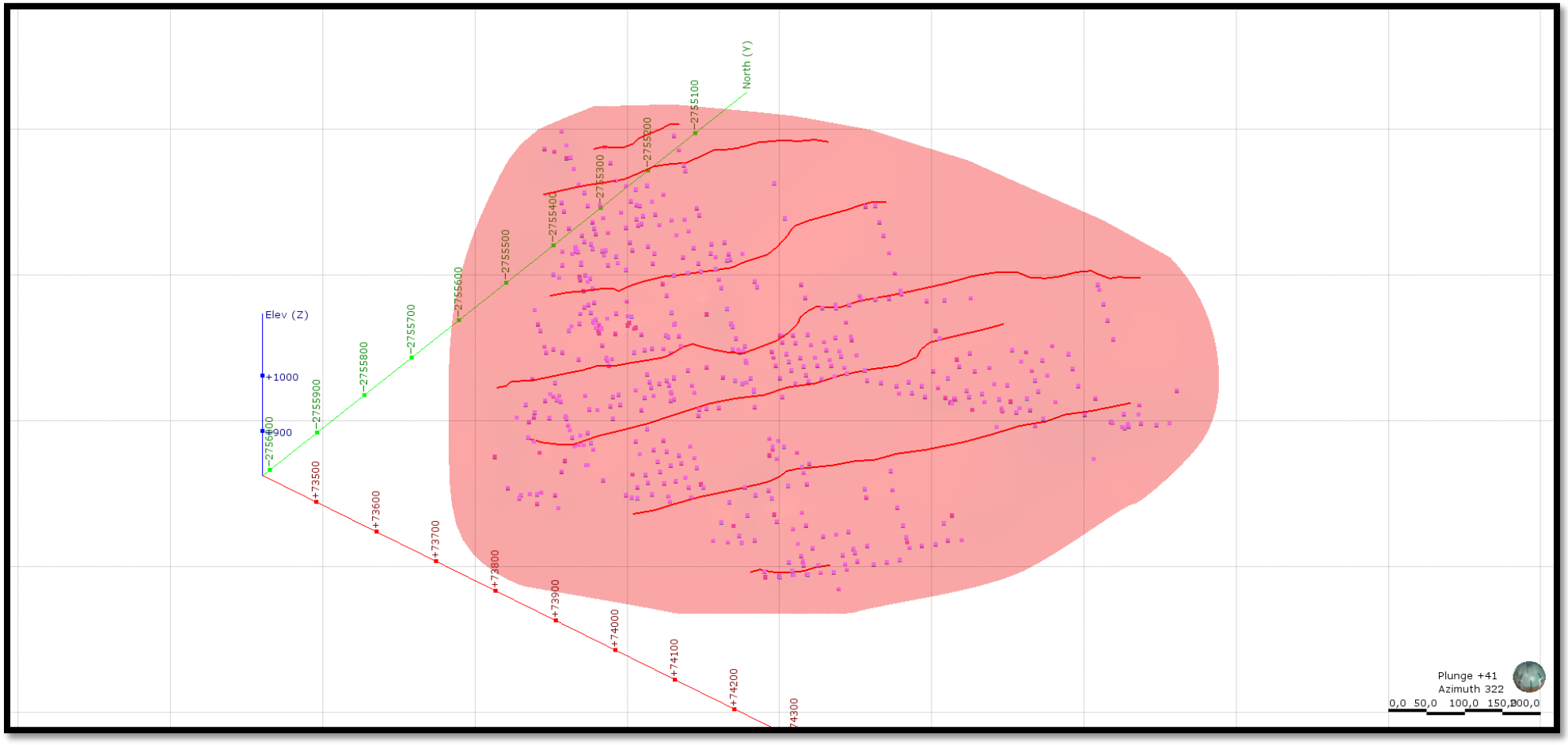

The boundary, hanging wall points, footwall points and polylines used to create the Gap Lower-Lode lode surface for the geological model.

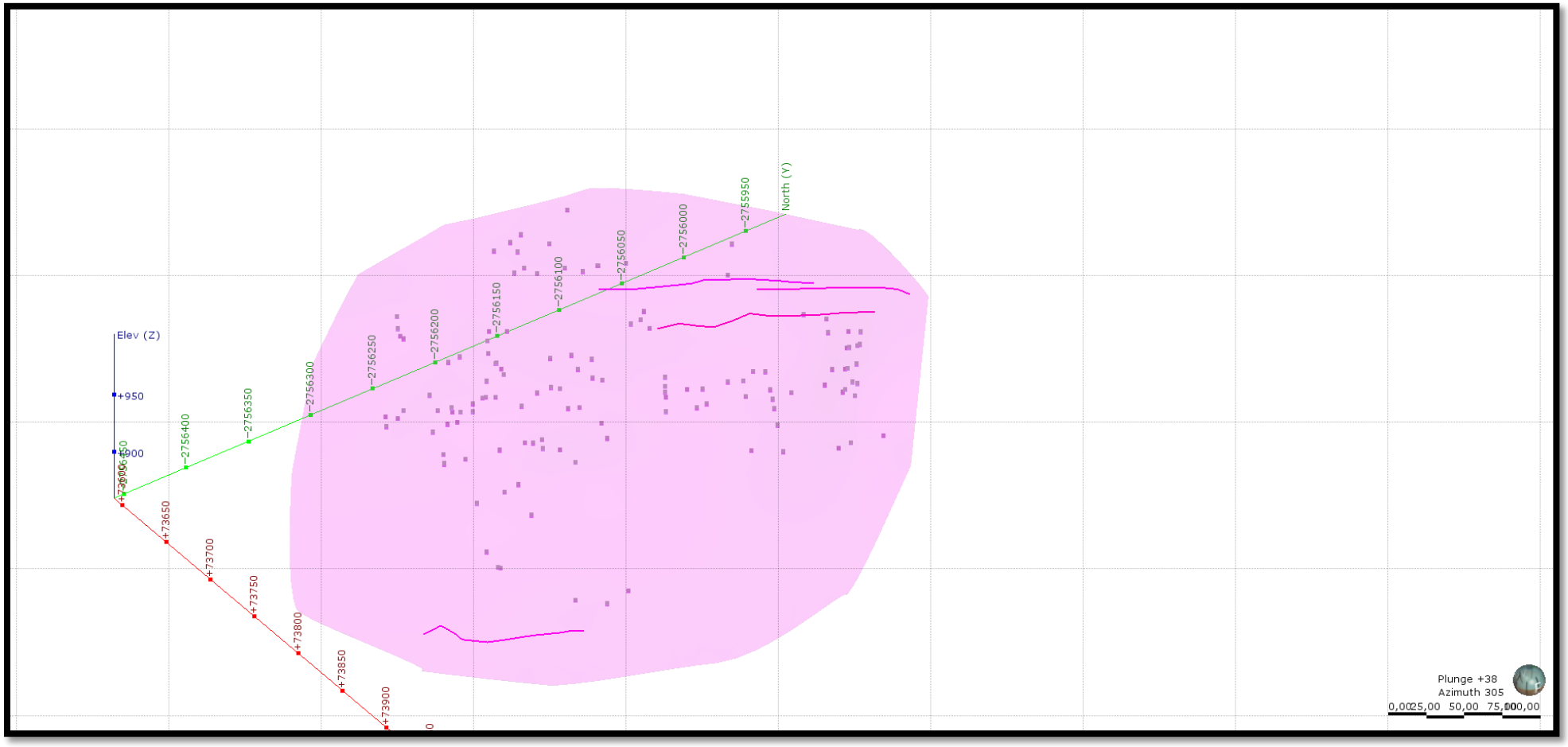

The boundary, hanging wall points, footwall points and polylines used to create the Gap Top-Lode lode surface for the geological model.

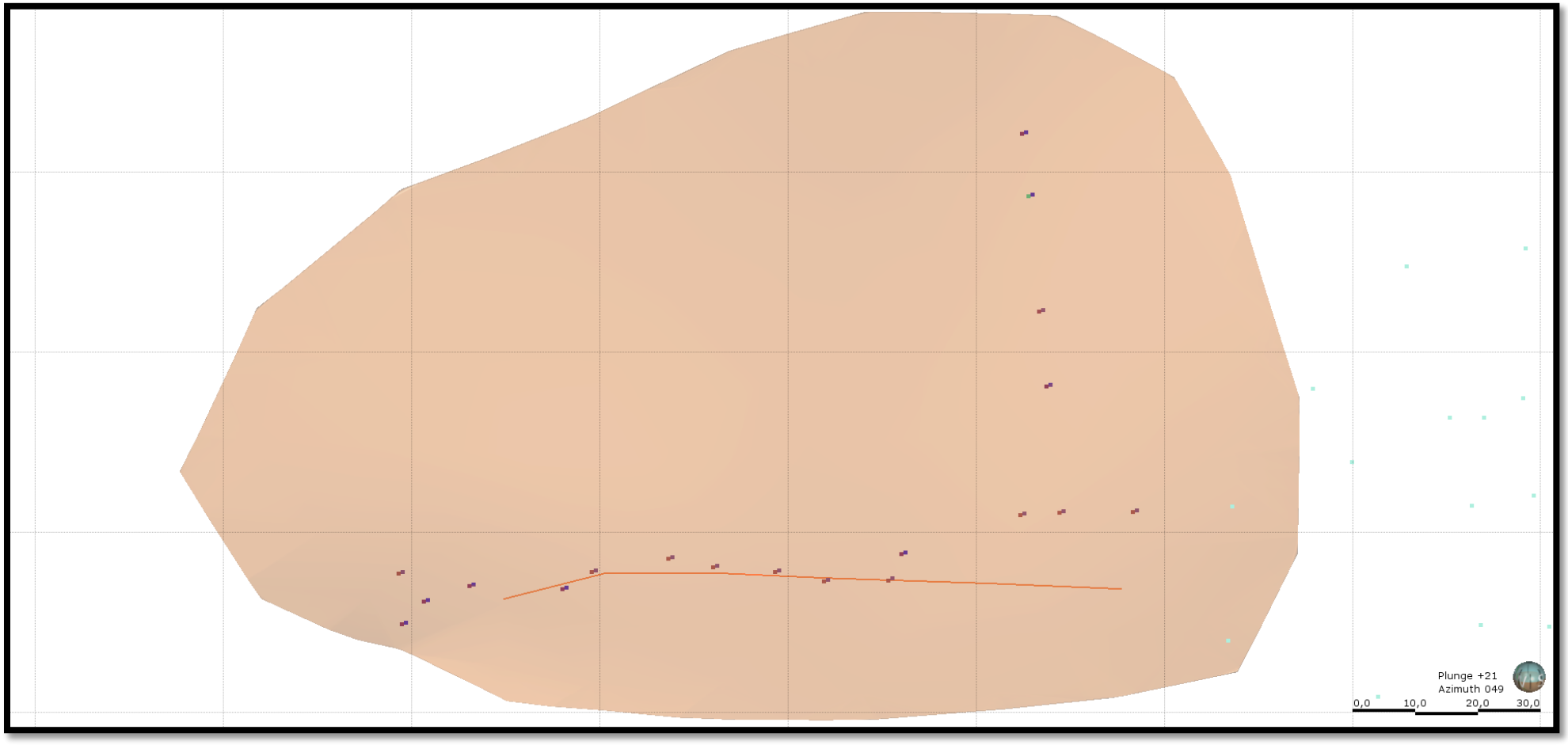

The boundary, hanging wall points, footwall points and polylines used to create the Government 1 lode surface for the geological model.

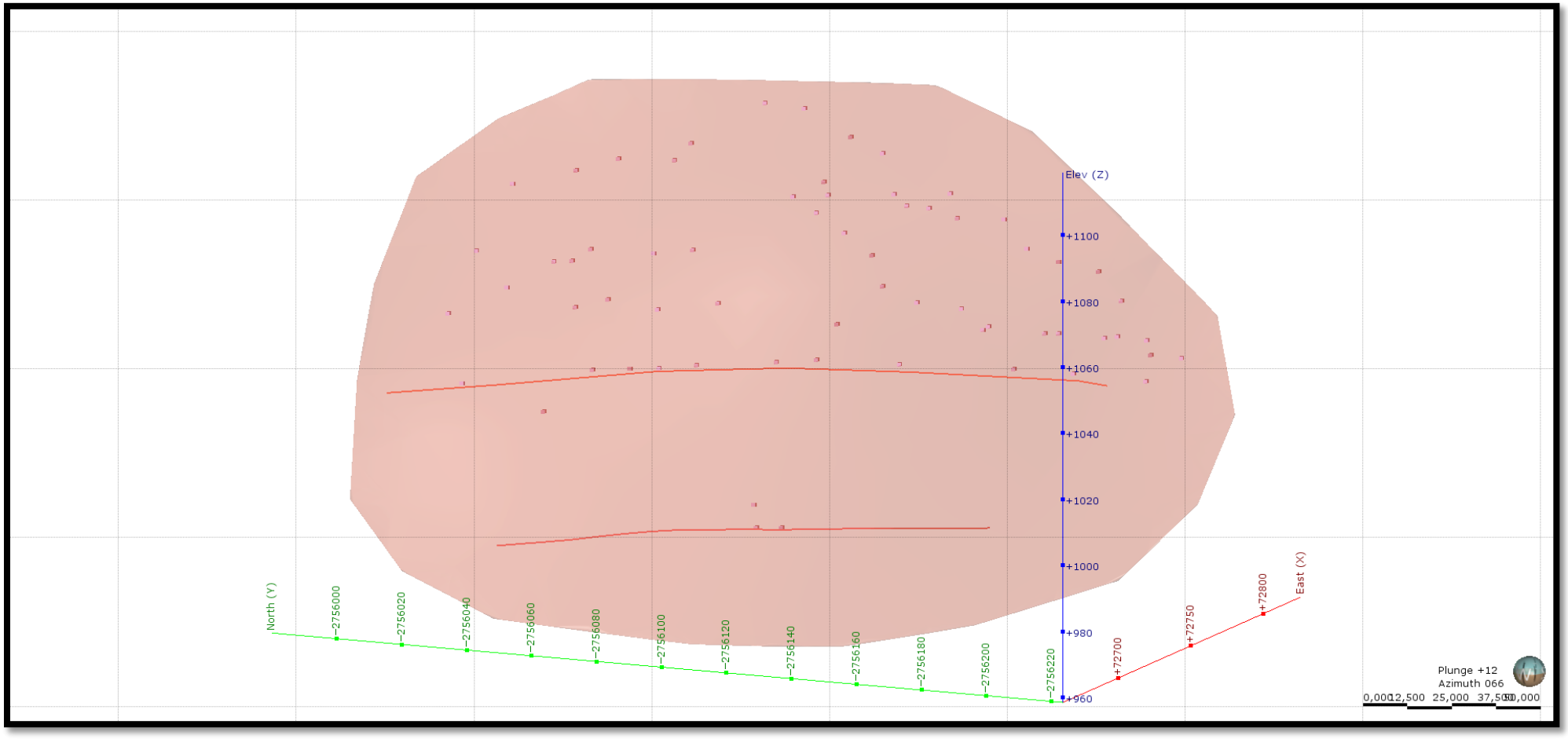

The boundary, hanging wall points, footwall points and polylines used to create the Government 2 lode surface for the geological model.

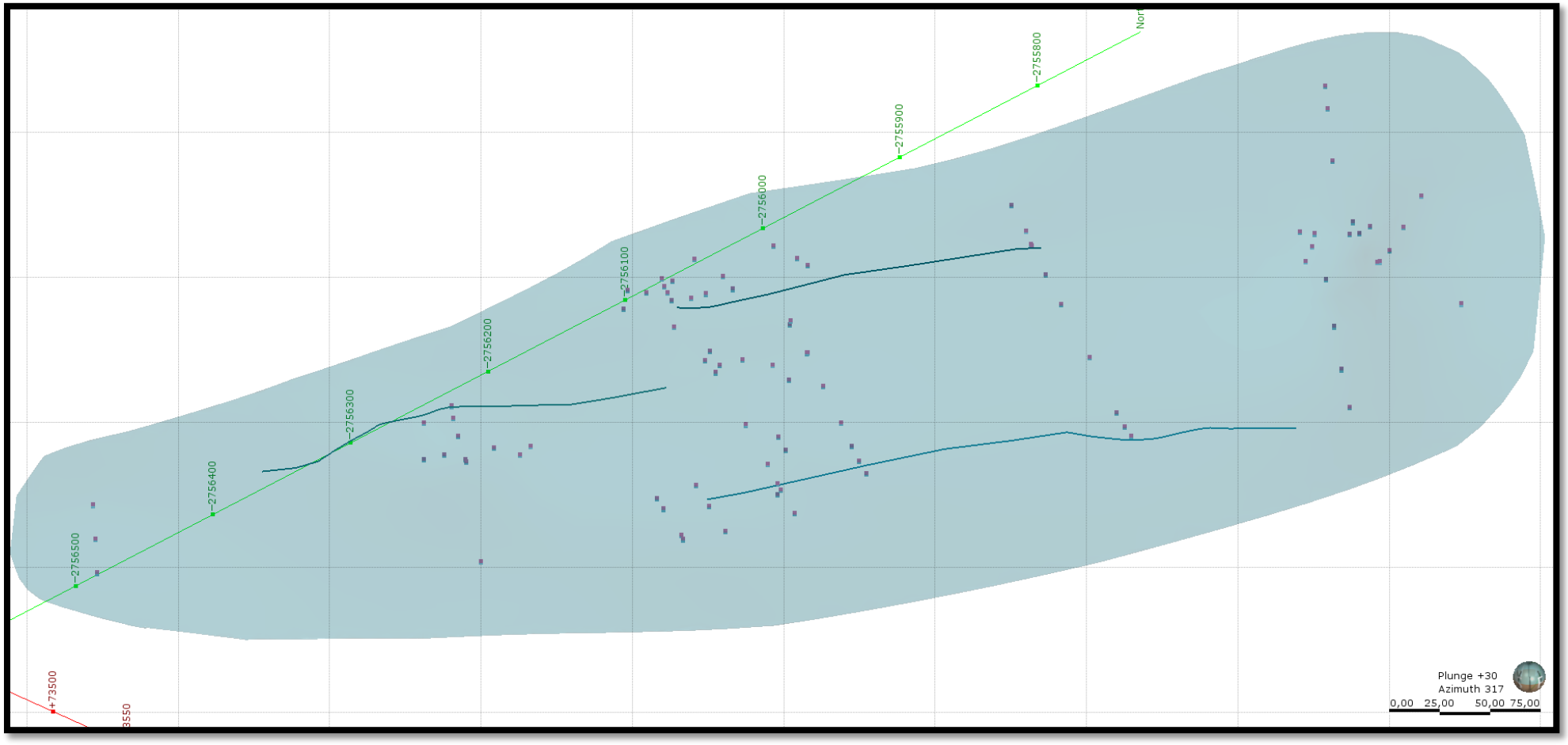

The boundary, hanging wall points, footwall points and polylines used to create the GS FW lode surface for the geological model.

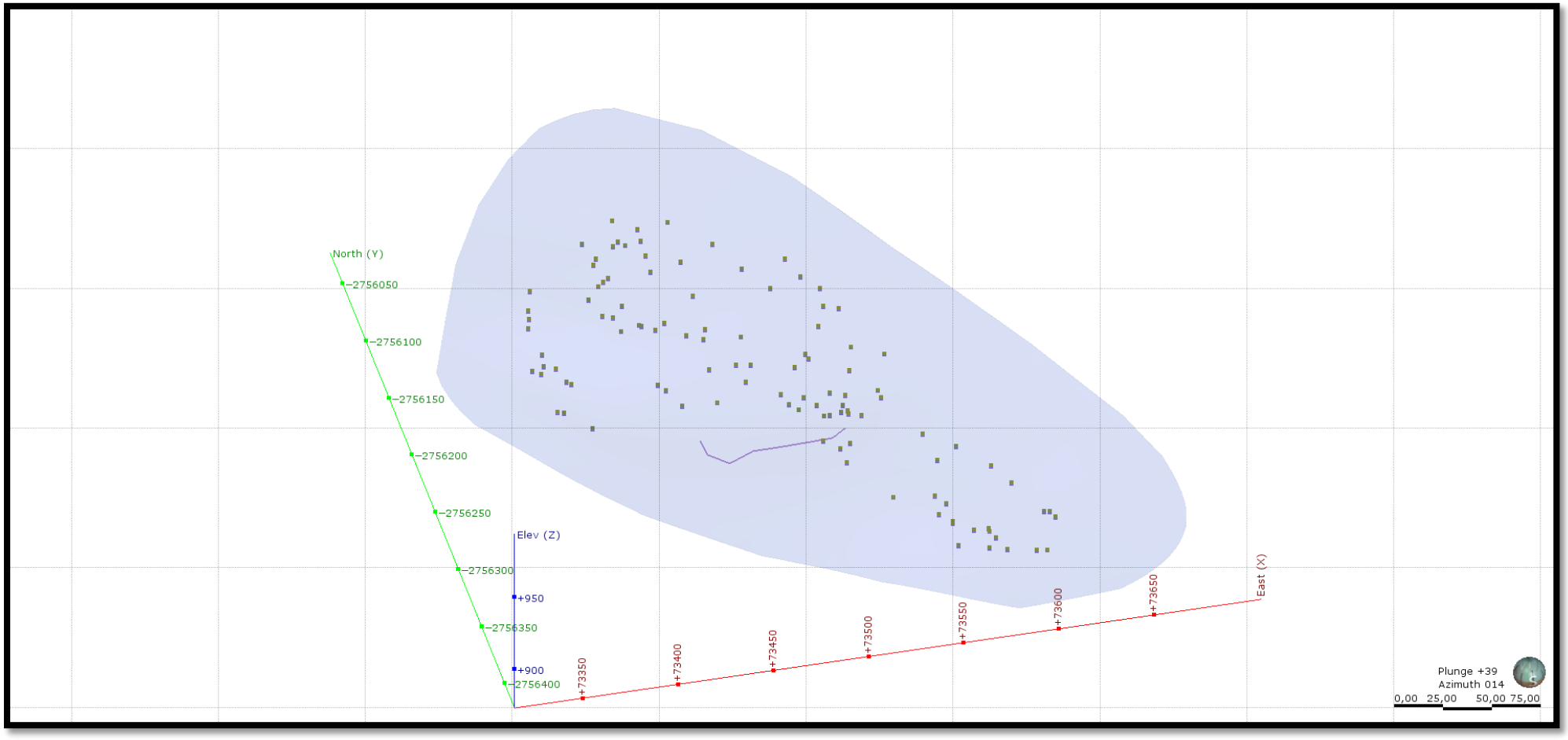

The boundary, hanging wall points, footwall points and polylines used to create the GS lode surface for the geological model.

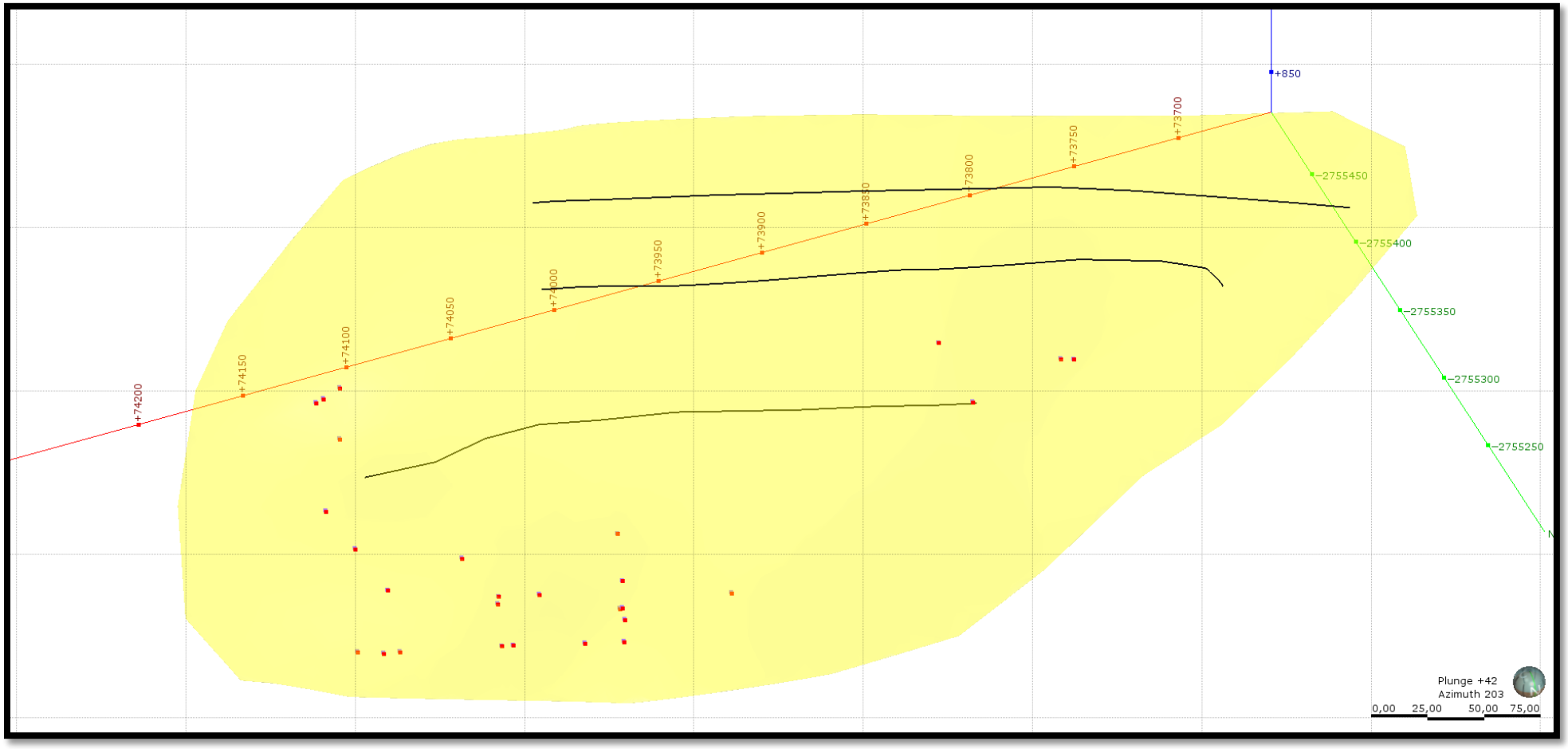

The boundary, hanging wall points, footwall points and polylines used to create the Hosking Fissure lode surface for the geological model.

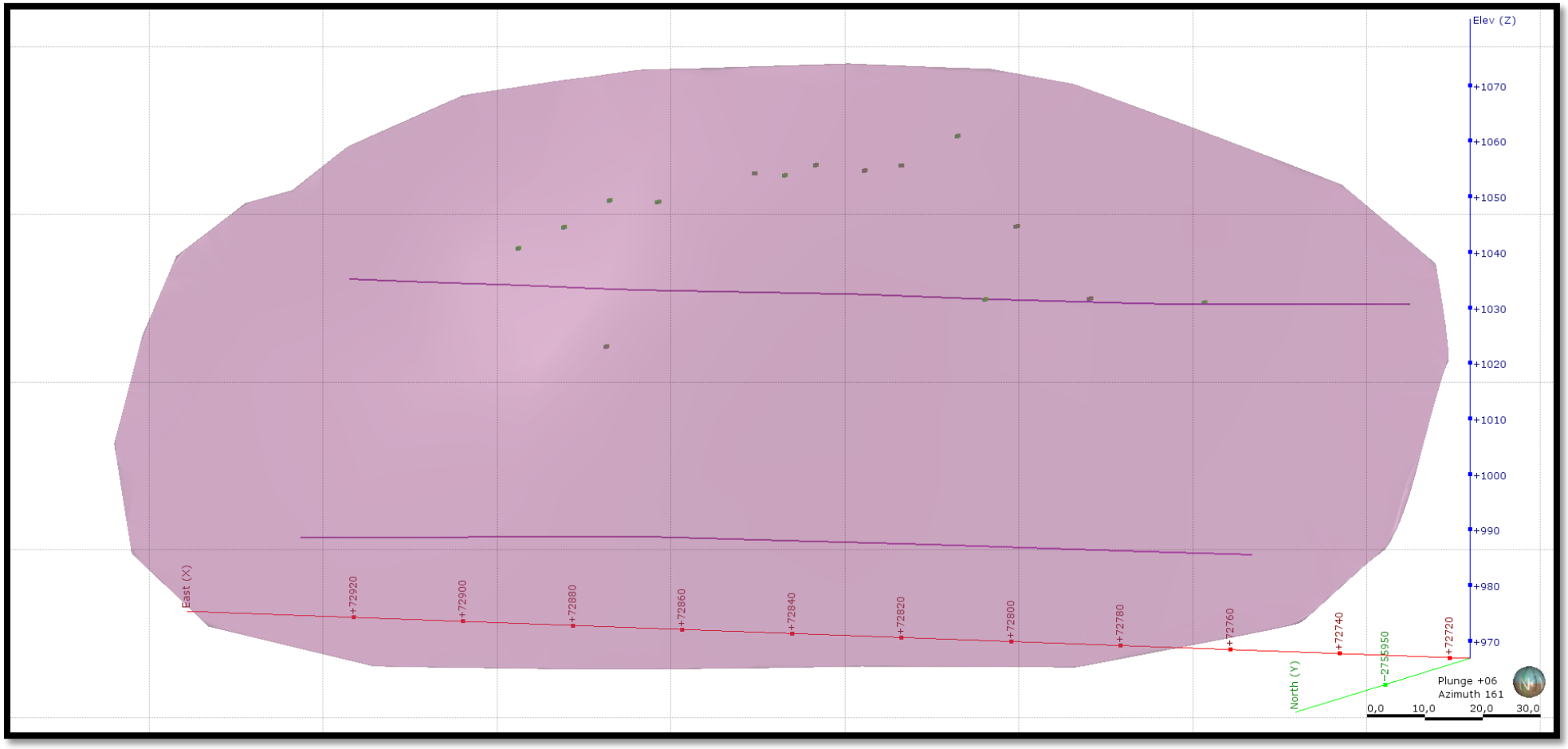

The boundary, hanging wall points, footwall points and polylines used to create the JB-Lode lode surface for the geological model.

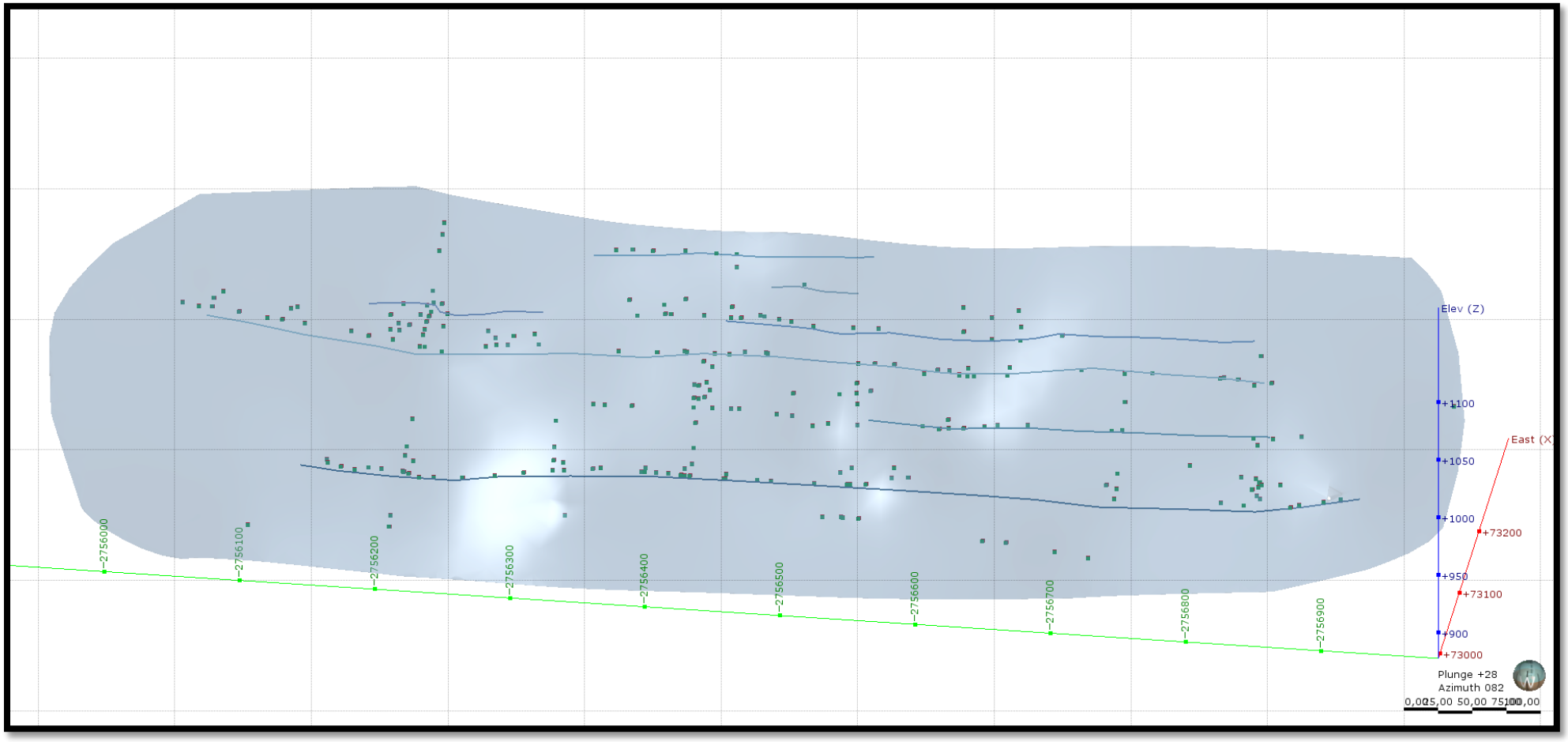

The boundary, hanging wall points, footwall points and polylines used to create the MC2 lode surface for the geological model.

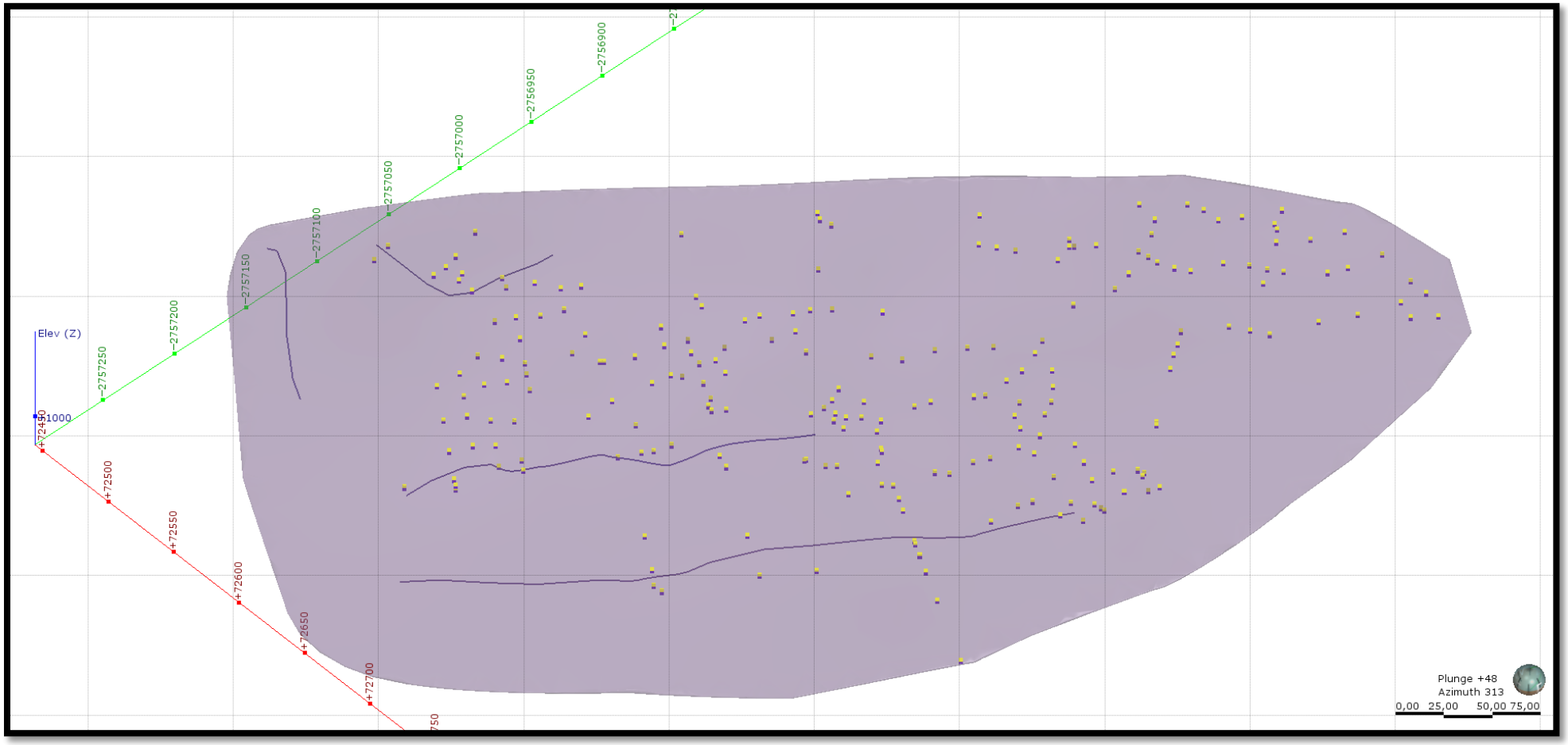

The boundary, hanging wall points, footwall points and polylines used to create the MD-Lode lode surface for the geological model.

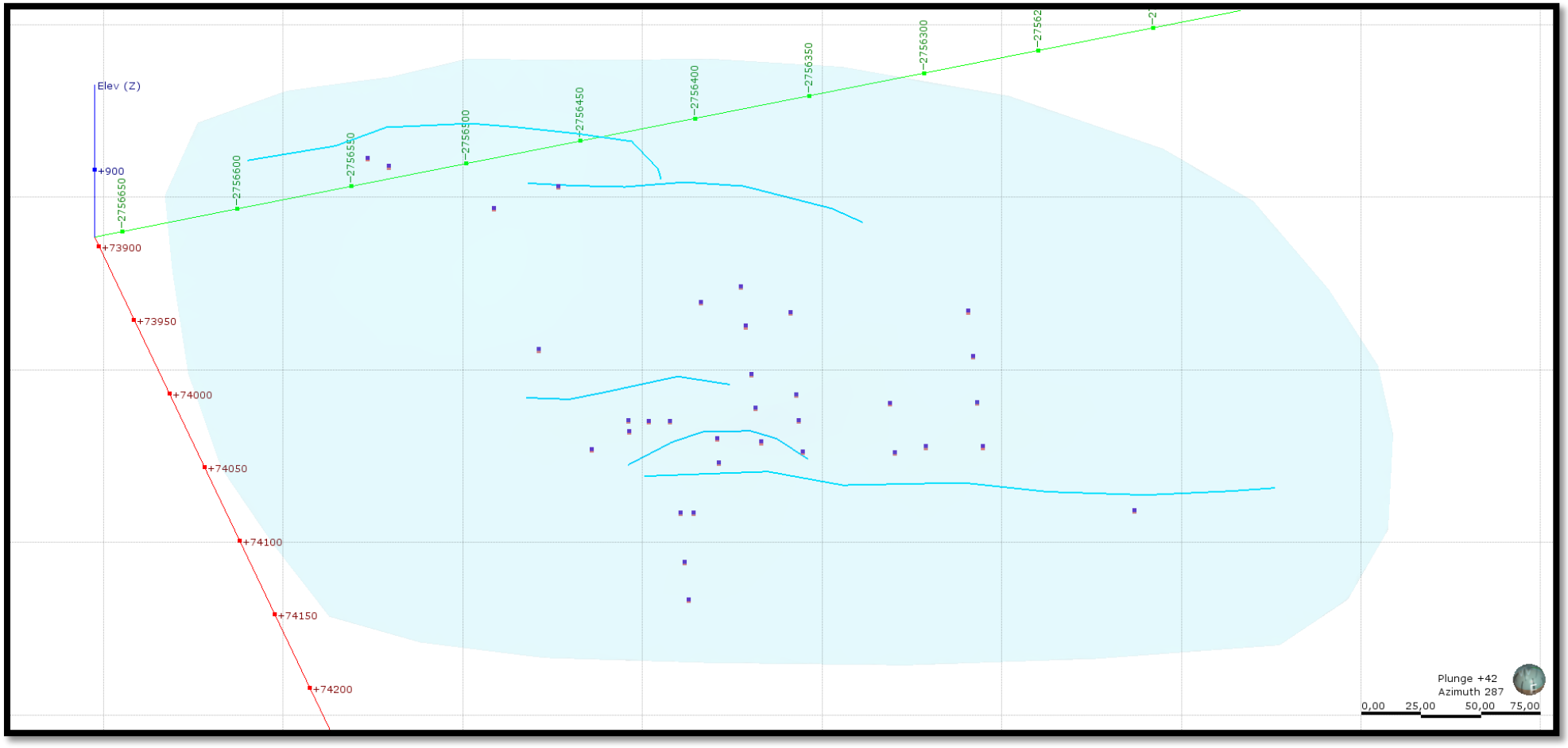

The boundary, hanging wall points, footwall points and polylines used to create the New New-Lode lode surface for the geological model.

CC

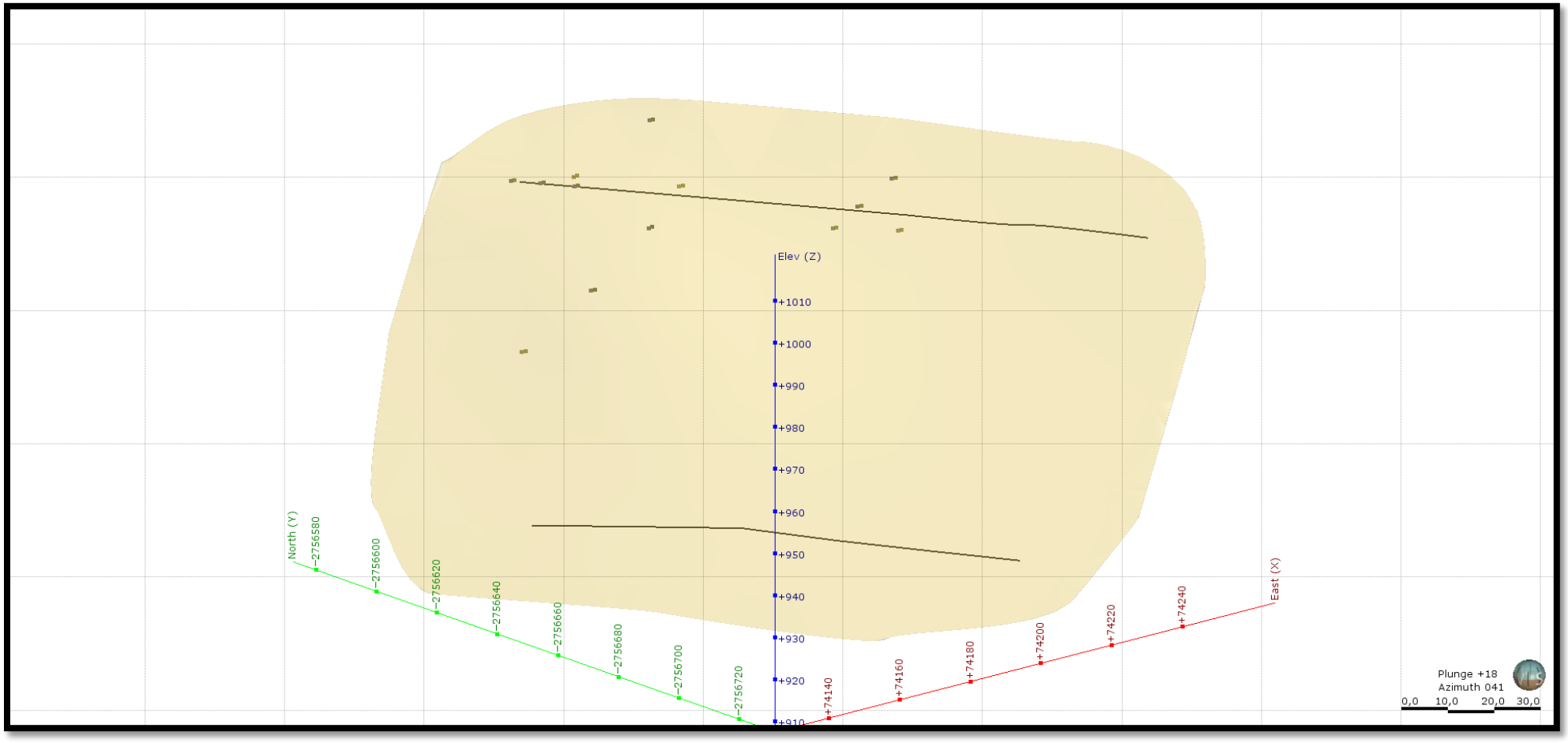

The boundary, hanging wall points, footwall points and polylines used to create the New Strike lode surface for the geological model.

DD

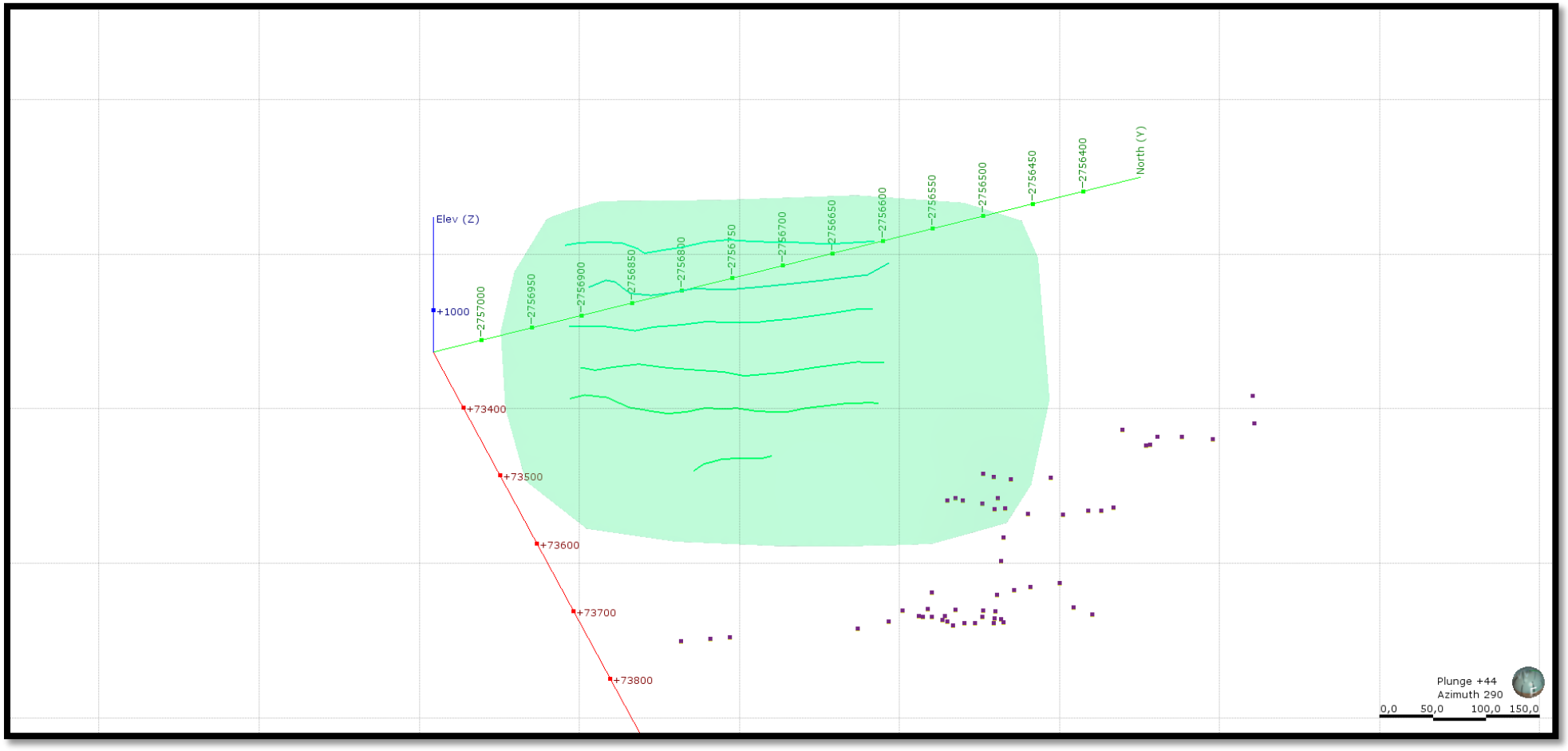

The boundary, hanging wall points, footwall points and polylines used to create the Spruit Extension-Lode lode surface for the geological model.

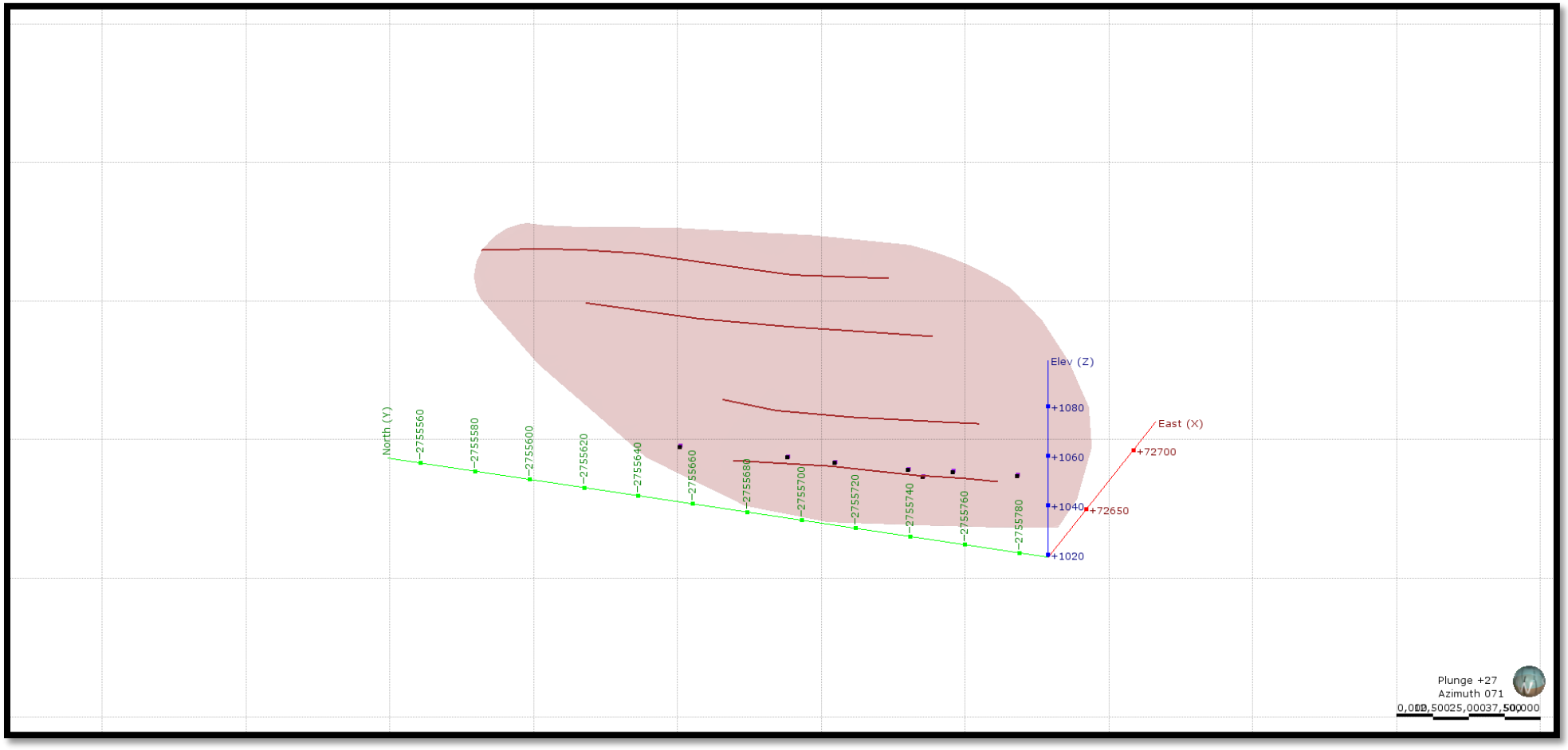

The boundary, hanging wall points, footwall points and polylines used to create the Trench-Lode lode surface for the geological model.

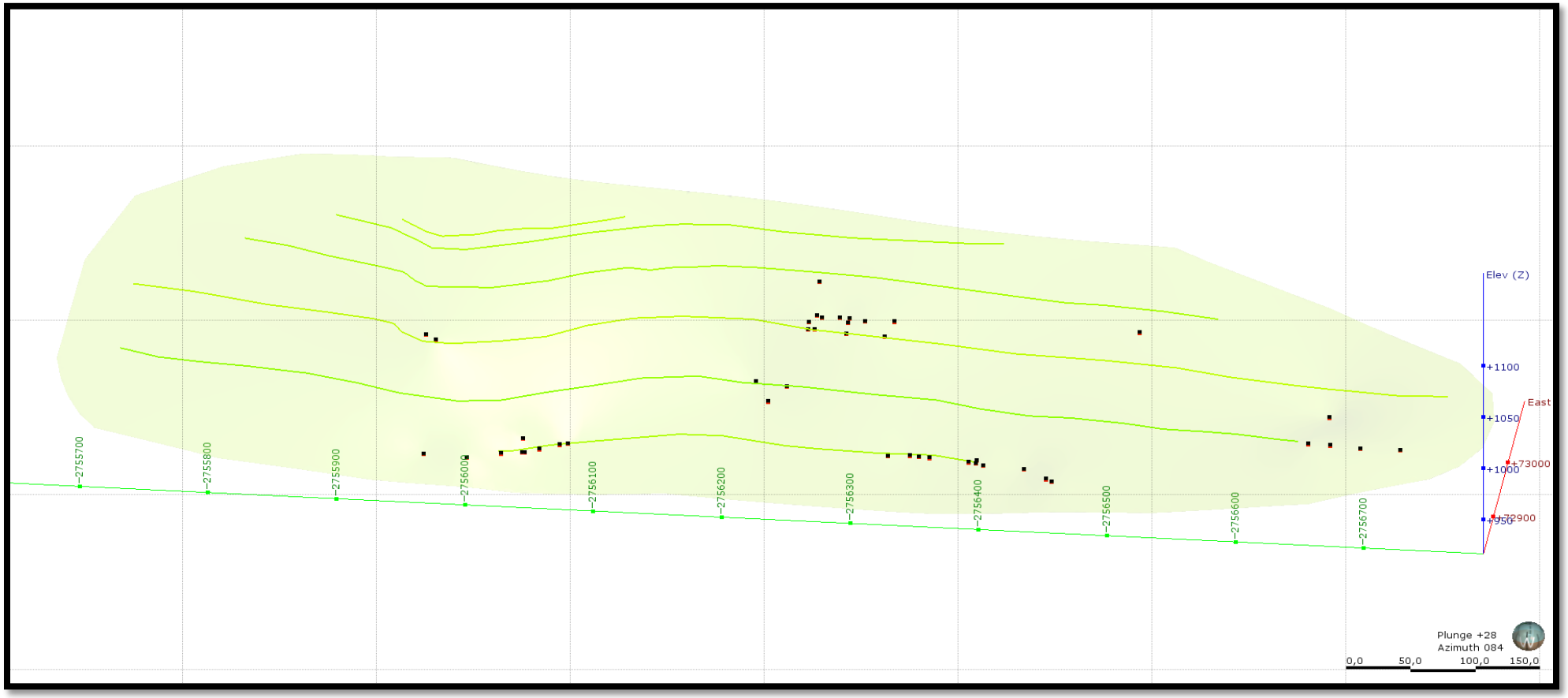

The boundary, hanging wall points, footwall points and polylines used to create the West Workings Fissure lode surface for the geological model.

11. APPENDIX 3: PLANNED DRILLHOLE COLLAR FILES IMPORTED AS POINTS TO GET THE ADJUSTED COLLAR ELEVATION THAT FITS THE TOPOGRAPHY

BH id	X-Coordinate	Y-Coordinate	Collar Elevation
PB1	73861.09	-2754409.88	1104.86
PB2	72693.26	-2755625.48	1145.51
PB3	73779.89	-2755221.78	1110.31
PB4	73493.08	-2756222.55	1172.44
PB5	75537.12	-2756130.8	1170.4
PB6	73171.23	-2755074.81	1153.2
PB7	72868.76	-2754678.89	1118.95
PB8	75153.22	-2757044.63	1082.86
PB9	73884.54	-2755274.23	1159.72
PB10	75473.31	-2754371.37	1117.57
PB11	73058.79	-2756672.33	1161.32
PB12	72993.57	-2754487.07	1164.14
PB13	73832.16	-2754946.32	1083.83
PB14	75198.62	-2754498.57	1165.03
PB15	72344.83	-2757322.97	1110.73
PB16	74286.02	-2754948.66	1114.69
PB17	73559.47	-2756892.89	1119.54
PB18	74048.43	-2755180.88	1100.07
PB19	73834.7	-2754346.04	1154.95
PB20	73387.27	-2755488.93	1104.57
PB21	73219.76	-2754294.47	1081.11
PB22	73700.97	-2756371.64	1148.05
PB23	73670.56	-2756196.6	1172.55
PB24	74972.65	-2754475.28	1123.57
PB25	73331.78	-2756200.91	1116.36
PB26	72316.62	-2755735.99	1085.69
PB27	73292.51	-2756813.42	1091.94
PB28	72869.63	-2754284.7	1120.75
PB29	74128.89	-2756159.15	1122.18
PB30	74000.71	-2756506.14	1094.81
PB31	75308.4	-2754114.01	1149.86
PB32	74860.31	-2754455.74	1148.55
PB33	73874.03	-2756631.95	1102.53
PB34	74090.06	-2755716.48	1086.6
PB35	72484.66	-2756829.32	1121.66
PB36	72972.02	-2757717.04	1115.32

PB37	72816.7	-2757828.17	1146.05
PB38	75322.37	-2757905.84	1137.42
PB39	75326.63	-2755305.23	1083.23
PB40	73945.79	-2757336.78	1130.4
PB41	74087.13	-2756782.14	1175.74
PB42	73642.04	-2754188.45	1156.32
PB43	74467.65	-2754301.24	1124.26
PB44	73865.54	-2755313.87	1126.61
PB45	74463.62	-2756150.8	1166.67
PB46	73317.38	-2755350.89	1081.45
PB47	73637.46	-2757871.91	1155.77
PB48	75063.27	-2757540.98	1143.34
PB49	74902.65	-2755579.16	1099.26
PB50	73082.67	-2757896.21	1079.58
PB51	75589.82	-2755301.66	1083.07
PB52	74726.63	-2755280.84	1133.86
PB53	74232.07	-2757361.81	1121.19
PB54	74449.2	-2754540.59	1081.09
PB55	72176.76	-2756460.46	1109.89
PB56	75419.76	-2754000.91	1107.96
PB57	74045.25	-2756632.38	1113.81
PB58	74617.31	-2756275.24	1094.55
PB59	73069.65	-2756714.48	1121.82
PB60	74520.92	-2756524.68	1082.74
PB61	74882.77	-2754364.37	1091.8
PB62	75581.38	-2756784.73	1095.05
PB63	73146.93	-2756246.69	1105.4
PB64	75468.84	-2754649.34	1131.87
PB65	75149.22	-2754086.33	1129.38
PB66	72421.37	-2757461.2	1120.56
PB67	74171.77	-2754022.26	1113.03
PB68	75410.36	-2756394.03	1111.58
PB69	72429.54	-2757387.8	1110.99
PB70	74468.44	-2754424.35	1129.61
PB71	73530.64	-2757191.63	1111.92
PB72	73810.25	-2755799.8	1110.61
PB73	72358.12	-2754342.22	1165.09

PB74	73794.65	-2755808.55	1113.56
PB75	73850.36	-2754819.4	1172.44
PB76	74841.73	-2754210.8	1142.78
PB77	74834.81	-2756815.42	1084.6
PB78	72937.88	-2756025.26	1150.88
PB79	72339.85	-2754688.91	1105.81
PB80	73850.85	-2755557.68	1094.29
PB81	73829.23	-2756430.88	1161
PB82	74558.53	-2756156.83	1086.74
PB83	72212.66	-2756347.44	1168.23
PB84	72514.68	-2754468.58	1113.07
PB85	74871.27	-2755722.63	1170.6
PB86	73197.01	-2756709.03	1162.27
PB87	72223.73	-2753993.4	1153.11
PB88	74032.11	-2757924.22	1137.43
PB89	75318.84	-2757301.81	1140.7
PB90	73463.2	-2756712.78	1133.09
PB91	74993.1	-2755357.27	1087.7
PB92	74265.16	-2755385.16	1089.03
PB93	74945.46	-2756440.06	1170.24
PB94	72420.92	-2756977.5	1146.18
PB95	72993.84	-2757469.47	1115.79
PB96	75490.68	-2757389.12	1158.44
PB97	73773.61	-2754149.68	1107.92
PB98	73113.58	-2755899.51	1090.59
PB99	72345.65	-2755605.62	1085.22
PB100	73620.61	-2754168.93	1165.55
PB101	73853.86	-2754788.59	1113.7
PB102	72447.75	-2757837.88	1163.97
PB103	72274.86	-2755109.52	1156.37
PB104	73283.03	-2754953.55	1158.87
PB105	73552.91	-2754883.65	1172.94
PB106	73435	-2757431.71	1144.28
PB107	74568.75	-2756651.34	1156.33
PB108	72379.99	-2755862.88	1162.71
PB109	72216.82	-2755582.56	1089.38
PB110	75173.08	-2754186.82	1108.67

PB111	73751.36	-2755565.42	1137.63
PB112	74137.51	-2754373.93	1124.46
PB113	74412.03	-2754013.73	1147.63
PB114	74109.56	-2755056.48	1133.51
PB115	73006.22	-2756694.37	1137.53
PB116	74495.05	-2755872.14	1080.55
PB117	72689.62	-2754857	1156.26
PB118	74643.93	-2756579.58	1167.98
PB119	75399.59	-2754142.71	1150.95
PB120	74857.97	-2755170.6	1094.02
PB121	75058.8	-2757058.8	1081.42
PB122	73677.49	-2754375.26	1082.94
PB123	75511.04	-2757416.41	1159.07
PB124	74376.71	-2755739.96	1135.64
PB125	73832.99	-2757990.89	1134.74
PB126	75511.7	-2755353.42	1121.85
PB127	74886.67	-2757739.64	1167.43
PB128	73047.15	-2755331.83	1135.41
PB129	72720.93	-2754734.22	1143.97
PB130	72785.42	-2754469.81	1123.65
PB131	74134.9	-2757047.56	1083.66
PB132	74285.43	-2756222.23	1130.98
PB133	72770.54	-2756704.69	1092.9
PB134	73299.5	-2757662.94	1153.47
PB135	75005.9	-2756130.27	1145.45
PB136	73534.51	-2758001.1	1164.86
PB137	73749.35	-2755516.41	1152.56
PB138	74264.27	-2757964.49	1133.5
PB139	73003.44	-2757163.61	1138.43
PB140	75585.79	-2757839.35	1098.68
PB141	74024.97	-2753964.85	1148.23
PB142	72220.64	-2754532.69	1124.96
PB143	73341.22	-2758088.05	1127.09
PB144	73774.9	-2756048.69	1152.98
PB145	74967.52	-2757969.13	1162.42
PB146	74664.13	-2755869.73	1107.34
PB147	72354.15	-2754965.69	1141.2

PB148	73522.87	-2757106.77	1117.46
PB149	72288	-2754624.62	1153.79
PB150	72462.47	-2754742.34	1174.49
PB151	74185.09	-2757490.22	1101.42
PB152	72629.98	-2756990.85	1135.6
PB153	74997.69	-2757396.43	1110.3
PB154	72355.94	-2755486.12	1129.07
PB155	74497.07	-2754323.69	1132.16
PB156	73317.36	-2757497.69	1152.55
PB157	73008.3	-2758002.53	1090.95
PB158	72835.9	-2756480.19	1127.61
PB159	75304.55	-2754766	1164.8
PB160	73836.36	-2757715.12	1133.12
PB161	73956.06	-2755350.01	1167.63
PB162	75242.51	-2756668.51	1087.53
PB163	74605.21	-2756202.69	1091.91
PB164	74116.94	-2756337.96	1169.19
PB165	73010.69	-2756449.05	1099.4
PB166	72368.25	-2756623.42	1088.84
PB167	73803.62	-2754555.32	1105.43
PB168	72858.44	-2755849.56	1126.38
PB169	72339.25	-2755182.63	1154.87
PB170	74452.41	-2756794.63	1173.35
PB171	72437.16	-2754872.53	1166.05
PB172	72289.82	-2756568.65	1145.16
PB173	73946.49	-2755985.01	1105.01
PB174	73894.66	-2755505.8	1161.29
PB175	72449.42	-2757422.82	1102.18
PB176	73989.84	-2757938.3	1103.83
PB177	75374.99	-2754652.49	1101.99
PB178	73283.91	-2755718.53	1143.02
PB179	75238.2	-2757941.96	1170.59
PB180	75055.46	-2757209.06	1113.28
PB181	75381.32	-2756087.28	1139.25
PB182	73654.87	-2757536.23	1093.79
PB183	72383.83	-2756175.47	1080.65
PB184	72757.2	-2757823.09	1082.04

PB185	74447.41	-2754271.3	1136.33
PB186	75278.82	-2755431.98	1111.36
PB187	72515.45	-2756305.28	1097.95
PB188	73550.31	-2756483.28	1110.59
PB189	72287.5	-2756912.89	1165.41
PB190	73100.18	-2756782.1	1164.77
PB191	72795.74	-2756522.27	1148.41
PB192	75249.07	-2753963.16	1109.59
PB193	75370.68	-2756719.57	1102.01
PB194	73166.44	-2756604.49	1168.26
PB195	72904.94	-2754983.51	1090.21
PB196	73100.51	-2754978.77	1083.96
PB197	74764.23	-2754463.62	1116.33
PB198	75581.6	-2757457.75	1131.02
PB199	73340.2	-2755877.11	1139.15
PB200	73672.89	-2755349.19	1108.35
PB201	72674.25	-2755153.78	1160.1
PB202	73825.28	-2754700.66	1166.45
PB203	73481.59	-2754853.07	1087.43
PB204	72855.7	-2757005.05	1120.14
PB205	73154.94	-2753963.43	1119.25
PB206	74635.73	-2755626.51	1145.28
PB207	74256.5	-2756907.58	1096.52
PB208	72303.88	-2754863.2	1108.16
PB209	74893.45	-2757973.76	1143.28
PB210	72912.42	-2753994.77	1171.56
PB211	73855.13	-2758062.09	1114.71
PB212	75636.65	-2755436.47	1093.67
PB213	72845.74	-2755342.49	1111.1
PB214	73109.69	-2757748.89	1105.92
PB215	74033.73	-2757371.71	1170.81
PB216	72885.82	-2754921.55	1086.12
PB217	74309.59	-2754049.54	1134.2
PB218	75317.83	-2757090.92	1173.15
PB219	75434.75	-2754319.93	1128.82
PB220	74657.39	-2755528.9	1089.36
PB221	75617.18	-2755842.42	1113.5

PB222	73369.6	-2754466.35	1090.09
PB223	74903.79	-2757167.29	1083.61
PB224	75621.29	-2754107.1	1160.31
PB225	74463.79	-2754777.1	1167.61
PB226	73341.43	-2756417.96	1080.52
PB227	75248.93	-2754113.88	1130.23
PB228	72311.51	-2755115.01	1105.27
PB229	73767.22	-2756984.96	1127.45
PB230	74465.92	-2756118.33	1149.78
PB231	73691.78	-2754268.73	1133.12
PB232	72867.97	-2754492.29	1094.93
PB233	72803.02	-2754796.83	1119.33
PB234	72543.67	-2756740.38	1103.44
PB235	72843.93	-2757062.58	1163.3
PB236	72657.13	-2757954.3	1148.35
PB237	73185.64	-2755776.27	1125.33
PB238	72591.86	-2755393.85	1131.07
PB239	73105.55	-2756758.38	1160.97
PB240	75504.74	-2754290.94	1130.79
PB241	74048.27	-2754448.66	1086.09
PB242	72812.82	-2757720.12	1113.41
PB243	72896.62	-2755272.09	1158.19
PB244	72443.33	-2755570.37	1162.83
PB245	73758.36	-2756434.49	1149.81
PB246	73410.82	-2754048.54	1108.5
PB247	72173.4	-2755256.52	1109.63
PB248	73612.47	-2756039.41	1148.12
PB249	74750.62	-2755985.77	1127.25
PB250	72309.33	-2754157.63	1115.71
PB250	74476.59086	-2755053.39	1170.07
PB251	73777.77547	-2756461.8	1174.25
PB252	75147.98151	-2757720.06	1173.22
PB253	73238.48822	-2757081.46	1080.33
PB254	73723.73282	-2754527.85	1157.03
PB255	72751.39441	-2755713.79	1120.79
PB256	74925.78756	-2754565.16	1126.01
PB257	73289.89456	-2758054.72	1122.39

PB258	74514.48598	-2754168.68	1146.39
PB259	72941.7617	-2754444.79	1107.48
PB260	72383.05872	-2755681.33	1125.37
PB261	73131.26457	-2756808.47	1164.21
PB262	72865.66169	-2755542.15	1093.53
PB263	72740.78769	-2756671.57	1124.87
PB264	74036.41386	-2754490.49	1124.04
PB265	74214.60737	-2753995.21	1146.1
PB266	73683.68091	-2755254.23	1169.64
PB267	73691.08734	-2756838.19	1134.08
PB268	74643.69677	-2757676.91	1134.83
PB269	75063.13616	-2757073.88	1174.58
PB270	74429.23652	-2757333.17	1101.96
PB271	74077.85077	-2755740.73	1117.22
PB272	74685.46187	-2755378.28	1081.46
PB273	72682.8747	-2754168.69	1119.23
PB274	72204.27985	-2757011.95	1120.38
PB275	73387.43077	-2758106.9	1137.44
PB276	74663.99657	-2754202.25	1152.21
PB277	73175.9567	-2754556.4	1089.16
PB278	72749.50717	-2754922.85	1103.11
PB279	72438.18235	-2758018.11	1136.31
PB280	73130.25609	-2756191.56	1150.71
PB281	74176.21975	-2754986.33	1107.17
PB282	74274.69887	-2754981.15	1157.68
PB283	73928.96964	-2756575.88	1107.2
PB284	74641.357	-2755244.13	1135.39
PB285	72420.83358	-2756838.5	1151.28
PB286	74867.2074	-2754167.44	1117.66
PB287	72343.29461	-2757860.34	1168.08
PB288	73093.33863	-2755429.43	1128.78
PB289	73422.8465	-2755333.86	1093.01
PB290	74066.63708	-2755133.99	1086.22
PB291	74240.86353	-2755461.87	1148.76
PB292	72199.95036	-2754403.19	1172.15
PB293	75018.81832	-2756757.59	1156.26
PB294	73627.41952	-2757705.55	1171.99

PB295	74449.67234	-2757267.29	1157.33
PB296	75542.61273	-2756812.29	1153.27
PB297	74630.15649	-2756986.72	1123.97
PB298	74508.29879	-2757348.21	1136.36
PB299	74202.60916	-2757495.72	1135.61
PB300	73565.39256	-2754419.43	1100.49
PB301	73908.61043	-2754658.96	1117.43
PB302	72795.80392	-2754376.69	1159.71
PB303	75050.39566	-2757051.51	1175.85
PB304	73989.50483	-2756598.96	1127.06
PB305	74467.98223	-2755523.43	1080.72
PB306	74252.85313	-2757302.43	1120.82
PB307	74558.01501	-2755891.29	1134.39
PB308	72442.85375	-2756682.43	1139.57
PB309	74235.91816	-2756420.68	1104.43
PB310	73429.37335	-2755093.87	1082.81
PB311	72770.02586	-2756010.62	1105.85
PB312	74855.92228	-2755941.36	1146.75
PB313	73255.77952	-2756592.21	1121.84
PB314	73539.88298	-2754927.8	1117.11
PB315	73878.81478	-2756843.66	1101.53
PB316	74319.25623	-2756418.09	1083.4
PB317	74145.24134	-2756213.22	1131.5
PB318	73589.52393	-2757282.83	1154.34
PB319	75614.73462	-2755384.39	1143.81
PB320	74835.09145	-2754499.55	1142.55
PB321	73974.56652	-2753988.94	1114.95
PB322	74749.2199	-2754913.04	1115.67
PB323	73319.14568	-2757162.05	1103.07
PB324	74522.81536	-2755473.94	1117.88
PB325	73827.60507	-2754608.66	1117.54
PB326	72529.81968	-2756484.28	1122.81
PB327	73498.00331	-2757875.21	1101.35
PB328	72764.55659	-2754734.13	1102.92
PB329	72581.12318	-2756187.51	1144.24
PB330	74831.28218	-2754526.03	1096.09
PB331	72434.6239	-2756401.89	1087.37

PB332	73412.47869	-2754756.16	1150.4
PB333	74242.23578	-2754368.43	1148.67
PB334	73516.40173	-2755027.59	1171.9
PB335	72202.58395	-2757773.68	1139.44
PB336	75299.14312	-2757760.62	1145.11
PB337	74959.15002	-2757980.87	1094.89
PB338	75615.88222	-2757319.93	1166.31
PB339	73151.28747	-2757377.75	1143.93
PB340	74201.88824	-2755808.52	1162.89
PB341	74137.6333	-2756817.31	1171.11
PB342	72412.67617	-2757670.87	1166.87
PB343	75504.95526	-2755024.86	1144.64
PB344	75430.6107	-2756815.7	1171.63
PB345	75634.47882	-2754087.67	1134.54
PB346	72416.20132	-2756704	1090.9
PB347	74459.07767	-2754434.51	1150.92
PB348	73902.82431	-2757062.01	1081.55
PB349	72313.74933	-2756474.74	1122.49
PB350	73830.28703	-2756420.71	1143.49
PB351	75532.53198	-2758026.93	1153.8
PB352	75402.38472	-2756378.95	1165.37
PB353	74763.52626	-2754809.35	1127.91
PB354	74674.55043	-2756068.42	1138.35
PB355	74200.34845	-2756180.19	1148.92
PB356	73911.99604	-2757800.03	1153.54
PB357	72761.17166	-2756002.77	1161.27
PB358	74452.99135	-2757966.19	1167.75
PB359	72293.76991	-2757649.96	1127.32
PB360	75481.2666	-2756556.91	1171.38
PB361	72182.54417	-2754899.66	1131.83
PB362	73934.20146	-2755901.77	1162.14
PB363	74836.19484	-2754502.39	1176.68
PB364	73294.10373	-2757316.4	1140.63
PB365	75545.51659	-2757127.24	1174.23
PB366	73299.27242	-2757744.43	1135.63
PB367	75392.27401	-2755848.47	1102.25
PB368	73414.06607	-2756930.22	1172.7

PB369	75382.70594	-2758040.74	1082.24
PB370	72884.40193	-2755905.4	1129.64
PB371	74638.53635	-2757163.37	1143.76
PB372	74656.04293	-2757271.5	1164.59
PB373	73482.33111	-2756316.72	1129.99
PB374	73296.17351	-2754359.31	1166.48
PB375	75238.25223	-2754536.66	1104.95
PB376	72367.46384	-2756499.28	1090.08
PB377	74542.47057	-2754950.97	1107.47
PB378	73042.69717	-2756815.63	1120.99
PB379	72392.64447	-2755505.22	1143.66
PB380	73503.75536	-2756830.39	1156.52
PB381	75401.11529	-2756215.71	1151.36
PB382	72731.01614	-2754154.55	1152.31
PB383	73048.13615	-2754464.09	1088.87
PB384	74086.57912	-2756422.45	1100.59
PB385	72564.96858	-2755017.56	1126.69
PB386	74674.45337	-2756850.43	1168.29
PB387	74541.62844	-2754048.16	1128.67
PB388	74301.70253	-2757039.27	1156.08
PB389	74724.84176	-2755948.53	1160.16
PB390	75189.83187	-2755781.84	1114.51
PB391	73722.62834	-2755287.8	1141.67
PB392	75276.15163	-2757394.47	1136.69
PB393	75458.06757	-2755450.46	1137.74
PB394	72824.1804	-2757385.67	1156.22
PB395	73441.72577	-2756915.25	1142.29
PB396	73230.73027	-2754196.48	1126.2
PB397	75558.65698	-2756927.01	1095.98
PB398	72325.48471	-2754308.55	1132.81
PB399	74922.10582	-2755615.39	1128.45
PB400	72618.05173	-2757029.22	1171.95
PB401	73698.65207	-2756033.19	1099.56
PB402	74408.22723	-2754137.11	1127.67
PB403	75308.33265	-2757371.97	1088.35
PB404	73616.79225	-2756999.89	1094.99
PB405	73998.11328	-2757847.64	1147.8

PB406	75044.41149	-2754152.63	1150.3
PB407	75446.5586	-2756110.64	1144.96
PB408	75202.97616	-2754336.53	1162.12
PB409	74592.57717	-2755250.13	1144.82
PB410	72643.30312	-2755296.85	1126.05
PB411	75313.08121	-2757099.95	1174.83
PB412	72673.86075	-2757820.14	1110.44
PB413	75164.89333	-2756120.01	1089.29
PB414	74820.39201	-2756278.13	1112.2
PB415	74480.74225	-2755249.15	1143.37
PB416	75551.51657	-2755337.44	1172.02
PB417	72835.44623	-2756731.15	1147.5
PB418	75393.80288	-2757989.87	1171.71
PB419	75095.34325	-2757976.64	1096.75
PB420	73502.39321	-2754496.21	1117.73
PB421	73378.92999	-2755003.05	1102.26
PB422	73290.21759	-2754063.03	1109.46
PB423	73269.91137	-2755175.07	1099.31
PB424	73797.40697	-2755367.84	1115.67
PB425	73049.61163	-2757692.44	1133.97
PB426	74534.22837	-2756854.46	1128.85
PB427	74885.67205	-2754541.52	1151
PB428	75035.1448	-2756859.77	1148.63
PB429	75571.79206	-2755269.68	1163.77
PB430	73057.97267	-2756931.04	1167.02
PB431	73305.16752	-2754610.32	1086.95
PB432	75183.27591	-2755286.23	1127.18
PB433	75599.44601	-2754604.9	1150.44
PB434	74178.33077	-2756906.16	1119.84
PB435	75622.93135	-2754064.44	1149.98
PB436	72921.41449	-2758054.47	1117.78
PB437	72876.20829	-2757858.59	1162.57
PB438	74195.02336	-2756281.33	1121.81
PB439	73263.6969	-2754690.41	1173.57
PB440	72627.10857	-2756679.73	1128.15
PB441	74100.07704	-2756790.64	1092.86
PB442	74653.837	-2757977.08	1154.27

PB443	72871.95082	-2756494	1147.22
PB444	73076.48985	-2755873.59	1107.02
PB445	73126.66119	-2757051.8	1147.47
PB446	74804.65219	-2757208.95	1130.27
PB447	73560.01915	-2754573.33	1155.31
PB448	73593.71147	-2757272.62	1079.46
PB449	72967.45984	-2755342.1	1109.14
PB450	75190.07907	-2756360.47	1095.99
PB451	73882.49222	-2754233.66	1087.16
PB452	75501.24087	-2755348.12	1115.77
PB453	72532.69906	-2754949.56	1133.31
PB454	72853.23023	-2756265.9	1098.51
PB455	74866.00974	-2755326.45	1143.07
PB456	75240.01898	-2754264.54	1150.09
PB457	74499.75921	-2754700.45	1106.23
PB458	72989.02642	-2755030.99	1084.1
PB459	75389.65925	-2755410.77	1103.56
PB460	74058.84687	-2757349.82	1146.12
PB461	75560.64354	-2757319.79	1098.41
PB462	73014.61579	-2758053.46	1143.14
PB463	75358.27456	-2755052.6	1114.23
PB464	73618.9398	-2756767.68	1143.45
PB465	73709.50156	-2754564.69	1132.87
PB466	72226.7724	-2753978.13	1085.38
PB467	72974.51693	-2755405.93	1124.81
PB468	75162.73507	-2756545.8	1130.03
PB469	72162.15721	-2755324.54	1172.91
PB470	75189.75419	-2755214.74	1166.31
PB471	73177.5264	-2755206.08	1130.25
PB472	72850.64204	-2757059.4	1091.66
PB473	74352.06359	-2754909.98	1094.57
PB474	74927.24762	-2756059.67	1145.43
PB475	74808.85073	-2755791.35	1108.45
PB476	72401.39744	-2755611.14	1092
PB477	72578.45669	-2755883.96	1153.6
PB478	74833.52974	-2754285.43	1094.9
PB479	72300.77645	-2756714.98	1125.79

PB480	74050.78036	-2755458.13	1111.23
PB481	73501.12269	-2755759.32	1121.09
PB482	74489.46826	-2755854.38	1101.9
PB483	74701.59635	-2755840.9	1156.11
PB484	75407.95333	-2755014.82	1084.06
PB485	73370.37193	-2754600.34	1113.88
PB486	75447.99127	-2755576.14	1113.95
PB487	74880.53055	-2757281.16	1109.74
PB488	72743.13986	-2756280.12	1129.19
PB489	72927.84392	-2755116.11	1147.25
PB490	74831.26023	-2757367.98	1119.52
PB491	74508.25732	-2754952.79	1156.15
PB492	72761.4993	-2755809.92	1175.38
PB493	73166.25165	-2756843.18	1161.76
PB494	72297.58858	-2757768.12	1156.02
PB495	74470.63079	-2758140.2	1150.71
PB496	73963.34855	-2754171.64	1118.62
PB497	73827.10201	-2755703.19	1146.93
PB498	74083.27235	-2754420.89	1129.82
PB499	75516.45524	-2755586.5	1133.53
PB500	73544.06655	-2756714.49	1137.77

12. APPENDIX 4: PLANNED DRILLHOLE DATA IMPORTED INTO LEAPFROG GEO

Drillhole Name	Easting	Northing	Elevation	Azimuth	Dip	Lift Rate	Drift Rate	Distance	Extension	Depth
PB1	73861.09	-2754409.88	1202.56	0	90	0	0	0	0	300
PB2	72693.26	-2755625.48	1158.91	0	90	0	0	0	0	300
PB3	73779.89	-2755221.78	1119.88	0	90	0	0	0	0	300
PB4	73493.08	-2756222.55	1098.11	0	90	0	0	0	0	300
PB5	75537.12	-2756130.80	1142.79	0	90	0	0	0	0	300
PB6	73171.23	-2755074.81	1140.74	0	90	0	0	0	0	300
PB7	72868.76	-2754678.89	1101.84	0	90	0	0	0	0	300
PB8	75153.22	-2757044.63	1138.85	0	90	0	0	0	0	300
PB9	73884.54	-2755274.23	1117.83	0	90	0	0	0	0	300
PB10	75473.31	-2754371.37	1126.53	0	90	0	0	0	0	300
PB11	73058.79	-2756672.33	1087.67	0	90	0	0	0	0	300
PB12	72993.57	-2754487.07	1111.24	0	90	0	0	0	0	300
PB13	73832.16	-2754946.32	1130.29	0	90	0	0	0	0	300
PB14	75198.62	-2754498.57	1125.49	0	90	0	0	0	0	300
PB15	72344.83	-2757322.97	1084.34	0	90	0	0	0	0	300
PB16	74286.02	-2754948.66	1119.23	0	90	0	0	0	0	300
PB17	73559.47	-2756892.89	1103.43	0	90	0	0	0	0	300
PB18	74048.43	-2755180.88	1117.01	0	90	0	0	0	0	300
PB19	73834.7	-2754346.04	1202.78	0	90	0	0	0	0	300
PB20	73387.27	-2755488.93	1158.46	0	90	0	0	0	0	300
PB21	74975.09	-2756928.07	1132.46	0	90	0	0	0	0	300
PB22	72377.71	-2754153.65	1130.17	0	90	0	0	0	0	300
PB23	74210.13	-2756371.62	1106.17	0	90	0	0	0	0	300
PB24	73042.2	-2756869.27	1091.17	0	90	0	0	0	0	300

PB25	72838.98	-2756401.50	1096.22	0	90	0	0	0	0	300
PB26	73332.53	-2755330.80	1164.75	0	90	0	0	0	0	300
PB27	72416.14	-2753994.58	1133.37	0	90	0	0	0	0	300
PB28	72429.11	-2755109.97	1100.4	0	90	0	0	0	0	300
PB29	75559.08	-2757150.17	1143.83	0	90	0	0	0	0	300
PB30	74596.47	-2757913.91	1123.47	0	90	0	0	0	0	300
PB31	72484.54	-2757849.00	1091.61	0	90	0	0	0	0	300
PB32	73009.79	-2757745.98	1120.53	0	90	0	0	0	0	300
PB33	73666.83	-2755098.10	1126.64	0	90	0	0	0	0	300
PB34	72387.15	-2756283.83	1097.18	0	90	0	0	0	0	300
PB35	73172.07	-2756942.01	1097.79	0	90	0	0	0	0	300
PB36	74390.84	-2755502.10	1108.77	0	90	0	0	0	0	300
PB37	73867.97	-2757244.25	1115.24	0	90	0	0	0	0	300
PB38	73436.13	-2755366.00	1158.46	0	90	0	0	0	0	300
PB39	72460.07	-2757262.15	1086.03	0	90	0	0	0	0	300
PB40	74157.21	-2756772.80	1115.28	0	90	0	0	0	0	300
PB41	72646.96	-2756998.25	1081.77	0	90	0	0	0	0	300
PB42	72860	-2756195.95	1105.08	0	90	0	0	0	0	300
PB43	73631.39	-2756686.62	1100.64	0	90	0	0	0	0	300
PB44	73894.87	-2756002.22	1096.11	0	90	0	0	0	0	300
PB45	74651.97	-2754557.88	1127.2	0	90	0	0	0	0	300
PB46	75597.82	-2757270.69	1145.01	0	90	0	0	0	0	300
PB47	72951.63	-2757618.77	1116.89	0	90	0	0	0	0	300
PB48	73387.94	-2756351.76	1097.12	0	90	0	0	0	0	300
PB49	75179.08	-2756421.28	1132.19	0	90	0	0	0	0	300

PB50	73440.5	-2754242.58	1122.31	0	90	0	0	0	0	300
PB51	74781.79	-2757935.37	1137.58	0	90	0	0	0	0	300
PB52	73670.71	-2758132.78	1100.61	0	90	0	0	0	0	300
PB53	73159.46	-2755775.49	1152.64	0	90	0	0	0	0	300
PB54	75516.5	-2754522.39	1122.38	0	90	0	0	0	0	300
PB55	73302.72	-2755299.13	1162.88	0	90	0	0	0	0	300
PB56	72964.12	-2754507.29	1110.15	0	90	0	0	0	0	300
PB57	73646.47	-2754209.47	1178.63	0	90	0	0	0	0	300
PB58	75008.14	-2757808.37	1145.37	0	90	0	0	0	0	300
PB59	72338.49	-2757305.07	1083.95	0	90	0	0	0	0	300
PB60	72711.36	-2755922.68	1109.61	0	90	0	0	0	0	300
PB61	73724.74	-2756334.60	1092.48	0	90	0	0	0	0	300
PB62	73723.69	-2755901.19	1101.75	0	90	0	0	0	0	300
PB63	75609.25	-2757788.50	1141.77	0	90	0	0	0	0	300
PB64	72267.75	-2755768.64	1098.81	0	90	0	0	0	0	300
PB65	75569.14	-2757900.66	1141.32	0	90	0	0	0	0	300
PB66	75560.5	-2754739.88	1118.64	0	90	0	0	0	0	300
PB67	74616.23	-2758006.24	1125.99	0	90	0	0	0	0	300
PB68	72753.77	-2757763.33	1109.91	0	90	0	0	0	0	300
PB69	74896.82	-2755800.04	1099.92	0	90	0	0	0	0	300
PB70	74571.58	-2757284.16	1117.07	0	90	0	0	0	0	300
PB71	74112.04	-2757295.88	1113.8	0	90	0	0	0	0	300
PB72	74564.52	-2754919.11	1118.5	0	90	0	0	0	0	300
PB73	74070.83	-2756452.11	1106.8	0	90	0	0	0	0	300
PB74	73207.49	-2757350.26	1111.53	0	90	0	0	0	0	300

PB75	72478.17	-2755109.03	1101.82	0	90	0	0	0	0	300
PB76	72720.3	-2756003.03	1105.36	0	90	0	0	0	0	300
PB77	74706.28	-2754651.25	1125.11	0	90	0	0	0	0	300
PB78	73922.31	-2756078.90	1095.01	0	90	0	0	0	0	300
PB79	72613.07	-2754642.27	1105.05	0	90	0	0	0	0	300
PB80	72539.92	-2757778.02	1093.61	0	90	0	0	0	0	300
PB81	73752.51	-2758127.94	1098.41	0	90	0	0	0	0	300
PB82	75228.45	-2755949.01	1115.2	0	90	0	0	0	0	300
PB83	73805.12	-2757537.14	1114.09	0	90	0	0	0	0	300
PB84	72397.25	-2757163.13	1080.91	0	90	0	0	0	0	300
PB85	74326.13	-2754800.35	1122.62	0	90	0	0	0	0	300
PB86	74790.06	-2756812.11	1124.16	0	90	0	0	0	0	300
PB87	75342.84	-2757375.63	1144.4	0	90	0	0	0	0	300
PB88	73714.65	-2757302.08	1115.74	0	90	0	0	0	0	300
PB89	74458.7	-2756994.54	1118.65	0	90	0	0	0	0	300
PB90	74774.01	-2754238.25	1134.25	0	90	0	0	0	0	300
PB91	72574.21	-2755393.66	1136.17	0	90	0	0	0	0	300
PB92	73897.35	-2754882.39	1133.31	0	90	0	0	0	0	300
PB93	75198.4	-2756100.08	1116.28	0	90	0	0	0	0	300
PB94	74076.89	-2755592.93	1107.48	0	90	0	0	0	0	300
PB95	75514.42	-2756957.51	1143.56	0	90	0	0	0	0	300
PB96	74149.51	-2757606.50	1108.64	0	90	0	0	0	0	300
PB97	72543.95	-2754597.39	1109.96	0	90	0	0	0	0	300
PB98	75181.27	-2756135.14	1117.4	0	90	0	0	0	0	300
PB99	73548.66	-2754028.21	1126.28	0	90	0	0	0	0	300

PB100	73788.98	-2754637.82	1179.7	0	90	0	0	0	0	300
PB101	75203.28	-2755308.94	1110.43	0	90	0	0	0	0	300
PB102	74912.06	-2755217.15	1111.73	0	90	0	0	0	0	300
PB103	73514.81	-2757456.74	1115.61	0	90	0	0	0	0	300
PB104	74454.05	-2755295.68	1112.22	0	90	0	0	0	0	300
PB105	73664.04	-2754482.68	1172.11	0	90	0	0	0	0	300
PB106	74309.56	-2756404.71	1109.13	0	90	0	0	0	0	300
PB107	72244.17	-2754375.58	1127.53	0	90	0	0	0	0	300
PB108	75415.35	-2757044.80	1139.65	0	90	0	0	0	0	300
PB109	73002.37	-2755624.09	1161.42	0	90	0	0	0	0	300
PB110	74814.62	-2756155.12	1106.1	0	90	0	0	0	0	300
PB111	73054.03	-2754592.72	1108.97	0	90	0	0	0	0	300
PB112	74618.4	-2756163.67	1103.68	0	90	0	0	0	0	300
PB113	73124.36	-2756268.77	1104.22	0	90	0	0	0	0	300
PB114	73675.54	-2756269.05	1093.23	0	90	0	0	0	0	300
PB115	75506.42	-2757724.49	1142.66	0	90	0	0	0	0	300
PB116	74806.87	-2755456.42	1106.23	0	90	0	0	0	0	300
PB117	72389.16	-2755177.47	1099.51	0	90	0	0	0	0	300
PB118	73183.21	-2755168.04	1150.12	0	90	0	0	0	0	300
PB119	72544.94	-2754917.71	1097.6	0	90	0	0	0	0	300
PB120	73197.29	-2754103.37	1119.89	0	90	0	0	0	0	300
PB121	73174.07	-2755496.85	1171.4	0	90	0	0	0	0	300
PB122	72478.47	-2757025.40	1079.35	0	90	0	0	0	0	300
PB123	75465.5	-2756645.68	1149.23	0	90	0	0	0	0	300
PB124	73383.68	-2754850.00	1131.92	0	90	0	0	0	0	300

PB125	72503.15	-2753975.10	1133.58	0	90	0	0	0	0	300
PB126	74768.14	-2755498.40	1105.34	0	90	0	0	0	0	300
PB127	73446.03	-2757033.29	1106.05	0	90	0	0	0	0	300
PB128	72398.55	-2756655.09	1085.14	0	90	0	0	0	0	300
PB129	72614.61	-2753960.61	1133.95	0	90	0	0	0	0	300
PB130	73299.51	-2757048.83	1104.89	0	90	0	0	0	0	300
PB131	74333.33	-2757553.24	1108.82	0	90	0	0	0	0	300
PB132	74312.27	-2755643.21	1105.42	0	90	0	0	0	0	300
PB133	72388.57	-2757569.79	1089.92	0	90	0	0	0	0	300
PB134	74807.65	-2758007.40	1136.62	0	90	0	0	0	0	300
PB135	72289	-2757156.13	1080.09	0	90	0	0	0	0	300
PB136	74840.66	-2757616.42	1144.26	0	90	0	0	0	0	300
PB137	75351.84	-2756167.89	1130.73	0	90	0	0	0	0	300
PB138	75189.88	-2755193.94	1112.17	0	90	0	0	0	0	300
PB139	75157.69	-2757796.23	1144.37	0	90	0	0	0	0	300
PB140	74295.48	-2754637.43	1130.82	0	90	0	0	0	0	300
PB141	72822.81	-2754607.38	1104.36	0	90	0	0	0	0	300
PB142	72473.04	-2757274.88	1086.75	0	90	0	0	0	0	300
PB143	75615.87	-2755744.28	1127.21	0	90	0	0	0	0	300
PB144	72453.6	-2754963.15	1099.72	0	90	0	0	0	0	300
PB145	74226.68	-2757754.34	1107.33	0	90	0	0	0	0	300
PB146	75108.77	-2756091.73	1112.86	0	90	0	0	0	0	300
PB147	74487.21	-2757814.18	1114.34	0	90	0	0	0	0	300
PB148	74759.78	-2754124.60	1137.04	0	90	0	0	0	0	300
PB149	72444.63	-2757611.79	1091.8	0	90	0	0	0	0	300

PB150	74650.66	-2754971.15	1117.3	0	90	0	0	0	0	300
PB151	74252.77	-2757856.98	1108.36	0	90	0	0	0	0	300
PB152	72183.17	-2756472.83	1092.04	0	90	0	0	0	0	300
PB153	74045.61	-2754655.25	1143.83	0	90	0	0	0	0	300
PB154	73062.95	-2758017.02	1119.73	0	90	0	0	0	0	300
PB155	75210.54	-2757136.70	1140.84	0	90	0	0	0	0	300
PB156	74749.41	-2757745.67	1136.45	0	90	0	0	0	0	300
PB157	75176.95	-2754070.20	1135.67	0	90	0	0	0	0	300
PB158	72931.1	-2756994.56	1092.99	0	90	0	0	0	0	300
PB159	75063.36	-2754149.08	1134.42	0	90	0	0	0	0	300
PB160	74054	-2755481.68	1110.2	0	90	0	0	0	0	300
PB161	73712.7	-2756163.11	1094.28	0	90	0	0	0	0	300
PB162	73171.4	-2756386.41	1093.54	0	90	0	0	0	0	300
PB163	73802.95	-2756445.09	1094.76	0	90	0	0	0	0	300
PB164	74808.96	-2756131.50	1105.21	0	90	0	0	0	0	300
PB165	74325.76	-2756368.81	1108.05	0	90	0	0	0	0	300
PB166	73434.9	-2754146.27	1119.5	0	90	0	0	0	0	300
PB167	74574.01	-2755095.37	1116.09	0	90	0	0	0	0	300
PB168	74339.68	-2755363.09	1110.76	0	90	0	0	0	0	300
PB169	73191	-2757691.91	1128.49	0	90	0	0	0	0	300
PB170	73334.41	-2757661.31	1122.09	0	90	0	0	0	0	300
PB171	72302.74	-2755354.69	1095.6	0	90	0	0	0	0	300
PB172	75028.17	-2756483.00	1124.18	0	90	0	0	0	0	300
PB173	75436.7	-2755748.19	1120.77	0	90	0	0	0	0	300
PB174	74452.88	-2756434.69	1112.74	0	90	0	0	0	0	300

PB175	73839.93	-2758088.52	1099.71	0	90	0	0	0	0	300
PB176	73090.61	-2756736.69	1089.17	0	90	0	0	0	0	300
PB177	74563.54	-2758085.14	1123.91	0	90	0	0	0	0	300
PB178	72609.35	-2754177.49	1127.35	0	90	0	0	0	0	300
PB179	73852.44	-2755959.06	1097.35	0	90	0	0	0	0	300
PB180	72629.82	-2757172.33	1088.82	0	90	0	0	0	0	300
PB181	73204.44	-2755711.01	1155.04	0	90	0	0	0	0	300
PB182	75157.36	-2756114.58	1115.5	0	90	0	0	0	0	300
PB183	72193.61	-2757545.57	1083.71	0	90	0	0	0	0	300
PB184	74329.62	-2756951.67	1118.52	0	90	0	0	0	0	300
PB185	74099.82	-2756797.61	1115.12	0	90	0	0	0	0	300
PB186	73082.34	-2755656.07	1158.91	0	90	0	0	0	0	300
PB187	72795.42	-2756308.96	1099.11	0	90	0	0	0	0	300
PB188	74061.33	-2754696.40	1141.3	0	90	0	0	0	0	300
PB189	75496.6	-2757024.20	1141.43	0	90	0	0	0	0	300
PB190	74124.07	-2755799.79	1100.7	0	90	0	0	0	0	300
PB191	73789.8	-2754669.67	1170.96	0	90	0	0	0	0	300
PB192	72874.81	-2756462.06	1092.93	0	90	0	0	0	0	300
PB193	74496.42	-2757960.28	1118.34	0	90	0	0	0	0	300
PB194	72166.9	-2755163.02	1103.97	0	90	0	0	0	0	300
PB195	74882.19	-2757070.28	1132.35	0	90	0	0	0	0	300
PB196	75035.11	-2757063.80	1137.3	0	90	0	0	0	0	300
PB197	72441.42	-2757843.59	1090.12	0	90	0	0	0	0	300
PB198	74834.26	-2756895.44	1126.97	0	90	0	0	0	0	300
PB199	73584.24	-2754819.52	1143.52	0	90	0	0	0	0	300

PB200	73740.89	-2755955.80	1099.32	0	90	0	0	0	0	300
PB201	75349.85	-2755018.20	1115.32	0	90	0	0	0	0	300
PB202	75084.7	-2754239.86	1132.47	0	90	0	0	0	0	300
PB203	75192.61	-2754529.14	1124.68	0	90	0	0	0	0	300
PB204	73166.12	-2755605.89	1162.13	0	90	0	0	0	0	300
PB205	75452.99	-2756744.32	1147.08	0	90	0	0	0	0	300
PB206	74626.96	-2755505.10	1107.12	0	90	0	0	0	0	300
PB207	75631.18	-2755049.36	1117.32	0	90	0	0	0	0	300
PB208	75178.76	-2756144.84	1117.86	0	90	0	0	0	0	300
PB209	72762.93	-2756922.50	1083.13	0	90	0	0	0	0	300
PB210	73091.33	-2754832.48	1111.21	0	90	0	0	0	0	300
PB211	74735.17	-2755298.20	1112.07	0	90	0	0	0	0	300
PB212	74445.44	-2756202.03	1103.02	0	90	0	0	0	0	300
PB213	72462.75	-2755029.88	1099.49	0	90	0	0	0	0	300
PB214	74749.43	-2756530.64	1116.75	0	90	0	0	0	0	300
PB215	73136.24	-2756659.51	1089.03	0	90	0	0	0	0	300
PB216	75350.82	-2757274.52	1142.98	0	90	0	0	0	0	300
PB217	74761.96	-2755356.24	1110	0	90	0	0	0	0	300
PB218	74632.78	-2754344.40	1132.93	0	90	0	0	0	0	300
PB219	74439.93	-2755149.25	1114.69	0	90	0	0	0	0	300
PB220	73619.45	-2758134.40	1103.69	0	90	0	0	0	0	300
PB221	73635.98	-2756814.07	1102.02	0	90	0	0	0	0	300
PB222	74191.12	-2755428.16	1110.04	0	90	0	0	0	0	300
PB223	73802.14	-2755479.21	1114.83	0	90	0	0	0	0	300
PB224	72739.93	-2757624.83	1101.24	0	90	0	0	0	0	300

FFF

PB225	74138.28	-2756973.16	1115.16	0	90	0	0	0	0	300
PB226	74407	-2754696.45	1124.24	0	90	0	0	0	0	300
PB227	75007.44	-2757768.05	1146.29	0	90	0	0	0	0	300
PB228	74962.69	-2755274.44	1110.13	0	90	0	0	0	0	300
PB229	74742.05	-2757934.69	1134.97	0	90	0	0	0	0	300
PB230	73894.18	-2757721.72	1108.52	0	90	0	0	0	0	300
PB231	74472.18	-2755328.90	1111.69	0	90	0	0	0	0	300
PB232	74433.68	-2756512.66	1114.69	0	90	0	0	0	0	300
PB233	74179.84	-2754261.36	1153.7	0	90	0	0	0	0	300
PB234	75375.63	-2754328.00	1128.71	0	90	0	0	0	0	300
PB235	74857.14	-2757774.61	1143.86	0	90	0	0	0	0	300
PB236	73871.83	-2757649.32	1110.61	0	90	0	0	0	0	300
PB237	75272.96	-2757321.29	1144.21	0	90	0	0	0	0	300
PB238	72247.13	-2756045.67	1098.22	0	90	0	0	0	0	300
PB239	75455.74	-2757712.94	1143.07	0	90	0	0	0	0	300
PB240	73395.83	-2755249.05	1159.51	0	90	0	0	0	0	300
PB241	72749.16	-2757253.49	1093.21	0	90	0	0	0	0	300
PB242	73740.82	-2756390.19	1092.59	0	90	0	0	0	0	300
PB243	74562.87	-2754347.33	1133.58	0	90	0	0	0	0	300
PB244	74975.62	-2755008.50	1114.92	0	90	0	0	0	0	300
PB245	72322.4	-2755662.00	1099.82	0	90	0	0	0	0	300
PB246	72841.38	-2754678.17	1101.37	0	90	0	0	0	0	300
PB247	73875.18	-2754271.31	1193.34	0	90	0	0	0	0	300
PB248	72522.05	-2756625.45	1086.02	0	90	0	0	0	0	300
PB249	74063.52	-2754524.85	1154.74	0	90	0	0	0	0	300

GGG

PB250	73486.79	-2753994.59	1120.55	0	90	0	0	0	0	300
PB251	73777.78	-2756461.80	1094.442	0	90	0	0	0	0	300
PB252	75147.98	-2757720.06	1146.188	0	90	0	0	0	0	300
PB253	73238.49	-2757081.46	1104.788	0	90	0	0	0	0	300
PB254	73723.73	-2754527.85	1181.342	0	90	0	0	0	0	300
PB255	72751.39	-2755713.79	1156.611	0	90	0	0	0	0	300
PB256	74925.79	-2754565.16	1125.435	0	90	0	0	0	0	300
PB257	73289.89	-2758054.72	1121.647	0	90	0	0	0	0	300
PB258	74514.49	-2754168.68	1140.06	0	90	0	0	0	0	300
PB259	72941.76	-2754444.79	1112.984	0	90	0	0	0	0	300
PB260	72383.06	-2755681.33	1102.729	0	90	0	0	0	0	300
PB261	73131.26	-2756808.47	1091.96	0	90	0	0	0	0	300
PB262	72865.66	-2755542.15	1167.726	0	90	0	0	0	0	300
PB263	72740.79	-2756671.57	1083.278	0	90	0	0	0	0	300
PB264	74036.41	-2754490.49	1164.627	0	90	0	0	0	0	300
PB265	74214.61	-2753995.21	1153.492	0	90	0	0	0	0	300
PB266	73683.68	-2755254.23	1123.854	0	90	0	0	0	0	300
PB267	73691.09	-2756838.19	1105.129	0	90	0	0	0	0	300
PB268	74643.7	-2757676.91	1124.485	0	90	0	0	0	0	300
PB269	75063.14	-2757073.88	1138.192	0	90	0	0	0	0	300
PB270	74429.24	-2757333.17	1112.494	0	90	0	0	0	0	300
PB271	74077.85	-2755740.73	1100.059	0	90	0	0	0	0	300
PB272	74685.46	-2755378.28	1110.242	0	90	0	0	0	0	300
PB273	72682.87	-2754168.69	1127.073	0	90	0	0	0	0	300
PB274	72204.28	-2757011.95	1079.774	0	90	0	0	0	0	300

HHH

PB275	73387.43	-2758106.90	1119.951	0	90	0	0	0	0	300
PB276	74664	-2754202.25	1136.328	0	90	0	0	0	0	300
PB277	73175.96	-2754556.40	1113.863	0	90	0	0	0	0	300
PB278	72749.51	-2754922.85	1096.998	0	90	0	0	0	0	300
PB279	72438.18	-2758018.11	1088.644	0	90	0	0	0	0	300
PB280	73130.26	-2756191.56	1109.833	0	90	0	0	0	0	300
PB281	74176.22	-2754986.33	1119.925	0	90	0	0	0	0	300
PB282	74274.7	-2754981.15	1118.579	0	90	0	0	0	0	300
PB283	73928.97	-2756575.88	1108.149	0	90	0	0	0	0	300
PB284	74641.36	-2755244.13	1114.372	0	90	0	0	0	0	300
PB285	72420.83	-2756838.50	1080.05	0	90	0	0	0	0	300
PB286	74867.21	-2754167.44	1135.075	0	90	0	0	0	0	300
PB287	72343.29	-2757860.34	1087.144	0	90	0	0	0	0	300
PB288	73093.34	-2755429.43	1175.877	0	90	0	0	0	0	300
PB289	73422.85	-2755333.86	1160.54	0	90	0	0	0	0	300
PB290	74066.64	-2755133.99	1117.811	0	90	0	0	0	0	300
PB291	74240.86	-2755461.87	1109.048	0	90	0	0	0	0	300
PB292	72199.95	-2754403.19	1128.403	0	90	0	0	0	0	300
PB293	75018.82	-2756757.59	1131.161	0	90	0	0	0	0	300
PB294	73627.42	-2757705.55	1114.841	0	90	0	0	0	0	300
PB295	74449.67	-2757267.29	1113.838	0	90	0	0	0	0	300
PB296	75542.61	-2756812.29	1148.973	0	90	0	0	0	0	300
PB297	74630.16	-2756986.72	1120.899	0	90	0	0	0	0	300
PB298	74508.3	-2757348.21	1114.127	0	90	0	0	0	0	300
PB299	74202.61	-2757495.72	1109.64	0	90	0	0	0	0	300

PB300	73565.39	-2754419.43	1157.69	0	90	0	0	0	0	300
PB301	73908.61	-2754658.96	1165.797	0	90	0	0	0	0	300
PB302	72795.8	-2754376.69	1117.914	0	90	0	0	0	0	300
PB303	75050.4	-2757051.51	1137.367	0	90	0	0	0	0	300
PB304	73989.5	-2756598.96	1110.022	0	90	0	0	0	0	300
PB305	74467.98	-2755523.43	1108.629	0	90	0	0	0	0	300
PB306	74252.85	-2757302.43	1112.578	0	90	0	0	0	0	300
PB307	74558.02	-2755891.29	1098.744	0	90	0	0	0	0	300
PB308	72442.85	-2756682.43	1083.966	0	90	0	0	0	0	300
PB309	74235.92	-2756420.68	1108.2	0	90	0	0	0	0	300
PB310	73429.37	-2755093.87	1138.581	0	90	0	0	0	0	300
PB311	72770.03	-2756010.62	1107.489	0	90	0	0	0	0	300
PB312	74855.92	-2755941.36	1101.259	0	90	0	0	0	0	300
PB313	73255.78	-2756592.21	1090.996	0	90	0	0	0	0	300
PB314	73539.88	-2754927.80	1136.544	0	90	0	0	0	0	300
PB315	73878.81	-2756843.66	1112.603	0	90	0	0	0	0	300
PB316	74319.26	-2756418.09	1109.861	0	90	0	0	0	0	300
PB317	74145.24	-2756213.22	1096.947	0	90	0	0	0	0	300
PB318	73589.52	-2757282.83	1114.471	0	90	0	0	0	0	300
PB319	75614.73	-2755384.39	1119.136	0	90	0	0	0	0	300
PB320	74835.09	-2754499.55	1127.83	0	90	0	0	0	0	300
PB321	73974.57	-2753988.94	1170.895	0	90	0	0	0	0	300
PB322	74749.22	-2754913.04	1117.802	0	90	0	0	0	0	300
PB323	73319.15	-2757162.05	1107.429	0	90	0	0	0	0	300
PB324	74522.82	-2755473.94	1109.19	0	90	0	0	0	0	300

PB325	73827.61	-2754608.66	1191.42	0	90	0	0	0	0	300
PB326	72529.82	-2756484.28	1092.561	0	90	0	0	0	0	300
PB327	73498	-2757875.21	1118.787	0	90	0	0	0	0	300
PB328	72764.56	-2754734.13	1098.446	0	90	0	0	0	0	300
PB329	72581.12	-2756187.51	1099.782	0	90	0	0	0	0	300
PB330	74831.28	-2754526.03	1127.239	0	90	0	0	0	0	300
PB331	72434.62	-2756401.89	1095.028	0	90	0	0	0	0	300
PB332	73412.48	-2754756.16	1133.431	0	90	0	0	0	0	300
PB333	74242.24	-2754368.43	1144.431	0	90	0	0	0	0	300
PB334	73516.4	-2755027.59	1133.931	0	90	0	0	0	0	300
PB335	72202.58	-2757773.68	1084.253	0	90	0	0	0	0	300
PB336	75299.14	-2757760.62	1143.609	0	90	0	0	0	0	300
PB337	74959.15	-2757980.87	1139.798	0	90	0	0	0	0	300
PB338	75615.88	-2757319.93	1145.243	0	90	0	0	0	0	300
PB339	73151.29	-2757377.75	1113.952	0	90	0	0	0	0	300
PB340	74201.89	-2755808.52	1100.157	0	90	0	0	0	0	300
PB341	74137.63	-2756817.31	1115.575	0	90	0	0	0	0	300
PB342	72412.68	-2757670.87	1090.499	0	90	0	0	0	0	300
PB343	75504.96	-2755024.86	1116.383	0	90	0	0	0	0	300
PB344	75430.61	-2756815.70	1144.476	0	90	0	0	0	0	300
PB345	75634.48	-2754087.67	1132.688	0	90	0	0	0	0	300
PB346	72416.2	-2756704.00	1083.221	0	90	0	0	0	0	300
PB347	74459.08	-2754434.51	1132.08	0	90	0	0	0	0	300
PB348	73902.82	-2757062.01	1113.713	0	90	0	0	0	0	300
PB349	72313.75	-2756474.74	1092.307	0	90	0	0	0	0	300

KKK

PB350	73830.29	-2756420.71	1095.027	0	90	0	0	0	0	300
PB351	75532.53	-2758026.93	1141.115	0	90	0	0	0	0	300
PB352	75402.38	-2756378.95	1144.217	0	90	0	0	0	0	300
PB353	74763.53	-2754809.35	1120.718	0	90	0	0	0	0	300
PB354	74674.55	-2756068.42	1101.547	0	90	0	0	0	0	300
PB355	74200.35	-2756180.19	1098.518	0	90	0	0	0	0	300
PB356	73912	-2757800.03	1106.285	0	90	0	0	0	0	300
PB357	72761.17	-2756002.77	1107.346	0	90	0	0	0	0	300
PB358	74452.99	-2757966.19	1116.543	0	90	0	0	0	0	300
PB359	72293.77	-2757649.96	1087.063	0	90	0	0	0	0	300
PB360	75481.27	-2756556.91	1150.308	0	90	0	0	0	0	300
PB361	72182.54	-2754899.66	1112.447	0	90	0	0	0	0	300
PB362	73934.2	-2755901.77	1097.689	0	90	0	0	0	0	300
PB363	74836.19	-2754502.39	1127.758	0	90	0	0	0	0	300
PB364	73294.1	-2757316.40	1109.239	0	90	0	0	0	0	300
PB365	75545.52	-2757127.24	1143.279	0	90	0	0	0	0	300
PB366	73299.27	-2757744.43	1126.489	0	90	0	0	0	0	300
PB367	75392.27	-2755848.47	1123.15	0	90	0	0	0	0	300
PB368	73414.07	-2756930.22	1103.152	0	90	0	0	0	0	300
PB369	75382.71	-2758040.74	1140.079	0	90	0	0	0	0	300
PB370	72884.4	-2755905.40	1127.395	0	90	0	0	0	0	300
PB371	74638.54	-2757163.37	1120.497	0	90	0	0	0	0	300
PB372	74656.04	-2757271.50	1122.104	0	90	0	0	0	0	300
PB373	73482.33	-2756316.72	1095.738	0	90	0	0	0	0	300
PB374	73296.17	-2754359.31	1119.939	0	90	0	0	0	0	300

PB375	75238.25	-2754536.66	1124.205	0	90	0	0	0	0	300
PB376	72367.46	-2756499.28	1091.449	0	90	0	0	0	0	300
PB377	74542.47	-2754950.97	1118.172	0	90	0	0	0	0	300
PB378	73042.7	-2756815.63	1089.653	0	90	0	0	0	0	300
PB379	72392.64	-2755505.22	1103.81	0	90	0	0	0	0	300
PB380	73503.76	-2756830.39	1101.513	0	90	0	0	0	0	300
PB381	75401.12	-2756215.71	1137.802	0	90	0	0	0	0	300
PB382	72731.02	-2754154.55	1126.991	0	90	0	0	0	0	300
PB383	73048.14	-2754464.09	1112.822	0	90	0	0	0	0	300
PB384	74086.58	-2756422.45	1106.268	0	90	0	0	0	0	300
PB385	72564.97	-2755017.56	1099.08	0	90	0	0	0	0	300
PB386	74674.45	-2756850.43	1121.857	0	90	0	0	0	0	300
PB387	74541.63	-2754048.16	1142.647	0	90	0	0	0	0	300
PB388	74301.7	-2757039.27	1117.941	0	90	0	0	0	0	300
PB389	74724.84	-2755948.53	1099.662	0	90	0	0	0	0	300
PB390	75189.83	-2755781.84	1109.771	0	90	0	0	0	0	300
PB391	73722.63	-2755287.80	1120.796	0	90	0	0	0	0	300
PB392	75276.15	-2757394.47	1145.215	0	90	0	0	0	0	300
PB393	75458.07	-2755450.46	1115.429	0	90	0	0	0	0	300
PB394	72824.18	-2757385.67	1098.424	0	90	0	0	0	0	300
PB395	73441.73	-2756915.25	1103.087	0	90	0	0	0	0	300
PB396	73230.73	-2754196.48	1119.986	0	90	0	0	0	0	300
PB397	75558.66	-2756927.01	1146.461	0	90	0	0	0	0	300
PB398	72325.48	-2754308.55	1126.88	0	90	0	0	0	0	300
PB399	74922.11	-2755615.39	1101.141	0	90	0	0	0	0	300

PB400	72618.05	-2757029.22	1082.019	0	90	0	0	0	0	300
PB401	73698.65	-2756033.19	1097.535	0	90	0	0	0	0	300
PB402	74408.23	-2754137.11	1143.691	0	90	0	0	0	0	300
PB403	75308.33	-2757371.97	1144.644	0	90	0	0	0	0	300
PB404	73616.79	-2756999.89	1107.749	0	90	0	0	0	0	300
PB405	73998.11	-2757847.64	1105.244	0	90	0	0	0	0	300
PB406	75044.41	-2754152.63	1134.415	0	90	0	0	0	0	300
PB407	75446.56	-2756110.64	1136.172	0	90	0	0	0	0	300
PB408	75202.98	-2754336.53	1129.777	0	90	0	0	0	0	300
PB409	74592.58	-2755250.13	1114.178	0	90	0	0	0	0	300
PB410	72643.3	-2755296.85	1142.215	0	90	0	0	0	0	300
PB411	75313.08	-2757099.95	1140.132	0	90	0	0	0	0	300
PB412	72673.86	-2757820.14	1102.727	0	90	0	0	0	0	300
PB413	75164.89	-2756120.01	1116.026	0	90	0	0	0	0	300
PB414	74820.39	-2756278.13	1110.046	0	90	0	0	0	0	300
PB415	74480.74	-2755249.15	1113.495	0	90	0	0	0	0	300
PB416	75551.52	-2755337.44	1117.378	0	90	0	0	0	0	300
PB417	72835.45	-2756731.15	1082.536	0	90	0	0	0	0	300
PB418	75393.8	-2757989.87	1140.398	0	90	0	0	0	0	300
PB419	75095.34	-2757976.64	1139.862	0	90	0	0	0	0	300
PB420	73502.39	-2754496.21	1140.232	0	90	0	0	0	0	300
PB421	73378.93	-2755003.05	1135.663	0	90	0	0	0	0	300
PB422	73290.22	-2754063.03	1120.076	0	90	0	0	0	0	300
PB423	73269.91	-2755175.07	1146.228	0	90	0	0	0	0	300
PB424	73797.41	-2755367.84	1116.977	0	90	0	0	0	0	300

PB425	73049.61	-2757692.44	1123.826	0	90	0	0	0	0	300
PB426	74534.23	-2756854.46	1119.902	0	90	0	0	0	0	300
PB427	74885.67	-2754541.52	1126.461	0	90	0	0	0	0	300
PB428	75035.14	-2756859.77	1133.251	0	90	0	0	0	0	300
PB429	75571.79	-2755269.68	1117.431	0	90	0	0	0	0	300
PB430	73057.97	-2756931.04	1093.478	0	90	0	0	0	0	300
PB431	73305.17	-2754610.32	1121.303	0	90	0	0	0	0	300
PB432	75183.28	-2755286.23	1110.624	0	90	0	0	0	0	300
PB433	75599.45	-2754604.90	1120.322	0	90	0	0	0	0	300
PB434	74178.33	-2756906.16	1116.017	0	90	0	0	0	0	300
PB435	75622.93	-2754064.44	1133.852	0	90	0	0	0	0	300
PB436	72921.41	-2758054.47	1121.155	0	90	0	0	0	0	300
PB437	72876.21	-2757858.59	1121.469	0	90	0	0	0	0	300
PB438	74195.02	-2756281.33	1098.229	0	90	0	0	0	0	300
PB439	73263.7	-2754690.41	1118.666	0	90	0	0	0	0	300
PB440	72627.11	-2756679.73	1083.185	0	90	0	0	0	0	300
PB441	74100.08	-2756790.64	1115.049	0	90	0	0	0	0	300
PB442	74653.84	-2757977.08	1128.33	0	90	0	0	0	0	300
PB443	72871.95	-2756494.00	1091.406	0	90	0	0	0	0	300
PB444	73076.49	-2755873.59	1142.894	0	90	0	0	0	0	300
PB445	73126.66	-2757051.80	1100.597	0	90	0	0	0	0	300
PB446	74804.65	-2757208.95	1132.117	0	90	0	0	0	0	300
PB447	73560.02	-2754573.33	1152.806	0	90	0	0	0	0	300
PB448	73593.71	-2757272.62	1114.284	0	90	0	0	0	0	300
PB449	72967.46	-2755342.10	1176.865	0	90	0	0	0	0	300

OOO

PB450	75190.08	-2756360.47	1130.524	0	90	0	0	0	0	300
PB451	73882.49	-2754233.66	1191.61	0	90	0	0	0	0	300
PB452	75501.24	-2755348.12	1116.236	0	90	0	0	0	0	300
PB453	72532.7	-2754949.56	1097.464	0	90	0	0	0	0	300
PB454	72853.23	-2756265.90	1100.987	0	90	0	0	0	0	300
PB455	74866.01	-2755326.45	1109.596	0	90	0	0	0	0	300
PB456	75240.02	-2754264.54	1131.276	0	90	0	0	0	0	300
PB457	74499.76	-2754700.45	1123.316	0	90	0	0	0	0	300
PB458	72989.03	-2755030.99	1128.357	0	90	0	0	0	0	300
PB459	75389.66	-2755410.77	1113.537	0	90	0	0	0	0	300
PB460	74058.85	-2757349.82	1114.003	0	90	0	0	0	0	300
PB461	75560.64	-2757319.79	1144.334	0	90	0	0	0	0	300
PB462	73014.62	-2758053.46	1119.567	0	90	0	0	0	0	300
PB463	75358.27	-2755052.60	1115.069	0	90	0	0	0	0	300
PB464	73618.94	-2756767.68	1100.251	0	90	0	0	0	0	300
PB465	73709.5	-2754564.69	1176.337	0	90	0	0	0	0	300
PB466	72226.77	-2753978.13	1136.016	0	90	0	0	0	0	300
PB467	72974.52	-2755405.93	1177.374	0	90	0	0	0	0	300
PB468	75162.74	-2756545.80	1134.965	0	90	0	0	0	0	300
PB469	72162.16	-2755324.54	1098.144	0	90	0	0	0	0	300
PB470	75189.75	-2755214.74	1111.97	0	90	0	0	0	0	300
PB471	73177.53	-2755206.08	1154.954	0	90	0	0	0	0	300
PB472	72850.64	-2757059.40	1091.972	0	90	0	0	0	0	300
PB473	74352.06	-2754909.98	1119.589	0	90	0	0	0	0	300
PB474	74927.25	-2756059.67	1105.867	0	90	0	0	0	0	300

PB475	74808.85	-2755791.35	1099.442	0	90	0	0	0	0	300
PB476	72401.4	-2755611.14	1104.755	0	90	0	0	0	0	300
PB477	72578.46	-2755883.96	1106.867	0	90	0	0	0	0	300
PB478	74833.53	-2754285.43	1132.72	0	90	0	0	0	0	300
PB479	72300.78	-2756714.98	1083.21	0	90	0	0	0	0	300
PB480	74050.78	-2755458.13	1110.647	0	90	0	0	0	0	300
PB481	73501.12	-2755759.32	1123.807	0	90	0	0	0	0	300
PB482	74489.47	-2755854.38	1099.232	0	90	0	0	0	0	300
PB483	74701.6	-2755840.90	1098.794	0	90	0	0	0	0	300
PB484	75407.95	-2755014.82	1115.716	0	90	0	0	0	0	300
PB485	73370.37	-2754600.34	1127.081	0	90	0	0	0	0	300
PB486	75447.99	-2755576.14	1116.136	0	90	0	0	0	0	300
PB487	74880.53	-2757281.16	1139.31	0	90	0	0	0	0	300
PB488	72743.14	-2756280.12	1099.942	0	90	0	0	0	0	300
PB489	72927.84	-2755116.11	1143.329	0	90	0	0	0	0	300
PB490	74831.26	-2757367.98	1139.592	0	90	0	0	0	0	300
PB491	74508.26	-2754952.79	1118.425	0	90	0	0	0	0	300
PB492	72761.5	-2755809.92	1140.381	0	90	0	0	0	0	300
PB493	73166.25	-2756843.18	1094.121	0	90	0	0	0	0	300
PB494	72297.59	-2757768.12	1086.58	0	90	0	0	0	0	300
PB495	74470.63	-2758140.20	1121.169	0	90	0	0	0	0	300
PB496	73963.35	-2754171.64	1177.806	0	90	0	0	0	0	300
PB497	73827.1	-2755703.19	1107.746	0	90	0	0	0	0	300
PB498	74083.27	-2754420.89	1160.94	0	90	0	0	0	0	300
PB499	75516.46	-2755586.50	1118.448	0	90	0	0	0	0	300

QQQ

PB500	73544.07	-2756714.49	1099.821	0	90	0	0	0	0	300

13. APPENDIX 5: NUMBER OF LODES INTERSECTED

Hole Id	Number of lodes intersected
PB1	0
PB2	1
PB3	2
PB4	4
PB5	0
PB6	0
PB7	0
PB8	0
PB9	3
PB10	0
PB11	1
PB12	0
PB13	0
PB14	0
PB15	0
PB16	0
PB17	1
PB18	2
PB19	0
PB20	0
PB21	0
PB22	0
PB23	1
PB24	1
PB25	0
PB26	0
PB27	0
PB28	0
PB29	0
PB30	0
PB31	0
PB32	0

PB33	0
PB34	0
PB35	1
PB36	0
PB37	0
PB38	1
PB39	0
PB40	0
PB41	1
PB42	1
PB43	3
PB44	1
PB45	0
PB46	0
PB47	0
PB48	1
PB49	0
PB50	0
PB51	0
PB52	0
PB53	0
PB54	0
PB55	0
PB56	0
PB57	0
PB58	0
PB59	0
PB60	2
PB61	5
PB62	3
PB63	0
PB64	0
PB65	0

PB66	0
PB67	0
PB68	0
PB69	0
PB70	0
PB71	0
PB72	0
PB73	3
PB74	0
PB75	0
PB76	2
PB77	0
PB78	1
PB79	0
PB80	0
PB81	0
PB82	0
PB83	0
PB84	0
PB85	0
PB86	0
PB87	0
PB88	0
PB89	0
PB90	0
PB91	0
PB92	0
PB93	0
PB94	1
PB95	0
PB96	0
PB97	0
PB98	0

PB99	0
PB100	0
PB101	0
PB102	0
PB103	0
PB104	0
PB105	0
PB106	0
PB107	0
PB108	0
PB109	0
PB110	0
PB111	0
PB112	0
PB113	1
PB114	6
PB115	0
PB116	0
PB117	0
PB118	0
PB119	0
PB120	0
PB121	0
PB122	1
PB123	0
PB124	0
PB125	0
PB126	0
PB127	0
PB128	0
PB129	0
PB130	0
PB131	0

PB132	0
PB133	0
PB134	0
PB135	0
PB136	0
PB137	0
PB138	0
PB139	0
PB140	0
PB141	0
PB142	0
PB143	0
PB144	0
PB145	0
PB146	0
PB147	0
PB148	0
PB149	0
PB150	0
PB151	0
PB152	0
PB153	0
PB154	0
PB155	0
PB156	0
PB157	0
PB158	0
PB159	0
PB160	2
PB161	5
PB162	1
PB163	4
PB164	0

PB165	0
PB166	0
PB167	0
PB168	1
PB169	0
PB170	0
PB171	0
PB172	0
PB173	0
PB174	0
PB175	0
PB176	1
PB177	0
PB178	0
PB179	2
PB180	1
PB181	0
PB182	0
PB183	0
PB184	0
PB185	0
PB186	0
PB187	0
PB188	0
PB189	0
PB190	2
PB191	0
PB192	1
PB193	0
PB194	0
PB195	0
PB196	0
PB197	0

PB198	0
PB199	0
PB200	3
PB201	0
PB202	0
PB203	0
PB204	0
PB205	0
PB206	0
PB207	0
PB208	0
PB209	2
PB210	0
PB211	0
PB212	0
PB213	0
PB214	0
PB215	1
PB216	0
PB217	0
PB218	0
PB219	0
PB220	0
PB221	1
PB222	2
PB223	2
PB224	0
PB225	0
PB226	0
PB227	0
PB228	0
PB229	0
PB230	0

PB231	0
PB232	0
PB233	0
PB234	0
PB235	0
PB236	0
PB237	0
PB238	0
PB239	0
PB240	0
PB241	0
PB242	5
PB243	0
PB244	0
PB245	0
PB246	0
PB247	0
PB248	0
PB249	0
PB250	0
PB251	3
PB252	0
PB253	0
PB254	0
PB255	0
PB256	0
PB257	0
PB258	0
PB259	0
PB260	0
PB261	1
PB262	0
PB263	1

PB264	0
PB265	0
PB266	2
PB267	1
PB268	0
PB269	0
PB270	0
PB271	2
PB272	0
PB273	0
PB274	0
PB275	0
PB276	0
PB277	0
PB278	0
PB279	0
PB280	1
PB281	0
PB282	0
PB283	4
PB284	0
PB285	0
PB286	0
PB287	0
PB288	0
PB289	0
PB290	1
PB291	1
PB292	0
PB293	0
PB294	0
PB295	0
PB296	0

PB297	0
PB298	0
PB299	0
PB300	0
PB301	0
PB302	0
PB303	0
PB304	3
PB305	0
PB306	0
PB307	0
PB308	0
PB309	1
PB310	0
PB311	0
PB312	0
PB313	1
PB314	0
PB315	0
PB316	0
PB317	1
PB318	0
PB319	0
PB320	0
PB321	0
PB322	0
PB323	0
PB324	0
PB325	0
PB326	0
PB327	0
PB328	0
PB329	0

PB330	0
PB331	0
PB332	0
PB333	0
PB334	0
PB335	0
PB336	0
PB337	0
PB338	0
PB339	0
PB340	0
PB341	0
PB342	0
PB343	0
PB344	0
PB345	0
PB346	0
PB347	0
PB348	0
PB349	0
PB350	3
PB351	0
PB352	0
PB353	0
PB354	0
PB355	0
PB356	0
PB357	0
PB358	0
PB359	0
PB360	0
PB361	0
PB362	2

DDDD

PB363	0
PB364	0
PB365	0
PB366	0
PB367	0
PB368	1
PB369	0
PB370	2
PB371	0
PB372	0
PB373	4
PB374	0
PB375	0
PB376	0
PB377	0
PB378	2
PB379	0
PB380	1
PB381	0
PB382	0
PB383	0
PB384	3
PB385	0
PB386	0
PB387	0
PB388	0
PB389	0
PB390	0
PB391	3
PB392	0
PB393	0
PB394	0
PB395	1

PB396	0
PB397	0
PB398	0
PB399	0
PB400	2
PB401	3
PB402	0
PB403	0
PB404	1
PB405	0
PB406	0
PB407	0
PB408	0
PB409	0
PB410	0
PB411	0
PB412	0
PB413	0
PB414	0
PB415	0
PB416	0
PB417	2
PB418	0
PB419	0
PB420	0
PB421	0
PB422	0
PB423	0
PB424	3
PB425	0
PB426	0
PB427	0
PB428	0

PB429	0
PB430	1
PB431	0
PB432	0
PB433	0
PB434	0
PB435	0
PB436	0
PB437	0
PB438	1
PB439	0
PB440	1
PB441	0
PB442	0
PB443	1
PB444	0
PB445	0
PB446	0
PB447	0
PB448	0
PB449	0
PB450	0
PB451	0
PB452	0
PB453	0
PB454	0
PB455	0
PB456	0
PB457	0
PB458	0
PB459	0
PB460	0
PB461	0

GGGG

PB462	0
PB463	0
PB464	1
PB465	0
PB466	0
PB467	0
PB468	0
PB469	0
PB470	0
PB471	0
PB472	1
PB473	0
PB474	0
PB475	0
PB476	0
PB477	0
PB478	0
PB479	0
PB480	3
PB481	0
PB482	0
PB483	0
PB484	0
PB485	0
PB486	0
PB487	0
PB488	0
PB489	0
PB490	0
PB491	0
PB492	1
PB493	1
PB494	0

HHHH

PB495	0
PB496	0
PB497	3
PB498	0
PB499	0
PB500	2

C.467] C-MINE SURFACE CONTOURS MASTER COPY Scale 1:20 000

C.467

LEEUWPOORT

District Warmbad

SCALE 1 - 20 000

500 0 500 1000 1500

METRES

LEGEND

X + 52 000 m

X + 56 000 m

X + 60 000 m

X + 64 000 m

Y - 2 000 m

Y - 6 000 m

HARTEBEESTVLEY 510 KQ

KNOPPIESKRAAL 537 KQ

RIETFONTEIN 536 KQ

LEEUWPOORT 554 KQ

DRIEFONTEIN 553 KQ

RIETDAL 555 KQ

DOORNFONTEIN 155 JQ

RUSTENBURG

WARMBAD

ROODBERG

BRITS

PIENAARSRIVIER

LEEUWPOORT TOWNSHIP

Work Shop

Spruit

C1

Rio Rita

No 2

No 3

Gen WK

COMPOUND

FLOAT DUMP

SLIMES DAM

MARRIED QUARTERS

1213

1200

86

1180

1160

1140

1120

1179

1100

TN

80

C MINE SURFACE BOREHOLE AND STRUCTURAL CONTOURS SCALE 1:5000

C696

C696

CMS 82 CMS 81 CMS 80 CMS 79 CMS 77 CMS 78 CMS 76

CMS 129 -60° E.O.H 504m 0.10 @ 1017m 0.10 @ 904m Repl Diesen

X+54 000 X+54 500 X+55 000 X+55 500 X+56 500 X+57 000

1120m 1130m 1140m 1150m 1160m 1170m

NEK HG ADIT CEMETERY RIO RITA SPRUIT EXIT CNS

CMS 47 CMS 124 CMS 126 CMS 43 CMS 64 CMS 65 CMS 70 CMS 75 CMS 107 CMS 74 CMS 72 CMS 140 CMS 92 CMS 60 CMS 57 CMS 67 CMS 73 CMS 104 CMS 117 CMS 108 CMS 62 CMS 56 CMS 52 CMS 71 CMS 102 CMS 110 CMS 23 CMS 55 CMS 51 CMS 101 CMS 112 CMS 44 CMS 68 CMS 66 CMS 69 CMS 58 CMS 105 CMS 59 CMS 91 CMS 109 CMS 54 CMS 42 CMS 100 CMS 115 CMS 139 CMS 106 CMS 63 CMS 46 CMS 40 CMS 83 CMS 114 CMS 89 CMS 90 CMS 49 CMS 48 CMS 103 CMS 86 CD C 8 CMS 111 CMS 113 CMS 61 CMS 88 CMS 151 CMS 2 CMS 84 CMS 152 CMS 20 CMS 153 CMS 21 CMS 19 CMS 85 CMS 154 CMS 156 CMS 165 CMS 22 CMS 87 CMS 18 CMS 50 CMS 53 CMS 1 CMS 6 CMS 14 CMS 13 CMS 149 CMS 116 CMS 148 CMS 147 CMS 150 CMS 4 CMS 8 CMS 3 CMS 146 CMS 16 CMS 9 CMS 10 CMS 11 CMS 12 CMS 15 CMS 143 CMS 121 CMS 134 CMS 133 CMS 136 CMS 41 CMS 142 CMS 135 CMS 137 CMS 138 CMS 119 CMS 39 CMS 118 CMS 141 CMS 17 MC 2 MC 3 CMS 35 CMS 34 CMS 131 CMS 28 CMS 130 CMS 27 CMS 26 CE CMS 30 CMS 38 CMS 122 CMS 24 CMS 25 CMS 120 CMS 37 CMS 36 CMS 128 CMS 127 CMS 29 CMS 125 CMS 81 CMS 132 CMS 97 CMS 99 CMS 32 CMS 123 CMS 93 CMS 94 CMS 96 CMS 145 CMS 95 CMS 144 CMS 98 MC 1

ROOIBERG TIN LTD

C MINE

SURFACE BOREHOLE PLAN

1:5000

R.L. WALKER

L. BOOTH

----- APPROXIMATE SURFACE CONTOURS

..... BEDDED LODES

FISSURES + FAULTS

'C' MINE GEOLOGY, MINERALIZED LODES, STRUCTURE and SURFACE BOREHOLES

SCALE 1:5 000

C716

C716

ROOIBERG TIN LTD.

LEEUWPOORT 'C' MINE

GEOLOGY, MINERALIZED LODES, STRUCTURE, AND SURFACE BOREHOLES

SCALE 1: 5000

0 100 200

LEGEND

- SCHRIKKLOOF Fm. FLOW BANDED FELSITE — ROOIBERG GROUP
- SMELTERSKOP Fm. INTERBEDDED ARENITES + ANDESITIC LAVAS
- SHALE — BLAAUWBANK SHALE MEMBER — LEEUWPOORT FORMATION
- SHALY ARKOSE — BLAAUWBANK SHALE MEMBER — LEEUWPOORT FORMATION
- BOSCHOFFSBERG QUARTZITE MEMBER — LEEUWPOORT FORMATION
- 1610'L / 15° STRIKE, DIP and ELEVATION OF MINERALIZED LODE
- STOPED OUT AREA
- SURFACE BOREHOLES WITH PAYABLE VALUES
- SURFACE BOREHOLE WITH TRACE MINERALIZATION
- SURFACE BOREHOLE NO VALUES
- OLD SURFACE BOREHOLES NO NUMBERS

PREPARED BY: J.E. MISIEWICZ.

DRAUGHTED BY: T. COETSER. 1989

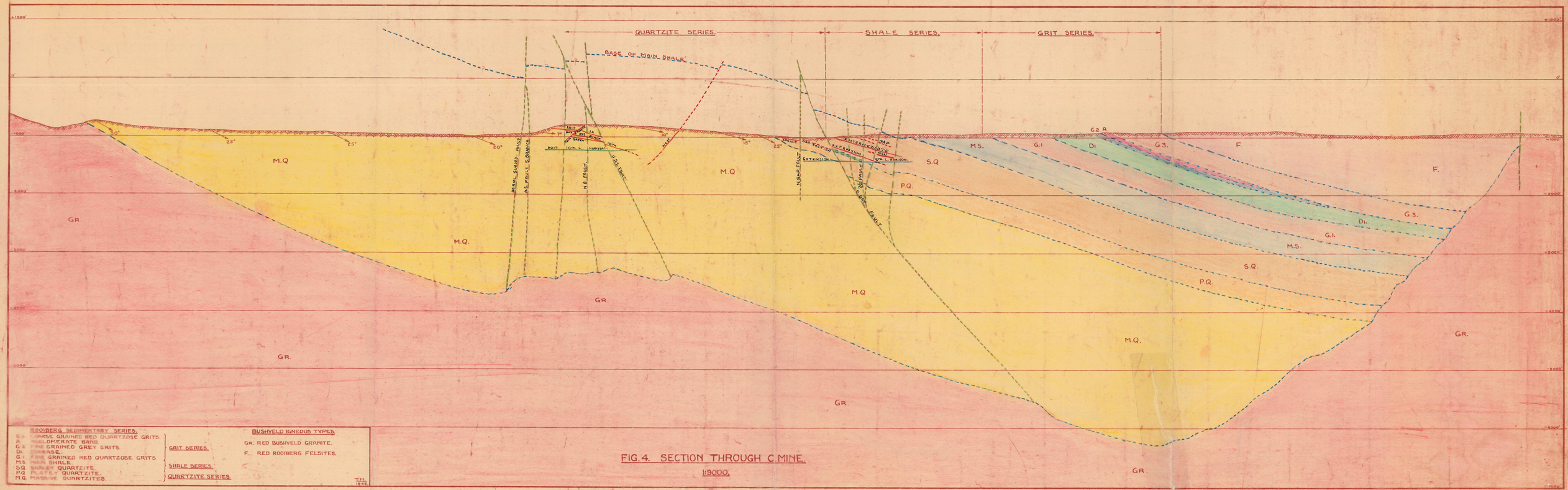

ROODIBERG SEDIMENTARY SERIES.

- G.3 COARSE GRAINED RED QUARTZOSE GRITS.
- A CONGLOMERATE BAND.
- G.2 FINE GRAINED GREY GRITS.
- D1 DOLERITE SILL.
- G.1 FINE GRAINED RED QUARTZOSE GRITS.
- M.S. MAIN SHALE.
- S.Q. SHALEY QUARTZITE.
- P.Q. PLATEY QUARTZITE.
- M.Q. MASSIVE QUARTZITES.

GRIT SERIES.
SHALE SERIES.
QUARTZITE SERIES.

BUSHVELD IGNEOUS TYPES.

- Gr. RED BUSHVELD GRANITE.
- F. RED ROODIBERG FELSITES.

T.H. 1942.

FIG.4. SECTION THROUGH C MINE.

1:9000.